Quantification of vegetation effects on shallow landslide probability at regional scales

Inauguraldissertation
der Philosophisch-naturwissenschaftlichen Fakultät
der Universität Bern

by:

Feiko Bernard VAN ZADELHOFF

from the Netherlands

29. March 2023

Supervisors:

Prof. Dr. Bettina SCHAEFLI
Bern University

Prof. Dr. Massimiliano SCHWARZ
Berner Fachhochschule

Copyright Notice

"The foremost quality of a good geographer is an intrinsic understanding of scale in both space and time"

Martin Hendriks, Utrecht University, 2012, personal communication

Abstract

Shallow landslides are the cause of considerable direct and indirect losses to individuals, enterprises and society as a whole. An increase in shallow landslide occurrence is often related to the loss of the protective effect of trees by deforestation. Methods of targeted reforestation, such as silvopastoralism, can in turn reduce the risk associated with shallow landslides considerably. The effective implementation of such systems can benefit from guidance in terms of tree placement, planting density, planting pattern, tree species selection and tree size development prediction. For this guidance, computational models can help greatly, in addition to expert knowledge, especially on a regional scale. In this work a quantitative, physically-based, tool to assess the influence of vegetation on shallow landslide occurrence is presented. The focus is specifically on rainfall-induced translational shallow landslides on a regional scale. The results of this tool are ideally incorporated into holistic analyses of site-specific tree benefits and co-benefits.

The tool as developed in this thesis is called SlideforMAP. It incorporates a probabilistic approach since the regional scale often poses challenges regarding heterogeneity in a range of parameters. Explicitly including this as uncertainty in the model can improve the model performance. Slope stability is computed by the limit equilibrium approach for a large number of randomly placed hypothetical landslide. The fraction of these hypothetical slides that are unstable, corresponds to local shallow landslide probability. The hydrological module is based on a topographic index and assumes a steady state sub-surface flux. All mechanical influences of vegetation are included with basal and lateral root reinforcement, being incorporated using the Root Bundle Model weibull approach on a single-tree basis. The model is calibrated and applied to three study areas (0.5 - 7.5 km^2) in Switzerland. Tree density is 33 to 73 trees/ha on average, but all study areas consist of distinct forested and non-forested sections. Soil thickness, soil cohesion, and the ratio between precipitation intensity and hydraulic saturated conductivity are found to be the most sensitive model parameters. Performance is measured against a 2005 landslide inventory and the Receiver Operator Curve analysis. Area Under the Curve values are between 0.64 and 0.93. It is proven that the single-tree based inclusion of mechanical effects significantly improves model performance, as compared to a forest stand approach.

To assess generalizability, SlideforMAP is applied in New Zealand silvopastoral systems in two small study areas (1.4 and 3.5 km^2). Over these areas a full calibration and validation of SlideforMAP and an improved version of SlideforMAP is performed. The improved version includes interception, passive earth pressure, root compression, a non-steady state approach to the lateral flux and a runoff coefficient. The runoff coefficient is dependent on cumulative precipitation and relates tree presence to increased macropore presence and subsequently to an increased runoff coefficient. The availability of RADAR-based precipitation data enables a more realistic precipitation input by finding a representative rainfall intensity. The non-steady state approach, runoff coefficients, representative rainfall intensity and novelties. The inclusion of such novelties did not improve model performance, which could be due to flaws in its methodology, the performance measure or site-specific reasons.

To place the application of SlideforMAP in context, it is compared to a statistical approach using binary logistical regression to shallow landslide susceptibility in New Zealand silvopastoral systems. For this a 2010 landslide inventory and a 2005 rainfall event are used. The model outputs are in agreement in approximately 70% of the study areas. Accountable for the remaining 30% are methodological differences, the heterogeneous input data in SlideforMAP and the difference in tree influence. SlideforMAP includes mechanical effects, where the statistical method implicitly includes all tree effects, but averaged over all trees. Practitioners are advised to prioritize

tree planting on areas where both models are in agreement and predict high shallow landslide susceptiblity.

SlideforMAP stands among other state of the art models focussed on vegetation effects on shallow landslide activity. This is due to the inclusion of single tree based lateral and basal root reinforcement and the tailoring to specific rainfall events. Further developments in SlideforMAP have enabled the application on large scales and for the analyses of specific components. All in all, land managers can benefit greatly by applying SlideforMAP to find the ideal targeted planting sites and stabilize the soil, as efficient as possible from a cost-benefit standpoint.

keywords: shallow landslides, probabilistic modelling, single-tree, root reinfrocement, hillslope hydrology

Acknowledgements

A PhD is not something one does alone. Everything presented in this thesis could only have materialized with help in many different forms from both seen and unseen people. Accordingly, I would like to extend gratitude to many people for the support they have shown me during the past three and a half years.

Thank you to Prof. Dr. Luuk Dorren for taking me under your wings during my internship and providing me with the opportunity for this PhD. To my supervisor Prof. Dr. Massimiliano Schwarz, thank you for providing me with the opportunity of doing this PhD and for all your valuable insights over the past years. To my supervisor Prof. Dr. Bettina Schaefli. Thank you for your kindness and making me feel welcome in the hydrology group. Throughout the PhD, I have admired your attention to detail. Your input has made everything we discussed better.

My PhD was funded by the New Zealand Ministry of Business, Innovation and Employment project "Smarter Targeting of Erosion Control" a.k.a. STEC. Thank you to the New Zealand taxpayer for seeing value in research, even when conducted from an office overseas.

During my two visits to New Zealand, I have been helped tremendously by the welcoming team of Landcare research/Manaaki Whenua. A specific thanks to Chris Phillips, leader of the STEC project, who made this PhD possible. Your insights and your hospitality have been invaluable. Also a specific mention for Raphael Spiekermann. Throughout the PhD, we've exchanged ideas, culminating in writing a paper together. I extend sincere gratitude for this and the warm welcome you've given me in New Zealand. Also a thank you to Gianluca, Julien and Ivo for making the fieldwork on poplar trees and the many visits to BurgerFuel during the first months of my PhD, an experience I still look back on fondly.

I would like to thank Dr. Rens van Beek. In the process of supervising both my bachelor and master thesis, you laid the foundation for my interest in physical geography. It is during your lectures and conversation in your office, that I first came into contact with most of the concepts treated in this thesis.

I've been pleased staying in contact with many people I've met before this PhD adventure. They helped in reminding me there's so much more in the world. Thank you Pieter, my former colleague for all your enthusiasm during our conversations on our mutual interest in GIS. Thank you Sven, Harke and Emmy for how we've kept kept in touch and for providing distractions from the work. Thank you to my brother Kristian and friends Stijn, Onno, Luuk, Amanda, Folckert, Maria, Sien and Ruud, for your visits to me in Switzerland and for welcoming me when I came for a visit back home.

I owe a lot of gratitude to Sara for providing me with a place to work, for giving your opinion on drafts, for making me feel more at home in Switzerland, but most of all for the happiness and laughter we've shared.

Lastly a well meant thank you to my parents, Albert and Annette, for instilling in me a curiosity to the world around us and the perseverance to find out how things work.

Contents

List of Figures

List of Tables

List of Symbols

Symbol*	Description	Dimension	Unit of prevalent expression
A	Surface area	L^2	m^2
C	Soil cohesion	$M/(L \cdot T^2)$	kPa
c	Circumference	L	m
CA	Contributing area	L^2	m^2
C_{int}	Interception	L	mm
D	Distance	L	m
DBH	Tree Diameter at Breast Height	L	m
F	Force	$(M \cdot L)/T^2$	N
g	Gravitational acceleration	L/T^2	$m\,s^{-2}$
H_{soil}	Soil thickness	L	m
H_{tree}	Tree height	L	m
I	Precipitation intensity	L/T	$mm\,s^{-1}$
K_{sat}	Saturated hydraulic conductivity	L^3/T	$m^3\,s^{-1}$
L	Length	L	m
m	Mass	M	kg
P	Total precipitation	L	mm
P_{ls}	Shallow landslide probability	$-$	%
P_{water}	Water pressure	$M/(L \cdot T^2)$	kPa
Q	Lateral flux	L^3/T	$m^3\,s^{-1}$
RR	Root reinforcement	$M/(L \cdot T^2)$	kPa
r	resolution	L	m
s	Slope angle	$-$	$^\circ$
SF	Safety factor	$-$	-
T	Soil transmissivity	L^2/T	$m^2\,s^{-1}$
t	Time	T	s
V_{mac}	Macropore flow velocity	L/T	$m\,s^{-1}$
ρ	Density	M/L^3	$kg\,m^{-3}$
θ	Topographic wetness index	L	-
ψ	Runoff coefficient	$-$	-

*sets of symbols are included as one, without subscripts

1 Introduction

1.1 Ratio for this work

This work was funded by the STEC (Smarter Targeting of Erosion Control) project. The STEC project is a multi-disciplinary project funded by the New Zealand Ministry of Business, Innovation and Employment (MBIE) that aims at developing strategies to reduce erosion in New Zealand pasture lands. The contribution of this thesis, within the project, is to provide a model to quantify the influence of trees on the reduction of rainfall-induced shallow landslide initiation. This contribution aligns with two of the five primary project goals. These project goals are i) finding an understanding of the spatial and temporal patterns of erosion and ii) quantifying sediment mitigation performance. This thesis addresses some of the key knowledge gaps in shallow landslide modelling. These knowledge gaps are primarily related to the computation of spatial variability of tree effects, the upscaling of tree effects and the complex influences of trees on hillslope hydrology and subsequently on slope stability.

1.2 Background

The support for research in erosion mitigation measures (such as by the STEC project) in New Zealand, is related to challenges the country faces. The development of the landscape in New Zealand has been exceptional due to its abruptness, as compared to other parts of the world (Fuller & Rutherfurd, 2022). Up until human settlement, median erosion rates were low due to intensive vegetation cover. This is despite 70% of the country consisting of steep to very steep terrain with high erosive potential (van Kraayenoord, 1968). Spikes in erosion rate and landscape evolution occurred only periodically due to extreme events, such as volcanic eruptions (Fuller & Rutherfurd, 2022). Initial Maori settlements, estimated to have started around 1280 AD, caused modest disturbance and later European settlements, with large-scale permanent deforestation for cattle farming, instigated extensive disturbance (Fuller & Rutherfurd, 2022). A total of 57% of original forests have been cleared (van Kraayenoord, 1968). Many parts of New Zealand now suffer from high rates of erosion since losing the protective effect of vegetation, with the remaining patches of native forest having significantly lower erosion rates (Fuller & Rutherfurd, 2022). Small-sized (50-500 m^2) shallow landslides are one of the primary contributors to this high erosion rate (Betts et al., 2017; De Rose, 2013; Dymond et al., 2016). The landscape is still adjusting to this wide-spread disturbance of deforestation by landslide activity (Crozier et al., 1980), leading to a decrease in average soil depth through time (De Rose, 2013). An extreme example of erosion is a 1977 event in the Wairarapa region of New Zealand, in which 40% of the region was directly affected by shallow landslides (Crozier et al., 1980). All this makes the New Zealand pasture lands an excellent study area for shallow landslide mapping and the testing of shallow landslide susceptibility models.

The occurrence of shallow landslides is observed throughout the world and their effects have a global impact (Glade et al., 2005). Shallow landslides and shallow landslide induced erosion cause considerable damage to landowners and others that are directly involved, but also to the

landscape and society as a whole. Shallow landslides can themselves be the instigators of debris flows (Kuriakose et al., 2009) and large wood mobilization (Cislaghi et al., 2018). An analysis of casualties due to natural hazards from 1946-2015 in Switzerland (Badoux et al., 2016) shows 74 landslide related casualties, with six percent of the country susceptible to landsliding (Lateltin et al., 2005). No distinction here is made between deep-seated and shallow landslides. Worldwide, 66 million people live in areas with a high landslide-risk and the annual monetary damages from landslides are in the billions of US dollars (Kjekstad & Highland, 2009a).

The protective effect of vegetation in reducing risk, related to many types of gravitational hazards, has been known for a long time. Strategies have developed around the world, to effectively apply this protective effect (de Jesús Arce-Mojica et al., 2019; Moos, 2018). In Switzerland, the NaiS (Nachhaltigkeit und Erfolgskontrolle im Schutzwald) (Frehner et al., 2005) handbook provides guidelines to managers to achieve a sustainable protective effect from forests, tailored to the protective forest location and the type of natural hazards to be expected. As an alternative to the clear-cuts as sometimes seen in production forests, some specific planting and management techniques have been developed. A venerable and effective technique is the management of forests by coppicing (Dazio et al., 2018a), where instead of entirely removing mature trees, they are cut down in regular intervals and sprouts from the stumps rejuvenate the tree and, in case of certain tree species, the root system (Vergani et al., 2017). This manages to significantly decrease the post-disturbance period of minimal protection (Masi et al., 2021; Sakals & Sidle, 2004; Schmidt et al., 2001; Steinacher et al., 2009). Throughout the world, different variations of silvopastoral land use are applied (Spiekermann, 2022). This land use consists of trees planted at low density with the land between trees used for grazing of cattle. New Zealand has a unique silvopastoral system with year-round cattle grazing (McIvor et al., 2011), relying heavily on non-native poplar and willow trees (van Kraayenoord, 1968). In New Zealand the development of large scale Silvopastoral systems can prevent long-term soil erosion, preferably with poplars and willows as they grow fast, withstand wet conditions and have high transpiration rates (Wilkinson, 1999). On landslide-prone locations the standard spacing of 15 m between trees is not sufficient for significant hazard reduction. Closer spacing of trees, however, tends to lead to canopy closure and loss of pasture productivity, leaving farmers with a dilemma (McIvor et al., 2011).

The risk associated with shallow landslides and the opportunities for prevention, established a desire to predict hazard patterns and effectiveness of mitigation measures (Debele et al., 2019). To increase understanding, a classification of risk is required. Many countries or regions have specific guidelines for this classification. In Figure 1.1 an example of risk classification as a function of event magnitude and probability, as used in Switzerland, is given. This can be applied specifically to aid zoning of shallow landslide hazard.

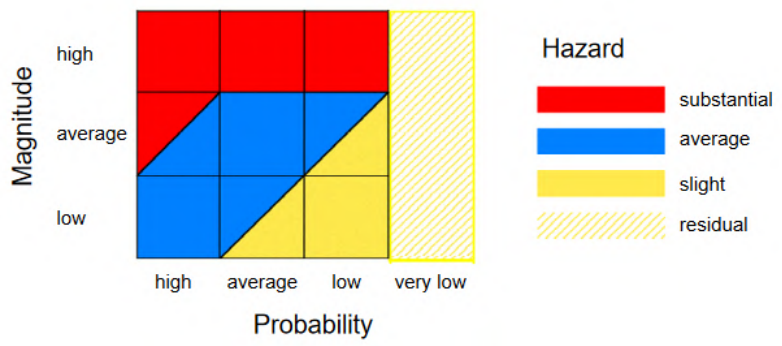

FIGURE 1.1: Hazard categories, as defined by the Swiss Federal Office of the Environment, based on probability and magnitude of an event. Figure adopted from Loat and Petrascheck (1997).

As seen in Figure 1.1, risk analyses generally agree that a residual hazard remains despite mitigation measures (Loat, 2003). Alongside hazard reduction, reducing exposure and vulnerability is an essential part of risk reduction (Loat, 2003). Expert knowledge and extrapolation from past events can effectively classify risk, but it has its shortcoming, especially on larger scales. These include limited resources and unconscious biases (Spiekermann et al., 2015). This is where regional scale models can aid with classifying risk. In this thesis, regional scale is defined as an area between 1 to 1000 km^2. An additional strength of many models is the ability to run scenarios. In the case of shallow landslide modelling, these scenarios can be related to modelling risk under design rainfall events. Rainfall induced shallow landslides may increase in frequency due to the increased frequency of extreme precipitation events. Scherrer et al. (2016) analyzed precipitation from 1901-2014 throughout Switzerland and found an average 10.4 % increase in annual maximum daily precipitation. Models can help translating this precipitation increase to an increase in risk. Another interesting feature is the modelling of the potential reduction in risk from implementing mitigation measures. Often used measures of mitigation are converting unforested areas to forest, increasing density of current forests, improved management in forests or non-nature based measures (often referred to as geotechnical interventions) (de Jesús Arce-Mojica et al., 2019). Comparing model outputs of mitigation measures helps in reliable cost-benefit analyses that aid decision-makers to effectively use available resources.

1.3 Research objective

The overall goal of this research is to provide a model to quantify the effectiveness of vegetation in reducing shallow landslide occurrence. This will be a probabilistic model and focussed on rainfall-induced shallow landslides on a regional scale. Ideally this model will benefit a wide variety of stakeholders including farmers, practitioners, policy makers, landowners and research institutes. Applying the model should require as little information on topography, soil and climate as possible. In order to make this model accurate and reliable, it should be well tested, embedded in current knowledge and find appropriate solutions for current knowledge gaps. In order to achieve a reliable and accurate assessment of vegetation influence, the following objectives are defined to include in or assess by the model:

- Include mechanical tree influence on slope stability at a single-tree scale and both in the horizontal and vertical dimensions, based on the Root-Bundle Model weibull (RBMw) as developed by Schwarz et al. (2013).

- Develop a methodology to include and analyze different vegetation scenarios in the modelling of shallow landslide susceptibility to enable model users to optimize vegetation planting and/or management.
- Calibrate and validate the model under realistic rainfall conditions, tree location, tree dimension and triggered shallow landslides to assess its real-world performance and value.
- Develop a dynamic methodology to sub-surface water and compare it to a steady-state assumption to assess whether a dynamic approach to hydrology can increase the performance of the model. This is because on the regional scale in natural environments, rainfall and the runoff response are rarely if ever, steady-state processes.
- Develop a methodology to include the influence of vegetation on lateral groundwater flow.
- Assess the ability of the model to accurately predict shallow landslide susceptibility and vegetation influence on shallow landslide susceptibility. Compare the model with its probabilistic strategy to a comparable model with a statistical modelling strategy.

1.4 Thesis structure

This thesis is based on papers as published during the PhD. The papers are formatted as chapters with each a preface summarizing the goal of the paper and its submission details. Following this introduction, chapter 2 presents the literature review and scientific background to this thesis's topics. For readers knowledgeable in any of the respective fields, the review of some topics may feel quite basic. This is deliberate, as it is the author's conviction that well-establishing and defining common knowledge paves the way for a deeper understanding of shallow landslide probability estimation and mitigation effectiveness. The literature review is followed by chapter 3, where the seven study areas that have been used in this thesis and to which our shallow landslide susceptibility model has been applied, are presented systematically. Chapter 4 is the first paper of the thesis. It's published in the Copernicus journal Natural Hazards and Earth sciences (date of acceptance 26-06-2022). The first paper presents the shallow landslide susceptibility model, named and henceforth referred to as SlideforMAP. Chapter 5 is the second paper, submitted to Ecological Engineering (date of submission 27-01-2023). In it, SlideforMAP is validated and it presents improvements in the hydrological module of the model. Chapter 6 is the third paper submitted to Geomorphology (date of submission 16-01-2023). The performance of SlideforMAP (uncalibrated) is compared to a statistical approach to shallow landsldie probability. An overarching objective of this thesis is the applicability of the SlideforMAP tool by stakeholders. For this, chapter 7 gives guidelines on application, tree distribution scenarios and tree influence parameter acquisition as well as documentation on thought-provoking modelling approaches. In chapter 8, a synthesis of the work is provided, followed by the overall conclusions and outlook in chapter 9. Finally, chapter 10, is a combination of the supplementary materials of the published papers.

The modelling of shallow landslide initiation in this thesis includes concepts from distinct disciplines. The disciplines are: i) geotechnics; for the forces controlling shallow landslide occurrence. ii) Hydrology; for the temporal and spatial distribution of soil and groundwater assumed responsible for initiation. iii) Forestry; for vegetation development and its influence on the geotechnical and hydrological modules of the model. Background to information from all three disciplines is given in the literature review (chapter 2).

2 Literature review

2.1 Shallow landslides

Landslides are a distinct type of slope failure and subsequent movement, defined by displacement along a clear shearing surface (Varnes, 1978). The landslide movement is considered rotational (along a curved shear plane) or translational (along a slope-parallel shear plane) (Varnes, 1978). Landslides are commonly triggered by rainfall events (De Vita et al., 1998, e.g) or by earthquakes (Croissant et al., 2019). Sub-types of landslides are shallow and deep-seated landslides. No universally accepted distinction between these two exists, but shallow landslides are generally considered relatively small, above regolith and one time events (Shou & Chen, 2021). In Switzerland all landslides with a shear plane depth < 2 m, are classified as shallow landslides (Lateltin, 1997). In this thesis the focus is specifically on rainfall-triggered translational shallow landslides.

Shallow landslide initiation is dependent on hydrology, root strength, soil conditions, topography and precipitation (Wu & Sidle, 1995). The hydrological influence is less pronounced for landslides triggered by short but extreme rainfall events (Sidle & Bogaard, 2016). Wet conditions (Geertsema et al., 2009) and land use change (Gorsevski et al., 2006) correlate directly to an increase in landslide activity. On short time scales ($< 10^3$ years), vegetation is the most effective stabilizing measure (Debele et al., 2019; Phillips et al., 2021).

The distribution in shallow landslide size is independent of its triggering event (Malamud et al., 2004) and does not correlate well to topography, lithology and vegetation presence (Bellugi et al., 2021). The minimum size is controlled by forces along the boundary, such as passive earth pressure, and correlates mainly to soil depth (Milledge et al., 2014). The maximum size is hypothesized to be dependent on heterogeneity in local conditions (Milledge et al., 2014). Malamud et al. (2004) performed a meta analysis on shallow landslide size distribution from studies all over the world and developed an inverse gamma based equation, to fit the distribution. The distribution is site specific and requires calibration.

2.2 Shallow landslide modelling

In the sections below an overview of the fundamentals in shallow landslide modelling is given. This starts with general modelling principles and subsequently narrows its focus specifically to shallow landslide stability modelling.

2.2.1 Modelling principles

Computational modelling to predict future shallow landslide occurrence is essential for prevention of damage (Zieher et al., 2017) and assessing the effectiveness of mitigation measures (de Jesús Arce-Mojica et al., 2019). It could be suggested that reducing processes to their physical basis comes closest to reality. However, this is generally not the case (Beven, 2000; Sivapalan et al., 2003). Computational models are, generally, attuned in their methodology to answer specific

questions. Several factors, as listed below, have been found throughout literature to challenge reductionist and complex approaches.

- Physical processes become near-infinitely complex on smaller scales, meaning we will never be able to reproduce them, not being in the possession of such computational power (Dooge, 2005).

  We cannot reliably model every raindrop in a rainfall event.

- A landscape inherently has a developmental history that influences events happening today and in the future (e.g. Iida, 1999). This history is shaped by events like landslides, rainfall, earthquakes, volcanic eruptions and past land use. Even if we can perfectly model processes, we have no reliable point in time to define as initial state of a system to model from. For this we have to make measurements and/or assumptions.

  A major rainfall event >50 years ago and subsequent landsliding still has an effect on current soil thickness. This effect in turn can be influenced by extreme rainfall events even further back, creating a constant 'background' heterogeneity.

- Reductionism and complexity may lead to good representation of individual processes but fails to model feedback mechanisms and emerging properties of a system as a whole (Beven, 2000; Spiekermann, 2022).

  Trees provide shade for cattle changing their behaviour and limiting nutrient distribution, leading to reduced tree growth elsewhere.

- Even if model complexity leads to better results in the temporal and spatial domain, the computational power may be so high or parametrization so complex that practitioners resort to simpler methods for answering specific question (e.g Beven et al., 2020; Phillips et al., 2021).

  Someone wanting to know the best management strategy for protection forest, may want a specific answer to that question and is not interested in the exact shape, location and timing of shallow landslides.

The arguments mentioned above indicate, that all developers include a certain degree of simplifications in their models (Beven & Kirkby, 1979). Savenije (2009) even goes so far as stating a model can better best be described as a hypothesis. Describing the degree to which simplifications are made, the degree of uncertainty and the verification of the model procedure, is good practice (Pechlivanidis et al., 2011; SafeLand, 2011). The level of model complexity should be related to the goal(s) of the model in terms of expected user and desired output accuracy, reliability and flexibility. Attuned to these needs different model types can be selected (Beven, 2012), of which the commonest are listed below (SafeLand, 2011).

- Physically based models: These models try to approximate the complexity of processes in reality as close as possible. The more physical a model is, the less calibration is required (Pechlivanidis et al., 2011).

- Conceptual models: These models represent physical processes, but an independent measurement of variables is mostly not possible and dependent on calibration (Pechlivanidis et al., 2011).

- Statistical models: Also known as black-box models. These models find empirical relationships between input and response variables, without the explicit inclusion of the processes involved (SafeLand, 2011).

In practice though, many models are hybrids that use different approaches for distinct modules in the model (Pechlivanidis et al., 2011). Conceptual and physically based models can either be deterministic or probabilistic. In deterministic models, the input parameters are single values and a unique output is given. Deterministic models are considered the most objective (SafeLand, 2011). SHALSTAB (Dietrich & Montgomery, 1998) and TRIGRS (Baum et al., 2002a) are examples of deterministic models in the context of shallow landslide occurrence. Probabilistic models take samples from a distribution as input, rather than single values. The output accordingly is not exact, but expressed in probabilities. Examples of probabilistic shallow landslide models are SINMAP (Pack et al., 1998), HIRESS (Rossi et al., 2013) and PG_TRIGRS (Salciarini et al., 2017). For most applications the probabilistic output needs to be converted in distinct classes (Zhang, Zhao, et al., 2018). Dependent on the situation, probabilistic models can perform better (Park et al., 2013) and are better tools for establishing safety criteria (Ang & Tang, 1975).

Calibration of shallow landslide models improves the model performance (e.g. Zieher et al., 2017). Calibration is never perfect though, and errors arise from various sources (Binley et al., 1991; Liu et al., 2018). One of the best performing calibration procedures is GLUE (Beven & Binley, 1992; Ratto et al., 2001; Xue et al., 2018). It calibrates to observed data, with optional constraints of a priori knowledge. In the procedure, calibration error due to poor boundary conditions, poor measurements or in the model structure are distinguished and quantified. As little parameters as possible should be calibrated for best results (Refsgaard, 1997) and calibration to multiple ground truths can improve calibration quality (Franks et al., 1998). Subsequent model validation is essential to independently show the accuracy and reliability of a model (SafeLand, 2011) and enable interpretation of results (Chung & Fabbri, 2003). Validation should be performed on a distinct spatial and/or temporal dataset, different from the calibration dataset (Chung & Fabbri, 2008; Guzzetti, Reichenbach, et al., 2006; Klemeš, 1986).

2.2.2 Slope stability

The limit equilibrium approach is most commonly used to assess the stability of a slope (Murgia et al., 2022; Phillips et al., 2021). This approach expresses the stability in a safety factor, which is the fraction of resisting force (numerator) and the sum of driving force (denominator), as given in Equation 2.1. A Safety Factor < 1.0 indicates a slope is unstable.

$$SF = \frac{F_{\text{res}}}{F_{\text{par}}} \tag{2.1}$$

In two dimensions the safety factor of a block of soil can be computed with as little as two terms, being the shear strength as resistance force and the tangential force as driving force. This does however overlook important components, such as soil cohesion, lateral and basal root reinforcement (see section 2.4.2), suction stress and pore water pressure (see section 2.3). Rainfall induced shallow landslides are commonly triggered by an increase in pore water pressure in the saturated part of the soil column. Increasing pore pressure is correlated directly to a decrease in shear strength via Bishop's approach (Bishop, 1955). This is the trigger mechanism that is included in the Safety Factor computation of the SlideforMAP model. The safety factor computation with all components for SlideforMAP, adopted from chapter 4, is given in equation 2.2 below.

$$SF = \frac{C_{\text{soil}} + RR_{\text{lat, tens}} + RR_{\text{bas}} + RR_{\text{lat, comp}} + EP + (g \cdot m_{\text{tot}} \cdot \cos(s) - P_{\text{water}}) \cdot \tan(\phi)}{g \cdot m_{\text{tot}} \cdot \sin(s)} \tag{2.2}$$

The driving force is the weight of a soil block ($g \cdot m_{\text{tot}} \cdot \sin(s)$), consisting of the gravitational acceleration, the moving mass and the sine of the slope angle. The resisting force is composed of the soil cohesion (C_{soil}), the lateral root reinforcement ($RR_{\text{lat, tens}}$), the basal root reinforcement (RR_{bas}), the root compression ($R_{\text{lat, comp}}$), the passive earth pressure (EP) and the soil shear strength ($g \cdot m_{\text{tot}} \cdot \cos(s) - P_{\text{water}}) \cdot \tan(\phi)$). The shear strength consists of the gravitational acceleration, the moving mass, the cosine of the slope angle, the water pressure and the tangent of the friction angle. Many models use a version of the force balance, with specific choices on what components to include, how to include components and which components to neglect. Suction stress (ignored in SlideforMAP) is often included in models using the analytical approach of Lu et al. (2010). Many models ignore the passive earth pressure, but this can be relevant, especially in deep soils (Murgia et al., 2022).

Pore water pressure is dependent on the depth to groundwater, i.e. the water table. Ignoring the velocity component in Bernoulli's energy balance equation, irrelevant under any realistic soil water flux velocities, the water table equals the hydraulic head (Hendriks, 2010). The hydraulic head, expressed in m, is given in equation 2.3 below.

$$h = z + \frac{P_{\text{water}}}{\rho_{\text{water}} \cdot g} \tag{2.3}$$

In this equation h is the hydraulic head [m], z is the elevation head [m], P_{water} is the pressure [N/m^2], ρ_{water} is the water density [kg/m^3], g is the gravitational acceleration [N/m^2]. In practical application, a reference value for elevation head is used. This is usually an impervious layer or impervious bedrock interface (Hendriks, 2010). In the unsaturated zone, both air and water is in the pores, so the mechanical energy can't be determined as easily as in the saturated zone. It is usually expressed as matric potential and is expressed with a minus sign since it's a stabilizing force. The absolute value of the matric potential is known as suction. An example of the pressure head, gravitational head and matric potential in a soil column is given in Figure 2.1 below.

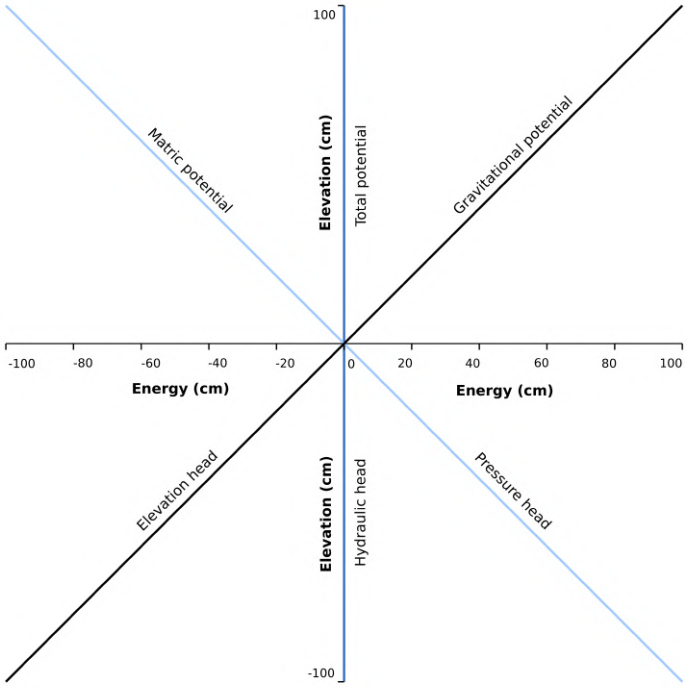

FIGURE 2.1: Displaying water pressure in a soil column under hydrostatic conditions for the saturated and the unsaturated zone. Figure adopted from Hendriks (2010, p. 144).

Converting hydraulic head [m] to pressure [Pa] and assuming the bedrock interface as reference, the pore water pressure is expressed by rewriting equation 2.3 as: $P_{\text{water}} = \rho_{water} \cdot g \cdot h$. Despite the forces related to pore water pressure development being small in comparison to other forces in the force balance (equation 2.2), it is their short timescale of variability that makes pore water pressure a common trigger of shallow landslides. This timescale is hours to days for heavy rainfall events (e.g. Askarinejad et al., 2012).

2.3 Hydrological concepts and groundwater table development

As stated in section 2.2.2, shallow landslides are initiated by groundwater table rise, whose development is in the hydrological domain. Hydrology is the flow of water through bedrock, soil or surface (Dingman, 2015). Especially on large spatial scales (basin and catchment scales) the water balance takes a central role in hydrological modelling (Hendriks, 2010; Luo et al., 2015). A simplified version of this balance in given in equation 2.4 below.

$$Q = P - ET + \frac{\Delta S}{\Delta t} \tag{2.4}$$

In this equation, P is the precipitation, Q is the outflow (discharge or runoff are also often used as terms, depending on scale and process), ET is the evapotranspiration and $\Delta S / \Delta t$ is the change in storage. ET includes interception that subsequently evaporates. In this version no distinction is made between overland and sub-surface runoff. Forest presence reduces total runoff considerably thanks to increased transpiration (Dingman, 2015). In wet forests, the evaporation resulting from interception can be more important than transpiration (Dingman, 2015). When potential evaporation exceeds available rainfall, we speak of a water limited system, the other way around is an energy limited system.

The transfer of surface water to subsurface water takes place though infiltration (Green & Ampt, 1911). Infiltration in the upper soil decreases matric potential, meaning the total pressure head increases, leading to downward flow where the water first spreads to the unsaturated and possibly to the saturated zone afterward. On the other hand, evaporation may increase matric potential in the upper soil, facilitating upward flow. The incompressible nature of water and landscape inclination affect infiltration, leading to a lateral flux in groundwater. This flux is a notable part of the water cycle in most climatic zones in the world and most active in unconfined aquifers (Dingman, 2015). Lateral redistribution by means of soil and vegetation heterogeneity is highly significant on small and large scales (Bierkens, 2008). The lateral groundwater flux between two points can be expressed by the Darcy equation (Darcy, 1856). In three dimensions, this is expressed as follows:

$$Q = k_{sat} \cdot A_{cross} \cdot \frac{\Delta h}{\Delta x} \tag{2.5}$$

In this equation, Δh is the difference in hydraulic head between two points. Δx is the horizontal distance between said points. A_{cross} is the cross-sectional area of the flow. k_{sat} is the saturated hydraulic conductivity, which is dependent on soil type. For the unsaturated zone, k_{sat} is replaced with the unsaturated hydraulic conductivity, which is additionally dependent on matric potential. Matric potential does not linearly increase with Volumetric Water Content (VMC) leading to the definition of soil type specific Soil Water retention curves (e.g van Genuchten, 1980).

A robust numerical method for solving (ground) water flow both in the vertical and horizontal domain is the Richards equation (Richards, 1931). Using this is computationally very intensive, which has led to the development of simplifications. One such is TOPMODEL (Beven & Kirkby, 1979). It is a simplification, that does not target to quantify local water fluxes (Ambroise et al., 1996), but aims to find a spatially explicit regional prediction of the groundwater table from topographic attributes (Beven, 1997). It does this by assuming a topographic index, composed of contributing area and slope angle and is predictive of relative wetness. The available water from infiltrated rainfall is scaled according to this topographic index, to compute an absolute water table. Despite the simplifications, TOPMODEL serves its purpose for many applications (Beven et al., 2020; Bouilloud et al., 2010). The key assumption in TOPMODEL is that of equilibrium runoff (i.e. steady-state runoff) parallel to the slope. Equilibrium runoff is very rare in natural watersheds (Dingman, 2015; Kutílek & Nielsen, 1994). The same simplification is applied in TOPOG (Montgomery & Dietrich, 1994) that computes the spatially explicit groundwater table directly from the topographic index, rainfall intensity and transmissivity. Another simplification assuming no temporal variability (Ponce & Hawkins, 1996) is the Curve Number (CN) method (Division, 1986), where the water table is derived from topographic and land use attributes.

Overcoming the steady-state simplification, but maintaining the practicability of models like TOPMODEL remains a challenge to this day (Buytaert et al., 2008). Many attempts have been made though (Ducharne, 2009). An intuitive approach is to consider TOPMODEL as the baseflow and add linear resevoir outflow (Gascoin et al., 2009) or artificial wetting in the root zone (Koster et al., 2000). Other improvements are allowing multiple flow directions (Wolock & McCabe, 1995), calibrating the topographic index (Lamb et al., 1997), allowing different transmissivity profiles (Ambroise et al., 1996), flux propagation by a wave equation (Beven & Freer, 2001) or time-dependent contributing area (Blazkova et al., 2002). Others point out that, despite its simplifications, TOPMODEL performs surprisingly well (Takeuchi et al., 2008; Yang et al., 2000), even in forested environments (Moore & Thompson, 1996). This could be due to the extent of topographic control in groundwater flux (Ducharne et al., 2000). It could also be that another factor significantly influences the groundwater table that neither TOPMODEL, nor any of its improvements, account for. A good candidate could be rainfall heterogeneity (Sivapalan et al.,

1997; Tsai, 2008).

2.3.1 Preferential flow

One common aspect in the complexity of both vertical and lateral water fluxes is heterogeneity in soil and groundwater transmissivity (Mooney & Morris, 2008; Wiekenkamp et al., 2016). This is observed in virtually all soil types (Koestel & Jorda, 2014; Mooney & Morris, 2008) and is especially profound in forested hillslopes with mature trees (Bodner et al., 2014; Hu et al., 2020; Sidle et al., 2001). This heterogeneity is referred to as preferential flow and consists of distinct processes such as fingered flow, funnel flow (flow blockage) and macropore flow (Lin et al., 2005). Macropore flow occurs due to small pores having a higher suction force than larger pores leading to them storing water with bypass flow occurring in interconnected larger pores, referred to as macropores (Beven & Germann, 2013). Interconnected vertical and horizontal macropores are created by tree roots, erosion, bedrock fractures, organic enrichment and animal burrows (Sidle et al., 2001). This theoretical background is the basis of the dual porosity, also referred to as two water worlds, modelling approach (Gerke & van Genuchten, 1993; Rinderer & Seibert, 2012; Shao et al., 2015) with the larger pores participating in throughflow and the smaller pores storing immovable water (McDonnell, 2014) or allowing limited mixing (Sternagel et al., 2019). There is still no universal definition of macropores (Beven & Germann, 1982) and therefore no unambiguous approach incorporating macropore flow in hydrological approaches, despite its importance on hillslope and catchment scale (Beven & Germann, 2013). This could be related to the complexity of preferential flow paths as shown in tracer experiments (Flury et al., 1994; van Schaik, 2009). In the vertical domain, preferential flow increases infiltration rates and subsequently decreases overland flow (Weiler & Naef, 2003). Preferential flow can significantly increase the reaction time of the water table on hillslope scale to a rainfall event (Askarinejad et al., 2012; Germann & Beven, 1981; Torres et al., 1998). Especially in forests and under intense rainfall, macropore infiltration and lateral flux regulates the water table, with vertical matrix infiltration playing a very limited role (Amatya, 2016). When macropores are numerous and large, macropore flow velocity can be in the same order of magnitude as overland flow (Beven & Germann, 1982; Gao et al., 2018). Throughflow in macropores with the mobilization old water by wave-like effects, confirmed to occur by isotope analysis (Weiler & McDonnell, 2007), increases reaction time even further (Beven & Germann, 1982; Torres et al., 1998; Weiler & McDonnell, 2007). This has led to the choice for wave equations to model lateral flux propagation in certain approaches (e.g. Beven & Freer, 2001; Germann & Beven, 1985).

2.3.2 Runoff coefficient

Discharge can be separated in a baseflow component of a semi-steady state deeper groundwater flux and a quickflow component (Amatya, 2016; Edwards et al., 2015). The quickflow component is highly variable (Post & Jakeman, 1996) and complex in its dependence on rainfall and catchment characteristics (Beven, 2000) such as potential for preferential flow. This complexity can be conceptualized into a runoff coefficient, a fraction between 0 and 1, correcting discharge (Baiamonte, 2020). One of the first inclusions of a runoff coefficient to estimate discharge, is in the rational method (Mulvaney, 1851) shown below:

$$Q = A_{cat} \cdot I \cdot \Psi \tag{2.6}$$

In this function Q is the quickflow. It is a function of the catchment area (A_{cat}), the rainfall intensity (I) and the runoff coefficient (Ψ). A correct estimation of the quickflow helps in prediction of flood intensity and the effect of mitigation measures. In these cases, the relative contribution of surface and sub-surface flow is poorly understood, as the runoff coefficient does not make this

distinction (Naef et al., 1994; Scherrer, 1996). From local to catchment scale, the sub-surface contribution is considered significant (Ahuja & El-Swaify, 1979; Markart et al., 2015). In the spatial domain, land use in the contributing area is arguably the most important predictor of the runoff coefficient (Markart et al., 2006; Markart et al., 2017; Scherrer, 1996; Uhlenbrook & Leibundgut, 2002; Zhang et al., 2013). This land use predictability is recognized and incorporated in many rainfall-runoff schemes such as ZEMOKOST (Markart et al., 2015), the curve number method (Division, 1986) and the HBV model (Bergström, 1976; Seibert, 1996). Considering the temporal domain, the runoff coefficient generally increases the longer a rainfall event takes (Antonetti, 2017; Antonetti et al., 2017). This is due to the cumulative precipitation filling up available storage and delayed runoff reaching the outlet at which the runoff coefficient is examined. This is supported by Naef et al. (1994), who found that estimations from travel time alone and not including storage, overestimate discharge.

2.4 Vegetation influence

Of all vegetation types, trees have by far the most significant influence on landslides (Arnone et al., 2016; Greenway, 1987). This influence can be subdivided into hydrological and mechanical mechanisms (Greenway, 1987). The hydrological mechanisms consist of increased infiltration, evapotranspiration, interception and an increase in preferential flow paths (Stokes et al., 2014). These mechanisms can decrease landslide initiation by preventing soils from reaching critical saturation level (Masi et al., 2021). Mechanical mechanisms of vegetation influence are: root reinforcement (section 2.4.2), surcharge, buttressing (roots, stems, branches braiding in each other), deep anchoring, bedrock fracturing, particle binding and increasing wind shear (Greenway, 1987; Masi et al., 2021). These mechanical mechanisms affect the forces along a hillslope directly (Giadrossich et al., 2017, e.g). Deep-seated landslides are not significantly affected by the mechanical effects of trees (Van Beek et al., 2007). The hydrological regulatory effects can be relevant though (Moos, 2018). Root reinforcement specifically, is an important mechanism by which shallow landslides as large as 1000 m^2 can be stabilized (Schwarz, Preti, et al., 2010). The degree of protection is dependent on the slope angle, soil cohesion, friction angle (Schwarz et al., 2016) and soil depth (Steinacher et al., 2009).

2.4.1 Tree co-benefits

Trees not only serve as protection against shallow landslides, but against other natural hazards as well. Rockfall is reduced by 10% to 90% as a result of forests (Moos, 2018). Bank erosion can be effectively reduced by root reinforcement from riverbank trees (Docker & Hubble, 2008; Gasser et al., 2019). Trees in the proximity of rivers can however, be mobilized as large wood and increase flooding and other hazards downstream (Gasser et al., 2019). Co-benefits, other than natural hazard prevention, are found as well. For example, the use of acacia (Power et al., 2003) and kanuka (Mackay-Smith et al., 2021) trees in silovpastoral systems, increases nitrogen concentration in the soil, benefiting pasture productivity. Other co-benefits are: shade for cattle, carbon sequestering, timber production, as well as cultural and recreational value (Mackay-Smith et al., 2021).

2.4.2 Root reinforcement

Roots of any type of vegetation offer a resistance when stretched, i.e. stress is applied. This resistance is known as root reinforcement. Root reinforcement in the context of slope stability is the force resisting movement of a soil block stemming from the stretching of roots. This root reinforcement can be subdivided in lateral and basal root reinforcement. Basal root reinforcement acts along the shear plane of a shallow landslide and lateral root reinforcement acts on the

sides of a shallow landslide (Cohen & Schwarz, 2017b). The ability of a root to resist stretching is dependent on multiple factors. Root tensile strength [Pa] increases exponentially with decreasing root diameter (Cohen & Schwarz, 2017b). Overall however, due to their larger surface area, coarse roots are more significant for root reinforcement than small roots (Cohen & Schwarz, 2017b). Root tensile strength is also highly dependent on tree species (Watson & Marden, 2004), by means of variability in root stiffness (Fan et al., 2021).

2.4.2.1 Root reinforcement measurements

There are several methods for measuring the maximum tensile strength of single roots. Direct measurements can be obtained in a laboratory environment, by mechanically stretching the root till breakage. Several weaknesses of the laboratory environment have been pointed out, related to the fact that it is not a realistic representation of actual root reaction in the soil to movement-induced stretch. In nature, roots can i) be dead as opposed to alive, where the drying of the root influences tensile strength (Vergani et al., 2016). ii) In-situ interact with the soil matrix, which adds friction resistance and soil bonding (Fan et al., 2021; Watson & Marden, 2004). iii) Be pulled out of the soil rather than break (Watson & Marden, 2004). To combat these shortcomings, in-situ root tensile strength measurement techniques were developed. A drawback is that when roots are close together, mechanical interactions with neighbouring roots affect measurement quality (Giadrossich et al., 2013). Another drawback is the fact that soil conditions at time of the pullout test affect the measurement. Roots under drier conditions generally give more resistance than under wet conditions (Fan et al., 2021).

Upscaling of these measurements requires knowledge on root architecture. For this the Root Area Ratio (RAR) is an often used method. RAR is the fraction of root surface to total surface area looking perpendicularly at a vertical slice of soil. This method does not distinguish between thin and thick roots (Docker & Hubble, 2008). For poplar trees, RAR decreases exponentially with depth, with few large sinker roots growing deep (Douglas et al., 2010; McIvor et al., 2009). Excavation of a root system, counting single roots per depth class and measuring root diameter is the most complete method, to analyze root architecture (e.g. Giadrossich et al., 2020; Ngo et al., 2023). Root development through time has conflicting results that are likely highly dependent on site conditions (Vine, 1980) and planting technique (Douglas et al., 2016). McIvor et al. (2007) found structural root growth in Veronese poplars to be negligible for the first 5 years after planting, but Phillips et al. (2014) found in a poplar and willow trial that root length grows to 2.5-5.5 m within a year. McIvor et al. (2009) showed that root mass increases exponentially with tree DBH. These measurement could lay the basis for calibrated allometric relationships.

2.4.2.2 Root reinforcement modelling

A challenge in root reinforcement modelling is the scaling of measured tensile strength to estimate root reinforcement over a larger scale, to be applied in slope stability models. A first attempt at this has been made by Wu et al. (1979), who developed the Wu model. It assumes root force is dependent on root density and root diameter. This is upscaled to an additional soil cohesion and, by including landslide dimensions, added to the shear strength (F_{res} in equation 2.1). Assuming the breaking of roots all at once overestimates root reinforcement (Schwarz, Preti, et al., 2010). Therefore, as a reaction to the 'all breakage at once' method of the Wu Model, the Fibre Bundle Model (FBM) was developed (Pollen & Simon, 2005). This model includes progressive failure of roots under increasing tensile strength, as a function of root diameter. A further development on this method is the Root Bundle Model weibull (RBWw) (Schwarz et al., 2013). It approximates the progressive tensile stress and breakage of roots in a moving soil block, by a

weibull function. All roots are assumed to break as it is the most frequent reaction to stress, especially for larger roots (Cohen & Schwarz, 2017b). This function is calibrated to measurements on root architecture and single root tensile strength. It performs well under natural conditions with roots of various diameter (Schwarz et al., 2013) and can be applied conveniently in slope stability models. A comparison of the root reinforcement as function of displacement from the RBMw vs. the Wu model is given in Figure 2.2 below.

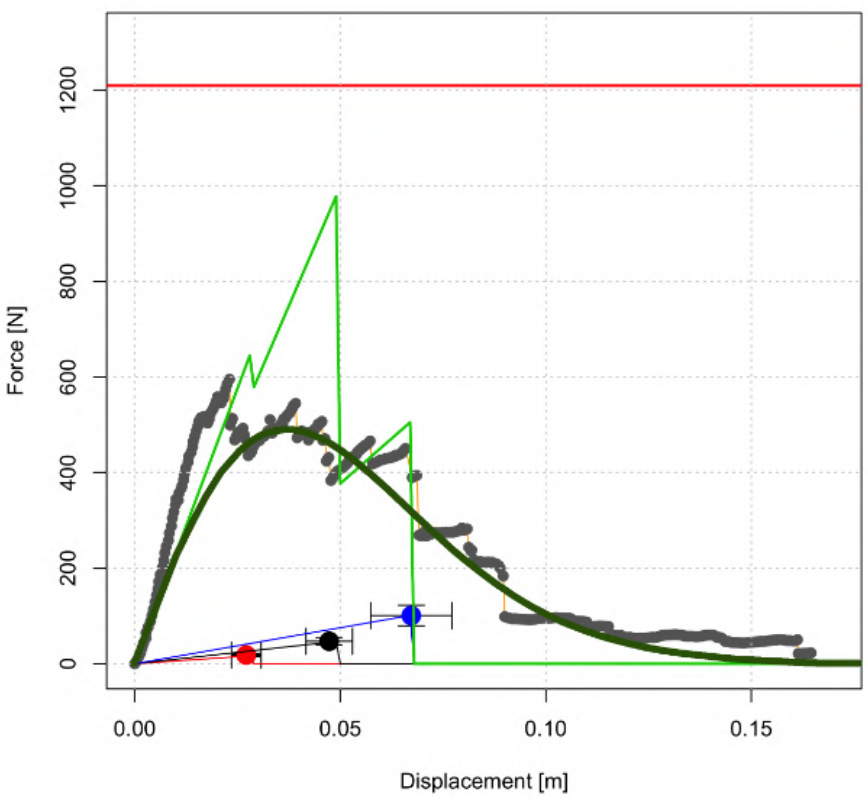

FIGURE 2.2: Example of the application of RBMw with root tensile force (root reinforcement) as a function of soil block displacement. In grey is the measured tensile force of a root bundle with roots of variable diameter. In light and dark green is the RBMw fit with different exponents of the weibull distribution. The red, black and blue dots are single root pull-out tests. The red line represents the Wu model, where tensile force is not a function of displacement. Figure adopted from Schwarz et al. (2013).

2.5 State of the art

2.5.1 Slope stability models with vegetation effects

Capturing the influence of spatial and temporal variability of vegetation in shallow landslide modelling remains challenging, especially on the regional scale where only few attempts have been made (Masi et al., 2021). One example of this is tRIBS-VEGGIE. This was designed as a hydrological model with a dynamic vegetation module (Ivanov et al., 2008; Lepore et al., 2013). Arnone et al. (2016) coupled this model with the RBM (Schwarz, Lehmann, et al., 2010) approach to basal root reinforcement and a slope stability computation. RBM parametrization is based on laboratory tests on tensile strength. Land use is classified in distinct vegetation groups, where trees are assumed homogeneous. The authors underscore the difference between species

in protective effect (Arnone et al., 2016). Shortcomings are neglecting lateral root reinforcement, laboratory-based tensile strength estimates and assumptions on root topology.

Scheidl et al. (2022) coupled ZEMOKOST (section 2.3.2) and a slope stability model with the iLand model that simulates forest stands and disturbances. Interestingly their application found no negative effect of disturbances and considers them a net positive as they accelerate landscape adaptability. Schmaltz et al. (2019) developed the LAIM model with raster-based temporal development of forest cover. It contains four forest classes and forest development is expressed by a change in Leaf Area Index (LAI). Vegetation influence on slope stability is linked to the LAI. Slope stability under various developmental stages was assessed by Coupling LAIM with STARWARS as hydrological and PROBSTAB as slope stability module (Beek, 2002). A probabilistic approach to shallow landslide susceptibility with vegetation inclusion is PRIMULA (Cislaghi et al., 2017; Cislaghi et al., 2018). It includes both lateral and basal root reinforcement on the forest stand scale, with averaged DBH and an average distance between trees.

Including single tree distribution, development and heterogeneity explicitly in shallow landslide susceptibility models is a recent development. This could be related to challenges in upscaling tree-scale measurements or assumptions to local, regional or catchment scale (Williams & Scott, 2009). Among the first to explicitly model single trees are Schmidt et al. (2001) and Roering et al. (2003), who identified an effective root reinforcement dependent on distance from trees in Oregon forests with the Wu root reinforcement model. This approach confirmed the observation that shallow landslide occur disproportionately in forest gaps. The model of Huang et al. (2021) includes root reinforcement from single tree with four distinct root types. Lateral root reinforcement is related to RAR empirically. The hydrological module consists of a lateral flux dominated system computed with an analytical solution to the Richards equation. The soil layer is split in a root and non-root layer with a distinctive hydrological conductivity. Schmaltz and Mergili (2018) developed a single-tree based stability approach, using a paraboloid root system architecture approximation. Root reinforcement influence on shallow landslide initiation is computed on a raster cell basis. On the hillslope scale, SOSlope is the first model to include both single tree root tension and compression forces, for the initiation and progression of shallow landslides (Cohen & Schwarz, 2017a).

A statistical approach that goes beyond forest/non-forest classification is that by Schmaltz et al. (2017), which uses forest classes as predictions in a statistical analysis of shallow landslide occurrence. Spiekermann et al. (2021) went down to the single-tree level in a statistical approach specifically for the application in New Zealand silvopastoral lands.

2.5.2 Data and extrapolation techniques

The application of single-tree based vegetation effects with existing trees, requires reliable data on the location of single-trees. Additionaly tree dimension (height and/or DBH) and species classification can be desired. Canopy height model (CHM) based single tree detection is an effective technique with the added benefit of having a measure for tree height (e.g. Menk et al., 2017). A CHM is generated by subtracting a Digital Terrain Model (DTM) from a Digital Surface Model (DSM). LiDAR (Light Detection And Ranging of Laser Imaging Detection And Ranging) can help to construct a detailed CHM or single-tree detection can occur directly from LiDAR derived point clouds (Korpela et al., 2007). Inaccuracies occur mostly from small trees being obscured by large trees (Korpela, 2004). Single tree detection and species classification is possible by combining Sentinel 2 optical imagery and Aerial Laser Scanning (airborne LiDAR) (Plakman et al., 2020). Conifer tree detection is highly accurate, deciduous trees are more challenging (Plakman et al., 2020). Species classification, in general, is still a challenging topic (Plakman et

al., 2020). For the parts of trees below the surface, Ground-penetrating RADAR (GPR) is a novel technique. It can non-intrusively identify large roots (Barton & Montagu, 2004) and additionally preferential flow paths (Guo et al., 2014).

In areas with quick runoff, temporal and spatial variabiliy of a rainfall event is an essential input for the accurate lateral flux computation (Cristiano et al., 2019; Keijsers et al., 2011). This is why the availability of high spatial and temporal resolution RADAR data improves shallow landslide susceptibility modelling (Crosta & Frattini, 2003). When no data is available but high spatial and temporal variability is desired, synthetic rainfall generators can be a solution (Benoit & Mariethoz, 2017).

2.5.3 Process understanding and uncertainty

Advancement in knowledge of processes and uncertainty sources has not always resulted in better models (Buytaert et al., 2008). Certain sources of uncertainty are rarely addressed, even in state of the art shallow landslide susceptibility models. This may be a conscious choice (see chapter 2.2) as exact predictions on shallow landslide timing, location and subsequent ideal mitigation procedure are considered unrealistic. This is too strongly dependent on localized heterogeneity (von Ruette et al., 2013). In addition to the often cited "local inhomogeneities and heterogeneity", possible sources of uncertainty in most, if not all, shallow landslide models are listed below.

- Drainage basins do not necessarily constitute isolated hydrological units (Hendriks, 2010). Infiltration in tilted high-permeability layers or faults and subsequent exfiltration can effectively transport water from the surface of one drainage basin to the other.
- Local pore water pressure can be influenced by leakage and artesian flow through fractured bedrock layers (Montgomery et al., 2002), which most models assume impermeable. The significance of this effect, however, is not supported in other studies with other study areas (e.g D'Amato Avanzi et al., 2004; McGuire et al., 2016).
- The inclusion of negative effects of vegetation, such as increased infiltration (Greenway, 1987) on shallow landslide triggering is rarely included (de Jesús Arce-Mojica et al., 2019).
- Depth to regolith, i.e. soil depth, is still poorly understood, though highly important in the modelling slope stability (Phillips et al., 2021). This is currently most often based on extrapolations of in-situ measurements, but could benefit from taking landscape characteristics and development into account (McDonnell et al., 2007).

2.6 Summary

Shallow landslide disposition is controlled by topography and shallow landslide initiation (often) is a hydrological process. The degree of simplification in shallow landslide susceptibility models, should be related to the question the models aims to answer. Shallow landslide susceptibility models are subdivided in physically-based, conceptual and statistical models. These models, in turn, can either adopt a deterministic or a probabilistic approach. Calibration improves the performance of most models and validation is essential to interpret model results. Shallow landslide occurrence is usually assessed with the Safety factor in the limit equilibrium approach, where all forces acting along a potential failure plane are included. In this approach, landslide initiation is related to an increase in pore water pressure. Pore water pressure in turn relates to the local groundwater table. Simplifications to estimate the groundwater table from topographic metrics are the TOPMODEL and TOPOG approach. The presence of macropores,

which in turn is influenced by vegetation, is influential in the local groundwater table and subsequent shallow landslide initiation. These macropores, among other effects, can be included in hydrological approaches using runoff coefficient curves.

The most effective nature-based shallow landslide mitigation measure is the planting and management of tree stands. The strongest stabilizing effect of trees is through the tensile strength of roots, i.e. root reinforcement, both on the horizontal and vertical plane of a moving soil block. The RBMw model is the most detailed model for the inclusion of root reinforcement, as it includes a propagating failure mechanism. This model is calibrated by field measurements in which root diameter, distance from tree and tree species is important. Current models, especially those focussed on nature-based mitigation measures, see the added benefit of including vegetation effects on a forest stand or single tree basis. Currently the most advanced models in this regard are tRIBS-VEGGIE, PRIMULA, LAIM and SOSlope. The recent development of remote sensing techniques, most importantly LiDAR, has facilitated this. Challenges remain, not only due to the detailed inclusion of vegetation effects, but also in terms of soil depth and groundwater table estimation at a regional scale.

3 Study areas

3.1 Description

In this chapter, the study areas of this thesis to which SlideforMAP has been applied, are presented in a uniform way. These are, three study areas in Switzerland and four in New Zealand. Provenance of the input data is given in additionally. More details to the study areas are given in their respective chapters. Study areas in Switzerland were selected on the availability of detailed spatial data and overlap with a complete and accessible shallow landslide inventory by Rickli and Graf (2009). Study areas in New Zealand were adopted in context of the STEC project. The study areas were selected for their availability of LiDAR data, previous research at the sites and high shallow landslide occurrence (Spiekermann et al., 2021). On average, the geographical locations of the study area have an energy-limited water balance (Dingman, 2015), indicating a permanent groundwater system. An overview of the study area locations is given in below.

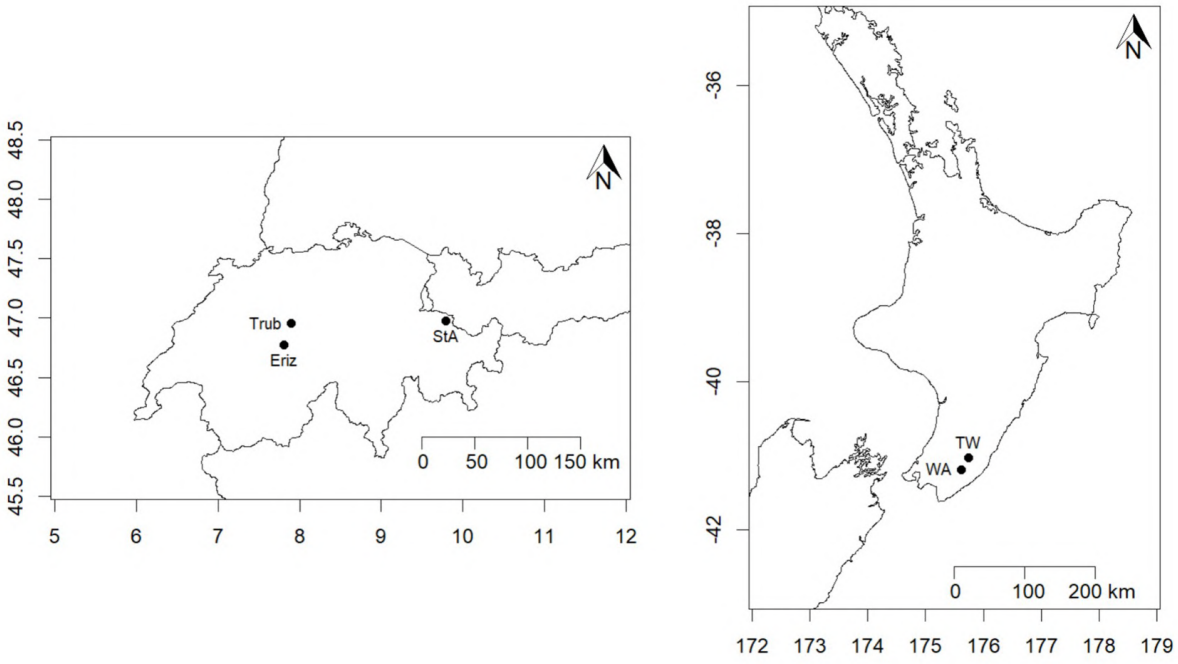

FIGURE 3.1: Location of the study areas in Switzerland and on New Zealand's north island. The New Zealand study areas overlap and are presented as two rather than four for clarity. TW is an abbreviation for Te Whanga. WA is an abbreviation for Waikoukou. All coordinates are in WGS84.

A table with a overview of the study areas, with names and chapters as used in this thesis, is given in Table 3.1 below.

TABLE 3.1: General overview of all the study areas as used in this thesis. The chapter, in which the study area is applied, is indicated.

Name	Short name	Country	Size (km^2)	Chapter
Eriz	Eriz	Switzerland	7.48	4
Trub	Trub	Switzerland	1.00	4
St. Antönien	StA	Switzerland	0.55	4
Te Whanga portion	TW portion	New Zealand	3.51	5
Waikoukou portion	WA portion	New Zealand	1.43	5
Te Whanga farm	TW farm	New Zealand	17.21	6
Waikoukou farm	WA farm	New Zealand	4.62	6

The study areas in New Zealand overlap, with a smaller portion of the Te Whanga and Waikoukou farm presented in chapter 5. This was decided because the calibration procedure, which is computationally intensive, requires a smaller study area. Orthophotos, with shallow landslides that have been recorded in the study areas, are presented in Figure 3.2 and 3.3 . Background to the shallow landslide inventories is given in section 3.1.5.

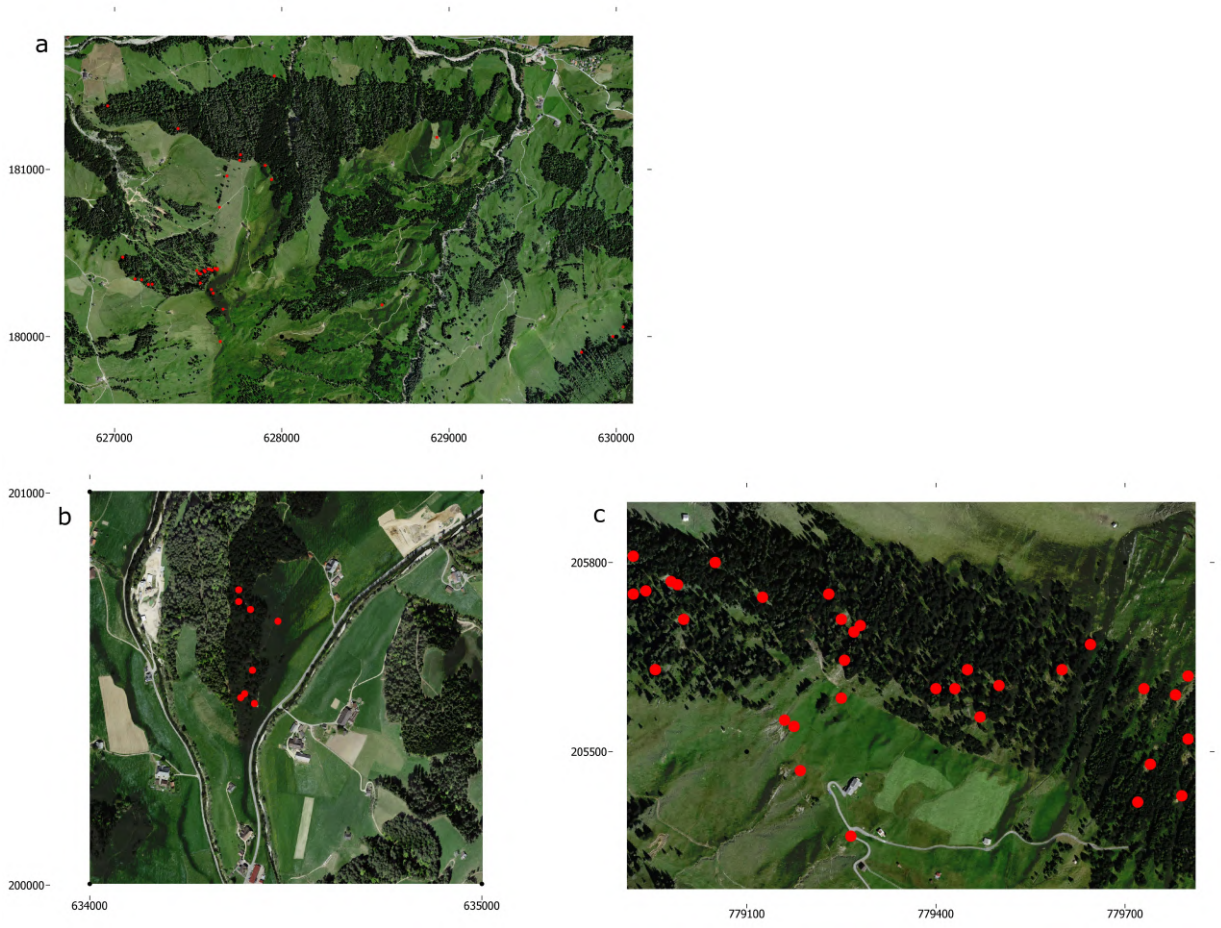

FIGURE 3.2: Orthographic overview of Swiss study areas as used in this Thesis. a) Eriz, b) Trub, c) StA. Coordinate system for study areas in Switzerland is "Swiss CH1903/LV03" (EPSG:21781). Inventoried shallow landslides are indicated as red dots, scaled to average landslide size.

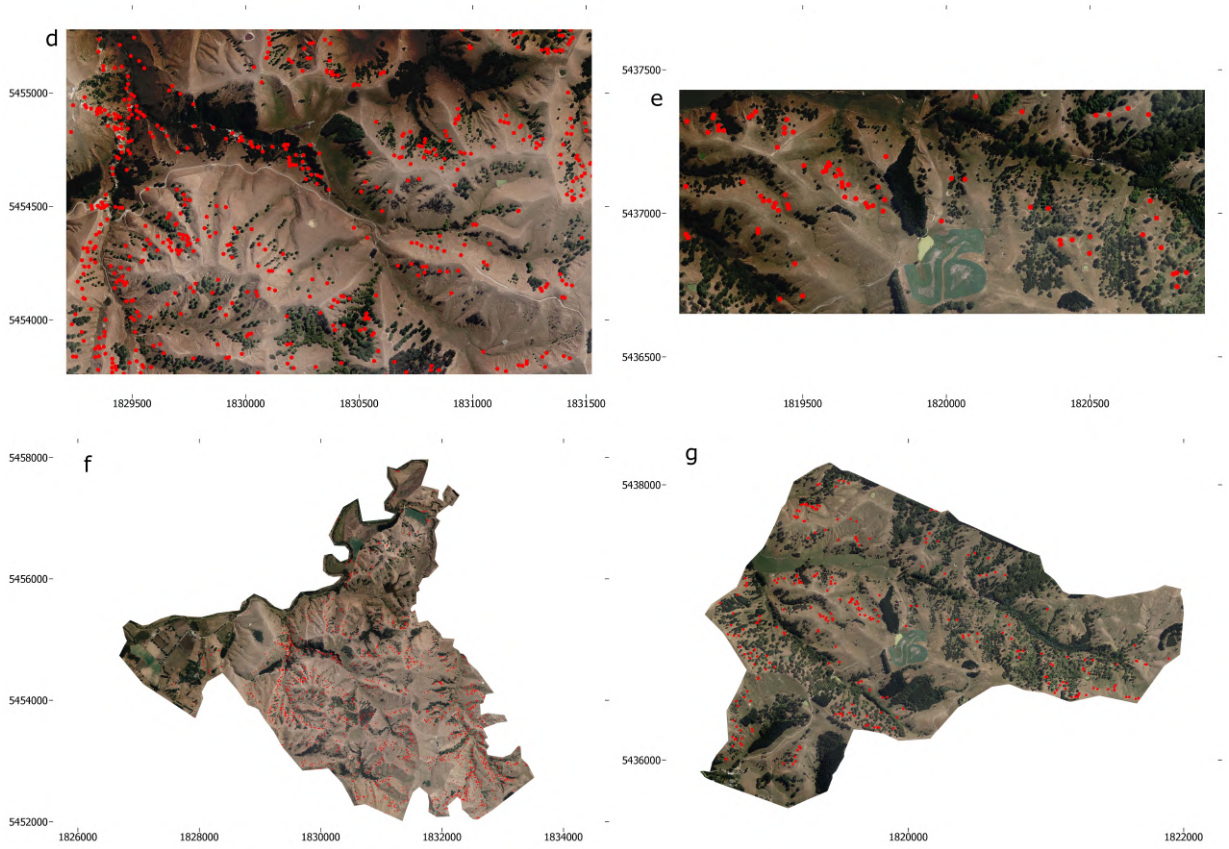

FIGURE 3.3: Orthographic overview of New Zealand study areas as used in this Thesis. d) TW portion, e) WA portion, f) TW farm, g) WA farm. Coordinate system for study areas in New Zealand is "NZGD2000 / New Zealand Transverse Mercator 2000" (EPSG:2193). Inventoried shallow landslides are indicated as red dots, scaled to average landslide size.

3.1.1 Elevation data

A DTM for the Swiss study areas is freely available at 2 m resolution (Swisstopo, 2018). For the New Zealand study areas, a 1 m resolution LiDAR derived DTM is used (Spiekermann et al., 2021). This raster was resampled (bi-linear technique) to a 2 m resolution. The decision to apply 2 m resolution DEM (and DEM derivatives) for both study areas, despite higher resolution availability was a combination of computational reasons, comparability and the indication that increasing DTM resolution does not necessarily improve model performance (chapter 4).

3.1.2 Precipitation data

Gridded hourly precipitation totals for New Zealand are available through the MOANA dataset (Moana Project Team, 2021). This interpolated grid is based on RADAR data. It has a spatial resolution of 4 km and covers the years of 2000 to 2020. No gridded precipitation data is available for our sites in Switzerland. Weather station data is available, but for sites outside of the study areas with questionable representativeness. It was chosen, not to use this data.

3.1.3 Vegetation data

A DTM and DSM of 0.5 m resolution are available for the Swiss study areas. The DTM and the DSM were both acquired from the SwissAlti3D database (Swisstopo, 2018), where aerial laser-scanning is applied. the absolute difference between these raster produces a CHM. Single trees are detected from the CHM using using a local maxima detection method as described in the work of Eysn et al. (2015) and Menk et al. (2017). Since the results of this detection method are influenced by the resolution and smoothness of the input data (Eysn et al., 2015), a pre-processing methodology is applied. This methodology is described in chapter 4, section 4.3.2. No species classification is performed.

In New Zealand, trees for the study areas have been mapped using available LiDAR data from 2013/14 in the Wellington region (Spiekermann et al., 2021). Processing has been performed using the PyCrown model (Zörner et al., 2018) and species classification by a Support Vector Machine (SVM) as described in Spiekermann et al. (2021). The data includes the X and Y coordinate of the tree, the tree crown height and the predicted species (Either Eucalyptus, Kanuka, Poplar/Willow, Pine or undefined).

Characteristics of the vegetation for the study areas, based on the data and methods as described above, are given in Figure 3.2. Tree height is converted to DBH using the relationship: $DBH_{\text{tree}} = (H_{\text{tree}})^{1.25} \cdot 0.01$, where DBH_{tree} [m] is the Diameter at Breast Height of a given tree and H_{tree} [m] its height. This equation and its background, is presented in chapter 4 (equation 4.16). A novel approach to single-tree detection using only orthophotos is presented and applied in chapter 6. However, for comparison and consistency, the results presented here are from the original methods as described above.

TABLE 3.2: Study area number of trees, average tree size and tree density. * These are different from the numbers as presented in chapter 4, since it measured stem density in the forested parts of the study area, not an average over the entire study area. ** These numbers are different from the total number as presented in chapter 6, due to not including a 1 km buffer around the farm here.

Name	**Number of trees**	**Average tree density** trees/ha	**Average DBH** m
Eriz	38923	52 *	0.51
Trub	7267	73 *	0.55
StA	1796	33 *	0.31
TW portion	3747	11	0.21
WA portion	2304	16	0.34
TW farm	15394 **	9	0.22
WA farm	10725 **	23	0.32

The density of trees is higher in our study areas in Switzerland, as compared to New Zealand. This reflects a difference in land use, which can be well observed in Figure 3.2 and 3.3. In the Swiss study areas, a significant portion of the area is forest covered, whereas the New Zealand study areas are dominated by a silvopastoral system with space planted trees. Tree size, expressed in DBH, is generally higher in the Swiss trees, indicating a mature well managed forest. Comparing the average DBH and tree density for the New Zealand study areas gives an indication that the trees in the Waikoukou farm are larger and denser planted. This corresponds to the earlier and more far reaching adoption of the silvopastoral system in the Waikoukou farm as expressed during personal communication with the farm manager.

3.1.4 Soil data

Soil data is directly used in chapter 6. In this chapter, soil thickness and soil texture class are derived from S-map soil mapping for New Zealand (Manaaki Whenua - Landcare Research, 2019). These are polygons, based on land use classification and field validation. For Switzerland no soil data has been used, as the relating parameters have been calibrated.

3.1.5 Shallow landslide inventory

An inventory with a total of 668 shallow landslides that occurred between 1997 and 2012 in Switzerland, has been compiled by the Swiss Federal Office for the Environment (Rickli & Graf, 2009). The inventory contains a total of 203 fields, with various data, resulting from extensive field observations. The majority of the slides were triggered by a major precipitation event in August 2005. For the New Zealand areas, a manually corrected automated landslide scar identification algorithm is used (Spiekermann et al., 2021). The total number of landslides in the dataset is 43069. This inventory is based on aerial imagery from 2010 and the majority of the slides were triggered by precipitation events in 2005 and 2006. From both inventories, the X-coordinate, Y-coordinate and scar surface area are taken into account. Additionaly, the estimated soil thickness from the Swiss inventory is used to correlate soil thickness to slope angle (see chapter 4, Appendix). An overview of the inventoried number of landslides in the study area and their properties is given in Table 3.3 below.

TABLE 3.3: Study area inventory characteristics. The triggered area is given as percentage of the total study area. *These numbers are different from the total number as presented in chapter 6, due to not including a 1 km buffer around the farm here.

Name	**Number slides**	**Mean landslide size** m^2	**Scarred area** % of total
Eriz	37	126.0	0.06
Trub	8	310.4	0.25
StA	33	240.9	1.44
TW portion	500	45.0	0.97
WA portion	78	68.0	0.42
TW farm	1663 *	69.3	0.67
WA farm	250 *	73.4	0.40

The Swiss areas have a higher average shallow landslide size compared to the ones in New Zealand. The difference could be rooted in the fact that the Swiss inventory is manually assembled by experts, whereas in New Zealand an algorithm and orthophotos are used. It could also be related to differences in landscape heterogeneity and soil parameters. The proportion of the study areas triggered varies slightly, with New Zealand generally having a higher proportion of the landscape scarred. The notable exception is the St. Antönien study area, which shows the highest scar density of all the study areas.

4 Introducing SlideforMAP

Full title:

Introducing SlideforMAP; a probabilistic finite slope approach for modelling shallow landslide probability in forested situations

Feiko Bernard van Zadelhoff[1], Adel Albaba[1], Denis Cohen[2], Chris Phillips[3], Bettina Schaefli[4], Luuk Dorren[1,5], Massimiliano Schwarz[1,5]

Natural Hazards and Earth Science Systems (Copernicus journal)
Volume 22, issue 8, 2611–2635, DOI:10.5194/nhess-22-2611-2022

Submitted: 19 May 2021, revised: 13 June 2022, accepted: 26 June 2022, published: 15 August 2022

This publication aims to be a foundational paper for the thesis. It introduces SlideforMAP as a probabilistic physically-based approach, to assess shallow landslide probability at a regional scale. The SlideforMAP methodology is applied and its performance measured on steep forested areas in Switzerland. The improvement of computing vegetation influences on a single tree scale as compared to uniform assumptions is quantified.

[1] Bern University of Applied Sciences - HAFL, Länggasse 85, CH-3052 Zollikofen, Switzerland
[2] COSCI Ltd.
[3] Manaaki Whenua - Landcare Research, Lincoln, New Zealand
[4] Institute of Geography (GIUB) & Oeschger Centre for Climate Change Research (OCCR), University of Bern, 3012 Bern, Switzerland
[5] Int. ecorisQ Association, P.O. Box 2348, 1211 Geneva 2, Switzerland

Abstract

Shallow landslides pose a risk to infrastructure and residential areas. Therefore, we developed SlideforMAP, a probabilistic model that allows for a regional assessment of shallow landslide probability while considering the effect of different scenarios of forest cover, forest management and rainfall intensity. SlideforMAP uses a probabilistic approach by distributing hypothetical landslides to uniformly randomized coordinates in a 2D space. The surface areas for these hypothetical landslides are derived from a distribution function calibrated on observed events. For each generated landslide, SlideforMAP calculates a factor of safety using the limit equilibrium approach. Relevant soil parameters are assigned to the generated landslides from log-normal distributions based on mean and standard deviation values representative for the study area. The computation of the degree of soil saturation is implemented using a stationary flow approach and the topographic wetness index. The root reinforcement is computed by root proximity and root strength derived from single tree detection data. The ratio of unstable landslides to the number of generated landslides, per raster cell, is calculated and used as an index for landslide probability. We performed a calibration of SlideforMAP for three test areas in Switzerland with a reliable landslide inventory, by randomly generating 1000 combinations of model parameters and then maximising the Area Under the Curve (AUC) of the Receiver Operation Curve. The test areas are located in mountainous areas ranging from 0.5 – 7.5 km^2 with mean slope gradients from 18 - 28°. The density of inventoried historical landslides varies from 5 – 59 slides/km^2. AUC values between 0.64 and 0.93 with the implementation of single-tree detection indicated a good model performance. A qualitative sensitivity analysis indicated that the most relevant parameters for accurate modeling of shallow landslide probability are the soil thickness, soil cohesion and the precipitation intensity/transmissivity ratio. Furthermore, we show that the inclusion of single tree detection improves overall model performance compared to assumptions of uniform vegetation. In conclusion, our study shows that the approach used in SlideforMAP can reproduce observed shallow landslide occurrence at a catchment scale.

keywords: mountain forest, shallow landslide probability, probabilistic modelling, single tree detection, root reinforcement

4.1 Introduction

Landslides pose serious threats to inhabited areas world-wide. They are the cause of 17% of the fatalities due to natural hazards in the period of 1994–2013 (Kjekstad & Highland, 2009b). Average annual monetary losses over the period of 2010–2019 are approximately 25 billion US dollars (Munich RE, 2018). In addition, Swiss Re Institute (2019) notes a significant increase in damages by hydrologically related natural hazards over the past 5 years, including hydrologically-triggered shallow landslides. This has been attributed to increased urbanization in risk-prone areas and to an increase in heavy rainfall events. Furthermore, Swiss Re Institute (2019) notes that the modelling of shallow landslides is underdeveloped compared to the severity of the danger they pose. In mountainous regions, landsliding is a prominent natural hazard. For instance, in the Alpine parts of Switzerland, 74 people have died as a result of landslide events between 1946 and 2015 (Badoux et al., 2016). The annual cost of landslide protective measures alone is approximately 15 million CHF each year (Dorren et al., 2009). No distinction is made between deep-seated and shallow landslides in these numbers. Rain induced shallow landslides are one of the most important and dangerous types of mass movement in mountainous regions (Varnes, 1978). Shallow landslides are defined as translational mass movement with a maximum soil thickness of 2 m and are the main focus in this paper. Fortunately, improvements in hazard assessment have significantly decreased the number of shallow landslide related deaths over

the past decades (Badoux et al., 2016). This general trend is also supported by long-term data (Munich RE, 2018). The fatality decrease is related to better organizational measures regarding hazards, such as warning based evacuations and road closures. Biological measures, such as management of protection forests, also play a role in mitigation of natural hazards. The latter role is especially important for (shallow) landslides, rockfall, snow avalanches and debris flows (Corominas et al., 2014).

Modelling of shallow landslide triggering has been an ongoing process. Shallow landslide probability has been modelled mostly using a deterministic approach (Corominas et al., 2014). The deterministic approach is defined by using average values of risk components and resulting in a univariate result (Corominas et al., 2014). An example of a deterministic approach in this sense is the SHALSTAB model of (Baum et al., 2002b) and SLIP (Montrasio et al., 2011), the latter showing good results in assessing soil saturation in a spatially heterogeneous way. In a comparative research it was noted that the SHALSTAB approach was not representative for the spatial variability of the parameters at a small scale (Cervi et al., 2010). In recent decades, the development of probabilistic models and statistical methods has improved model performance for quantifying landslide probability and the interpretation of their results (Corominas et al., 2014). In statistical methods e.g. Baeza and Corominas, 2001, there is no explicit accounting of physical processes. Probabilistic methods could take physical processes into account and additionally quantify the reliability of the results considering the probability distribution of values of one or more input parameters (Salvatici et al., 2018). The output is a probability rather than a univariate result. A prime example of a probabilistic model in SINMAP (Pack et al., 1998). Generally, these models perform better than deterministic ones (Park et al., 2013; Zhang, Wu, et al., 2018), likely due to natural landslides having a mode of movement significantly controlled by internal inhomogeneities and discontinuities in the soil (Varnes, 1978). These control mechanisms are unpredictable at small-scales, making it hard for deterministic models to identify exact locations of instabilities and adjust the heterogeneous parametrization accordingly. Below we go into more detail on the initiation of shallow landslides.

Initiation of instability is a process that combines mechanical and hydrological processes on different spatial and temporal scales and can thereby be very localized, with successive movement increasing the magnitude of the event (Varnes, 1978). In alpine environments, instabilities are typically triggered by rainfall, leading to soil wetting and ensuing increase of pore pressure, which destabilizes the soil and can then initiate soil movement. An increase in pore pressure can build up in minutes to months following a rainfall event (Bordoni et al., 2015; Lehmann et al., 2013), where rapid pore pressure changes are attributed to macropore flow and slow pore pressure changes to the matrix water flow. The higher the horizontal hydraulic conductivity of the soil, the faster pore pressure changes can develop (Iverson, 2000). The reaction of pore pressure to rainfall is variable and highly dependent on soil type. A key experimental study is the work of Bordoni et al. (2015) in which in-situ measurements were taken on a slope with clayey–sandy silt and clayey–silty sand soils that experienced a shallow landslide. It showed that intense rainfall and a rapid increase of pore pressure were the triggering factors of the landslide. Over the duration of the measurements, comparable saturation degrees have been reached both during prolonged and intense rainfall events. Prolonged rainfall did not result in the pore pressure required to trigger a shallow landslide. Similar behaviour has been observed in an artificially triggered landslide in Switzerland (Askarinejad et al., 2018; Askarinejad et al., 2012; Lehmann et al., 2013). In the first wetting phase (year 2008), homogeneously induced rainfall with a duration of 3 days, an accumulated rainfall of 1700 mm and an intensity of 35 mm/hr, induced a maximum pore water pressure of 2 kPa at 1.2 m soil depth, resulting in no landslide. In the second phase of the experiment (year 2009), the rainfall was heterogeneous, with a maximum intensity of 50 mm/hr in the upper part of the slope that induced an increase of pore water

pressure up to 5 kPa at 1.2 m soil depth, resulting in the triggering of a shallow landslide. The triggering was reached after 15 hours with a cumulative rainfall of 150 mm. In addition, a computational study by Li et al. (2013) showed that at a high rainfall intensity (80 mm/hr), the pore water pressure at a depth of 1 m reached a constant value within 1 hour. For a lower intensity of 20 mm/hr, this took approximately 3 hours. This shows that landslide triggering is related to a fast build up of pore water pressure proportional to rainfall intensity. The work of Wiekenkamp et al. (2016) suggests that preferential flow dominates the runoff in a heterogeneous catchment during extreme precipitation events. Water can move downslope very rapidly through macropores (in experimental conditions) under both saturated and unsaturated conditions (Mosley, 1982). The role of macropores can be important in a closed soil structure or in the presence of a shallow impermeable bedrock, where they control the soil hydrological behavior. Further examples of the influence of macropores on hillslope hydrology in various soil types are presented in the work of Weiler and Naef (2003) and Bodner et al. (2014). Additionally, Torres et al. (1998) demonstrates the strong role of macropore in preferential flow paths for landslide triggering in an artificial rain experiment in a loamy sandy soil. Montgomery et al. (2002) and Montgomery and Dietrich (2004) also underline the importance of macropore flow, but state that the vertical flow governs response time and build up of pore pressure rather than the lateral flow in their study areas.

The mechanical aspect of shallow landslide initiation usually results from local instabilities that could extend indefinitely in a infinite constant slope if the shear resistance is low (Varnes, 1978). In complex topography, however, the passive earth pressure at the bottom of the triggering zone reacts with a resisting force, contributing thereby to landslide stabilisation (Cislaghi et al., 2018; Schwarz et al., 2015). It is important to note here that the passive earth pressure is activated in a later phase of the triggering of a shallow landslide and should not be added to active earth pressure or tensile forces acting along the upper half of the shallow landslide (Cohen & Schwarz, 2017b).

Besides hydrology, slope and soil characteristics, vegetation plays a key role in landslide triggering (Corominas et al., 2014; González-Ollauri & Mickovski, 2014; Greenway, 1987; Salvatici et al., 2018). The role of vegetation can be subdivided in hydrological and mechanical effects. Vegetation influences the effective soil moisture by interception, increased evapotranspiration and increased infiltration (Greenway, 1987; Masi et al., 2021). Over the short timescale with intense rainfall these hydrological effects are negligible, but do play an important role in pre-event disposition of slope instability (Feng et al., 2020). Among the mechanical effects, root reinforcement, mobilized during soil movement, is an essential component (Greenway, 1987; Schwarz, Preti, et al., 2010). It is a leading factor in the failure criterion for many vegetated slopes (Dazio et al., 2018b). In modelling studies, the influence of root reinforcement on slope stability is often quantified as an apparent added cohesion (Borga et al., 2002; Wu et al., 1979). This apparent cohesion in turn can be added in the limit equilibrium computation of a Safety Factor (SF). Using a Monte Carlo approach of this method (Zhu et al., 2017), it was found that the SF can gain up to 37% stability when including vegetation root reinforcement. In another study in New Zealand, trees showed an effect on soil stability up to 11 meter away from their position and had the ability to prevent 70% of instability events (Hawley & Dymond, 1988). Computational research furthermore shows that root reinforcement by the larger roots is dominant over the smaller roots, even though they are far less numerous (Vergani et al., 2014). The planting pattern and management of the vegetation can have a profound effect on root reinforcement and thus on slope stability (Sidle, 1992). Therefore a detailed approach to calculate the spatial distribution of root reinforcement is important for slope stability calculations. Root reinforcement can be subdivided into two major components: Basal root reinforcement and lateral root reinforcement. Basal root reinforcement is the anchoring of tree roots through the sliding plane into

the deeper soil. Lateral root reinforcement is the reinforcement from roots on the edges of the potential slide that stick into the soil outside of the potential slide (Schwarz, Preti, et al., 2010). In contrast, the mechanical influence of vegetation weight on slope stability is often considered negligible (Steinacher et al., 2009). In current shallow landslide probability modelling, whether deterministic or probabilistic, root reinforcement is generally modelled in a simplified way, for example by including homogeneous root reinforcement (Montgomery et al., 2000). These methods limit the evaluation of the effects of different forest spatial properties such as forest structure, and the contribution of different root reinforcement mechanisms to slope stabilisation (Schwarz et al., 2012). In order to overcome this limitation, we develop a shallow landslide probability model, named SlideforMAP. To ensure a wide applicability, SlideforMAP is designed for a regional scale. In concrete terms this means SlideforMAP should be applied to study areas of 1 - 1000 km^2. The main objectives of this work are to:

- Present the SlideforMAP model as a tool for shallow landslide probability assessment
- Show a calibration of SlideforMAP through a performance indicator over three study areas with 78 field recorded shallow landslide events in Switzerland
- Analyze the expected improvement in the performance of SlideforMAP with a detailed inclusion of vegetation
- Provide a qualitative sensitivity analysis and identify the parameters that are of greatest influence on the slope stability

Strong emphasis within the SlideforMAP framework and this paper is put on the quantification of root reinforcement on a regional scale. We will show the effect of accurate, quantitative, representation of root reinforcement has on slope stability over three study areas. Simplifications, lack of a temporal component and calibration constraints make it impossible to use SlideforMAP as an exact forecast tool. The main application for SlideforMAP is as a tool to quantify the effects of vegetation planting, growth and/or management for land managers in relation to shallow landslides.

4.2 Methods: SlideforMAP

4.2.1 Probabilistic modelling concept

SlideforMAP is a probabilistic model that generates a 2D raster of shallow landslide probability (P_{ls}). It is an extension of the approach of Schwarz, Preti, et al. (2010) and Schwarz et al. (2015). It generates a large number of hypothetical landslides (HLs, singular: HL) within the limits of a pre-defined region of interest. These HLs are assumed to have an elliptic shape and are characterized by a mix of deterministic and probabilistic parameters, from which the landslide stability is computed following the limit equilibrium approach (section 4.2.2). The probabilistic parameters are the HL location, its surface area and its soil cohesion, internal friction angle and soil thickness parameters (drawn from appropriate random distributions). The location and surface area are approached in a probabilistic way to compute a spatial probability distribution. The soil parameters are probabilistic because we assume their variation is high and important in mountainous environments. The deterministic parameters include several vegetation parameters and hydrological soil parameters. A key originality of the approach stems from the fact that the vegetation parameters can be derived from single-tree scale information (section 4.2.5). The number of generated landslides is high enough such that each point in a region of interest is overlain by multiple HLs from which a relative P_{ls} can be estimated by considering the ratio of unstable HLs. A general flow chart of SlideforMAP is given in Figure 4.1. More details on the modules follow in the subsequent sections.

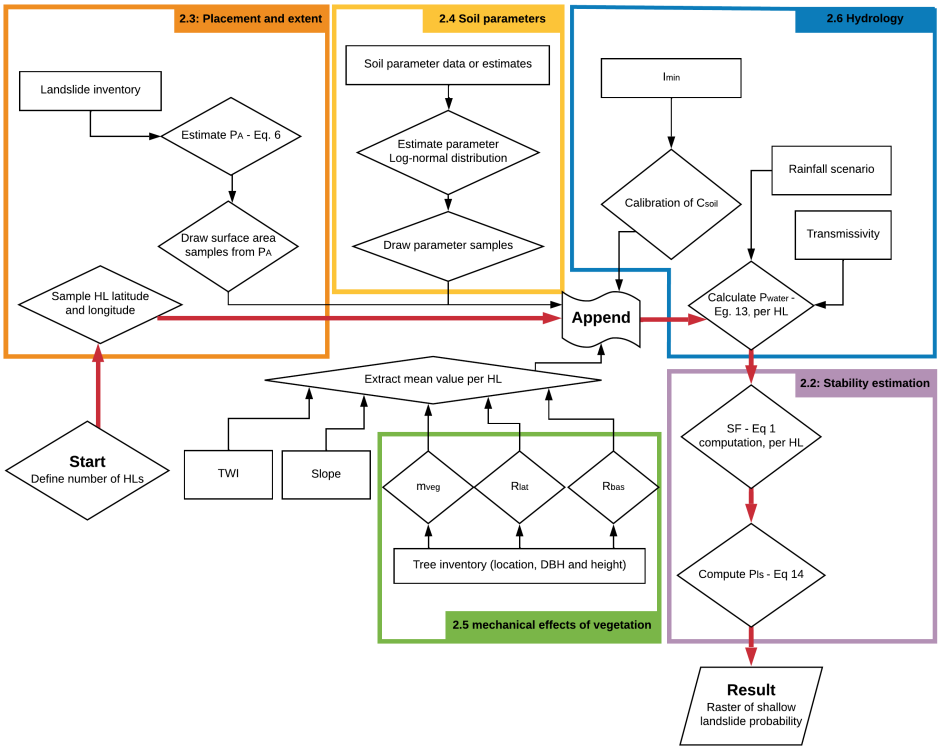

FIGURE 4.1: Flowchart of the computational steps in SlideforMAP. Separate sections are outlined in colors. The central workflow is highlighted.

4.2.2 Stability estimation

The estimate of the stability of each HL is calculated following the limit equilibrium approach (described well in the work of Day (1997)). In this method, a landslide is assumed to be stable if its safety factor (SF) is greater than 1.0. The SF is computed as the ratio of the parallel to slope stabilizing forces and the destabilizing ones:

$$SF = \frac{F_{\text{res}}}{F_{\text{par}}}, \tag{4.1}$$

where F_{par} [N] is the force parallel to the slope, F_{res} [N] is the maximum mobilized resistance force. The assumed forces that act upon a hypothetical landslide are schematically shown in Figure 4.2.

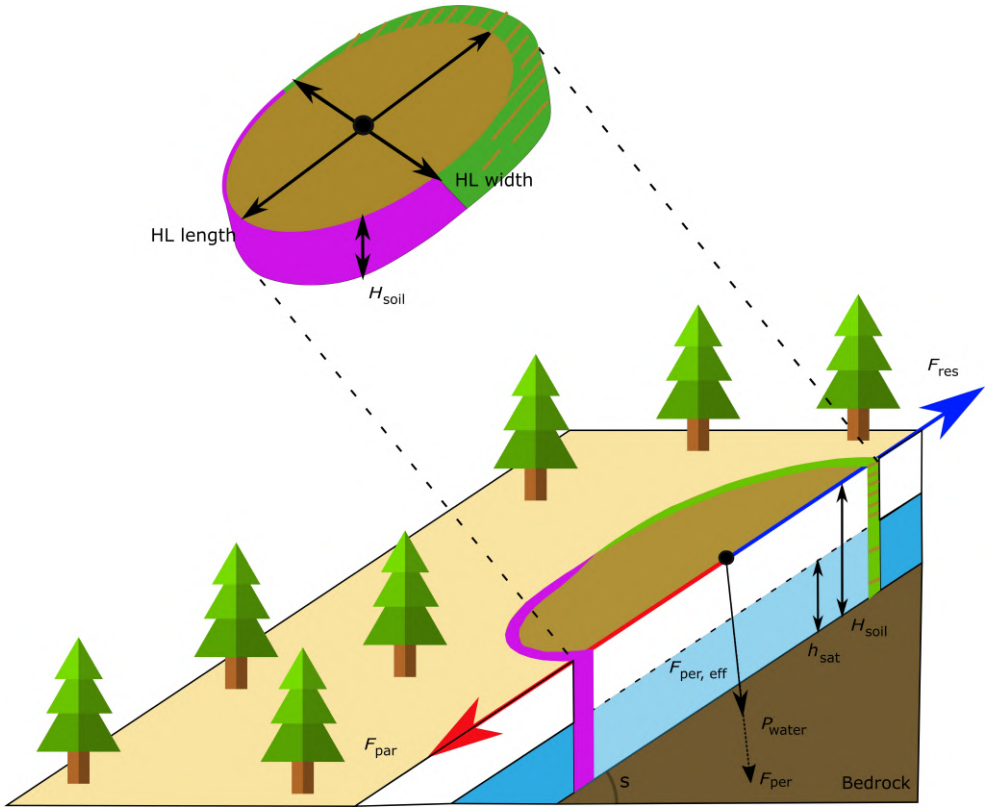

FIGURE 4.2: Schematic overview of the forces acting upon a hypothetical landslide, as assumed in SlideforMAP. The blue arrow, F_{res}, indicates the stabilizing forces and the red arrow, F_{par}, indicates the destabilizing forces. Lateral root reinforcement only acts upon the green part of the hypothetical landslide, where tension takes place. In purple is the compression zone in the shallow landslide. Basal root reinforcement and soil shear strength act on the whole potential failure surface.

As seen in Figure 4.2, all landslides are assumed to be elliptical (Rickli & Graf, 2009) with a ratio between length and width, $l_{wr} = 2$. The forces assumed in SlideforMAP are typical for the second stage of the activation phase: the displacement at which lateral root reinforcement is maximized under tension along the tension crack and at which passive earth pressure and lateral root compression are assumed to not be fully mobilized (Cohen & Schwarz, 2017b). The magnitude of the stabilisation's effects under compression considerably change depending on the stiffness of the landslide material and the dimension of the landslide. The quantification of those effects are still a challenge for slope stability calculation at large scales. In order to develop a conservative approach, we neglect those effects in the stability calculations of SlideforMAP. The tension crack is assumed to span the entire upper half of the circumference of the HL and has an assumed length in the range of 0.01 - 0.1 m (Schwarz et al., 2015) depending on the root distribution. This behaviour of progressive shallow landslide failure with a tension crack opening up in the upper half of a shallow landslides is described in detail in Cohen et al. (2009) and Askarinejad et al. (2012). This is different from the assumptions taken in most landslide models involving root reinforcement e.g. Montgomery et al., 2000; Schmidt et al., 2001, that assume lateral root reinforcement to be activated at the same time along the entire landslide perimeter. Quantification of the forces in the safety factor calculation follows the limit equilibrium assumptions. This method is outlined in equations 4.2 to 4.5 below:

$$F_{par} = g(m_{soil} + m_w + m_{veg}) \cdot \sin(s), \tag{4.2}$$

$$F_{\text{res}} = \frac{c_{\text{ls}}}{2} \cdot R_{\text{lat}} + F_{\text{res,bas}}, \tag{4.3}$$

$$F_{\text{res,bas}} = A_{\text{ls}} \cdot C_{\text{soil}} + A_{\text{ls}} \cdot R_{\text{bas}} + F_{\text{per,eff}} \cdot \tan(\phi), \tag{4.4}$$

$$F_{\text{per,eff}} = g \cdot (m_{\text{soil}} + m_{\text{w}} + m_{\text{veg}}) \cdot \cos(s) - P_{\text{water}}, \tag{4.5}$$

In these equations, m_{soil} is the soil mass [kg], m_{w} is the mass of the water [kg], m_{veg} is the vegetation mass [kg], g is the gravitational acceleration assumed at 9.81 [m/s^2], s is the slope [°], c_{ls} is the circumference of the landslide [m], R_{lat} is the lateral root reinforcement [N/m], $F_{\text{res,bas}}$ is the basal resisting force, A_{ls} [m^2] is the area of the landslide, C_{soil} [Pa] is the soil cohesion [Pa], R_{bas} is the basal root reinforcement [Pa], $F_{\text{per,eff}}$ is the effective perpendicular resisting forces [N], ϕ is the angle of internal friction [°] and P_{water} is the water pressure [Pa].

4.2.3 Placement and extent

The location of the center of mass of the HLs is generated from two uniform distributions covering the latitudinal and longitudinal extent of the study area. HLs on the edge of the study area are taken into account as well, though cut to the extent of the study area in the later spatial processes of SlideforMAP. The total number of HLs is determined by multiplying the landslide density parameter (ρ_{ls}) with the total surface area of the study area. This number is then uniformly sampled with replacements from the latitudinal and longitudinal distribution. The value of ρ_{ls} should be high enough such that each raster cell of the study domain is covered by several HLs. The HL surface area is sampled from an inverse gamma distribution following the work of Malamud et al. (2004), which showed that the probability distribution of shallow landslide surface areas follows an inverse gamma distribution (Johnson & Kotz, 1970). The parameterization of a three parameter inverse gamma distribution is shown in equation 4.6 below.

$$P_{A_{\text{ls}}} = \frac{1}{a \cdot \Gamma(\rho)} \left(\frac{a}{A_{\text{ls}} - s} \right)^{(\rho+1)} e^{\left(\frac{-a}{A_{\text{ls}} - s}\right)}, \tag{4.6}$$

where A_{ls} is the area of the landslide, $P_{A_{\text{ls}}}$ is the probability of A_{ls}, Γ is the gamma function, a, ρ and s are parameters. These distributional parameters are estimated using the landslide surface area data of the inventory (section 4.3). The estimation is based on minimizing the Root Mean Square Error (RMSE) between the histogram counts (size of histogram bins = 10) of the surface areas from the inventory and the distribution of equation 4.6. Users can follow this approach with an inventory or use a custom parametrization. The maximum HL surface area is set for all case studies based on the maximum surface area observed in the landslide inventory. This maximum is set to 3000 m^2, based on the rounded up maximum value of a well-distributed landslide inventory in Switzerland (section 4.3.3), but users can vary this parameter.

4.2.4 Soil parameters

Steep-sloped mountainous areas are prone to extreme and unpredictable heterogeneity in soil parameters (Cohen et al., 2009). This makes a heterogeneous deterministic parameterization inaccurate, even if based on observations. To overcome this limitation, a probabilistic approach in the parameterization of soil parameters of the model is applied. Values of soil cohesion and internal friction angle of each HL are randomly generated from independent probability distributions. This is an approach similar to the one taken in Griffiths et al. (2009), who use the log-normal distribution for soil cohesion only and Pack et al. (1998) who use a uniform distribution for soil cohesion and friction angle. We choose the log-normal distributions in our

parametrization because it has shown to give a good fit (Figure 4.11 with a comparison to a normal distribution in the Appendix; Corresponding code in the supplementary material), it ensures generating positive values only and its accuracy has been shown in Griffiths et al. (2009). The distribution is parametrized by the mean and the standard deviation of observed samples. The mean and the standard deviation are based on different information such as field soil classification or a geotechnical analysis. The soil cohesion in our computations is assumed to be representative for saturated, drained and unconsolidated conditions. Soil thickness is parametrized following a different approach to account for the shallow soils found on steep slopes. An initial soil thickness (h_{soil}) is derived from a log-normal distribution. This is then multiplied by a correction factor which is a function of slope inclination as shown in equation 4.7. Soil thickness is defined here perpendicular to the slope as opposed to soil depth, that is measured in the vertical direction.

$$H_{\text{soil}} = h_{\text{soil}}\big(1 - P_{\mathcal{N}}(S \leq s|\mu_1, \sigma_1)\big), \tag{4.7}$$

where H_{soil} [m] is the soil thickness and s is the observed slope, extracted for the HL. $P_{\mathcal{N}}(S \leq s|\mu_1, \sigma_1)]$ is the cumulative normal distribution of the slope S with $\mu_1 = a \cdot m_h$ and $\sigma_1 = b \cdot \sigma_h$. m_h and σ_h are the mean and standard deviation of the slope angle of shallow landslides from an inventory or a best guess. a and b are estimated by fitting data from a landslide inventory containing slope angle and soil thickness. Other relations than used by SlideforMAP to correct the soil thickness to the slope e.g. Prancevic et al., 2020 are possible as well.

4.2.5 Mechanical effects of vegetation

Three properties of vegetation are included in the model. These are vegetation weight, lateral root reinforcement and basal root reinforcement. SlideforMAP only incorporates trees and ignores possible effects by shrubs, grasses and other vegetation. This choice is due to the fact that trees are predominant in influencing slope stability (Greenway, 1987). Single tree detection (Korpela et al., 2007; Menk et al., 2017) serves as a basis to estimate these properties. Single tree position and dimensions are derived from a Canopy Height Model (CHM), which is the difference between the Digital Surface Model (DSM) and the Digital Elevation Model (DEM), using a local maxima detection method (LMD) described in the work of Eysn et al. (2015) and Menk et al. (2017). First, the trees are rasterized. The resolution of this raster has to exceed the effective radial dimension of the trees, in order to calculate representative vegetation parameter values at stand scale. The weight of the tree is calculated by using the tree height and the Diameter at Breast Height (DBH), assuming that the trees are cone shaped. The tree mass, m_{veg}, used in equation 4.2 and 4.5, is calculated assuming a mean tree density (ρ_{tree}) of 850 kg/m^3. Root reinforcement is added in the model using the method proposed by Schwarz et al. (2012), which relates the root reinforcement to the distance to a tree, the size of the tree and the tree species. Two rasters are computed. A raster with the nearest distance to a tree (D_{trees}) and a raster with the average DBH of all trees within an assumed maximum distance of root influence ($D_{\text{trees,max}}$), set at 15 m. We compute actual lateral root reinforcement for a given grid cell as a function of maximum lateral root reinforcement and soil thickness, which reduces maximum lateral root reinforcement. The maximum lateral root reinforcement, RR_{max} [N/m], is computed as a function of D_{trees} and DBH (Gehring et al., 2019; Moos et al., 2016) according to equation 4.8 below:

$$RR_{\text{max}} = (c \cdot DBH) \cdot \Gamma_{PDF}\left(\frac{D_{\text{trees}}}{DBH \cdot 18.5}\middle|\alpha_1, \beta_1\right), \tag{4.8}$$

In equation 4.8, c is a fitting parameter in N/m^2 based on the work of Schwarz, Preti, et al. (2010). DBH is in [m]. The $\Gamma_{\text{PDF}}(x|\alpha_1, \beta_1)$ is the gamma probability density function (Γ_{PDF}) evaluated as function of x with shape parameter α_1 and rate parameter β_1. Both α_1 and β_1 are dimensionless.

The parameters should ideally reflect any knowledge about how root reinforcement decreases with distance for specific tree species. The general Γ_{PDF} is written as:

$$\Gamma_{PDF}(x|\alpha,\sigma) = \frac{x^{\alpha-1}e^{-x/\sigma}}{\sigma^{\alpha}\Gamma(\alpha)}, (x,\alpha,\sigma > 0), \tag{4.9}$$

In this equation α and σ are the shape and scale parameter. The rate parameter, β, as used in this research, is defined as $1/\text{scale}$. Soil thickness reduces the effects of lateral root reinforcement that contributes to stabilize a shallow landslide. This decrease of lateral root reinforcement with soil thickness is obtained as follows:

$$R_{\text{lat}} = RR_{\text{max}} \cdot \int_0^{H_{\text{soil}}} \Gamma_{\text{PDF}}\left(H\middle|\alpha_2,\beta_2\right) dH, \tag{4.10}$$

In this equation $\Gamma_{\text{PDF}}(H|\alpha_2,\beta_2)$ is the Γ_{PDF} for the normalized root distribution over the soil thickness with shape parameter α_2 and rate parameter β_2. In this equation β_2 has the unit [m] in order to make the integral of the Γ_{PDF} dimensionless. SlideforMAP computes this integral by numerical approximation. This method computes the root reinforcement where only one tree can influence a cell. A spatially representative minimum root reinforcement value is calculated in a stand assuming a triangular lattice (Giadrossich et al., 2020). Under this assumption, three root systems interact additively. Basal root reinforcement, R_{bas} is assumed to be proportional to lateral root reinforcement and dependent on soil thickness according to the relation shown in equation 4.11:

$$R_{\text{bas}} = RR_{\text{max}} \cdot \Gamma_{\text{PDF}}\left(H_{\text{soil}}|\alpha_2,\beta_2\right), \tag{4.11}$$

where $\Gamma_{\text{PDF}}\left(H_{\text{soil}}|\alpha_2,\beta_2\right)$ is the normalized root distribution in the vertical direction. The Γ_{PDF} in this application the unit [m^{-1}] which leads to a unit of [Pa] for the term R_{bas}, under the assumption of isotropic conditions.

4.2.6 Hydrology

The hydrological module in SlideforMAP is based on the TOPOG model (O'Loughlin, 1986), which includes a specific topographic index as inspired by Kirkby (1975). In this framework we specifically assume macropore flow dominates hillslope hydrology. The identical model is used in the SHALSTAB stability model (Montgomery & Dietrich, 1994) and SINMAP (Pack et al., 1998). It is assumed that the saturated soil fraction of each cell holds a relation to its specific catchment area, its slope angle, a constant precipitation intensity and the soil transmissivity (equation 4.12). This is in close correspondence to the parameterization used in the widely used TOPMODEL (Beven & Kirkby, 1979). Limitations of this approach is the assumption of uniform soil transmissivity, no inclusion of initial conditions, steady-state flow and lateral flow governing of soil moisture pattern. These limitations and generalizations make the model insufficient in capturing detailed hydrological pattern, especially in mountainous regions modelled by SlideforMAP. Despite this, we assume the approach to be suitable for a general pattern of saturated fraction and subsequent pore pressure. In addition to this shortcoming we ignore the apparent hydrological cohesion (Chae et al., 2017) prominent in unsaturated fine and clayey soils, but of little prominence in other conditions (Montrasio & Valentino, 2008). The saturated soil fraction, h^*_{sat} [-], of a soil column is defined in equation 4.12 below:

$$h^*_{\text{sat}} = \frac{I \cdot CA}{T \cdot b \cdot \sin(s)}, \tag{4.12}$$

I [m/s] is the constant precipitation intensity, T [m^2/s] is the transmissivity, CA is the contributing catchment area [m^2], s is the slope inclination [°], and b is the contour length [m] that in our

model corresponds to the cell size (see section 4.3.2 for details on its computation). We assume dominant macropore flow, which has the ability to quickly drain a catchment and potentially reach a state of stationary flow. Using this estimated h^*_{sat}, pore water pressure is computed as:

$$P_{\text{water}} = H_{\text{soil}} \cdot \cos(s) \cdot h^*_{\text{sat}} \cdot g \cdot \rho_{water}, \tag{4.13}$$

where P_{water} [Pa] is the pore water pressure (used in equation 4.5), H_{soil} [m] is the soil thickness, s is the slope angle, g=9.81 m/s^2 is the gravitational acceleration, ρ_{water} is the density of water assumed equal to 998 kg/m^3. The same value for water density is used in the computation of the water mass in the HL.

4.2.7 Model initialisation

The model has a total of 3 probabilistic parameters and 15 deterministic parameters (Table 4.1). The deterministic parameters as well as the distributional parameters for the probabilistic parameters are determined from in-situ data or from literature (section 4.3). In a first step of the workflow for the application of SlideforMAP, after assigning the deterministic parameter values and sampling a value for each probabilistic parameter, a minimum value of soil cohesion is computed for each HL to obtain stable conditions (safety factor, SF >= 1.0) under uniform a precipitation intensity of 28.3 mm/day or 1.2 mm/hr. This threshold of precipitation intensity is chosen according to Leonarduzzi et al. (2017), who statistically analyzed over 2000 landslides in Switzerland over the period 1972–2012 and found this as a triggering threshold. The minimum value of soil cohesion is obtained by equating F_{par} (equation 4.2) and F_{res} (equation 4.3). If the minimum value of soil cohesion is larger than the sampled soil cohesion, the soil cohesion is updated to the minimum value. This procedure can be altered by users when another threshold or no threshold at all applies.

TABLE 4.1: An overview of all variable model parameters of SlideforMAP. The second to last column indicates the source of the default value. The last column indicates whether the default is global or specific for this research in Switzerland (CH).

Parameter	Description	Default value	Unit	Source	Extent
m_{d}	Soil thickness mean	1	m	Estimate	Global
σ_{d}	Soil thickness standard deviation	0.25	m	Estimate	Global
m_{C}	Soil cohesion mean	2	kPa	Estimate	Global
σ_{C}	Soil cohesion standard deviation	0.5	kPa	Estimate	Global
m_{ϕ}	Angle of internal friction mean	30	°	Estimate	Global
σ_{ϕ}	Angle of internal friction standard deviation	4	°	Estimate	Global
ρ_{ls}	Density of the random generated landslides	0.1	HL/m^2	Estimate	Global
ρ_{soil}	Dry soil density	1500	kg/m^3	Estimate	Global
T	Soil transmissivity	0.1	m^2/s	Estimate	Global
I	The precipitation event that is tested	10	mm/hr	Estimate	Global
I_{min}	Precipitation intensity threshold for instability	1.2	mm/hr	Leonarduzzi et al. (2017)	CH
r_{xy}	Raster resolution of the SlideforMAP run	2	m	Estimate	Global
l_{wr}	Ratio between length and width of the landslides	2	-	Estimate	Global
c	Fitting parameter for the lateral root reinforcement	25068.54	-	Gehring et al. (2019)	CH
α_1	Shape of root distribution in horizontal direction	0.862	-	Gehring et al. (2019)	CH
β_1	Rate of root distribution in horizontal direction	3.225	-	Gehring et al. (2019)	CH
α_2	Shape of root distribution in vertical direction	1.284	-	Gehring et al. (2019)	CH
β_2	Rate of root distribution in vertical direction	3.688	m	Gehring et al. (2019)	CH
$D_{\text{trees,max}}$	maximum distance for influence of tree roots	15	m	Estimate	Global
ρ_{tree}	Density of a tree	850	kg/m^3	Estimate	CH
ρ_{water}	Density of water	998	kg/m^3	Estimate	Global

4.2.8 Landslide probability computation

After model initialisation, SF (equation 4.1) is computed for each of the generated HLs. Based on the SF for all generated HLs, landslide probability per raster cell (with the resolution of the original DEM), P_{ls}, is computed as:

$$P_{ls} = \frac{n_{us}}{n_{HL}}, \tag{4.14}$$

where n_{us} is the number of unstable HLs, i.e. of HLs with SF<1.0 and n_{HL} is the total number of generated HLs (the HLs are overlapping). Both per raster cell. Finally, this results in a raster of shallow landslide probability on a resolution of the input DEM.

4.3 Data

4.3.1 Study areas

Three study areas were chosen to test SlideforMAP based on the availability of elevation data and detailed records of historical shallow landslide events (Figure 4.3), each varying in size and location to test the robustness and the general applicability of the model.

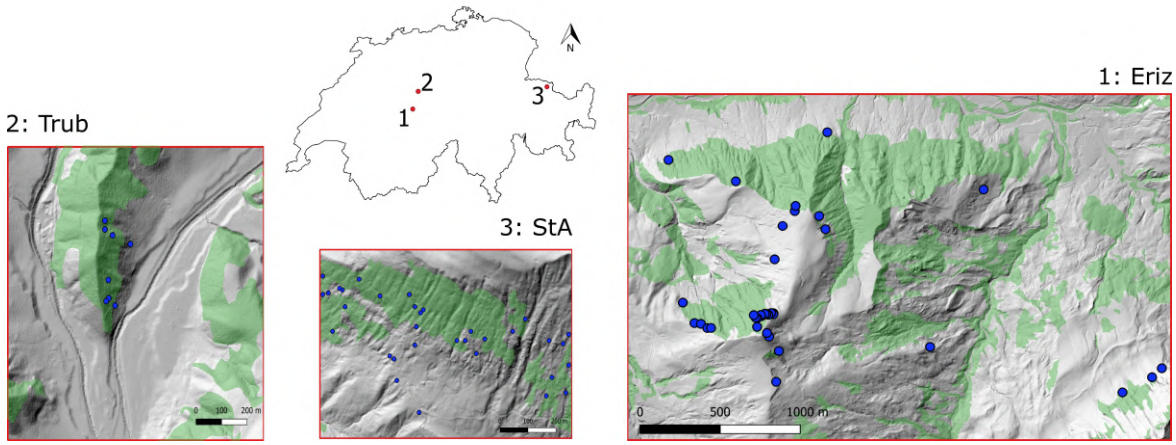

FIGURE 4.3: Locations of the study areas in Switzerland with observed Shallow landslide occurrence over the period 1997 - 2012 (blue dots); the case study names are given according to nearby villages: Trub, St. Antönien and Eriz. Forest covered area is presented in green. Source of forest cover: Federal Office of Topography Swisstopo (Swisstopo, 2020). Source of hillshade: Federal Office of Topography Swisstopo (Swisstopo, 2018).

The geological formations in the Eriz study area vary from Oligocene freshwater Molasse in the lower northern part, morainic material in the central part and Cretaceous Limestone in the highest parts. Forests are dominated by spruce (*Picea abies*), except for the lower regions where broad-leaved trees are dominant. In the Trub study area, the dominant geological formation is Miocene Marine Molasse and forests are dominated by spruce. In the St. Antönien (from here forward abbreviated to 'StA') study area, the dominant geological formation is Flysch (Prättigauer Flysch), partially covered by till (Moos et al., 2016). The forest in this study area is also dominated by spruce (Moos et al., 2016). Further characteristics of the study areas are given in Table 4.2.

TABLE 4.2: Study area characteristics. Meteorological data is from the HADES yearly average precipitation for the time period 1981 - 2010 (Frei et al., 2020). Shallow landslide number and density from the inventory in section 4.3.3.

Name	**Centre coordinate** lat;lon (WGS84)	**Surface area** km^2	**Mean prec.** mm/year	**Elevation** m.a.s.l.	**Number of slides**	**Slide density** Slides/km^2	**Mean slope** °
Eriz	7.81; 46.78	7.54	1700	960 - 1750	37	4.9	20.4
Trub	7.90; 46.96	1.00	1620	820 - 1020	8	8.0	18.3
StA	9.80; 46.98	0.56	1310	1540 - 2010	33	58.9	27.5

4.3.2 Input data

To accurately measure P_{ls} for each study area, the following data are required.

- Digital Surface Model (DSM) and Digital Elevation Model (DEM)
- Average and standard deviation values for soil cohesion, thickness and friction angle
- A representative landslide inventory containing at least:
  - Average landslide soil thickness
  - Landslide surface area

In addition to the DEM, the DSM is applied in the vegetation module of SlideforMAP. The DEM and the DSM are both acquired from the SwissAlti3D database (Swisstopo, 2018), which makes use of aerial laserscanning (ALS). Both the DSM and DEM are available at a resolution of 0.5 m. As an alternative to the use of a landslide inventory and the DSM for single tree identification, users can also use synthesized values for the parameters derived from this data. After pit filling, the DEM is used to compute a slope map following the method of Zevenbergen and Thorne (1987). The topographic wetness index θ for Figure 4.4 is computed on a raster cell basis based on the 2 m DEM using equation 4.15.

$$\theta = \frac{CA}{b \cdot \sin(s)}, \tag{4.15}$$

where CA is the specific upslope catchment area, b is the contour length and s is the slope angle. To avoid numerical problems for elongated catchments, θ is computed using a 2 km buffer around the catchment. The large buffer size is chosen arbitrarily, but can be reduced by other users. The standard D8 method is applied for the computation of the upslope catchment area from the DEM (O'Callaghan & Mark, 1984). For single tree detection, the FINT algorithm (Menk et al., 2017) is used. Since the results of such detection methods are strongly influenced by the resolution and smoothness of the input data (Eysn et al., 2015), we applied the LMD method to the canopy height model (CHM). This canopy height model is computed by subtracting the DEM from the DSM and is resampled to a resolution of 1, 1.5 and 2 m. In addition, three different Gaussian filters were applied on the 1 m resolution CHM. These three filters have a radius of 3, 5 and 7 cells and a standard deviation of 2 m. To identify the input data that leads to LMD results with the highest accuracy, we evaluated the identified trees in three randomly selected forest inventory plots with an area of 20 m x 20 m for each study site. In these plots, we visually identified all recognisable tree crowns, on the basis of aerial photos (Swisstopo, 2017) and the CHM. The identified trees were then compared to the LMD result, using the difference in the number of detected trees. The input data leading to the most accurate results in all three study sites was the 1 m resolution CHM with a Gaussian filter of a 3 cells radius and with the fixed standard deviation of 2 m. This combination has been applied to the entire area of the three study

sites. To estimate the DBH from the tree heights of all detected trees, the following empirical equation (Dorren, 2017) was used:

$$DBH_{\text{tree}} = \frac{(H_{\text{tree}})^{1.25}}{100}, \tag{4.16}$$

where DBH_{tree} [m] is the diameter at breast height of a given tree and H_{tree} [m] its height. Details resulting from the LMD method for the three study areas are shown in Table 4.3.

TABLE 4.3: Vegetation parameters in the study areas. Source of forest cover: Federal Office of Topography Swisstopo (Swisstopo, 2020). Source of hillshade: Federal Office of Topography Swisstopo (Swisstopo, 2018).

Study area	**Trees identified**	**Forest cover** %	**Mean stem density** Stems/ha	**Mean DBH** m	**Std. deviation DBH** m
Eriz	38923	32	165	0.51	0.27
Trub	7267	26	270	0.55	0.30
StA	1796	27	120	0.31	0.18

The lateral and the basal root reinforcement (equations 4.10 and 4.11) are parameterized using the values from Gehring et al. (2019) (α_1 = 0.862, β_1 = 3.225, c = 25068.54, α_2 = 1.284, β_2 = 3.688). In their work, the calibration was performed on beech (Fagus Sylvatica) stands over varying elevations. Our study areas, however, are predominantly vegetated by spruce trees. Therefore a discrepancy in the estimated root reinforcement will likely arise. Unfortunately, this is the only published set of calibrated values.

4.3.3 Landslide inventory

A landslide inventory is required to quantify a distribution for slope, surface area and soil thickness for the HLs. This inventory does not necessarily have to be well distributed in the study area, or even be present in the area. However, it should be representative of the conditions in the area of interest as much as possible. A dataset of 668 shallow landslides that occurred between 1997 and 2012 in Switzerland has been created by the Swiss Federal Office for the Environment (Rickli et al., 2019). Statistical information on the landslides can be seen in Figure 4.4. We assume the properties in this inventory to be representative for shallow landslides in Switzerland. All landslides are triggered by rainfall and the majority of the landslides are shallower than 1.5 m (Figure 4.4). The landslides in the StA and Trub area took place in 2005 during or shortly after heavy rainfall in August. The landslides in the Eriz area from 2012 are related to heavy rainfall in July. Exact precipitation amounts and intensities are unknown. The data is formatted with centre points and surface area of the shallow landslide initiation area. In our analysis we assume they have an elliptical shape.

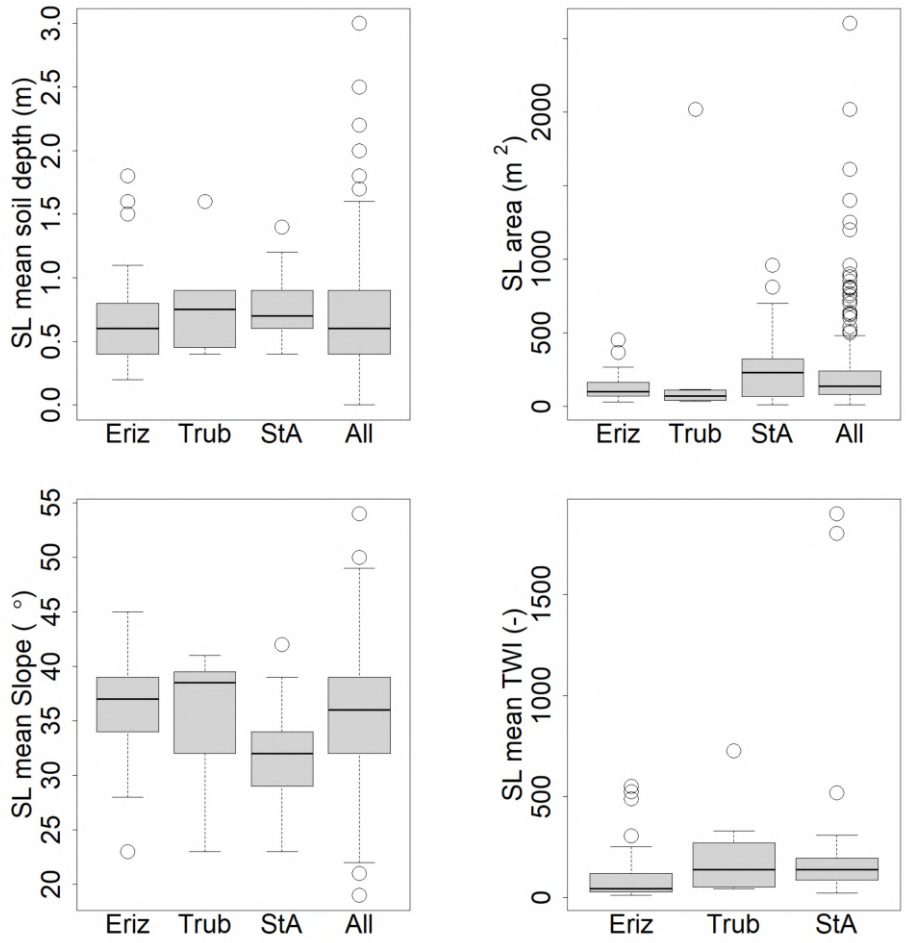

FIGURE 4.4: Overview of landslide properties for the studied regions. Top row: mean soil thickness (left) and the surface area (right) of the shallow landslide (SL) for the test areas and the total inventory; bottom row: mean slope (left) and mean TWI (right). The box plots show the 25, 50 and 75 percentiles, the whiskers extend to 1.5 times the length between the 25 and 75 percentile. Outliers are marked as circles. The TWI was extracted from the TWI raster cells that lie inside the landslide inventory polygons.

The inventory is used to estimate the parameters for the surface area distribution used in SlideforMAP (equation 4.6), via minimization of the RMSE between observed frequencies and theoretical frequencies. The estimated values of the parameters are: a = 1.40, ρ = 1.5^{-4} m^2, s = 4.28^{-8} m^2. In addition, the inventory is used to calibrate the a and b parameters for the soil thickness correction factor as used in equation 4.7. For the fitting (Appendix, Figure 4.12) of the correction factor we use classes of inclination of 2.5 degrees and the soil thickness values corresponding to 95^{th} percentile. This best fit for equation 4.7 was obtained with the values of a = 1.47 and b = 0.50.

4.3.4 Model calibration and sensitivity analysis

The model has a total of 21 parameters that are derived from observed data, from literature or that are set to default values; their values, given in Table 4.1, are not further varied in the model behavior analysis due to their assumed low variance. The remaining parameters can potentially influence the landslide probability, mostly given their variation as observed in nature. These parameters are: I_{min}, l_{wr}, c, α_1, β_1, α_2, β_2, $D_{trees,max}$, ρ_{tree}, ρ_{water}. The remaining 12 parameters are

then calibrated by Monte Carlo simulation, drawing a high number of parameter samples for all calibration parameters and evaluating the corresponding model performance based on the Area Under the Curve (AUC) method (Fawcett, 2006; Metz, 1978). We hereafter first present the used performance evaluation method, followed by the parameter sampling method used for the calibration as well as for the sensitivity analysis. In addition, we present four vegetation parameter scenarios that are developed to test the potential influence of vegetation. Due to the limited size of the landslide inventory, we do not include an independent validation of SlideforMAP.

4.3.4.1 Model performance evaluation

The basis of the application of the AUC method is a spatial representation of the landslide inventory in a boolean raster (0 = no past landslide present, 1 = past landslide present). For each randomly generated parameter set, the simulated P_{ls} (section 4.2.8) is also converted to a boolean raster, by selecting a threshold to assign 0 or 1. Overlaying the inventory raster on the modelled raster, results in a confusion matrix with four possible combinations, as shown in Table 4.4.

TABLE 4.4: The confusion matrix, resulting from the comparison of a reference boolean raster and a raster corresponding to a simulation.

		Model	
		True	**False**
Inventory	**True**	True positive (TP)	False negative (FN)
	False	False positive (FP)	True negative (TN)

A so-called Receiver Operator Curve (ROC) can be obtained by computing the values of the confusion matrix for all unique values in the simulated raster as threshold values and for each plotting the sensivitiy, TP/(TP+FN), against the specificity , TN/(TN+FP). The area under the ROC curve is the AUC and defines the accuracy of the model on a scale of 0.5 - 1.0, where 0.5 is being no better than a random guess and 1.0 is a perfect prediction.

4.3.4.2 Parameter sampling and qualitative sensitivity

The parameter samples for the Monte Carlo-based model calibration and the subsequent sensitivity analysis are generated using the Latin Hypercube Sampling (LHS) technique (McKay et al., 1979). This makes use of semi-random samples of variables over pre-defined ranges. The outcome of a Monte Carlo-based calibration is highly influenced by the ranges chosen for the parameters. For this reason, parameter ranges were chosen as realistically as possible. To estimate the parameter ranges for soil properties, soil types in USCS classes are taken from the shallow landslide inventory (a total of 377 had their soil type listed). Soil types present more than ten times are taken into account and aggregated into a hybrid table of soil cohesion and angle of internal friction values per soil type based on the values given in the work of Dysli and Rybisar (1992) and VSS-Kommission (1998) (see Appendix, Table 4.10). In order to obtain a realistic range for the soil cohesion, first the mean soil cohesion (weighted on USCS soil type occurrence) is computed and then the weighted standard deviation is subtracted and added twice to the weighted mean. This is to account for 95% of the variation in the observed soil cohesion (assuming a normal distribution). The same procedure is performed for the angle of internal friction. The range of transmissivity values is obtained by taking the saturated hydraulic conductivity from the work of Freeze and Cherry (1979) for the respective soil classes and by multiplying these saturated hydraulic conductivities with the minimum and maximum soil thickness of the soil class. From the resulting list of possible transmissivity values per soil class, the minimum and maximum are taken for the LHS range. For the precipitation intensity, four depth duration values are defined. These correspond to a duration of 1 hour and 24 hours with subsequent

return periods of 10 and 100 years. The duration of 1 to 24 hours is in line with the SlideforMAP assumption of quick macropore-flow dominated lateral groundwater flow. The return periods of 10 and 100 years were chosen arbitrarily in line with forest management timescales. Precipitation intensities are computed using data from the work of Jensen et al. (1997) and the methodology as described in the work of HADES (2020). An overview of the intensity - return period rainfall values is given in Table 4.5.

TABLE 4.5: Rainfall intensity [mm/h] for specific duration and return periods, used to define the boundaries in the sensitivity analysis D = duration, T = return period.

	D = 1 h T = 10 y	**D = 1 h T = 100 y**	**D = 24 h T = 10 y**	**D = 24 h T = 100 y**
Eriz	32	48	4	5
Trub	30	42	4	5
StA	30	43	4	4

The R-script implementing the sampling methodology and a description is included in the supplementary material. The minimum and maximum value from Table 4.5 are used as the range in the sensitivity analysis (Table 4.6). The maximum value for vegetation weight is taken from a biomass study in Switzerland by Price et al. (2017). For the other parameters, realistic ranges have been assumed. In Table 4.6 an overview is given of the tested parameters and the ranges used to generate the parameter samples. The precipitation intensity and transmissivity together determine the saturation degree of the soil (equation 4.12) and are therefore prone to equifinality. We grouped them as an additional parameter, the I/T ratio.

TABLE 4.6: Parameters used in the SlideforMAP qualitative sensitivity analysis and corresponding ranges for parameter sampling via LHS. RR_{max} and W_{veg} are given as spatially uniform parameters and not computed by the methodology in section 4.2.5. This is to create scenarios that are comparable with and without single-tree detection.

Parameter	**Unit**	**Description**	**LHS Range**
ρ_{ls}	m^{-2}	Density of the randomly generated landslides	0.02 - 0.10
ρ_{soil}	kg/m^3	Dry soil density	1.00 - 1.50
m_d	m	Mean soil thickness	0.20 - 1.80
σ_d	m	Standard deviation of the soil thickness, as a fraction of m_d	0.00 - 0.50
m_C	kPa	Mean saturated soil cohesion	0.00 - 12.5
σ_C	kPa	Standard deviation of the soil cohesion, as a fraction of m_C	0.00 - 0.50
m_ϕ	°	Mean angle of internal friction	24.00 - 41.50
σ_ϕ	°	Standard deviation of the angle of internal friction	0.00 - 5.00
T	m^2/s	Soil transmissivity	10^{-8} - 10^{-3}
I	mm/h	The precipitation event that is tested	4.0 - 48.0
I/T	m^{-1}	Ratio between precipitation and transmissivity	8.9^{-3} - 1390
RR_{max}	N/m	Maximum lateral root reinforcement	0.00 - 15.0
W_{veg}	$tonne/m^2$	The weight of the vegetation	0.00 - 0.10

For the model calibration and qualitative sensitivity analysis, 1000 LHS parameter sets were generated per study area by drawing samples from the ranges in Table 4.6. The number 1000 was chosen arbitrarily for computational constraints. The vegetation is set to a global uniform vegetation, which results in constant root reinforcement and vegetation weight in space. This is necessary because the same runs are used for model calibration and for model sensitivity analysis, where we need such uniform vegetation to ensure that the sensitivity of the (hypothetical)

vegetation has an effect on all raster cells of the whole study area (and not only on the actually vegetated cells). The parameter set with the highest AUC value is retained for model calibration. In addition, all 1000 parameter sets are used for a qualitative sensitivity analysis. The response variables are the AUC as a measure for accuracy and the ratio of unstable landslides as a measure for instability. The AUC is chosen for the sensitivity analysis as the main response variable since it expresses the performance relative to the independent landslide inventory. We then consider AUC as a generalized measure of parameter likelihood (Beven & Binley, 1992) and assess how selected best parameter sets (e.g. the best 10 % out of the 1000 sampled sets) are distributed (parameter subsampling).

4.3.4.3 Vegetation parameter scenario analysis

SlideforMAP has potential in testing the effect of different vegetation scenarios on the landslide probability. For this research, besides the reference scenario for model calibration and sensitivity analysis (global uniform vegetation), three additional scenarios are tested: i) without vegetation, ii) with uniform vegetation in forested areas and iii) with a fully diverse vegetation based on single-tree detection. The single-tree version uses the input data as mentioned in section 4.3.2. The forested areas are defined as areas where the single tree detection method leads to a lateral root reinforcement (Figure 4.9) which is not equal to zero.

4.4 Results

4.4.1 Sensitivity analysis

We use the 1000 model simulations corresponding to the 1000 generated parameter sets per study area for a sensitivity analysis of the model. The objective of this analysis is to quantify how the distribution of AUC values and of the landslide probability vary as a function of the parameters. Applying the parameter subsampling technique (see section 4.3.4.2), we see that for some parameters, the histogram shape (i.e. their marginal distribution) does not significantly deviate from the initial uniform distribution (from which we sampled), even if we retain only the best 10% (in terms of AUC) of all parameter sets (Figure 4.5). This apparent lack of sensitivity does not necessarily mean that the model is not sensitive to this parameter; in fact, the sensitivity could be hidden by strong parameter correlation (see Bárdossy, 2007, for a discussion of how uniform marginal distributions can result from strong parameter correlation). Our addition of the I/T ratio gives a hint at such behaviour. From Figure 4.5 it appears that the sensitivity to AUC of the I/T ratio is slightly stronger than either the precipitation or transmissivity independently. Some parameters, in exchange, show very strong sensitivity of their marginal distributions if only the best (in terms of AUC) parameter sets are retained. For the Trub case study (Figure 4.5), we see that the mean thickness m_d, the mean cohesion m_C, the I/T ratio and the transmissivity show a well defined maximum around the parameter values retained for calibration (the best performing ones). This suggests a good sensitivity of the model to these parameters in terms of model performance. Two of these three parameters also show a clear sensitivity if we retain subsamples that lead to successively higher unstable landslide ratio (Figure 4.6): high unstable ratios are obtained for high m_d values or for low m_C. Also for RR_{max}, highest ratios are clearly obtained for low lateral root reinforcement values (for all three case studies, Figure 4.6, Supplementary Material 10.2, 10.4). For transmissivity, while it shows a clear effect on model performance, the relation between its marginal distribution and the ratio of unstable landslides is less visible.

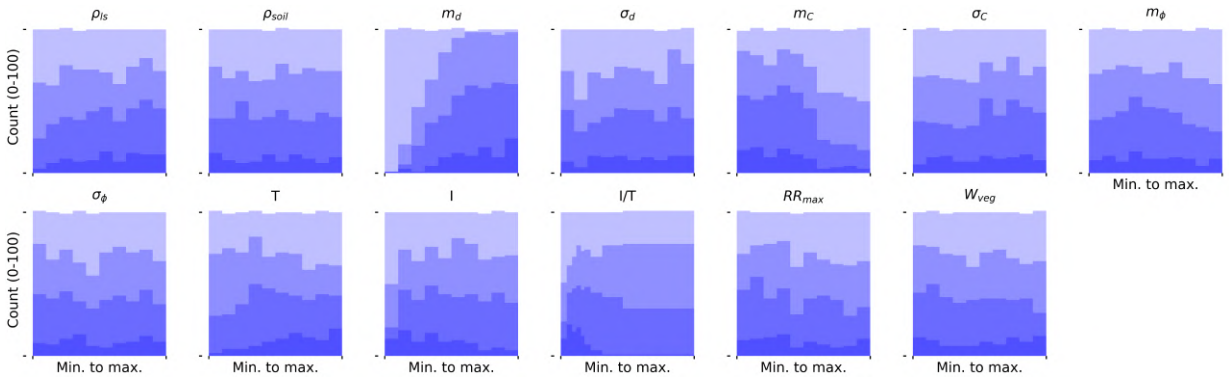

FIGURE 4.5: Histograms of different subsamples of the LHS parameter sets for the Trub study area. The shading (from light to dark) corresponds to subsamples retaining only the x% highest parameter sets in terms of AUC; the shown fractions are: 1, 0.7, 0.4, 0.1.

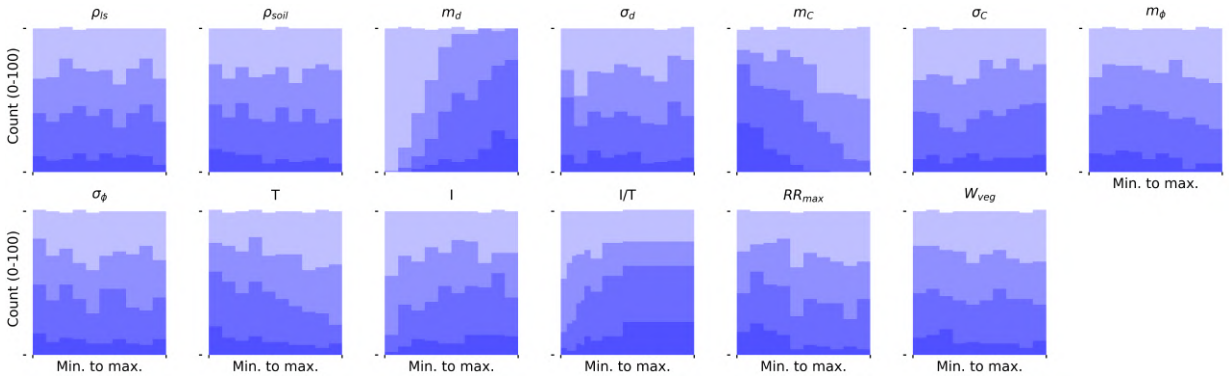

FIGURE 4.6: Histograms of different subsamples of the LHS parameter sets for the Trub study area. The shading (from light to dark) corresponds to subsamples retaining only the x% highest parameter sets in terms of Unstable ratio; the shown fractions are: 1, 0.7, 0.4, 0.1.

4.4.2 Model calibration

Based on the generated 1000 parameter sets, we identified the parameter set that resulted in the highest AUC value and assumed this to be an optimal calibration of the model. These calibrated parameter sets for each study area and their AUC values are shown in Table 4.7 together with the ratio of generated HLs that are unstable.

TABLE 4.7: Outcome of the Monte Carlo-based calibration: the parameter sets per study area resulting in the highest AUC value. The last row shows the ratio of unstable HL resulting from these parameter sets.

Parameter	**Eriz**	**Trub**	**StA**
ρ_{ls}	0.095	0.041	0.093
ρ_{soil}	1.40	1.20	1.49
m_d	1.62	1.02	1.78
σ_d	0.32	0.13	0.31
m_C	4.29	1.75	2.51
σ_C	0.43	0.32	0.30
m_ϕ	34.0	29.3	26.0
σ_ϕ	0.37	1.39	0.92
T	0.000148	0.000473	0.000582
I	40.3	24.2	14.0
I/T	0.077	0.014	0.007
RR_{max}	12.3	4.7	10.3
W_{veg}	0.05	0.02	0.03
AUC	0.924	0.940	0.693
Unstable ratio	0.197	0.308	0.387

Parameter consistency between the study areas appears to be visible in ρ_{soil}, m_d, m_C, σ_C, m_ϕ, σ_ϕ, T and W_{veg}. Other parameters show stronger variation, relative to their LHS range, between case studies. A realization of the shallow landslide probability computed with SlideforMAP for the three areas with their calibrated parameter set is given in Figure 4.7.

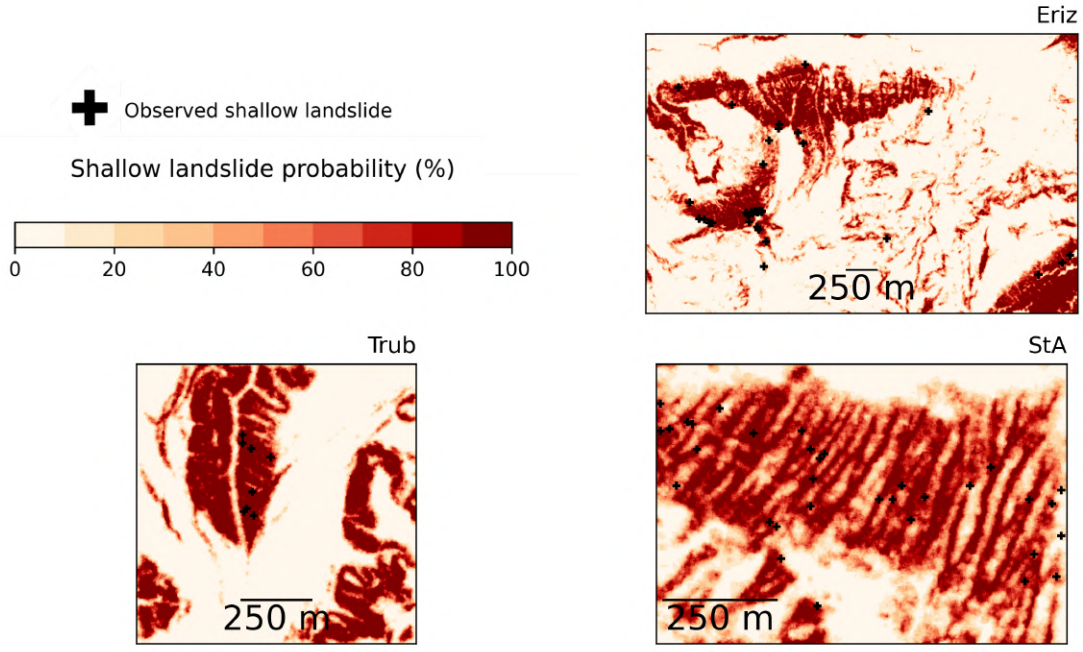

FIGURE 4.7: Overview of the landslide probability of the study areas simulated with the calibrated parameter sets of Table 4.7. Added as blue points are the observed landslides from the inventory.

In general, the model represents well the spatial distribution of the shallow landslides from the inventory. A cumulative plot of the shallow landslide probability for the study areas based on Figure 4.7 is given in Figure 4.8.

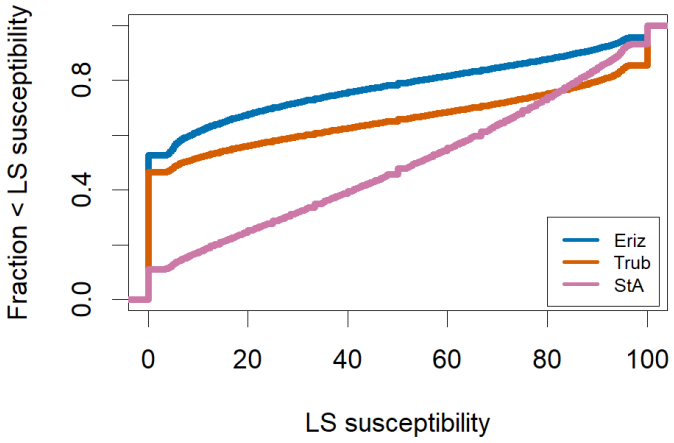

FIGURE 4.8: Cumulative plots for shallow landslide probability in the study areas, derived from the results in Figure 4.7.

4.4.3 Mechanical effects of vegetation

To test the impact of vegetation on the model behavior, we compare the different vegetation scenarios. The spatial distribution of lateral root reinforcement, resulting from single tree detection and SlideforMAP, is given in Figure 4.9.

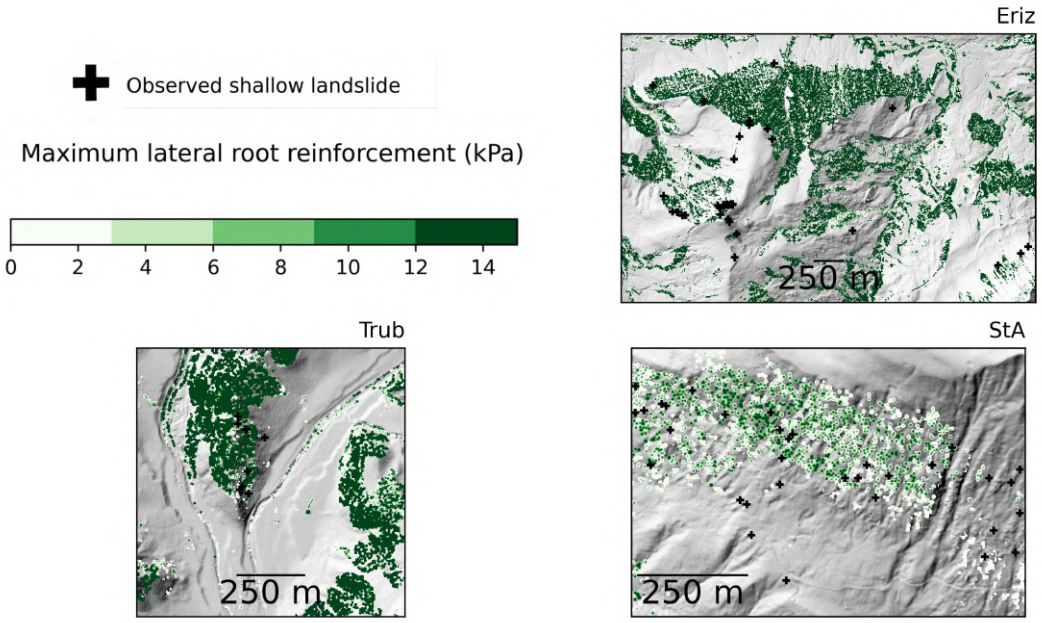

FIGURE 4.9: The spatial distribution of maximum root reinforcement (equation 4.8) in the study areas as used in SlideforMAP. Source of hillshade: Federal Office of Topography Swisstopo (Swisstopo, 2018)

The selected vegetation scenarios (no vegetation, global uniform vegetation, forest area uniform vegetation, single tree detection) affect the computation of the vegetation weight, the lateral root reinforcement and the basal root reinforcement. The latter is due to its dependence on lateral root reinforcement (equation 4.11). Accordingly, the vegetation scenario has a direct impact on SF (equation 4.1, 4.3, 4.4) and on P_{ls} (equation 4.14). For the analysis, we use the optimal parameter set from Table 4.7, obtained for a global uniform vegetation cover. The model runs are repeated 10 times to produce an average result and to show the variation from the probabilistic approach. Due to sampling from distributions, every realization produces a (slightly) different result. The resulting influence of the selected vegetation scenarios on AUC and on the ratio of unstable landslides is given in Table 4.8. The results from Table 4.8 and Table 4.9 display that the model is sensitive to the vegetation scenarios and that it predicts lower ratios of unstable ratios for vegetated scenarios as compared to the unvegetated scenario. This underlines the value of the model for future scenario analyses.

TABLE 4.8: AUC and unstable ratio under different vegetation scenarios with the optimal parameter sets of Table 4.7 and averaged over 10 runs. The "Overall" is composed of the mean value of all three study areas. In the global uniform vegetation scenario, the reference scenario is used during parameter optimisation.

		AUC				Unstable ratio			
		Overall	**Eriz**	**Trub**	**StA**	**Overall**	**Eriz**	**Trub**	**StA**
mean	Global uniform vegetation	0.808	0.910	0.844	0.669	0.299	0.197	0.311	0.388
	Forest area uniform vegetation	0.801	0.901	0.861	0.641	0.400	0.250	0.371	0.580
	Single tree detection	0.831	0.925	0.925	0.644	0.336	0.199	0.217	0.593
	No vegetation	0.785	0.880	0.854	0.622	0.475	0.309	0.413	0.704
Std. dev.	Global uniform vegetation	0.017	0.007	0.029	0.016	0.001	0.000	0.001	0.002
	Forest area uniform vegetation	0.021	0.008	0.039	0.016	0.001	0.000	0.001	0.002
	Single tree detection	0.012	0.005	0.011	0.021	0.001	0.001	0.001	0.001
	No vegetation	0.025	0.013	0.044	0.019	0.002	0.001	0.002	0.002

ROC curves corresponding to the scenarios with repetitions as presented in Table 4.8 are given in Figure 4.10. Significance of the differences between vegetation scenarios from Table 4.8 as given in Table 4.9.

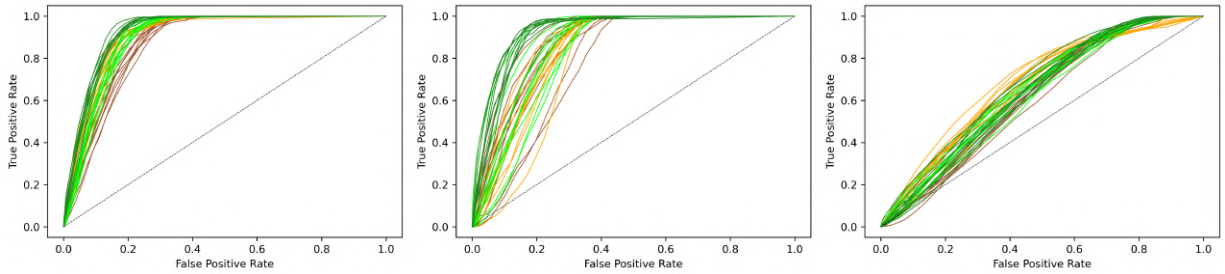

FIGURE 4.10: ROC curves of the 10 runs per vegetation scenarios from Table 4.8. Orange: Global uniform vegetation, light green: Forest area uniform vegetation, Dark green: Single tree detection, Brown: no vegetation. Corresponding study areas from left to right are: Eriz, Trub and StA.

TABLE 4.9: Significance of the difference in distribution between results of vegetation scenarios at a 90 and 99 % confidence level. Scenario names are shortened. Significance measured by Welch's t test (Welch, 1947). T (True) indicates a significant difference, F (False) indicates no significant difference. Three indicator per cell are related to the three study area, ordered as: Eriz, Trub, StA.

		99%			
		Global	Forest	Single	No
90%	Global	-	T,F,T	T,T,T	T,F,T
	Forest	T,F,T	-	F,T,F	T,F,F
	Single	T,T,T	T,T,F	-	T,T,F
	No	T,F,T	T,F,T	T,T,T	-

4.5 Discussion

It is important to point out that the inventory to which the model performance is calibrated plays a key role in all the results discussed below. The inventory was obtained after triggering rainfall events, for which the precipitation intensity, duration and the spatial distribution are not known precisely. Despite this shortcoming, the inventory represents a unique source of information and the spatial localisation of the landslides can be assumed to be of high quality. Below, we discuss the model behavior as a function of the different model parameter groups and the performance of the model and give directions for future research.

4.5.1 Soil parameters

The best performing parameter sets show high values for the soil thickness for all study areas (by comparing the values of Table 4.7 and Table 4.6). The qualitative sensitivity analysis (Figure 4.6) also shows that the highest unstable ratios are obtained for highest soil thicknesses; this indicates that a certain minimum soil thickness is required for landslide triggering, which is in line with previous findings by D'Odorico and Fagherazzi (2003) and by Iida (1999). In these studies, soil thickness is noted as the conditional factor for landslide triggering along with precipitation intensity and duration. The best performing parameter sets display cohesion values with a clear tendency to low values for all three study areas (Figure 4.6, Supplementary Material 10.4, 10.2), which suggests that the observed landslides can only be reproduced with low soil cohesion for all case studies. The mean angle of internal friction appears to show consistency for a low value (Table 4.7). The sensitivity of the AUC and unstable ratio on the angle of internal friction, however, appears to be small (Figure 4.6 and Figure 4.5).

4.5.2 Hydrological parameters

Soil transmissivity showed considerable sensitivity to the AUC (Figure 4.5) and the values are consistently high for all three case studies for the parameter range (Figure 4.7), which is a hint that a correct estimation of soil transmissivity is paramount for a reliable estimate of shallow landslide occurrence. Regarding precipitation intensity, we see variability between the best values for the three case studies and minor univariate sensitivity of the model performance or the model output (ratio of unstable landslides). The application of the TOPOG approach has the major shortcoming that it assumes a groundwater gradient parallel to the surface gradient. It has been shown in the past that this assumption decreases the accuracy of water content simulations as compared to distributed dynamic hydrological models (Grabs et al., 2009). However, as discussed earlier, it has also been shown in the past that macropore flow is omnipresent in landslide

triggering and SlideforMAP has been parameterized assuming an important role of macropore flow. In macropore-driven systems, steady-state groundwater flow can be reached (see Introduction), which implies that the TOPOG assumption holds well in this case. Due to the lack of detailed meteorological data, the precipitation intensity and duration is unknown. This makes computation on the exact pore pressure during the landslide event impossible. The precipitation intensity / transmissivity ratio (I/T) is assumed to include both precipitation intensity and transmissivity sensitivity. This is reflected in Figure 4.5 and Figure 4.6. The calibrated values for I/T ratio and subsequent pore pressure computation should be regarded as a measure for landslide propensity. In the landslide inventory underlying the study here, the dominant soil types are GM (silty gravel), GC (clayey gravel) and CL (low plasticity clayey silt); accordingly. Due to large pore size, we can assume that the TOPOG assumptions are valid for a wide range of the domain (for GM and GC soil type), even if it probably holds less well for the CL soil types.

4.5.3 Vegetation

A key aspect of the model is the use of single tree detection to parameterize vegetation, a method that was previously found by Menk et al. (2017) to be reliable to detect single trees and derive their DBH's from the detected tree heights for sloped forests. As mentioned in section 4.3.2, we found for the selected case studies that single tree detection provides the best results in terms of correct number of trees counted if applied on a 1 m resolution DSM with a 3 cell kernel Gaussian filter. This is in line with the results of Menk et al. (2017) who found in a similar scenario-testing approach that a 1 m resolution DSM with no Gaussian correction provided the most accurate results, noting, however, that the difference in performance between these two methods (with and without Gaussian filter) is small. In SlideforMAP, we do not only consider basal but also lateral root reinforcement. This is unique for shallow landslide probability models. As shown in the sensitivity analysis (Figure 4.6), RR_{max} has a clear effect on the ratio of unstable landslides, with low values leading to high ratios. In the SlideforMAP workflow and calibration, a fixed relationship between the lateral and the basal root reinforcement is assumed, accordingly, the model sensitivity cannot be attributed to R_{lat} or R_{bas}. Mobilization of the lateral root reinforcement in the SlideforMAP workflow is independent of time and not countered by passive earth pressure. A shortcoming in this parameterization of the effect of vegetation is the assumption of uniform forest structure and a uniform tree species (beech) within a landslide area. The field recordings in the StA area of Moos et al. (2016) show that the forest consists mainly of Norway spruce. For the Trub and Eriz area, visual interpretation of aerial photos allowed us to identify mixed forests with Norway spruce and beech. The latter are known for having a high root reinforcement and therefore the beech assumption will overestimate both the lateral and the basal root reinforcement (Gehring et al., 2019). Vegetation weight shows no clear relation to both the AUC and the unstable ratio (Figure 4.5, Figure 4.6). However, this does not mean that vegetation weight does not influence the response variables. The relationship could depend on other parameters and therefore obscured (Bárdossy, 2007). In contrast to the soil and hydrological parameters, vegetation configures both the magnitude and the spatial pattern of the probability. Vegetation can be modified by land management practices with relative ease (Amishev et al., 2014) and is therefore of ultimate importance in shallow landslide mitigation.

4.5.4 Implementation of the mechanical effects of vegetation

In Table 4.8 it can be seen that the vegetation scenario has a considerable impact on the modelled unstable ratio for all study areas. Unstable ratio is lowest in the single tree detection scenario for the Trub study area. In the StA and Eriz study area, it is the lowest for the uniform vegetation. We assume this is caused by the low calibrated uniform root reinforcement in Trub and a higher value in the other study areas (Table 4.7). Both single-tree detection and uniform vegetation are

determined to have the ability to decrease instability. From a practical perspective vegetating parts of a study area is more realistic than uniformly vegetating the whole area. Influence of the vegetation scenario on the AUC is present, with an absolute mean increase of 0.023 AUC points between single tree detection and uniform vegetation and to forest uniform vegetation and unvegetated of 0.030 and 0.046 AUC points respectively (Table 4.8). Additionally the performance improvement can be described relatively in terms of percentage of extra AUC gained (AUC range from 0.5 - 1.0) between two vegetation scenarios. For the overall single tree detection compared to uniform vegetation, forest uniform vegetation and no vegetation this is 8%, 10% and 16% respectively. Results in Table 4.9 show that the differences are relevant for the uniform scenario in all study areas at both a 90% and 99% confidence level. The difference between single tree detection and no vegetation is relevant for all confidence levels and study areas except for the StA study area at 99% confidence. The difference between single tree detection and forest uniform is more ambiguous, with notably a significant difference at a 90% confidence level in the Trub and Eriz study area. This is likely related to the forest uniform scenario being most close to single tree detection in the distribution of root reinforcement of all scenarios.

In both Eriz and Trub, the single tree detection is the best performing scenario. Our overall finding that the model output is sensitive to the vegetation scenario and gives second lowest values in unstable ratio and highest values in AUC for single-tree detection. We argue that even though the model is calibrated on a global uniform vegetation scenario (Table 4.7) and the single-tree detection gives a significantly better overall performance, single tree detection is more accurate in assessing shallow landslide susceptibility (Table 4.8 and Table 4.9). Adding to this explanation is that in these study areas, where slope angle is a highly predictive factor, even marginal gains in AUC due to vegetation are important and the result of extensive parameterization. Our analysis is in line with the findings of Roering et al. (2003), who state that single tree based modelling, including the tree dimensions, has the highest accuracy in the prediction of shallow landslides. Moreover, Vergani et al. (2014) state that a site specific estimation of vegetation and root extent is essential in the correct estimation of root reinforcement.

4.5.5 Model performance

As pointed out by Corominas et al. (2014), the absolute values of AUC are dependent on the characteristics of the study area. In larger areas, with low overall landslide activity, the AUC will overestimate the predictive performance. This most likely explains why the StA study area has a low overall AUC compared to Eriz and Trub (Table 4.8). In particular, StA study area shows a higher prevalence of steep slopes. The Trub and the Eriz study area show both relatively high AUC values, indicating high model performance, with very similar AUC values; this is in agreement with a similar occurrence of steep and gradual slopes in these areas. Another explanation for the discrepancy in model performance between the study areas could be the assumption that all trees are beech trees. This does not hold equally well for all three study areas. Based on visual inspection and on elevation, the mismatch between actual vegetation and this assumption is probably most pronounced in the StA area, where the dominant tree species appears to be Spruce. Though no published data is available, it can be estimated from the work of Moos et al. (2016) that the root reinforcement of a spruce forest is lower than that of a beech forest, but this cannot confirmed by our parameter analysis at this stage.

A comparison between the shallow landslide density (Table 4.2) and the calibrated unstable ratio (Table 4.7) shows moderate consistency. The Eriz and Trub study areas have a low unstable area corresponding to a low shallow landslide density. StA both has a higher landslide density and higher unstable ratio. From the consistency in Table 4.7 and the sensitivity analysis results of Figure 4.5, it can be concluded that the main configuration of the model lies in the parametrization

of the mean soil thickness, the mean cohesion and the I/T ratio. In addition, the vegetation scenario strongly influences the model performance and is of high influence on calculated shallow landslide probability (Table 4.8). Equifinality between the parameters in the qualitative sensitivity analysis is likely as it is very common in similar multi-parameter modelling (Beven & Binley, 1992). However, we believe, the sensitivity as observed in Figure 4.5 is valid and a qualitative indicator for important parameters in SlideforMAP. The calibrated optimal parameter set (Table 4.7) is still within realistic bounds as is the ranges for the sensitivity analysis. In addition, the calibrated combination of mean friction angle (26 - 34 °) and mean soil cohesion (1.75 - 4.29 kPa) are possible, according to Appendix Table 4.10. Finally, we would like to add here that the case study dependence of the used model performance measure is a limitation that typically occurs for all model performance measures that compare the model behavior to some reference model (Schaefli & Gupta, 2007) (the reference model for AUC is a random process). Accordingly, we cannot compare the performance of SlideforMAP to other published AUC values despite of the fact that values above 0.8 are considered as indicating good performance (e.g. Xu et al., 2012).

4.5.6 Comparison to other slope stability models

The main advantage of SlideforMAP to other models is the more realistic approach to implement root reinforcement. It includes a spatial distribution in both the basal and lateral root reinforcement and the focus on second stage of the activation phase in accordance with the Root Bundle Model as described in Gehring et al. (2019). Compared to previous slope stability models that include the effect of root reinforcement, SlideforMAP uses a more realistic implementation of root reinforcement based on recent knowledge of shallow landslides triggering mechanisms and root reinforcement activation (Cohen & Schwarz, 2017b; Schwarz et al., 2012; Schwarz et al., 2013). In particular, only part of the lateral root reinforcement under tension is considered for the force balance calculation. Moreover, the spatial distribution of root reinforcement as function of forest structure is included. The assumptions made in SlideforMAP allow a probabilistic calculation at regional scale that are not possible with more complex models such as SOSlope (Cohen & Schwarz, 2017a). In comparison to more simple models based on infinite slope calculations such as SINMAP and SHALSTAB (Montgomery & Dietrich, 1994; Pack et al., 1998), SlideforMAP considers the effect of lateral root reinforcement on landslide of different sizes. SINMAP with a homogeneous root reinforcement is comparable to our global uniform vegetation scenario (Table 4.8). A version of SINMAP with no root strength is comparable to our no vegetation scenario. When no vegetation data is available or complexity is not desired, these are valid option to assess shallow landslide susceptibility in a probabilistic way.

A hydrological and slope stability model identical to SlideforMAP is applied in Montgomery et al. (2000), which is used to estimate sediment yield resulting from forest clearing. This is comparable to our global uniform vegetation scenario as well. Their result of a high significance of root reinforcement is in line with our findings. Other differences in the model approach are the assumption of fixed landslide dimensions, including soil thickness. In addition, the root reinforcement is assumed to act around the full perimeter of the landslide. In its approach, SlideforMAP shares many similarities with PRIMULA, as developed by Cislaghi et al. (2018), which applies a probabilistic approach and a spatially distributed root reinforcement as well. the PRIMULA root reinforcement is based on a stand scale approach rather than single-tree detection though. The AUC values in this paper are higher, but that could be the result of different characteristics of the study areas and our parameter optimization by the qualitative sensitivity analysis. Other differences as compared to PRIMULA are their assumption of lateral root reinforcement along the entire landslide perimeter, the inclusion of lateral soil cohesion simultaneously with lateral root cohesion, the assumption of rectangular shaped landslides rather than elliptical ones and a different landslide surface area distribution. 3DTLE (Hess et al., 2017) is a

deterministic landslide susceptibility model with a similar detailed spatially heterogeneous inclusion of root reinforcement. Differences are their deterministic approach and the assumption of a simultaneous maximum of tension and compression forces.

4.5.7 Future research

SlideforMAP uses a relatively simple hydrological module to estimate soil saturation. The used TOPOG approach could be improved and multiple papers have presented simple to more advanced rewriting of formulas (e.g. Beven & Freer, 2001; Blazkova et al., 2002). Common denominator is the inclusion of time dependency, since the stationary flow assumption rarely, if ever, holds in nature. This time dependency is a solution to simulate a different response to a precipitation event at different locations within a study area. Future work could also focus on improving the vegetation module by including different tree species (those that are often used in protection forest) in the parametrization of lateral root reinforcement (equation 4.10). For practical application of SlideforMAP we have not found a specific lower boundary in landslide density, to still generate reliable results. More specific testing on this would be useful for future application of SlideforMAP. A comparison between SlideforMAP and SHALSTAB and/or SINMAP would be interesting. It can validate whether the uniform vegetation scenario in SlideforMAP produces similar results to these models in terms of shallow landslide probability. Finally doing a validation over study areas with a larger shallow landslide inventory would be a vital procedure to further analyze the SlideforMAP model.

4.6 Conclusions

In this paper, we present a probabilistic model to assess shallow landslide (landslides with a scar thickness < 2 m) probability. The main motivation to develop yet another model is to provide a detailed inclusion of the influence of root reinforcement. Its application is illustrated based on three mid-elevation case studies from Switzerland, for which a detail landslide inventory is available. The model has a total of 21 parameters, of which 12 are calibrated using the AUC of the Receiver Operator Curve as performance measure to identify the best parameter set among a large set generated using Latin hyper cube sampling. The AUC maximum values for the three study areas vary between 0.64 and 0.93 under a single tree detection vegetation scenario, which reflects an overall good model performance. Our model parameter analysis has shown that soil thickness, precipitation intensity to transmissivity ratio and soil cohesion, are the key parameters to predict slope stability in the studied mountainous regions. A major focus of the presented work was the assessment of the model's ability to study scenarios of vegetation distribution. Comparison of different scenarios ranging from uniform to single-tree detection-based vegetation clearly showed that the model output, in terms of shallow landslide probability, is sensitive to the spatial distribution of vegetation. Additionally, in two of our three study areas, the single-tree detection scenario provides significantly (Welch's t test confidence > 99 %) higher AUC values. Accordingly, the model is fit for future scenario analysis, including e.g. different protection forest management scenarios. In fact, a single-tree scale model parameterization provides the opportunity to run hypothetical vegetation scenarios reflecting on small scale managements strategies or disturbances. Future improvements in the hydrological approach, concerning a more catchment based approach to compute saturation degree, could likely further improve the performance of SlideforMAP.

Appendix

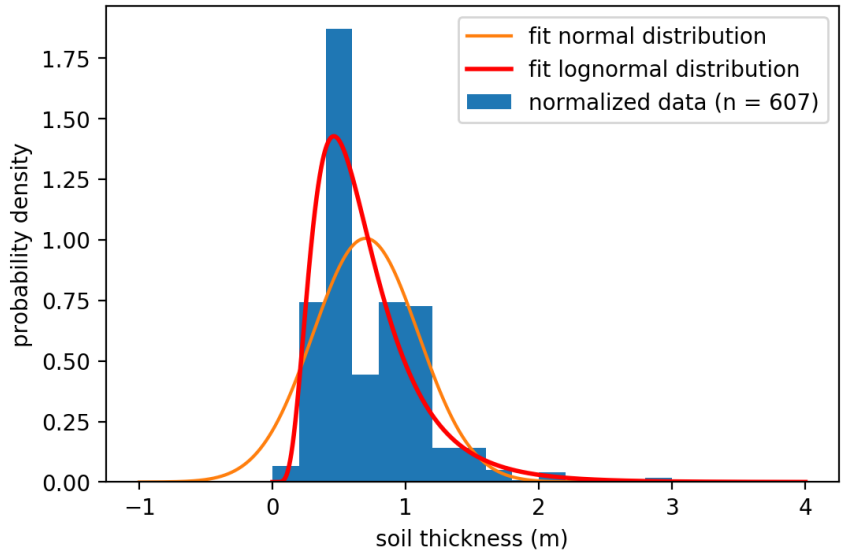

FIGURE 4.11: Plot of the probability density of the soil thickness data from the BAFU dataset as used in this paper. The best fit is given of a normal and a log-normal distribution. The mean square errors are 0.096 and 0.053 for the normal and log-normal fit respectively.

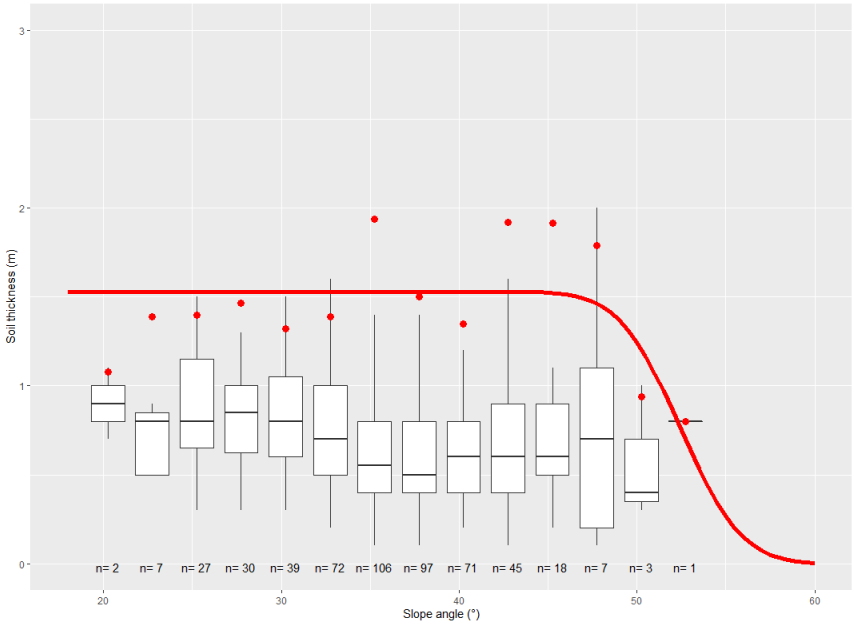

FIGURE 4.12: Shallow landslide Slope soil thickness relationship as used in this research. Boxplots are classes with a width of 2.5 Slope units. The red dots are the 95th percentile per class. The red line is the fit of equation 4.7 to the 95th percentiles.

TABLE 4.10: The hybrid table for the soil cohesion and angle of internal friction for the relevant set of USCS soil classes. Derived from laboratory experiments (Dysli & Rybisar, 1992; VSS-Kommission, 1998) and combined in this research to exclude values that seemed unrealistic.

USCS soil class	**Mean soil cohesion**	**Std. dev. soil cohesion**	**Mean friction angle**	**Std. dev. friction angle**
SM	0	0	34.5	5.0
CL-ML	0.4	1.3	32.7	4.8
GM	0.0	0.0	35.0	5.0
GC-GM	5.0	5.0	33.0	3.0
CL	6.2	11.3	27.1	5.2
OL	2.5	5.0	32.8	2.2
GC	20.0	52.9	31.4	3.6

Acknowledgements

We thank the STEC (Smarter Targeting of Erosion Control) project by the Ministry of Business, Innovation and Employment of New Zealand for the financial support. In addition we would like to thank the two anonymous reviewers and a community review by David Milledge. Their contribution was of great improvement to the quality of this paper.

5 Application and validation of SlideforMAP

Full title:

Application and validation of SlideforMAP for assessing shallow landslide probability in New Zealand hill country

Feiko Bernard van Zadelhoff*[1,2], Bettina Schaefli[2], Chris Phillips[4], Massimiliano Schwarz[1,3]

Ecological engineering (Elsevier journal)
Submitted, under review, preprint DOI: 10.5281/zenodo.7615348

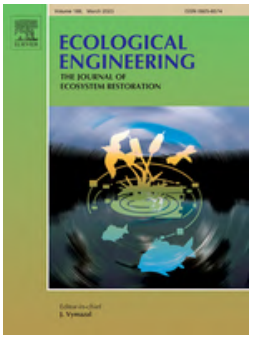

Submitted: 27 January 2023
https://zenodo.org/record/7615348

This manuscript builds on the previous paper, where SlideforMAP is introduced. It presents multiple improvements in the hydrological module by including temporal variabiliy in reaction to a rainfall event dependent on topography and vegetation presence. These improvements are applied and validated in a silvopastoral system in New Zealand.

[1] Bern University of Applied Sciences - HAFL, Länggasse 85, 3052, Zollikofen, Switzerland
[2] Institute of Geography (GIUB) & Oeschger Centre for Climate Change Research (OCCR), University of Bern, 3012 Bern, Switzerland
[3] Int. ecorisQ Association, P.O. Box 2348, 1211 Geneva 2, Switzerland
[4] Manaaki Whenua - Landcare Research, Lincoln, New Zealand

Abstract

Shallow landslides are an important erosion process in New Zealand hill country. To mitigate this, silvopastoral land use is often adopted. In such an environment, the correct placement of trees can improve slope stability. In this paper, we demonstrate the application of a shallow landslide model to identify optimal patterns of tree location. The model, SlideforMAP, is specifically designed to assess single tree location. We use an extended version of SlideforMAP with a dynamic computation of the soil saturation by a macropore flow rainfall-runoff computation and a runoff rate coefficient for subsurface flow. The model is calibrated and validated for two New Zealand locations using observed data from a total of 578 shallow landslides identified in a 2010 inventory, partly related to an extreme precipitation event that occurred in March 2005. Single tree data containing tree location, height and species is included. The calibrated model parameters resulted in deep soils with low soil cohesion, low friction angle and high saturated conductivity. This indicates silt dominated soils, which is in agreement with available soil maps. Slight but inconsistent improvements in the accuracy are gained from the improved hydrological approach. Differences between the improvement and the original SlideforMAP are attributed to the non-steady-state approximation of sub-subsurface flow, rather than to the vegetation-influenced runoff rate coefficient. The optimized tree location pattern suggests that effective shallow landslide prevention in our study areas obtained by trees on slopes between 20° and 30° and under a lateral flux greater than 0.001 m^2/s, i.e. mid-slope areas. SlideforMAP can help to visualize these areas more precisely and considering local soil conditions. This is a support tool for landowners and practitioners to optimally reduce erosion while maintaining productivity.

keywords: shallow landslide probability, probabilistic modelling, catchment-scale, silvopastoral systems, runoff coefficient

5.1 Introduction

Shallow landslides are a direct hazard for humans and infrastructures. Additionally, they cause indirect effects on ecosystem services due to the loss of fertile soil and the mobilisation of sediments (Douglas et al., 2013). This is a concern in New Zealand, where past deforestation has caused a noticeable increase in shallow landslide activity that increased the volume of mobilised sediments at catchment scale and induced surface sheet and rill erosion (McIvor et al., 2011). A study in New Zealand hill country, an area with steep sloped pastoral farming, showed that approximately 15% of sediment is mobilised and recruited from rainfall-triggered shallow landslides (Reid & Page, 2003). This erosion causes unwanted effects ranging from land degradation to water quality reduction (McIvor et al., 2011; Reid & Page, 2003). An often applied measure to prevent shallow landsliding in New Zealand is the space-planting of trees, also known as silvopastoralism. This method enables erosion mitigation while maintaining pasture production (Mackay-Smith et al., 2021). Although this approach is applied in practice, research gaps remain concerning the effectiveness of silvopastoral systems (Mackay-Smith et al., 2021; Spiekermann et al., 2021). Shallow landslide probability can be modelled with different types of approaches and models, ranging from local to global models and with a probabilistic, deterministic or statistical approach (Murgia et al., 2022). Such models are essential for a holistic evaluation of land uses in the context of shallow landslide risk assessment (Mackay-Smith et al., 2021) and for the prioritisation of bio-engineering measures at regional scale.

A key challenge for shallow landslide modelling is the quantification of hydrological processes and involved vegetation processes, which are fundamental to quantify the spatial distribution

of shallow landslide probability at hillslope to catchment scale. On the local scale, root reinforcement dominates this spatial distribution (Cohen & Schwarz, 2017b; Schwarz, Lehmann, et al., 2010; Schwarz, Preti, et al., 2010; Vergani et al., 2017). A number of challenges, related to data availability, scale and representation of vegetation management exist in modelling vegetation influence on shallow landsliding (Phillips et al., 2021) and accordingly, stakeholders often resort to simple models.

The influence of trees on shallow landslide probability has been discussed in several studies (e.g. Masi et al., 2021; Murgia et al., 2022). These studies generally consider trees as slope stabilizing actors (Schmaltz et al., 2017; Stokes et al., 2014; van Zadelhoff et al., 2022). However, differences in root reinforcement between tree species, tree age and tree location are often poorly understood and insufficiently included in slope stability models (Masi et al., 2021; Stokes et al., 2014). The inclusion of these local differences was shown to improve the reliability of slope stability models (Rickli & Graf, 2009). This improvement resulted from the inclusion of a spatio-temporal dynamic forest as compared to spatially uniform values of vegetation effect (Schmaltz et al., 2019). In addition, the work of van Zadelhoff et al. (2022) concluded that applying a spatially heterogeneous root reinforcement model consistently improved shallow landslide probability prediction. They used a state-of-the-art probabilistic landslide model, SlideforMAP, which was specifically developed to consider in detail the effect of tree root reinforcement over large regions (1-100 km^2), based on the detection of single trees.

One of the most challenging issues in the application of such event-based probabilistic models is the implementation of hydrological processes. Most of the coupled hydrological-shallow landslides models (e.g. TOPOG (O'Loughlin, 1986)) use a topographic-index approach (Beven & Kirkby, 1979) to model lateral subsurface flow. In this approach, the assumption is made that catchment-scale water storage is spatially "configured as if it was at steady state" (Beven et al., 2020). Such topographic-index approaches can relate average catchment-scale moisture conditions to a spatial, topography-based pattern of likely saturated areas, without necessarily providing correct local moisture conditions (Beven, 1997; Moore & Thompson, 1996). Apart from the often incorrect assumption that instantaneous catchment-scale moisture patterns are configured as for steady-state storage conditions, preferential flow, bedrock fractures, piping etc. (Blazkova et al., 2002) provide limitations. Shallow landslide susceptibility models using the topographic-index approach in their hydrological module generally mention the limitations of the approach, but argue that the benefits of the simplification (lower data and/or assumption requirements, faster computation enabling focus on larger areas) outweigh the shortcomings (Buytaert et al., 2008).

Besides the TOPOG approach, the rainfall-runoff modelling literature offers a few alternative methods to parsimoniously relate runoff generation to rainfall input and catchment physiographic conditions, i.e., to obtain estimates of runoff-available water without going through a full input-output streamflow model. One family of methods uses so-called runoff curves (Sitterson et al., 2018) to directly estimate the fraction of rainfall that becomes runoff from land use and rainfall properties. The empirical SCS curve number (CN) is the most well known of these methods (Rallison, 1980): it relates runoff coefficients to land use and soil type. A storage parameter provides temporal variability in the CN runoff coefficient. This method has however been developed for extreme events, namely for annual floods. We adopt here another runoff curve method, developed originally for Switzerland by Scherrer and Naef (2003) and Antonetti et al. (2017). These curves relate runoff coefficients to rainfall amounts and dominant runoff processes that are derived from land use and soil depth. There are only few other studies available that attempt a similar classification of dominant runoff processes (such as Hortonian overland flow or lateral subsurface flow) as a function of landscape characteristics, e.g. the work of Savenije

(2010), which uses the Height Above Nearest Drainage, HAND, as classifier.

In this paper, we analyze the performance of different hydrological assumptions in SlideforMAP. We choose SlideforMAP due to its assumed compatibility for silvopastoral systems, where modelling the influence on the single trees is paramount. We compare three different versions of the model. Firstly, the original version, referred to as SfM original. Secondly, the new improved version that includes a runoff coefficient, referred here as SfM (without extension of the name). Additionally this version overcomes the topographic-index approach by enabling a dynamic lateral groundwater flux approach. Thirdly, we also test a hybrid version with dynamical lateral groundwater flux but no runoff coefficient, which is called SfM hybrid. This hybrid version is tested to isolate the influence of the runoff coefficient for comparison. The main aim of this research is to analyze the change in model performance of the improved version. We test the improvements by independent calibration and validation of generated shallow landslide probability maps. The selected study areas are two shallow landslide-prone study areas in New Zealand hill country, dominated by silvopastoral land use.

5.2 Methods

5.2.1 SlideforMAP

The shallow landslide probability model SlideforMAP (van Zadelhoff et al., 2022) is based on the calculation of the Safety Factor (SF) for a high number (in the order of $10^5 - 10^7$, depending on study area size) of randomly located landslides (RLs, singular: RL) within a gridded study area domain and then assessing the landslide probability by taking the fraction of the amount of RLs with a SF < 1 to the total of the generated RLs overlapping a raster cell. Each RL has a random location and a surface area drawn from a calibrated inverse gamma distribution, with an assumed horizontally projected circular shape. For each RL, soil parameters are drawn from normal distributions and spatially variable parameters (slope angle, contributing area and root reinforcement) are obtained by averaging corresponding properties over the RL area. The SF for each RL is calculated based on a three dimensional force balance. The probabilistic approach has the advantage to explicitly incorporate the uncertainty in parameters values used for the SF calculations. Each single RL is indexed in the following equations with l, and the grids cells located within each RL are indexed with i.

5.2.2 General principle of the new hydrological module

The original version of SlideforMAP (van Zadelhoff et al., 2022), uses a steady-state assumption of runoff given a constant precipitation input for the calculation of the pore water pressure. To investigate the effect of temporal rainfall input variation and of related moisture conditions, we implemented a new hydrological module. The new approach is based on runoff coefficients that depend on cumulative precipitation and furthermore assumes that lateral runoff has spatially uniform mean velocity depending only on rainfall intensity. No distinction is made between surface runoff and subsurface runoff. Figure 5.1 shows an overview of the improved hydrological module and further details are given in the corresponding sections below.

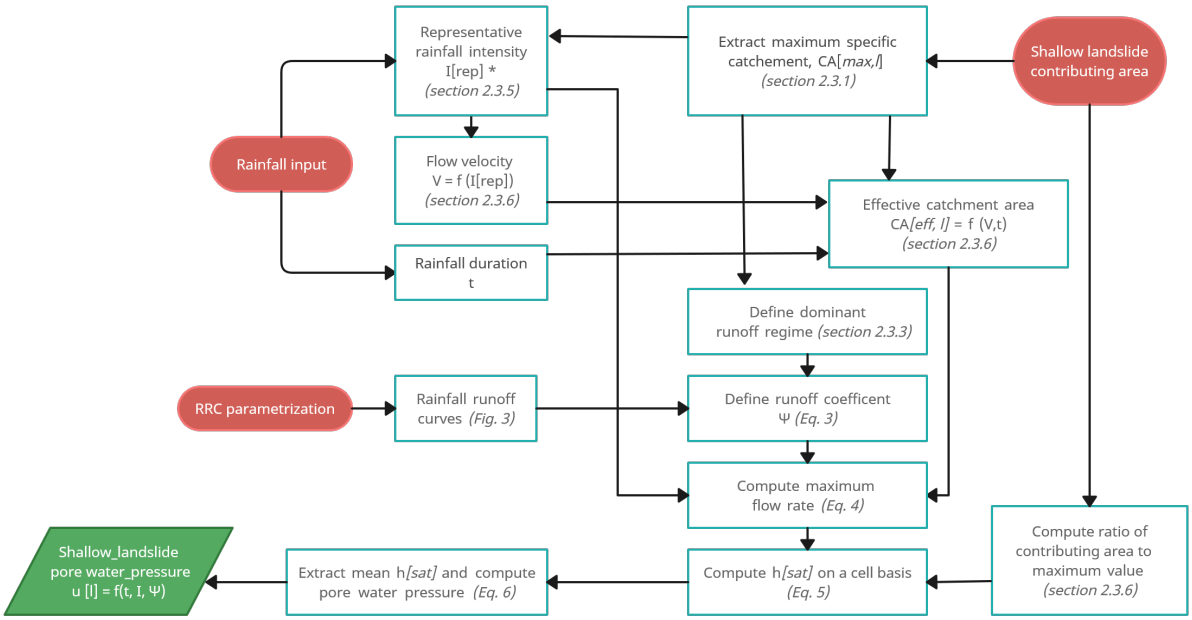

FIGURE 5.1: Flowchart of the new hydrological module; the outcome is computed pore pressure, which as outcome that is used for the slope stability computation. *Optional. The computation of I_{rep} is only relevant in case of on-steady rainfall input.

5.2.3 From rainfall to lateral sub-surface flow

5.2.3.1 Computation of maximum runoff-contributing area

The spatial extent of the contributing area for each RL is computed by the D8 - flow raster algorithm (Callaway et al., 2003) using Pysheds (Bartos, 2020) on a raster resolution of 5 m. Within a RL of index l, the raster cell with the highest value of contributing area ($CA_{max,l}$) is selected for the computation of the maximum lateral runoff contributing to the build up of the pore water pressure. This raster cell is indexed i_{max}. The $CA_{max,l}$ is used as a mask to extract properties such as mean slope inclination and mean root reinforcement within the contributing area. Based on the D8 - flow raster, the distance of each raster cell within the contributing area j to i_{max} is computed. The concept of the $CA_{max,l}$ is illustrated in Figure 5.2.

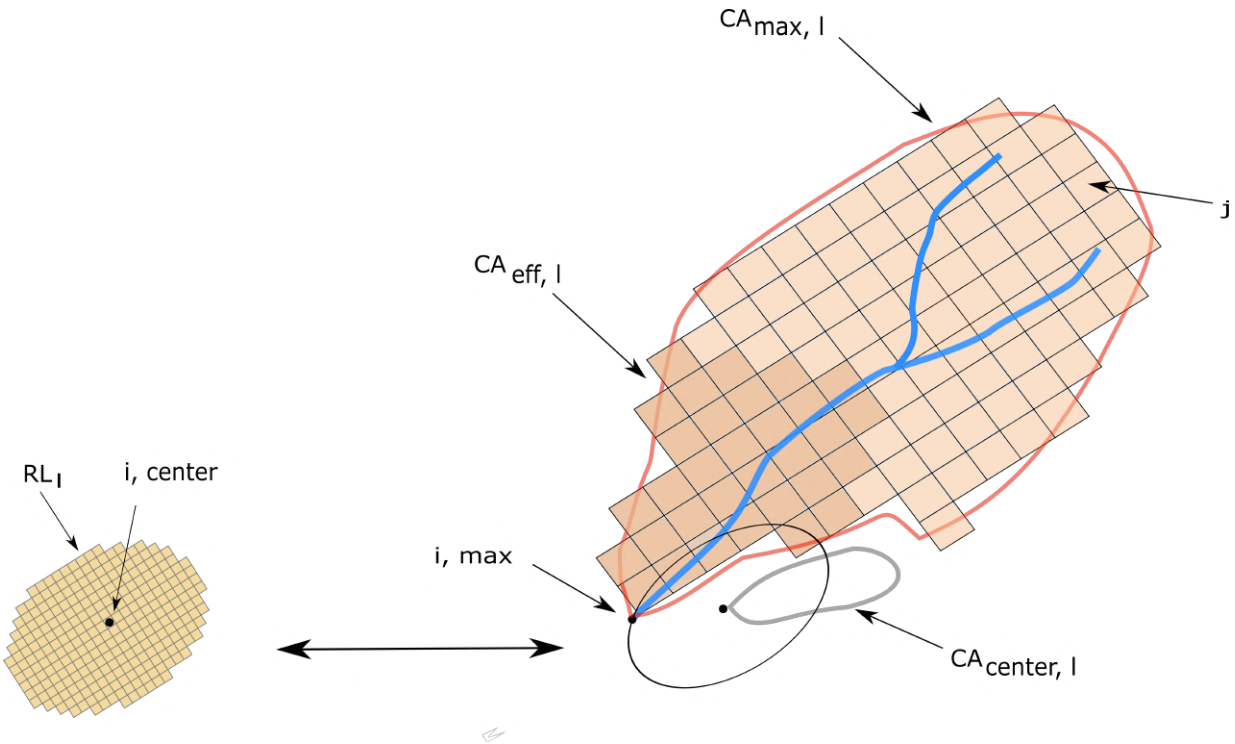

FIGURE 5.2: Schematic display of a RL with its hydrologically contributing area to its centre point in red and the maximum contributing area, $CA_{max,l}$, in orange. Grid resolution in the RL (2 m), with cells i and the contributing area (5 m), with cells j, is presented conceptually. The orange shaded area within the maximum contributing area of the RL highlights the effective contributing area, $CA_{eff,l}$, which is a function of precipitation intensity and duration (see section 5.2.3.6)

5.2.3.2 Interception

Tree interception is subtracted from the cumulative rainfall for each rainfall event, for each raster cell. A grid cell is assumed covered by foliage when $RR_{max} > 0$. For raster cells with foliage cover, cumulative interception is computed using Equation 5.1 (Aston, 1979).

$$C_{int} = C_{max}(1 - \exp(-kP/C_{max})), \tag{5.1}$$

where C_{int} [mm] is the interception storage and C_{max} the maximum interception storage capacity. P [mm] is the total rainfall and k is a shape parameter [-], which moderates the degree of water detention. C_{max} and k are arbitrarily assumed to be 4 mm (well within the 2.2 to 8.3 mm range for C_{max} measured on tree basis by Herwitz (1985).) and 0.03 respectively. All intercepted water is assumed to re-evaporate immediately after the rainfall event and to be lost from the system.

5.2.3.3 Runoff coefficient

After correction for interception, we estimate for each rainfall event a runoff coefficient at the scale of the larger hydrological contributing area, $CA_{max,l}$ of the RL l. This runoff coefficient is the fraction of rainfall that results in lateral water mobilization during a rainfall event (surface runoff and lateral subsurface flow). The rest of the rainfall-event water is stored in the soil or percolates to deeper layers. Accordingly, the runoff coefficient is linked to the degree of saturation of the soil, which is important in the computation of slope stability.

The runoff coefficient depends on rainfall event structure (intensity, duration) and on soil properties. Here we use the method suggested by Antonetti et al. (2017) to relate hillslope-scale runoff coefficients to cumulative rainfall of single rainfall events and to soil properties. The runoff coefficient is calculated for each raster cell RL l from the land use and rainfall properties in its $CA_{\max,l}$. Their method uses rainfall-runoff curves (RRCs) that relate runoff coefficients to cumulative rainfall for five different runoff types that regroup one or several dominant hydrological runoff processes (Table 5.1). The method was developed based on sprinkler experiments and expert knowledge. It does not include antecedent soil moisture.

TABLE 5.1: Runoff types approach of Antonetti et al. (2017); HOF = Hortonian overland flow, SOF = Saturation-excess overland flow, SSF = sub-surface flow, DP = Deep percolation. Runoff Types are sub-classified by numbers.

Runoff Type	**Dominant process**	**Response time**	**Soil depth**
1	HOF1, HOF2, SOF1	Immediate	Very shallow soils/exposed bedrocks
2	SOF2, SSF1	Slightly delayed	Shallow soils
3	SSF2	Delayed	Moderately deep soils
4	SOF3, SSF3	Strongly delayed	Deep soil
5	DP	Not contributing	Very deep soils, wetlands

The RRCs used here (Antonetti et al., 2017) are based on previous research in Switzerland (VAW, 1993) (Figure 5.3). We approximate their shape by fitting the general function:

$$\psi(P) = a + b \cdot \log_{10}(P - S), P > 0; S < P, \tag{5.2}$$

where ψ is the runoff coefficient, P [mm] is the total precipitation, S [mm] is critical rainfall amount before runoff starts , a and b are shape and scale parameters. Both the cumulative and the derived instantaneous version (runoff rate coefficient) of the RRCs are described with Equation 5.2. For the computation of the maximum pore water pressure, the instantaneous version is used. The use of these RRCs requires the determination of the runoff types. For Switzerland, a decision scheme to assign a runoff type to an area was proposed by (Scherrer & Naef, 2003). This decision scheme is based on soil type, slope angle, presence of macropores, soil depth, matrix permeability and soil water content before the rainfall event. This decision scheme and resulting classification has been developed for meadows and is not directly applicable to forested areas. However, it does consider the effects due to the presence of macropores and lateral preferential flow paths, which can be assumed to be influenced by the presence of tree roots. The presence of macropores can be assumed to increase the effective hydraulic conductivity in the subsurface and thus favour lateral flow, thereby reducing saturation-excess overland flow. An extensive adaptation of this decision scheme for forest types exists (Markart et al., 2011), but requires estimates for many input parameters. Based on previous research, we develop our own concise version for runoff type determination, including the effect due to roots. Firstly, a slope threshold is used to define areas with exposed bedrock, automatically classifying them as Runoff Type 1. We set this threshold to 50°. We assume all meadow and pasture areas have a slightly delayed runoff type (Runoff Type 2), which we call hereafter RT_{base}. Soil thickness is assumed to influence RT_{base}, as thicker soils can store more rainfall. The original method distinguishes deep and shallow soils and the limit between them is set to 1 m (Scherrer & Naef, 2003)), which we also adopt.

5.2.3.4 Accounting for macropores

The presence of vegetation in the contributing area is first of all taken into account via interception (section 5.2.3.2), but additionally also via the effect of roots on preferential flows in macropores. We introduce the notation of RT_{min}, which is the runoff type yielding the lowest possible runoff amount for a given soil thickness. For shallow soil, RT_{min} is the delayed runoff (Runoff Type 3), for deep soils, RT_{min} is the strongly delayed flow (Runoff Type 4). We assume that the minimum runoff rate coefficient is affected by the presence of vegetation due to an increase in macropore flow. We model this effect of macropores by scaling the runoff rate coefficient as a function of lateral root reinforcement (as proxy variable), which is a parameter that is used in the calculation of the Safety Factor, SF (see section 5.2.1).

For this runoff rate coefficient scaling, we define a fractional root reinforcement factor, called $F_{RR,l}$. $F_{RR,l}$ obtained as a fraction of the mean value of root reinforcement within the $CA_{\max,l}$ and an assumed reference value of maximum lateral root reinforcement $RR_{\max}$, which is set to 5 kN/m $F_{RR,l}$. The scaling of the runoff rate coefficient $\psi_{l,p}$ for a landslide RL and a cumulative precipitation P is then obtained as follows:

$$\psi_{l,p} = \psi_{RT_{min},p} + (\psi_{RT_{base},p} - \psi_{RT_{min},p}) \cdot F_{RR,l},\ 0 < \psi_l < 1 \tag{5.3}$$

where $\psi_{RT_{base},p}$ is the runoff rate coefficient corresponding to the base runoff type for landslide RL and cumulative precipitation P and $\psi_{RT_{min},p}$ is the corresponding minimum runoff rate coefficient. An example of the results of the possible runoff rate coefficients, assuming various $F_{RR,l}$ values, calculated with Equation 5.3 are shown in Figure 5.3. We assume that any Hortonian overland runoff contributes to the RL-scale runoff generation, re-infiltrates or connect to the macropores network within the RL and contributes to lateral subsurface flow and thus to pore water pressure.

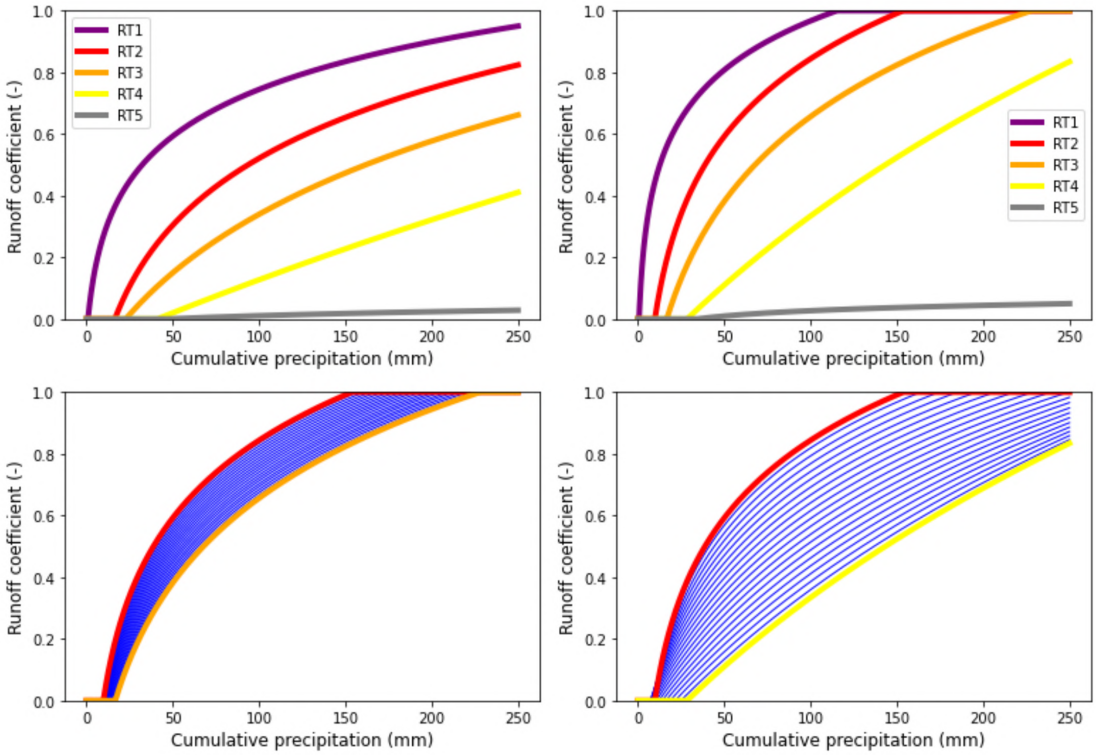

FIGURE 5.3: Rainfall-runoff curves according to the Runoff Types of Table 5.1. Top row shows the cumulative version of Antonetti et al. (2017) (left) and the corresponding derived instantaneous version (right). Bottom row shows our cumulative curves for shallow soils (thickness < 1 m), left, and for deep soils (thickness $>$ 1 m), right. For this the Scherrer and Naef (2003) soil thickness threshold was used. The blue curves in the bottom row show RRCs for 20 evenly distributed fractions of maximum root reinforcement.

The RRCs represent a simple tool to link rainfall and runoff. They have a solid theoretical basis as discussed in the work of Antonetti et al. (2017). Conceptually, the presence of macropores enhances the infiltration. In the first period of a rainfall event, this leads to a vertical preferential flow, which may saturate the lower horizons of the soil profile along a potential interface between the high permeability soil (with macropores) and a deeper low permeability horizons/bedrock. Once macropores are hydrologically connected, runoff is dominated by lateral surface or subsurface flow. These distinct phases of the runoff formation are the theoretical background for the RRCs in Figure 5.3.

5.2.3.5 Representative mean rainfall intensity

Applying the mean rainfall intensity from a rainfall event could lead to an underestimation of the maximum pore water pressure that in reality is more related to the peak intensity of a rainfall event. An example of such an underestimation is given in the Supplementary Material (Supp. material, Figure 10.6) where we applied a lateral flux example with an observed rainfall event using the hydrological module of SfM. To overcome this issue, we correct the mean precipitation intensity of an event by a correction factor (I_{corr}) to obtain a representative peak rainfall intensity (I_{rep}). This correction factor is the difference between the maximum soil water flux based on a dynamic precipitation intensity and the one based on a constant mean precipitation intensity. I_{corr} is assumed to be dependent on the following factors: contributing area extent, contributing

area elongation, macropore flow velocity, precipitation event duration and precipitation intensity variability in time.

We compute I_{corr} for a random 5% subset (for computational reasons) of the contributing areas in both of our study areas, with the inclusion of our runoff rate coefficient methodology. The results are plotted versus the contributing area size, which we expect to be the best and most practical predictor of this ratio (see Results section, Figure 5.8). The resulting relationship of I_{corr} to $CA_{\text{max},l}$ is then used to connect I_{corr} and $CA_{max,l}$ for all contributing areas. This method is applied to all model versions.

5.2.3.6 Effective contributing area

To compute the effective contributing area $CA_{\text{eff},l}$ from the maximum contributing area $CA_{\text{max},l}$, an estimation of lateral flow velocity is essential. We assume that this lateral flow velocity is dominated by the contribution of preferential macropore flow. Typical macropore flow velocity varies between 10^{-1} and 10^{-5} (Gao et al., 2018), with a geometric mean of $1.08 * 10^{-3}$ m/s. This can be 2-3 orders of magnitude higher than soil matrix mean flow velocity. Findings similar to this are reported in the work of Beven and Germann (2013).

Gao et al. (2018) reviewed and analyzed the relationship between precipitation intensity and macropore flow velocity in 76 global studies over different soils and land cover. We use the resulting linear relationship for all data points to define macropore velocity (V_{mac}) as a function of macropore diameter and rainfall intensity (Gao et al., 2018, Equation 2). It is assumed that the effective contributing area $CA_{\text{eff},l}$ [m^2] is a function of time (t), of lateral flow velocity and of total contributing area ($CA_{\text{max},l}$). We define the contributing fraction of the total contributing area by the fraction of cells that satisfy the condition: $L_c < tV_{mac}$, where L_c is the distance of a contributing area cell, c, to its outlet (cell within RL l with $CA_{\text{max},l}$). The effective contributing area $CA_{\text{eff},l}$ is then obtained by multiplying the contributing fraction with $CA_{\text{max},l}$. The lateral flux, $Q_{\text{max},l}$ [m^3/s], is calculated as a function of time, using Equation 5.4 (Montgomery & Dietrich, 1994):

$$Q_{max,l}(t) = I_{\text{rep}} \cdot CA_{\text{eff},l}(t) \cdot \psi(P). \tag{5.4}$$

In this equation, ψ [-] is the runoff rate coefficient, which is a function of the cumulative precipitation P. I_{rep} [m/s] is the representative precipitation intensity, obtained by multiplying the mean intensity I [m/s] with a multiplication factor I_{corr} [-]. This enables us to estimate the degree of saturation of each cell, i, in the RL as a function of time at the outlet using a modified TOPOG approach as below:

$$h^*_{\text{sat,i}}(t) = \frac{Q_{\text{max},l}(t) \cdot \left(\frac{CA_i}{CA_{\text{max},l}}\right)}{K_{sat} \cdot H_{\text{soil}} \cdot \sin(s_i) \cdot b}. \tag{5.5}$$

In this equation, CA_i is the specific contributing area for an individual cell i in the RL. K_{sat} [m/s] is the saturated hydraulic conductivity parallel to slope, averaged over the soil thickness. H_{soil} [m] is the soil thickness. s_i is the slope angle in degrees per cell i. b [m] is the raster cell resolution. Averaging $h^*_{\text{sat,i}}$ [-] over all cells gives the RL h^*_{sat}. Subsequent pore water pressure is computed as:

$$P_{\text{water}} = H_{\text{soil}} \cdot \cos(s) \cdot h^*_{\text{sat}} \cdot g \cdot \rho_w, \tag{5.6}$$

where P_{water} [Pa] is the pore water pressure, s is the average slope angle of the RL, g [9.81 m/s^2] is the gravitational acceleration, ρ_{water} [998 kg/m^3] is the density of water.

5.2.4 Passive earth pressure

Passive earth pressure acting as resistance force at the bottom of the RL is included applying the results of Cislaghi et al. (2019), in accord with the framework proposed by Schwarz et al. (2015). Root compressing forces in this calculation are included and estimated to be 10% of the lateral root reinforcement under tension (Cohen & Schwarz, 2017b; Schwarz et al., 2015). The contribution of passive earth pressure forces to RL stability are implemented by adding them to the other stabilizing forces (shearing forces and maximum tensile lateral root forces).

5.2.5 Model calibration and validation

The improved model has a total of 20 parameters. Three of these are probabilistic. An overview of the parameters is given in Table 5.2. We only retain four sensitive parameters (van Zadelhoff et al., 2022) for calibration and assign default values, estimates or literature values, to the remaining parameters (Table 5.2).

TABLE 5.2: An overview of all SfM parameters. Table is adapted from van Zadelhoff et al. (2022). The only difference is the substitution of the transmissivity by the saturated hydraulic conductivity K_{sat}. Transmissivity is the product of the K_{sat} and the soil thickness. The last column in the table indicates whether the parameter is to be calibrated.

Parameter	Description	Default value	Unit	Calibration
m_d	Soil thickness mean	1	m	Yes
σ_d	Soil thickness standard deviation	0.25	m	No
m_C	Soil cohesion mean	2	kPa	Yes
σ_C	Soil cohesion standard deviation	0.5	kPa	No
m_ϕ	Angle of internal friction mean	30	°	Yes
σ_ϕ	Angle of internal friction standard deviation	4	°	No
ρ_{ls}	Density of the random generated landslides	0.2	RLs/m^2	No
ρ_{soil}	Dry soil density	1500	kg/m^3	No
K_{sat}	Saturated hydraulic conductivity	0.1	m/s	Yes
I	The precipitation event that is tested	10	mm/hr	No
I_{min}	Precipitation intensity threshold for instability	1.2	mm/hr	No
r_{xy}	Raster resolution	2	m	No
l_{wr}	Ratio between length and width of the landslides	2	-	No
C_{max}	Maximum interception storage capacity	4	mm	No
k	Interception curve shape parameter	0.03	-	No
c	Fitting parameter for the lateral root reinforcement	25068.54	-	No
α_1	Shape of root distribution in horizontal direction	0.862	-	No
β_1	Rate of root distribution in horizontal direction	3.225	-	No
α_2	Shape of root distribution in vertical direction	1.284	-	No
β_2	Rate of root distribution in vertical direction	3.688	m	No
$D_{trees,max}$	maximum distance for influence of tree roots	15	m	No
ρ_{tree}	Density of a tree	850	kg/m^3	No
ρ_{water}	Density of water	998	kg/m^3	No

The calibration parameters and their corresponding ranges are given in Table 5.3. Contrary to our previous work, we do not include precipitation intensity because detailed rainfall data from RADAR imagery is available. Accordingly, saturated hydraulic conductivity (transmissivity in van Zadelhoff et al. (2022)) and mean soil thickness are the only calibration parameters in the computation of pore water pressure. Furthermore, parameters related to the vegetation are also not included in the calibrated parameter set; we use here single tree detected trees (section 5.3) and assign the parameters related to root reinforcement (c,α_1,β_1,α_2,β_2) directly based on the identified tree species (see section 5.3). This has proven to be the best performing method of including vegetation effects in SlideforMAP (van Zadelhoff et al., 2022). For calibration and validation, we use a split sample test, splitting the available observations into spatial subsets.

We divide the study area into 10,000 small subsets i.e. terrain units and subsequently classify the terrain units for either validation or calibration. Throughout the calibration and validation process, the classification is immutable.

TABLE 5.3: Parameters for the calibration with initial value ranges.

Calibration parameter	Unit	Description	Initial value range
m_{d}	m	Mean soil thickness	0.20 - 1.80
m_{C}	kPa	Mean saturated soil cohesion	0.00 - 12.5
m_{ϕ}	°	Mean angle of internal friction	24.00 - 41.50
K_{sat}	m/s	Saturated hydraulic conductivity	10^{-8} - 10^{-2}

For the split sampling, we arrange the terrain units by slope angle and then take a random 85% / 15% sample in a method similar to the performance evaluation in the work of Frattini et al. (2010), where it is suggested that a terrain unit based on slope angle, comprised of multiple grid cells, is a better terrain unit than single grid cells. The 85% / 15% ratio is a recommendation by Guzzetti, Reichenbach, et al. (2006).

We calibrate the model based on an iterative parameter sampling technique, which will not necessarily yield the best possible parameter set (which in any case would be spuriously influenced by observational uncertainties), but has the advantage of yielding additional insights into the parameter ranges that perform well (van Zadelhoff et al., 2022). The method uses a total of three parameter sampling cycles. For the first cycle, we sample 150 unique calibration parameter sets from the prior parameter ranges of Table 5.3 with Latin Hypercube Sampling (McKay et al., 1979). Each of these parameter sets is used to run the model twice (to account for the inherent probabilistic variation) and the corresponding model performance is evaluated with the Area Under the Curve (AUC) from the Receiver Operator Curve method (Metz, 1978). The AUC value is computed for each model run for all terrain units that were retained for calibration. For a given sampled parameter set, the mean AUC of the two runs is taken as performance evaluator. Subsequently, the 150 values sampled per calibration parameter are ordered and grouped into 0.1 percentile fractions, for which the mean AUC is computed.

The 5 fractions with the highest mean AUC value (i.e. 50% of the total fractions) are retained as prior range for the next sampling cycle. After the third sampling cycle, the single parameter set with the highest AUC values is retained as calibration parameter set and used in the subsequent validation. With the new model formulation for groundwater table and pore water pressure computation, a challenge is the fraction of RLs that are fully saturated, which can become unreasonably high. We remove calibration parameter sets that lead to saturated fractions higher than 0.5, which is a heuristic choice.

5.3 Data

For the application of SfM, we use two study areas in New Zealand that are dominated by silvopastoral farming. Location and overview of the areas is given in Figure 5.4. Digital terrain models (DTM) for the study areas were provided by Spiekermann et al. (2021). The DTM is resampled using bi-linear resampling to a resolution of 2 m. This corresponds to a resolution proven to give good results in SlideforMAP (van Zadelhoff et al., 2022).

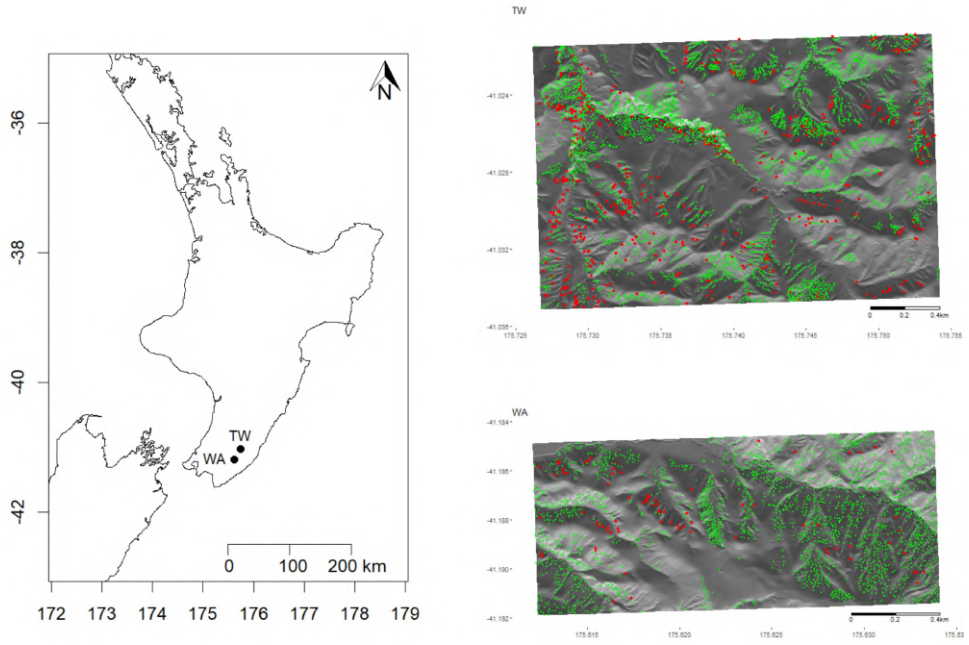

FIGURE 5.4: Location of the study areas in the Wellington region on New Zealand's North Island. Upper right is Te Whanga (short: TW), lower right is Waikoukou (short: WA). In green are given single tree locations, in red shallow landslides from the inventory. All coordinates are in WGS84.

A manually corrected automated landslide scar identification algorithm produced a dataset of 43069 shallow landslides (Spiekermann et al., 2021), which overlaps our study areas. We use 500 scars for Te Whanga and 78 for Waikoukou. 14 shallow landslides were excluded based on fieldwork that identified them as cattle trampling rather than shallow landslides. The aerial imagery is from 2010 and the identified shallow landslides are considered largely to be related to events in March 2005 and July 2006 (Spiekermann et al., 2021). An overview is given in Table 5.4.

TABLE 5.4: Study area characteristics. * Indicates the study area as used in Spiekermann et al. (2021). The size reduction of the study areas in this paper is for computational efficiency purposes.

Name	**Surface area** km^2	**Inventory** n landslides
Te Whanga	3.5	500
Te Whanga farm*	17.2	3271
Waikoukou	1.4	78
Waikoukou farm*	4.6	755

Gridded hourly precipitation totals are available through the MOANA dataset (Moana Project Team, 2021). This interpolated grid is based on RADAR data. To confirm internal consistency of the precipitation data in our study areas, double mass curves for all RADAR grid cells that overlap our study areas are given in Figure 5.5.

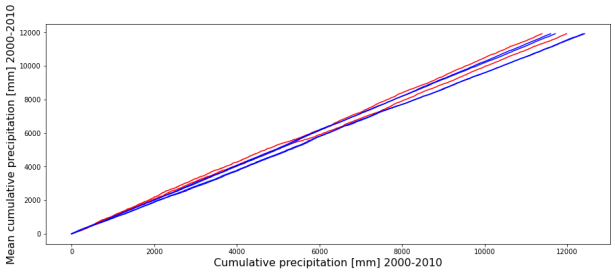

FIGURE 5.5: Double mass plot validation of precipitation data consistency. Shown is the cumulative precipitation of one raster cell over the entire RADAR data period (x-axis) plotted against mean cumulative precipitation of all raster cells (y-axis). Red: raster cells in the Waikoukou study area. Blue; raster cells in the Te Whanga study area.

This data is used to identify probable events that initiated shallow landslides and to give an idea of the corresponding precipitation intensity and return period. A plot of most extreme events and the computation of return periods in the study areas prior to the landslide inventory is shown in the Supp. Material (Figure 10.5). For model validation in both study areas, we focus on the March 2005 event. We retain this event because it has the highest return period for the RADAR observational period but we know that not all landslides were triggered by this single event. Details of the event are presented in Table 5.5 and in Figure 5.6. The event had a high variability of precipitation intensity and was more extreme (in terms of amounts) in Waikoukou than in Te Whanga, indicating significant spatial precipitation variation.

TABLE 5.5: The most extreme event from the two study areas over the period of 2000 - 2010. I is the precipitation intensity (mm/hr) and T is the return period (years).

	Te Whanga	**Waikoukou**
Event start	29-3-2005 05:00	29-3-2005 05:00
Duration	33 hours	33 hours
I	4.3 mm/hr	7.1 mm/hr
T	10 years	173 years

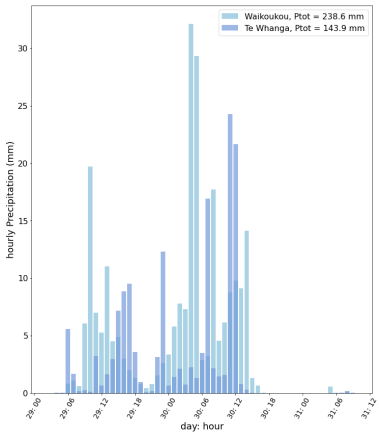

FIGURE 5.6: Hourly precipitation graph of the March 29-30 2005 precipitation event in the two study areas.

Trees in the study area have been mapped using available LiDAR data from 2013/14 in the Wellington region of New Zealand (Spiekermann et al., 2021), which was processed with the PyCrown model (Zörner et al., 2018) to delineate tree crowns. The center point X and Y of the tree crown is assumed to be the tree location. Properties of the inventoried shallow landslides as compared to the properties of the total study area are given in Table 5.6. We assume that no changes have taken places on trees between 2005 (time of the larger landslides events) and the LiDAR data collection.

TABLE 5.6: Properties of the inventoried shallow landslide scars as compared to the properties of the total study area. The average distance to the nearest tree, obtained as average over all raster cells, is computed after removing all distances > 15 m, beyond trees are assumed to exert no effect.

	Waikoukou		**Te Whanga**	
	Total study area	Shallow landslide scars	Total study area	Shallow landslide scars
Total surface area [ha]	142.6	0.6	351.7	3.4
Mean elevation [m.a.s.l.]	218.0	210.5	197.6	189.0
Mean slope angle [°]	19.9	26.4	21.5	28.6
Mean contributing area [m^2]	8432.3	100.3	4158.9	13089.1
Mean distance to nearest tree [m]	11.7	14.0	12.9	12.9

Species classification was conducted with a Support Vector Machine (SVM) and based on orthophotos (2010 - 2017) and the tree crown (Spiekermann et al., 2021). The resulting data includes the X and Y coordinate of the tree, the tree crown height and the classified species (eucalyptus, kanuka, poplar/willow, pine, undefined). Characteristics of the vegetation based on this data and of soil data in the two study areas is given in Table. 5.7.

TABLE 5.7: Study area characteristics. Soil depth and soil texture class are taken from S-map soil mapping for New Zealand (Manaaki Whenua - Landcare Research, 2019).

	Waikoukou	**Te Whanga**
Number of trees	2304	3747
Dominant tree species	Kanuka (52%)	Kanuka (50%)
Sub-dominant tree species	Poplar/Willow (32%)	Poplar/Willow (45%)
Tree density [Trees/ha]	16	11
Average tree height [m]	16.8	11.5
Dominant soil depth class	Shallow (41%)	Moderate deep (83%)
Sub-dominant soil depth class	Deep (30%)	Deep (16%)
Dominant soil texture class	Silt (100%)	Silt (91%)
Sub-dominant soil texture class	-	Loam (8%)

Parameterization of the maximum lateral root reinforcement as a function of tree distance is available for poplar (Ngo et al., 2023) and pine (*Pinus Radiata*) (Giadrossich et al., 2020). In the work of Spiekermann et al. (2021), a normalized tree influence with distance from the stem is given, based on a statistical analysis in the same study areas. We use their equations (shown in Figure 5.7) to extend our reclassification of the tree species for which we have no root reinforcement parametrization.

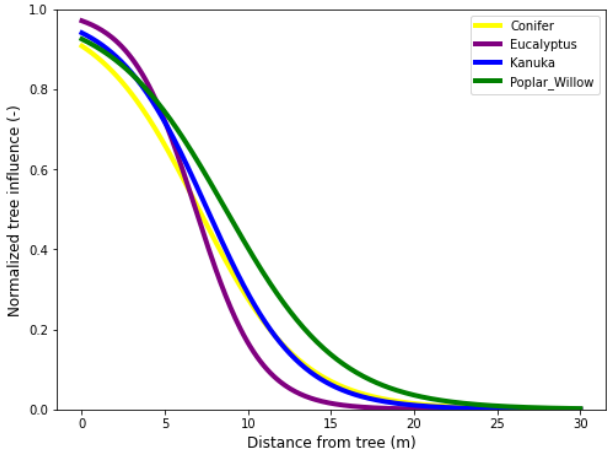

FIGURE 5.7: Normalized tree root influence as a function of distance from the stem. Parameterization based on Spiekermann et al. (2021, Figure 10).

Due to the incompatibility of the statistical method, which implicitly includes all vegetation effects, with our probabilistic physical method, we cannot relate the tree influence equations directly to root reinforcement, but have to use it is an indication. We choose to apply poplar root reinforcement parameterization for kanuka, eucalyptus and undefined trees. This is because, within the most effective distance (up to approximately 7 m), poplars exert a comparable vegetation influence (Figure 5.7) to the other tree species. A comparison between pine and kanuka trees shows that a standard kanuka stand provides a higher reinforcement for the first 8 years of growth, but lower reinforcement thereafter (Ekanayake et al., 1997). Root tensile strength of kanuka, before felling, is almost two times higher than that of pine (32.45 vs. 17.62 MPa) (Watson et al., 1999).

5.4 Results

We first present the analysis of the multiplication factors I_{corr} to obtain the representative rainfall intensity I_{rep} based on observed mean precipitation intensity per event, I. Figure 5.8 shows the simulation results for a single precipitation event, the one of March 2005 as a function of catchment area, for the full model. Corresponding results for a fixed runoff rate coefficient and no runoff rate coefficient scenario are given in the Supp. material (Figure 10.7 and Figure 10.8).

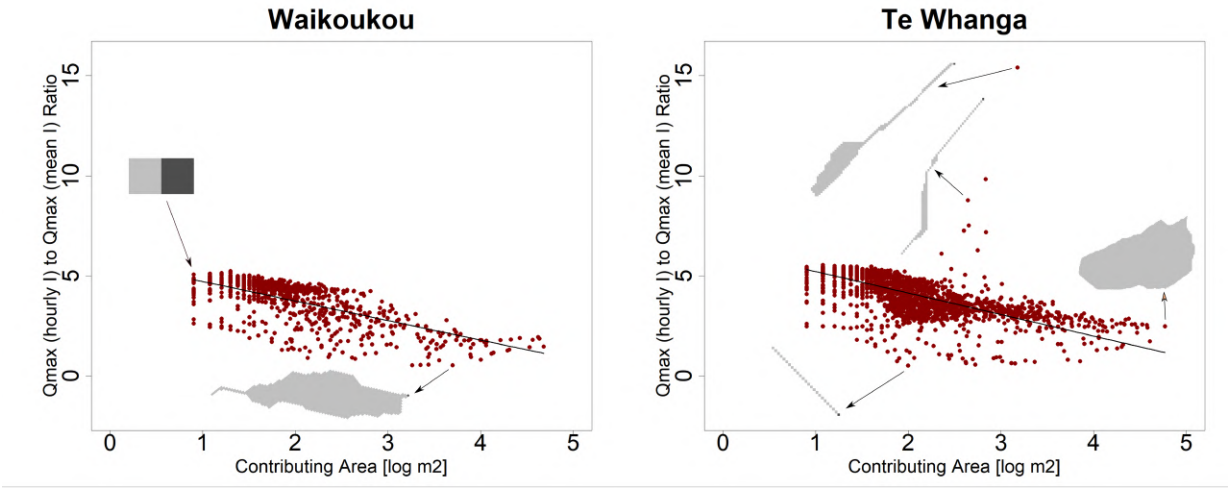

FIGURE 5.8: Ratio between the maximum lateral flow rate computed with an actual precipitation event and with a constant mean precipitation with a runoff rate coefficient dependent on lateral root reinforcement for the March 2005 event (with 33 h duration). Each point in the plot represents one RL. Soil thickness classification between deep and shallow soils is derived from random sampling. The shown regression lines are: The Waikoukou, intercept 5.7 and slope -0.98; The Te Whanga, intercept 6.3 and slope-1.08. To add context, for some outliers the contributing area outlines are given, with their outlet in black.

The identified relation between the flow ratios and contributing areas of Figure 5.8 matches our expectations, with large areas having a lower ratios. These ratios can be directly related to *I*corr because of the assumed linear relationship between throughfall and interception (equation 5.4). In small catchments, the infiltrated rainfall travels a small distance to the outlet and has a more instantaneous reaction. This means that the peak lateral flux is more directly related to the peak rainfall intensity, resulting in a large I_{corr}. For larger contributing areas, the flux at the outlet is a mixture of different precipitation intensities occurring at different locations in the contributing area at different moments in time, meaning the lateral flux corresponds better to the mean precipitation intensity of the event. This behaviour is visible for certain elongated contributing areas in Figure 5.8 for Te Whanga and for the example contributing area in Figure 10.6 with the inclusion of the runoff rate coefficient. Due to the dependency of the flow ratio on many factors and on the precipitation event, we are forced to make a generalization. We therefore use the identified relations between the flow ratio and the contributing area size in Figure 5.8.

5.4.1 Calibration and validation

The iterative parameter sampling leads to a consistent narrowing of the parameter ranges for the three model versions tested here (Table 5.8, corresponding dotty-plots are given in the Supp. Material, section 10). The calibration procedure is run at a shallow landslide density (ρ_{ls}) of 0.20 RLs/m^2. After calibrated parameter values are determined, these are input for a final split-sample run. This run and all subsequent results are computed with ρ_{ls} = 0.75 RLs/m^2 to make full use of computational efficiency.

TABLE 5.8: Overview of the calibration and validation results for the model versions of this study. Per study area, the first subgroup gives the calibrated parameter values and the narrowed parameter range from the last calibration cycle. The second subgroup gives metrics of performance. These are the AUC, The unstable fraction (UF), which is the fraction of random landslides that has a safety factor < 1.0 and the Saturated Fraction (SAF) which the fraction of Random landslides that has a relative saturation ($h^*_{sat,i}$) of 1.0 for the part (85% of the study area) of the study area used in the calibration. The last subgroup gives the same metrics for the part (15% of the study area) used for validation. Between brackets for SfM original and SfM hybrid (no Ψ) are the metrics when they are ran with the calibrated parameters from SfM.

	SfM		SfM original		SfM hybrid	
Waikoukou						
m_d [m]	1.32	(0.64-1.52)	0.98	(0.64-1.42)	1.41	(0.52-1.52)
m_C [kPa]	2.06	(0.06-2.04)	2.15	(0.09-2.05)	0.32	(0.06-2.03)
m_ϕ [°]	25.5	(24.0-29.6)	26.6	(24.1, 28.4)	25.7	(24.0-27.5)
K_{sat} [m/s]	0.0075	(0.0004-0.0075)	0.0006	(0.0005-0.0065)	0.0080	(0.0004-0.0081)
Calibration AUC	0.899		0.864	(0.910)	0.902	(0.899)
Calibration UF	0.124		0.357	(0.112)	0.251	(0.125)
Calibration SAF	0.0159		0.3446	(0.0152)	0.0143	(0.0162)
Validation AUC	0.863		0.814	(0.879)	0.878	(0.864)
Validation UF	0.128		0.357	(0.116)	0.255	(0.129)
Validation SAF	0.0172		0.3433	(0.0168)	0.0155	(0.0179)
Te Whanga						
m_d [m]	1.29	(1.09, 1.48)	1.44	(1.06-1.53)	1.48	(1.25-1.56)
m_C [kPa]	0.33	(0.03, 2.51)	1.56	(0.05-2.03)	0.64	(0.14-2.10)
m_ϕ [°]	27.4	(24.1-28.2)	28.2	(24.1-29.3)	28.0	(24.1-29.2))
K_{sat} [m/s]	0.0068	(0.0021-0.0074)	0.0056	(0.0004-0.0057)	0.0060	(0.0002-0.0063)
Calibration AUC	0.866		0.854	(0.848)	0.867	(0.865)
Calibration UF	0.232		0.129	(0.211)	0.201	(0.229)
Calibration SAF	0.0128		0.0153	(0.0126)	0.0131	(0.0117)
Validation AUC	0.896		0.888	(0.887)	0.896	(0.897)
Validation UF	0.224		0.125	(0.205)	0.194	(0.222)
Validation SAF	0.0169		0.0201	(0.0173)	0.0176	(0.0159)

Calibrated parameter values are largely consistent for the two case studies and the tested model versions, especially when compared to the initial parameter ranges. It is however important to note that the calibration parameter ranges and the values for different versions can only be compared qualitatively, since the exact value is dependent on model process uncertainties. Most notable is the low mean soil cohesion for SfM and SfM hybrid in both study areas and the low K_{sat} for SfM original for Waikoukou. This low K_{sat}, directly results in a high Saturated Area Fraction, SAF, of RLs. Calibration and validation metrics (AUC, SAF and UF) for the three compared model versions are largely consistent for the two case studies. Minor differences between the calibration and the validation metrics, is to be expected due to observational and modelling uncertainties (Arsenault et al., 2018; Beven & Binley, 1992). The random split sampling of the modelling domain into 85% for calibration and 15% for validation probably also plays a certain role.

Overall, we see that SfM performs marginally better than SfM original for both case studies, despite of their considerable difference in size (142.6 h versus 351.7 ha). The performance of SfM hybrid is closer to the one of the new version than to the one of SfM original for both study areas. One notable exception occurs in SfM original in the Waikoukou study area, here the calibrated

performance is worse than the performance using a different calibration set (SfM parameters). This can only indicate an inadequacy in our calibration procedure. A further indication for this is the deviancy in the calibrated K_{sat} and elevated degree of (34% of total RLs) complete soil saturation.

5.4.2 Hydrological module

The average pore water pressure resulting from the calibrated parameter values of Table 5.8 for SfM is shown in Figure 5.9 for Te Whanga. Corresponding results for Waikoukou are available in the Supp. Material Figure 10.14. The average pressure and difference to SfM original under SfM calibration, SfM original with unique calibration and the hybrid version are also listed. The spatial patterns of pore water pressure resulting from the retained parameter sets for each model, show small differences on the hillslope tops but strong differences close to the stream network. This difference reflects the distribution of contributing area and to a minor extend the location of single trees. Significant influence of the calibration can be seen as well related to values of K_{sat} and m_d, which do not so much influence the pattern, but the overall 'background' value of pore pressure.

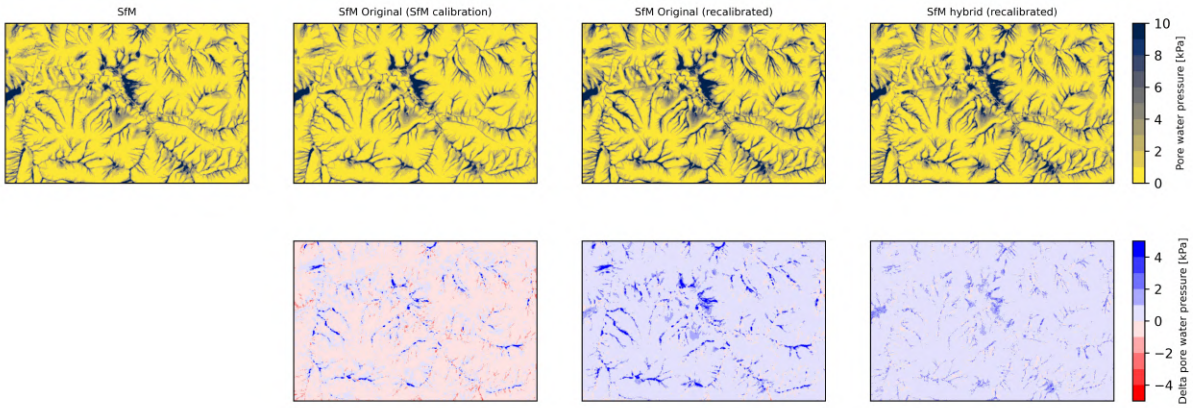

FIGURE 5.9: Calibrated pore water pressure in Te Whanga. Upper row, mean pore water pressure [kPa] from SfM, SfM original with SfM parametrization, SfM original, with unique calibration and SfM no hybrid; Lower row list the absolute difference in pore water pressure of the versions as compared to SfM.

5.4.3 Landslide probability

A key check that the model behaves well is the assessment of computed shallow landslide susceptibility on areas that have experienced landslides according to the inventory. Here we focus on SfM as it is the main result we want to present in this paper. SfM computed landslide probability maps resulting from the calibration parameters (Table 5.8) for the two study areas are given in Figure 5.10 and 5.11. The lower probability values in Waikoukou are noticeable. This correlates to the unstable fraction of surface area in Table 5.6, where it is shown that Te Whanga has a higher relative and absolute unstable area. This is also reflected in the calibration and validation results (Table 5.8), with Te Whanga having a higher unstable fraction resulting in the calibrated runs.

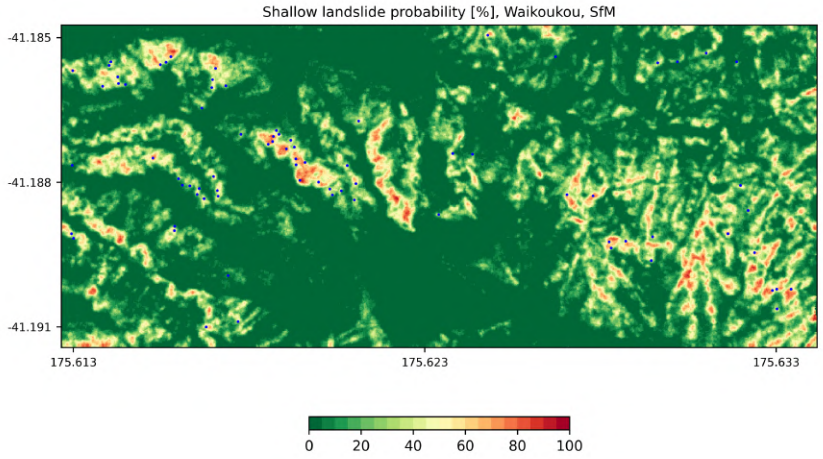

FIGURE 5.10: SfM Landslide probability results in Waikoukou

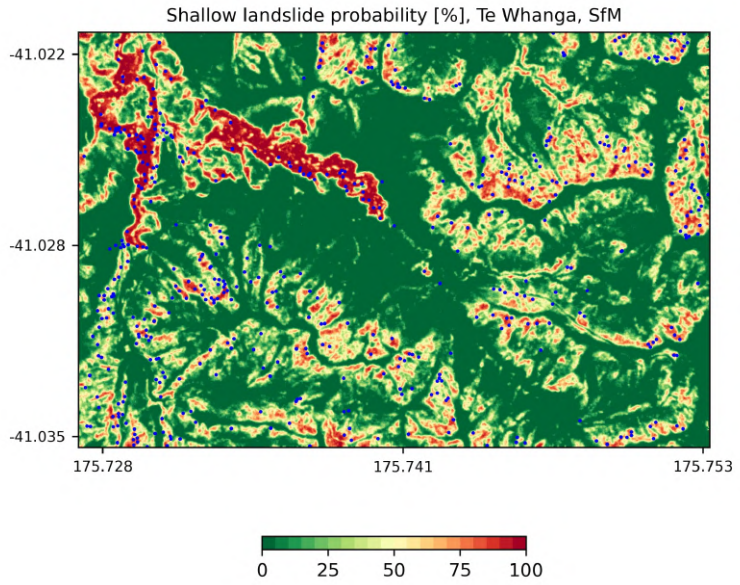

FIGURE 5.11: SfM Landslide probability results in Te Whanga

The computed distribution of susceptibility clearly shows that in both study areas SfM is generally capable of reproducing the shallow landslides from the inventory. This pattern appears to be dominated by slope angle. The similarity in validation AUC values, despite a significantly lower UF indicates that the pattern in landslide probability is important and the absolute probability values are arbitrary. Performance can be better visualized by making a cumulative graph of the probability values for both study areas and the inventoried landslide scars. This is displayed in Figure 5.12.

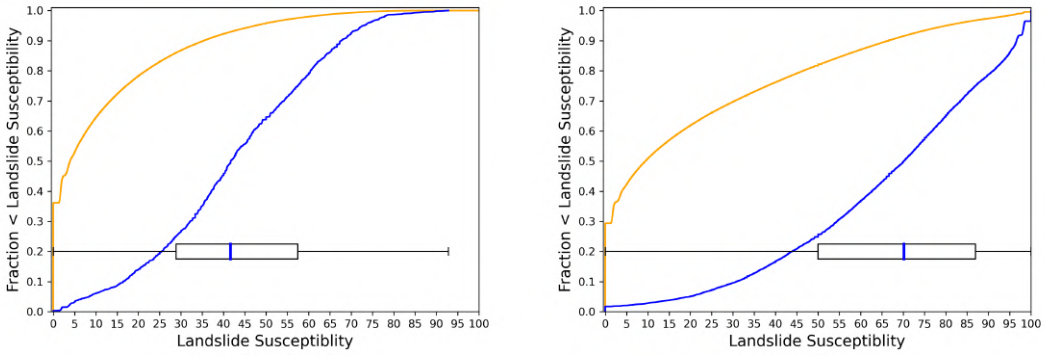

FIGURE 5.12: Left: Empirical cumulative distribution functions of the shallow landslide probability for the entire study area (orange) and the surface area from the landslides in the inventory (blue). In addition, the boxplot of the distribution of probability values for the landslide scars is shown. Figure Left: Waikoukou, Figure right: Te Whanga.

Here we see the same pattern as seen in Table 5.8 and in Figure 5.11 and 5.10, with Te Whanga having overall higher landslide probability values. Both study areas appear to have a well distinguishable curves for inventory probability values and overall probability values. In addition, we check if the hydrological model indicators are distributed similarly on the landslide area as compared to the total area. We present these as boxplots in Figure 5.13. We see a stronger discrepancy in all indicators for Waikoukou. For both study areas, the median and mean contribution coefficient ($CA_{\text{eff},l}/CA_{\text{max},l}$) and median runoff rate coefficient is higher for the landslide scars. Lateral root reinforcement is lower for the shallow landslide scars. There seems to be no significant difference in distribution in the shallow landslide size for all unstable RLs and the shallow landslide scars.

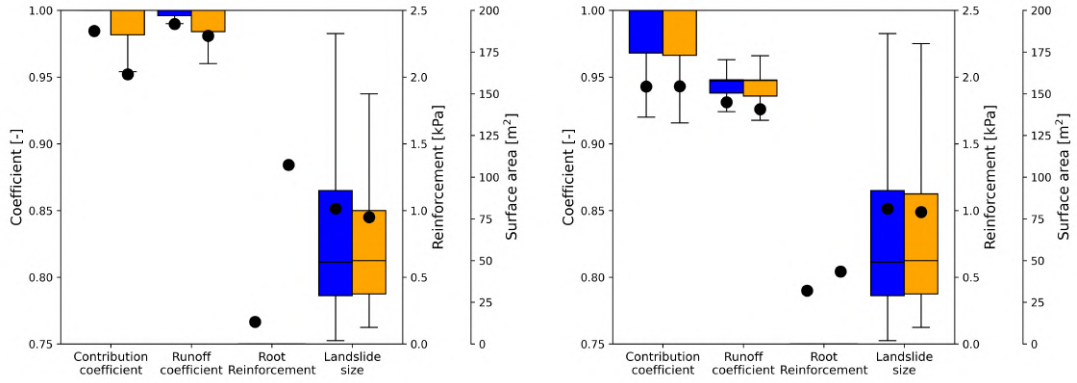

FIGURE 5.13: Boxplots of some key model indicators, of the entire study area (orange) and cells in the landslide inventory (blue). Key indicators are the contribution coefficient ($CA_{\text{eff},l}/CA_{\text{max},l}$), runoff rate coefficient (Ψ) and the lateral root reinforcement. Additionally, we added a boxplot of observed landslide size (size of landslides in the inventory in blue and the distribution of size of RLs that have a stability factor, SF<1 in orange; Figure Left: Waikoukou, Figure right: Te Whanga.

We also check the relationship of lateral flux with slope angle for the SfM results and the inventoried landslides in accordance with the methodology of Prancevic et al. (2020) in Figure 5.14. All RLs with a computed SF < 1.0 are plotted. Setting aside spatial variation in root reinforcement and soil parameters, these are the only indicators influencing the shallow landslide susceptibility pattern.

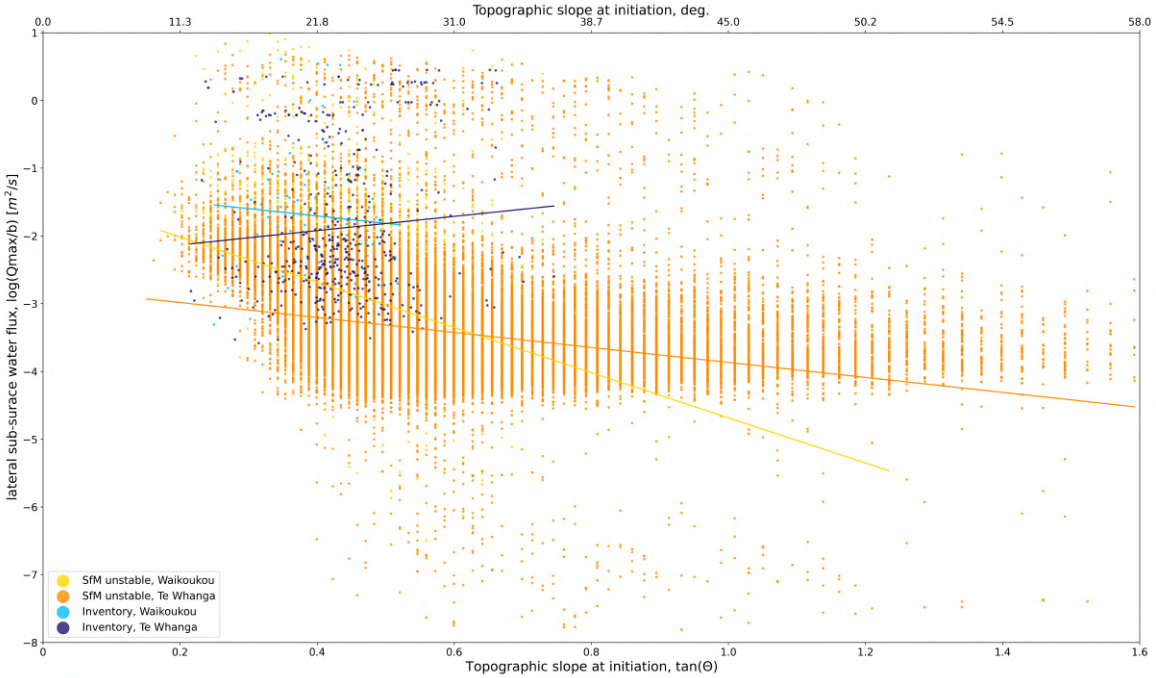

FIGURE 5.14: Computed lateral flux for the inventoried shallow landslide scars and the unstable random landslides from the calibrated SfM (random sample of 10% for better visibility), plotted versus the slope angle. Linear regressions (none significant) for the points are given.

It can be seen that the RLs mapped as unstable match the properties of the majority of the inventoried landslides, with a sweet spot on a slope angle between 20 to 30 ° and a specific discharge of 0.001 to 0.01 m^2/s. For both study areas, it appears the model classifies a wide range of slope angles and contributing areas (Figure 5.14) as unstable, decreasing the accuracy. The model tends to overestimate slope instabilities in steep slopes ($>$ 35 °). Especially since the inventory in Figure 5.14 displays quite a narrow slope range. The trendlines of the shallow landslide scars and the RLs do not match up well. It appears the inventory trendlines are influenced heavily by outliers with high lateral flux or from another perspective: the model overestimates instability in shallow landslides with a low computed lateral flux. We also see a subset of inventoried shallow landslides displaying a very high lateral flux, indicating they overlap with the bottom of hollows. SfM appears capable of classifying these areas as unstable.

5.5 Discussion

5.5.1 Limitations

The objective of the model improvements presented here was to improve the representation of the conditions of shallow landslides initiation, i) in hydrological terms, by pore water pressure and vegetation characteristics by root reinforcement and ii) in mechanical terms by means of passive earth pressure. However, uncertainties arise from model shortcomings, local inhomogeneities or from parts of the inventory not being related to our modelled event.

The large variation and magnitude in unstable fraction (UF, Table 5.8) through the study areas and model versions is remarkable. It is an order of magnitude higher than the actual fraction of the study areas that suffered shallow landsliding (Table 5.6). We believe the variation is partly related to variation in the calibrated mean soil cohesion. The overall large values of UF can

be due to the use of AUC as performance measure. The AUC may not be the best measure in validating physical models as it is a relative measure where the absolute probability values are ambiguous. For practitioners, we recommend relating shallow landslide probability values to said values in known landslide scars, akin to what is shown in Figure 5.12 as presented in this manuscript. Practitioners can decide how much of instability they want to capture and how much uncertainty they take into account by taking a certain fraction of actual landslide scars and extrapolating this to a threshold on the probability values.

5.5.2 SlideforMAP improvements

A key challenge in the use of observed precipitation events is how to account for effects related to precipitation falling on different parts of the contributing area and to subsequent different (unknown) surface or subsurface flow paths, which lead to a temporal dispersion of flow contributions at a point of interest (which is commonly addressed in rainfall-runoff modelling literature, (e.g. Rinaldo et al., 2006; Robinson et al., 1995)). This makes it challenging to relate properties of the precipitation event to the maximum lateral flux, which in turn relates to the highest pore water pressure. We tackle this here by converting precipitation to subsurface lateral flow by i) a runoff rate coefficient and ii) by correcting the reference precipitation for the size of the contributing area. Both improvements are, to the best of our knowledge, novel for comparable landslide models.

However, the difference in performance of between the model versions is negligible (Table 5.8). For Waikoukou, SfM original even performs better. For Te Whanga, where the majority of the inventoried landslides lie (500 vs 78), SfM (and SfM hybrid) perform slightly better than SfM original. The change in pore water pressure due to the hydrological improvements is visible 5.9. Comparing the pore water pressure of SfM to SfM original under similar calibration shows a higher modelled pressure on the ridges for SfM than for SfM original and a lower modelled pore water pressure in the valleys. The lower value in the valleys corresponds to a smaller $CA_{\text{eff},l}$ and the higher value on the ridges likely stems from the use of $CA_{\text{max},l}$ for scaling (rather than taking the mean contributing area of a RL as in SfM original, Equation 5.4 and 5.5).

Influence of the vegetation on the pore water pressure appears minor, as visible from the low difference in performance metrics between SfM and SfM hybrid. A multitude of reasons, or a combinations thereof, can be invoked: i) None of our improvements significantly distinguished unstable areas from stable areas and therefore the AUC measured performance does not improve. ii) The use of an area-relationship to find a representative rainfall intensity I_{rep}, as applied in both the original and in the new version is very effective and overrules performance gains related to any other improvement. A hint of this might be that near identical performance of SfM hybrid shows that at least the runoff rate coefficient is of little effect. iii) Our improvements in SfM do not capture the unique conditions of outliers in the inventory, especially in terms of contributing area. This is best seen in Figure 5.14. iiii) The AUC performance measure is not a good metric for capturing marginal gains in accuracy and therefore cannot highlight performance improvements.

Accordingly, from a landslide susceptibility perspective, we cannot definitively say if SfM or SfM original should be preferred for practical applications. We do however believe that our new hydrological module is closer to reality since stationary lateral flow conditions (as assumed in SfM original) are very rare in nature (Beven & Kirkby, 1979). Future work, and in particular additional case studies, will certainly yield additional evidence.

5.5.3 Vegetation

In SfM original, vegetation acts in a mechanical sense, by lateral/basal root reinforcement and vegetation weight. In SfM version, two additional hydrological effects are included, namely: reduction in the runoff rate coefficient near vegetation and a reduction in precipitation amount by interception. However, lateral root reinforcement can be assumed to be the vegetation parameter with the highest impact on slope stability computation in SfM: it was shown to be the most sensitive parameter in original SfM original (van Zadelhoff et al., 2022). In the Waikoukou study area, the difference in mean distance to trees between the whole study area and the inventoried landslides (Table 5.4) suggests a general propensity of shallow landsliding further away from the trees. This is also shown in Figure 5.13, where root reinforcement correlates with more stable areas. This effect is strongest in Waikoukou and less strong in Te Whanga. Regardless of the model version, of the calibrated parameter combinations or of the study area used, our validation AUC is above 0.8, indicating good predictive performance (El Khouli et al., 2009). We have assumed our trees to be either poplar or pine trees. This meant a reclassification of a large number of kanuka trees to poplar trees. Using statistical relationships on the relative effects of both tree species (Spiekermann et al., 2021), we argue the effects of this differences is small.

One main vegetation-dependent effects is not included in SfM: the effect of evapotranspiration (beyond evaporation of intercepted water) and the effect of heterogeneous infiltration in vegetated soils. Evapotranspiration can be assumed to be of minor importance during extreme precipitation events relevant for landslide triggering (Feng et al., 2020). However, evapotranspiration over longer time periods, possible coupled with an increased macropore presence, could reduce antecedent moisture in vegetated areas. This effect is partially addressed here with the estimated runoff rate coefficients. However, the calibration and validation results show that the way we implemented this effect did not lead to significantly different results, indicating either the antecedent moisture itself was not significant for this specific event or our implementation with the runoff curves was ineffective.

5.5.4 Research outlook

The availability of hourly rainfall data by the MOANA project helped in this research. This data avoids using precipitation intensity as a calibration parameter or making broad assumptions. This contributed to a more realistic validity test of our improvements with less uncertainty compensated by the calibrated parameters. We think this type of data creates opportunities for new concepts in rain-induced shallow landslide modelling as illustrated here. As discussed earlier in this paper, this is not the first attempt to overcome the stationary-flow assumption in landslide probability modelling. The presented method to overcome the stationarity assumption requires only a low number of parameters but was shown here to lead to only small improvements in terms of model performance. This might potentially be due to the fact that rainfall uncertainty largely dominates total modelling uncertainty, which is a well-known fact in hydrological modelling (e.g. McMillan et al., 2011; Sivapalan et al., 1997). Passive earth pressure is often neglected in shallow landslide models (Murgia et al., 2022). Here we implemented this pressure as its maximum mobilized amount. Cohen and Schwarz (2017b) numerically estimates that only a portion of this pressure is mobilized at any given moment of shallow landslide displacement. Definitive research and implementation of this portion could improve current models.

Finally, we would like to emphasize that plotting contributing area vs. slope angle from the inventoried shallow landslides (Figure 5.14) displays outlier landslides in terms of the combinations of lateral flux and slope angle, which still remains a mystery as these outliers are distant from the SfM sweet spot of slope angles between 20 - 30 $^{\circ}$ and a lateral flux between 0.001 to 0.01

m^2/s. One reason for these outliers might be the absence of antecedent moisture assumptions in the model, which could be improved in the future. In combination with more reliable spatial rainfall data, this might show more clearly if dynamic hydrology can perform better than the stationarity assumption under a variety of conditions.

5.6 Conclusion

In this study we calibrated, validated and compared the performance of the original version of SlideforMAP, an improved version and a hybrid version in two shallow landslide-prone study areas in New Zealand hill country. The improved model version includes the following new features: it computes an event-based effective contributing area per random landslide, a runoff rate coefficient based on root reinforcement in the contributing area and it includes passive earth pressure forces in the stability calculations. The calibrated and validated model parameters displays a tendency to deep soils, low soil cohesion a low friction angle and high saturated hydraulic conductivity, influenced by macropore flow. The improved version of SlideforMAP performs marginally better than the original model version in Te Whanga study area; in the Waikoukou study area performance is slightly worse, with a calibration imprecision in the results. The hybrid version, without runoff rate coefficient, performs near similar to the new version. This suggests that the inclusion of non-stationary flow, by means of an effective contributing catchment ($CA_{\text{eff},l}$), is the main model improvement. The runoff rate coefficient is either of little influence or to be inefficiently incorporated in our model.

In terms of case-study specific results, the obtained landslide probability maps for the two case studies show that shallow landslide occurrence in our study areas is concentrated on slopes between 20° and 30° and under a lateral flux higher than 0.001 m^2/s. This mostly corresponds to mid-slope regions, where enough contributing area is present and which could greatly benefit from space-planted trees. Overall, SlideforMAP has been shown to perform satisfactorily for the two case studies in New Zealand. Compared to the original three case studies in Switzerland (van Zadelhoff et al., 2022), the new test areas vary in soil composition, soil heterogeneity and precipitation regime. Accordingly, we consider the methodology of the model applicable in similar steeps-sloped environments, which opens interesting perspectives for practitioners to plan future vegetation-based landslide management measures.

Author contribution

F.Z. is the main writer. B.S. contributed to the manuscript and embedding this research within previous research. C.P. contributed funding for the study and assisted with the manuscript. M.S. contributed to the manuscript and the concepts of the model.

Competing interests

The authors declare no conflict of interest.

Acknowledgement

We extend our sincere thanks to Andrew Neverman from Manaaki Whenua Landcare Research and the MOANA project team for providing us with the MOANA hourly gridded rainfall data. Thanks to Raphael Spiekermann for providing the outline of the study areas, the digital elevation model of the study area at 1 m resolution, the inventory of trees containing height and

species and the 2010 landslide inventory. This research was supported by New Zealand Ministry of Business, Innovation and Employment research program "Smarter Targeting of Erosion Control (STEC, Contract C09X1804)".

6 Contrasting physical and statistical landslide susceptibility

Full title:

Contrasting physical and statistical landslide susceptibility models at the scale of individual trees: Implications for land management

Feiko Bernard van Zadelhoff*[1,2], Raphael I. Spiekermann*[3,4], Jan Schindler[3], Hugh Smith[3], Chris Phillips[3], Massimiliano Schwarz[1]

Geomorphology (Elsevier journal)
Submitted, under review, preprint DOI: 10.2139/ssrn.4347971

Submitted: 18 January 2023
http://dx.doi.org/10.2139/ssrn.4347971

This manuscript aims to be a generalizability and performance test case for SlideforMAP. We compare SlideforMAP to a statistical model in two New Zealand pastoral farms. Automated detection of tree location and species enable the detailed inclusion of vegetation effects and a comparison to how a statistical shallow landslide susceptibility method incorporates these effects. As far as we know, no research before specifically compared slope stability with single-tree based vegetation effects of two model philosophies.

[1] Bern University of Applied Sciences - HAFL, Länggasse 85, CH-3052 Zollikofen, Switzerland
[2] Institute of Geography (GIUB) & Oeschger Centre for Climate Change Research (OCCR), University of Bern, 3012 Bern, Switzerland
[3] Manaaki Whenua - Landcare Research, Riddet Rd, Palmerston North, New Zealand
[4] GeoSphere Austria, Hohe Warte 38, 1190 Vienna, Austria

* Author van Zadelhoff F.B. and Author Spiekermann R.I., made equal contribution to the work as presented in the manuscript and are considered joint-first authors

Abstract

Physically or statistically based approaches are widely used to quantify shallow landslide susceptibility. Despite the underlying data, methods, and assumptions being significantly different, there has been little quantitative work to evaluate the differences in model outcomes. Therefore, we compare previously developed physical and statistical shallow landslide susceptibility models for a study area in New Zealand's silvopastoral hill country. Both models include individual tree effects on slope stability. We use convolutional neural networks to delineate individual tree crowns and classify species at the scale of individual trees with regional aerial photography. SlideforMAP, a physically based probabilistic model that includes both lateral and basal root reinforcement, is adapted for application in silvopastoral landscapes. Root reinforcement models for physical modelling are subsequently developed for the most abundant tree classes based on allometric relationships to remotely sensed, above-ground metrics. In contrast, the statistical landslide susceptibility model uses binary logistic regression, including empirically derived tree influence models alongside topographic and lithological explanatory variables. Binary Logistic regression displays a better performance for our study area, resulting from the model being trained and tested on an inventory of past shallow landslide observations, whereas SlideforMAP makes predictions largely independent of past slope failures. SlideforMAP has the advantage of computing shallow landslide susceptibility for different rainfall scenarios coupled with specific return periods. The two predictions of landslide susceptibility within the study area were >70% in agreement. In terms of implications for land management, we recommend the advantages and limitations of both approaches should be considered by land managers in relation to their erosion control objectives. However, to increase performance of erosion and sediment mitigation, we suggest land managers prioritize tree planting in areas where the statistical and physical approach agree within the "high" susceptibility classification (8% of the study area). Comparing shallow landslide susceptibility scenarios based on potential trees and a treeless baseline can further improve targeted planting.

keywords: Landslide susceptibility, SlideforMAP, CNN: U-Net; MaskRCNN, individual trees, bioengineering

6.1 Introduction

Within the numerous examples of slope stability modelling studies that range from tree stand to national scale (e.g. Guzzetti, Galli, et al., 2006; Murgia et al., 2022; Reichenbach et al., 2018; Van Den Eeckhaut et al., 2006; van Westen et al., 2008), there are generally two data-driven approaches: i) physically based, and ii) statistical modelling. Physically based models quantify the balance of forces acting on slopes, commonly using a safety factor to determine local (in-)stability. They are used to simulate a range of soil hydrological conditions to investigate the effects of rainfall scenarios on slope stability (Wu & Sidle, 1995). However, due to data requirements relating to the soil physical parameters (cohesion, internal angle of friction, hydrological parameters) and to knowledge of failure mechanisms and of mass movement processes (e.g. depth of failure plane), physical, process-based models are best suited to the hillslope scale and are more challenging to implement at regional scales (Holcombe et al., 2012; Masi et al., 2021). For larger areas, simplifying assumptions must be made (Salvatici et al., 2018), which can result in poorer performance of physical models compared to statistical methods (e.g. Cervi et al., 2010). These limitations were partly overcome by the implementation of probabilistic approaches (e.g. van Zadelhoff et al., 2022). In physical models, the rainfall-induced landslide triggering susceptibility is the probability of landslide occurring conditional to a specific rainfall

scenario (Corominas et al., 2014).

Statistical landslide susceptibility modelling is an alternative approach to physical slope stability modelling. Statistical models differ from physically based, deterministic models by not attempting to directly represent the processes that control slope stability. Rather, and in the absence of soil geotechnical data, statistical models use readily available surrogate data (e.g. lithology, topographic data) to train models based on sites of previous landslide occurrence to predict where future landslides are likely to occur. In statistical terms, landslide susceptibility is the probability of future landslide occurrence for a specific areal unit given local environmental conditions (Brabb, 1984). Therefore, the data requirements are less limiting than for physical models. However, statistical models are based on the assumption that locations with physical characteristics similar to those where past failures have occurred, are also likely to fail in the future, given similar rainfall triggering event characteristics. Indeed, past observations provide "the key to the future" (van Westen et al., 2008) for statistically based models.

Few studies have compared the benefits, challenges, and assumptions underpinning statistical and physical landslide susceptibility models. In one of the few examples, the predictive performance of two statistical models (Weight of Evidence; Fuzzy Logic) were compared with a physical model (SHALSTAB), showing a significantly higher model performance of statistical over physical models. However, the utility of these different approaches to slope stability quantification in terms of knowledge gain (e.g., geomorphic plausibility; Steger et al. (2016)) has not been adequately investigated, nor have the implications for land management of model selection been explored. In this study, we provide a comprehensive comparison of two different models, using the most advanced developments at the individual tree scale – both in probabilistic, physically based modelling (SlideforMap; van Zadelhoff et al. (2022)) and in statistical modelling (Spiekermann et al., 2022b) of shallow landslide susceptibility. Both models include individual tree effects at landscape to regional scales; we compare their performance and utility for land managers in New Zealand's silvopastoral hill country.

While both models quantify slope stability and produce probabilities of future landslide occurrence (0–1), the required interpretation is very different and must be made with knowledge of the objectives and assumptions of the underlying methods. In this study, we therefore compare the underpinning theoretical frameworks, their assumptions, and implications for decision-making. Specifically, this study has the following objectives: i) to develop spatially distributed root reinforcement models for the most abundant tree species in the study area for inclusion in SlideforMap, and to contrast these estimates with empirically based tree influence models on slope stability (TIMSS; Spiekermann et al. (2021)); ii) To compare the spatial predictions of the two physical and statistical models and evaluate potential differences – both in terms of model performance and spatial variation of predictions. Moreover, we discuss the assumptions and sources of uncertainty of both models and explore the potential complementarity of statistical and physical modelling and potential implications for land management decisions.

Following a short review of methods used to capture tree effects in both physical and statistical slope stability models in section 6.2.2, landslide susceptibility models are implemented for two case studies in the Wairarapa, New Zealand (section 6.2.3 and 6.2.4). The reduction in landslide erosion due to existing vegetation is subsequently quantified with respect to a treeless baseline scenario (section 6.2.5). Additionally, we explore an additional rainfall scenario (5-year return period) with the physical approach to see how landslide susceptibility develops under more frequent rainfall conditions. Based on this, we consider whether tree planting to mitigate shallow landsliding would need to be significantly different using the assumed rainfall scenario as a triggering event compared to a rainfall event of higher magnitude and lower frequency (>100-year

return period).

Supported by the scenario modelling, we i) assess whether the recommended spatial patterns of mitigation measures differ for both modelling approaches and ii) determine the degree to which estimates of mitigation performance derived from the two different models are similar. Our findings are subsequently used to formulate recommendations for scientists, policy makers, and land managers regarding the use of physical and statistical models for the planning and implementation of vegetation-based mitigation measures of shallow landslides at local to catchment scales.

6.2 Methods

6.2.1 Study area

The study area comprises two farms (Sites 1 and 2) in the Wairarapa in the south-east of the North Island of New Zealand. These farms have a history of landslide and soil erosion research (Basher et al., 2018; De Rose, 2013; Douglas et al., 2013; Lambert et al., 1984; Spiekermann et al., 2021; Spiekermann et al., 2022b; Spiekermann, 2022). For the purposes of the modelling undertaken here, the study area was defined using a 1-km wide buffer zone added to the bounding box of the two farms (Figure 6.1; Site 1: 70.6 km2; Site 2: 24.3 km2). Both farms are underlain by predominantly Neogene-aged massive, poorly bedded mudstone and alternating sandstone and mudstone (Lee & Begg, 2002). Soils commonly have a dense subsoil zone of low permeability formed in loess that is the failure plane for many landslides (De Rose, 2013). Both sites also have small areas of coquina limestone outcrops. The terrain has low to moderate relief (<150 m) that is intensely dissected, with narrow ridge and spur crests, steep hillslopes mostly between 15°and 35°, and narrow valley floors. This topography is locally referred to as "hill country". Significant areas of colluvium (landslide debris) have accumulated along the bases of many slopes, and in mid- and upper-slope hollows. Mean annual rainfall is 1100 mm, characterised by winter maxima and summer droughts. However, this typical pattern can change during episodes of La Niña, which increases rainfall during summer months. Long duration, low intensity rainfall with low daily rainfall totals is typical (De Rose, 2013). Most landslide-generating storms do not have particularly high storm total or daily rainfall totals but occur when antecedent moisture conditions are high (Basher et al., 2018; De Rose, 2013).

Site 1 is a 1700-ha sheep and beef farm located east of Masterton in a region of steep pastoral hill country. The original native vegetation was cleared between 1860 and 1890 (Lambert et al., 1984). A major rainfall storm event led to widespread landsliding in 1977 (Crozier et al., 1980; De Rose, 2013; Glade, 2003). Soil conservation works in the form of space-planted poplar, willow, and eucalyptus trees began in the 1980s (Spiekermann et al., 2022b). Before the implementation of erosion mitigation measures, a woody vegetation cover was largely lacking. While planting has since been sustained, the density of trees on hillslopes differs greatly across the farm, with some hillslopes devoid of tree cover. Site 1 is thus representative of a "moderate" level of tree cover for New Zealand's pastoral hill country farms.

Site 2 is a 462-ha sheep and beef, mixed-species silvopastoral farm located at the upper catchment of the Waikoukou Stream and has had extensive soil and water conservation measures implemented since 1956. The main objectives of these conservation works were to intensively revegetate slopes and gullies prone to severe erosion, using poplars, willows, and protected seedlings of other species (e.g., Eucalyptus varieties). According to farm plan documents (Wairarapa Catchment Board, 1956), the early European land cover likely consisted of light bush, kānuka,

and fern, with heavier podocarp species in the wider valleys. Several remnants of kānuka remain distributed across the farm. Overall, there is a higher tree density across the farm of Site 2 compared with Site 1 (Spiekermann et al., 2022b), and therefore Site 2 more closely represents an "ideal" silvopastoral hill country farm.

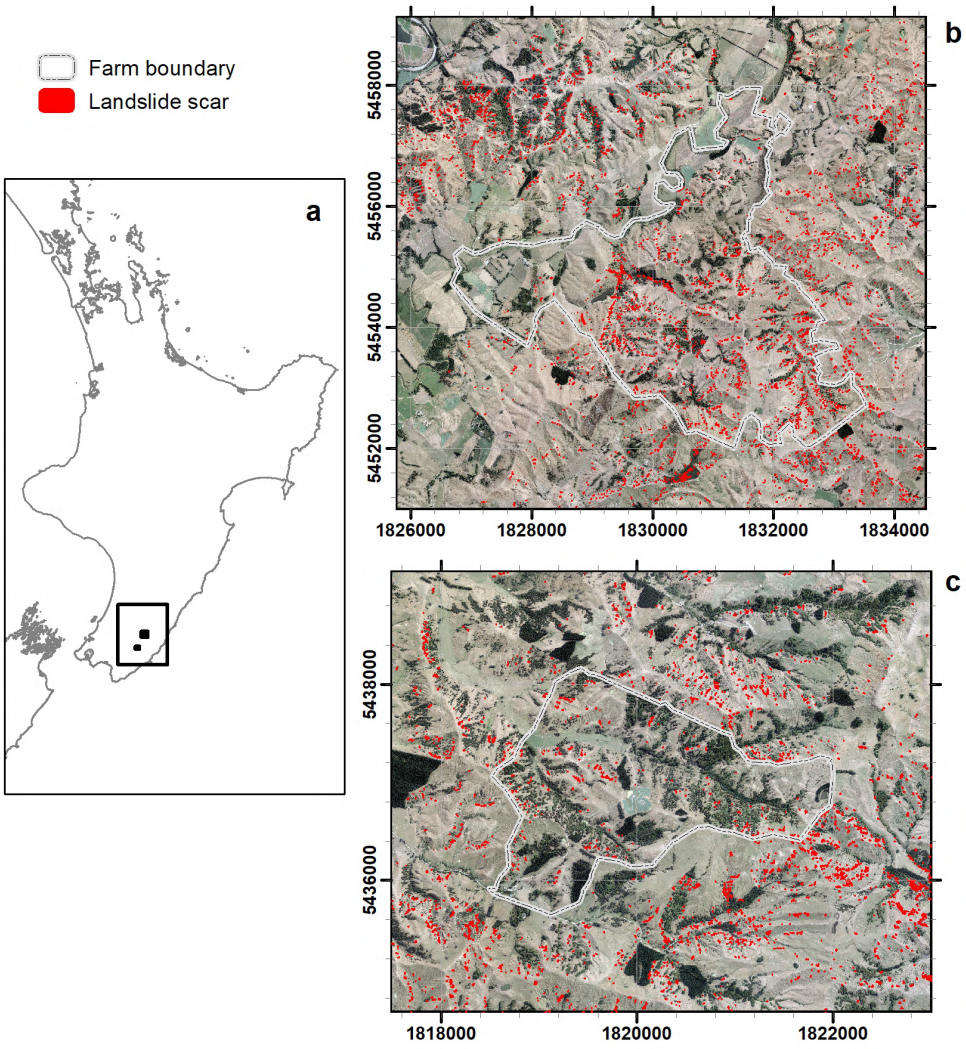

FIGURE 6.1: a) Study area location. b) Site 1. c) Site 2.

6.2.2 Integrating individual tree effects for slope stability modelling

6.2.2.1 Quantifying tree effects on slope stability in physical models

There are two direct effects by which vegetation influences slope stability: hydrological and mechanical. Vegetation modifies water infiltration and soil moisture content – most importantly through interception, increase of soil permeability, and evapotranspiration (Greenway, 1987; Phillips & Marden, 2005; Sidle & Ochiai, 2006). These functions gain in importance when modifying soil moisture within the contributing area upstream of a potential landslide location. Hydrological mechanisms that reduce pore-water pressures in the soil are beneficial, whereas processes that increase pore pressure are adverse. The mechanical effect through lateral root reinforcement, basal root reinforcement, and soil stiffening increases soil shear strength and thus promotes slope stability in shallow soils (Cohen & Schwarz, 2017b; Schmidt et al., 2001; Schwarz et al., 2015). This is achieved through increased strength of the composite rooted soil material

produced by the integrated interaction of roots and soil under different types of solicitations (tension, compression, shearing) (Reubens et al., 2007; Roering et al., 2003; Schmidt et al., 2001; Schwarz et al., 2011; Schwarz et al., 2013; Schwarz et al., 2015; Sidle & Ochiai, 2006; Styczen & Morgan, 2003). Moreover, the topology and morphology of root systems are important factors that determine the spatial arrangement and contribution of roots to soil reinforcement. The most effective mechanism relevant to shallow land sliding is through basal root reinforcement, which is achieved when roots penetrate the shear plane, thus increasing the basal shear strength (Schwarz, Lehmann, et al., 2010). Lateral root reinforcement governs the onset and size of shallow landslides (Roering et al., 2003; Schmidt et al., 2001; Schwarz, Lehmann, et al., 2010). The influence of root reinforcement on soil shear strength is usually expressed as an additional cohesion term (root cohesion c_r) (Wu, 1984) in the Coulomb failure criteria

$$S_{sr} = c'_s + c_r + (\sigma - \mu)tan(\phi') \tag{6.1}$$

where c'_s is the effective cohesion of the soil, σ is the normal stress due to the weight of the soil and water of the sliding mass, u is the soil pore-water pressure, and ϕ' is the effective internal friction angle of the soil that is assumed unaltered by the presence of roots. Some studies have shown that roots, in combination with other agents (e.g. fungi and bacteria), can change the structure of the soil and the stability of its aggregates, which results in an apparent shift of the grain size distribution, implying an apparent increase of the friction angle for low confining pressures (Bast et al., 2014; Graf et al., 2009). This effect is particularly relevant for the shallow organic horizons of the soils (0–40 cm depth) becoming much less important with increasing soil depth (e.g. within B or C horizons).

Root reinforcement models can be classified according to assumptions about root failure dynamics (Giadrossich et al., 2017). The 'all-at-once' breakage method or 'Wu/Waldron model' (Waldron, 1977; Wu et al., 1979) assumes simultaneous breakage of the roots. These models consider the root force independent of displacement and fully available at all displacement, that is, the maximum tensile strength is fully mobilised. Moreover, it is assumed that breakage of the root occurs at the shear plane. These are invalid assumptions, however, since breakage often occurs below the shear surface where the root diameter is smaller than at the shear plane (Giadrossich et al., 2017; Giadrossich et al., 2013; Hubble et al., 2010; Vergani et al., 2016). These limitations led to the development of field pull-out or shear tests and of root bundle models, which consider the dynamic stress-step (Pollen & Simon, 2005) or strain-step loading of a root system (Cohen et al., 2011; Schwarz et al., 2013; Schwarz, Lehmann, et al., 2010). The advantage of these models is that they consider root strength as a function of displacement.

6.2.2.2 Statistical approaches to quantifying tree effects

Previous statistical landslide susceptibility models were limited by their spatial representation of trees as predictor variables. Most models include land use or land cover data available at coarse scales (Knevels et al., 2021; Knevels et al., 2020; Reichenbach et al., 2014; Smith et al., 2021), for example, the Land Cover Data Base (LCDB) of New Zealand, which has been used for regional-scaled modelling of landslide susceptibility (Smith et al., 2021). At this scale, different types of vegetation cover (e.g., grasslands, deciduous hardwoods and mānuka/kānuka) are mapped at a minimum areal unit of 1 ha. However, these regional-scaled data are inadequate for capturing individual tree effects in silvopastoral systems (Figure 6.2).

Other authors include higher resolution variables derived from remotely sensed (satellite) imagery to represent physical vegetation characteristics (Wang et al., 2022), for example, the Normalized Difference Vegetation Index (NDVI), which is based on spectral reflectance measurements acquired in the red (visible) and near-infrared regions of the electromagnetic spectrum (Arabameri & Pourghasemi, 2019). High values of NDVI (close to 1) represent areas of dense green vegetation, and negative values indicate either an absence of vegetation or moisture-stressed vegetation (Gessesse & Melesse, 2019). Inclusion of NDVI-based variables, however, can be problematic due to the lack of a clear relationship between the index and the physical properties of vegetation that affect slope stability (Reichenbach et al., 2018), for example, deciduous trees outside the growing season can have NDVI values less than green pasture. Thus, the rationale for including higher resolution vegetation variables such as NDVI in a landslide susceptibility model is not adequately justified.

Of particular relevance for silvopastoral systems is the failure of such metrics that reflect properties of tree canopies (NDVI) to account for the spatial variation in the distribution and strength of roots and the hydrological interactions between trees and soil at the scale of the individual tree. Characteristics of individual tree canopies can reflect differences in vegetation composition, which can be useful for tree species classifications (Fassnacht et al., 2016) or relating canopy dimensions to above-ground biomass (Lau et al., 2019). Yet, the relationship between tree canopy and slope stability is more complex – primarily due to the nature of root system architecture and differences in root strength across vegetation species, which is not reflected by greenness in the canopy. Thus, tree effects on slope stability are spatially more heterogeneous than the more uniform tree canopy might suggest. While simple above ground measures of vegetation can improve on coarse-scaled land cover data, the significance of above-ground measures of vegetation with respect to slope stability needs to be carefully established (Reichenbach et al., 2018).

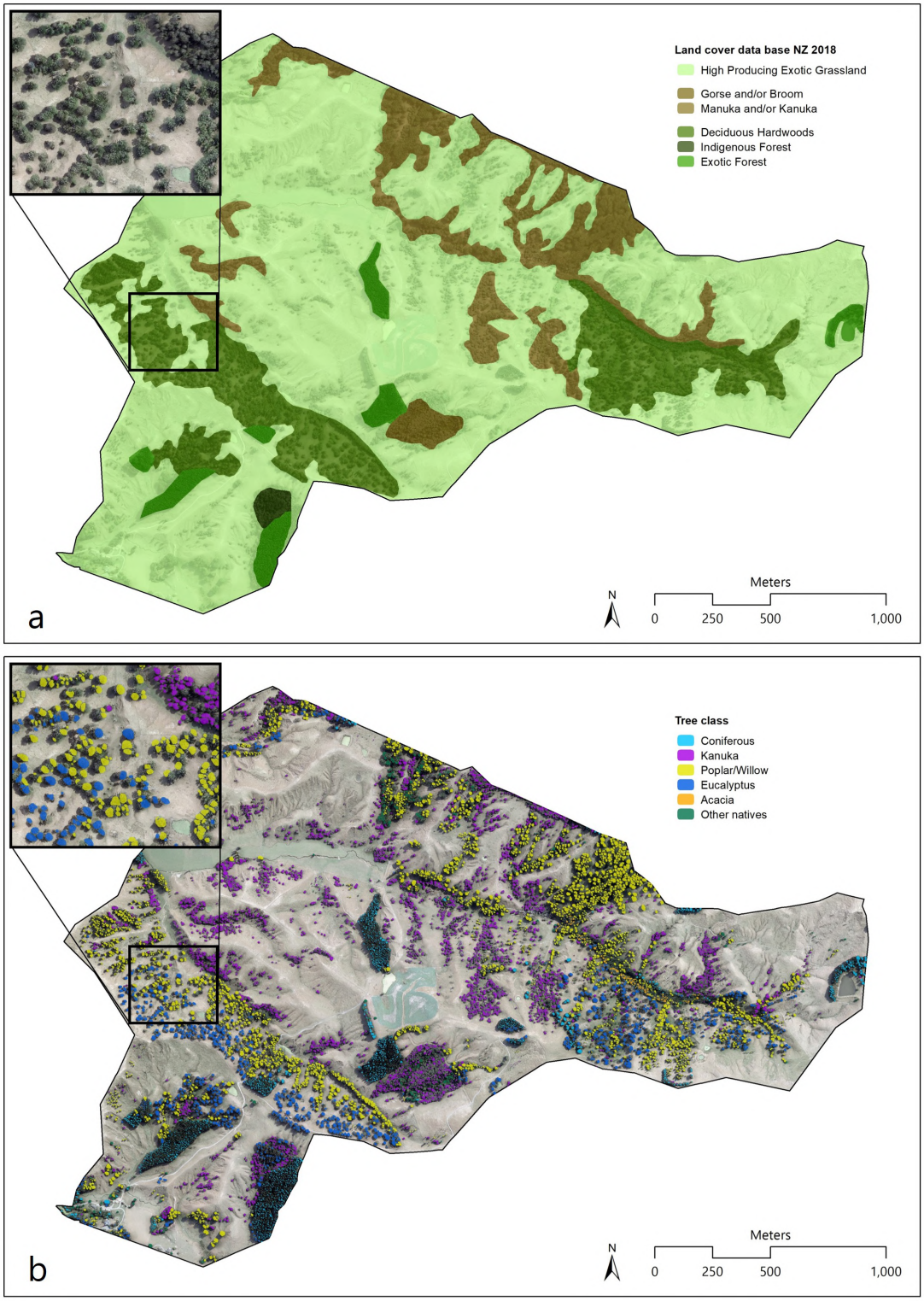

FIGURE 6.2: Implications of land cover data available at different scales: a) Regionally scaled land cover data are useful for regional landslide susceptibility modelling, but inadequate for capturing individual tree effects; b) High resolution remote sensing data enable individual trees to be identified and tree canopies classified.

Given these limitations, a novel approach for statistical landslide susceptibility modelling including individual tree effects was proposed by Spiekermann et al. (2022b) through use of Tree

Influence Models on Slope Stability (TIMSS; (Spiekermann et al., 2021)). The TIMSS represent the average influence of an individual tree on slope stability for the four most abundant tree types in the study area, fulfilling the following four criteria:

- Individual tree effects from different vegetation types (e.g., coniferous, poplar/willow) are captured;
- Local hydrological and mechanical effects are implicitly accounted for;
- Values are spatially distributed as a function of distance from tree (trunk);
- Contributions of neighbouring trees to slope stability are considered additive.

The method used to generate the TIMSS builds on that developed by Hawley and Dymond (1988), generating a two-dimensional spatial representation of individual tree influence normalised to a scale of 0–1. While the TIMSS fulfil the criteria for inclusion in a statistical model, since measurement units are largely irrelevant to statistical models, they do not quantify and model tree effects using physical measurements of force (N/m), which is a requirement for physical models. The outputs of these two different models for representing individual tree effects (root reinforcement and TIMSS) are included in the physical and statistical landslide susceptibility models in section 6.2.3 and 6.2.4.

6.2.2.3 Overcoming vegetation data limitations for silvopastoral systems with deep learning

Two proposed methods for estimating individual tree effects for inclusion in landslide susceptibility models were introduced: root reinforcement modelling (section 6.2.2.1) and through use of TIMSS (section 6.2.2.2). These approaches are adopted for landslide susceptibility modelling using physical and statistical modelling, respectively. Both methods rely on the identification of single trees. In this study we draw on most recent advances in remote sensing to delineate and classify individual trees for the study area. A convolutional neural network was trained using high resolution regional 4-band orthophotography. The advantage of this method over the previously published tree crown classifications in New Zealand's rural landscapes (e.g. Spiekermann et al., 2021) is that tree crowns are delineated and classified in the high resolution orthophotos without the need of a canopy height model (CHM). This enables temporal dynamics in tree cover to be captured through automated mapping and classification of trees in successive regional photography datasets.

Training data

Hand-annotated tree crowns mapped in 30-cm 4-band orthophotos (RGBI; Greater Wellington Regional Council, 2021) were labelled by tree species using field-based mapping undertaken by Spiekermann et al. (2021) in the study area. In total, 28,297 tree crowns across 22 different species were digitized on-screen and formed the basis for training convolutional neural networks. All varieties of coniferous species (e.g., radiata, spruce, cedar, Douglas fir) were grouped as conifers (4339 crowns). Similarly, all mapped poplar (Populus spp.) and willow (Salix spp.) were grouped into a second tree class (5645 crowns); the third class consists of eucalyptus (Eucalyptus spp., e.g. Eucalyptus globulus; 1414 crowns), the fourth includes kānuka (Kunzea spp.; 13661 crowns); the fifth class includes acacias (Acacia dealbata; 857 crowns); and the sixth class consists of indigenous species (2381 crowns) such as totara, (Podocarpus totara) and cabbage trees (Cordyline australis).

Convolutional neural networks for instance and species detection (MaskRCNN and UNet64)

First, all areas not mapped in the field, i.e., areas with no hand-annotated crown polgyons or species information, were masked out in the imagery to avoid model confusion. The tree-crown-level tree class information was subsequently burned into a label raster and used to train two CNNs; (i) an instance segmentation model (Mask Region-based Convolutional Neural Network (MaskRCNN; He et al. (2017)) as implemented in the Pytorch-based Detectron2 framework (Wu et al., 2019)) to identify and delineate individual tree crowns from RGB colour photography and (ii) a semantic segmentation model (UNet64 PyTorch implementation; Ronneberger et al. (2015)) for image-based species recognition at the pixel level. The first model is able to create detailed tree crown objects (without species information) outside the initial training areas. The second model was then used to produce a semantic segmentation map of tree species. Cross-validation using hold-out data not used during training was undertaken to quantify classification statistics of the raster predictions. The tree crown layer was then intersected with the raster map to calculate the mode of predicted class values for each tree crown, which was the method adopted to determine the most likely tree class. Finally, the classification statistics (precision, recall and F-measure) of the final tree level data were calculated using all available data.

6.2.3 Physical landslide susceptibility modelling with SlideforMAP

6.2.3.1 Model description

SlideforMap is a model developed to quantify landslide susceptibility on a regional scale with a direct inclusion of mechanical influence of vegetation. SlideforMAP applies the Root Bundle Model as presented in Schwarz, Lehmann, et al. (2010) and Schwarz et al. (2013). This makes for a spatially explicit, single-tree-based inclusion of both lateral and basal root reinforcement. Parametrizations of the model for three tree species are publicly available. These are European Beech (Gehring et al., 2019), Radiata Pine (Giadrossich et al., 2020), and Poplar (Ngo et al., 2023). SlideforMAP is a physically based probabilistic model that considers a force balance in 3-Dimensional volume of a large number (10^6+) of randomly generated landslides. To account for uncertainty on a local scale, certain parameters are sampled from distributions rather than using fixed values. This determines geotechnical soil parameters and random landslide surface area. To estimate the geotechnical parameter distribution, determination of a representative soil type is important. Like many physically based models, SlideforMap is conditioned to a constant precipitation rate. This precipitation rate is used to approximate actual rainfall events or for design rainfall scenarios usually associated with certain return periods. The output consists of a relative landslide probability map, conditional to the modelled precipitation event. A more detailed description of SlideforMap is given in van Zadelhoff et al. (2022).

6.2.3.2 Model parameterization

A 1-m resolution LiDAR-derived digital elevation model (DEM), as used in Spiekermann et al. (2022b), forms the basis of the spatial input. For computation reasons, this is bilinearly resampled to a resolution of 2 m. Slope angle and D8 flow accumulation (O'Callaghan & Mark, 1984) are computed from the 2-m DEM. Ideally, further parametrization of SlideforMap reflects available soil data and meteorological data. For the study area in this research, we access soil data from S-Map (Manaaki Whenua - Landcare Research, 2019). Soil depth and soil texture for our study sites are given in Table 6.1 and Table 6.2.

TABLE 6.1: Study site characteristics of S-map soil depth to hard rock. The SlideforMAP reference value is the mean of the class boundaries in S-map.

S-map soil depth class	Site 1	Site 2	SlideforMAP reference value
Deep	35 %	30 %	1.25 m
Moderately deep	60 %	30 %	0.73 m
Shallow	5 %	40 %	0.33 m
Very shallow	0 %	0 %	0.10 m

TABLE 6.2: Study area characteristics of S-map soil texture. SlideforMAP reference derived from mean class value in a geotechnical conversion table in VSS-Kommission and Engineers (2011)

S-map soil texture class	Site 1	Site 2	USCS soil type conversion	SlideforMAP reference mean soil cohesion	SlideforMAP reference mean friction angle	SlideforMAP reference Transmissivity
Clayey	7 %	0 %	CM	5.0 kPa	24.0 °	$10^{-}8$ m/s
Loamy	18 %	2 %	SW-SC	2.5 kPa	31.5 °	$10^{-}5$ m/s
Silty	75 %	98 %	ML	2.5 kPa	30.0 °	$10^{-}4$ m/s
Sandy	0 %	0 %	SW	0.0 kPa	38.0 °	$5^{-}4$ m/s

Our precipitation event intensity is that of the highest hourly intensity in the March 2005 event that is a likely trigger for many shallow landslides inventoried from the 2010 imagery (Spiekermann et al., 2021). Hourly gridded 4-km resolution RADAR data for the period 2000–2020 (Moana Project Team, 2021) enables us to estimate the hourly maximum intensity during this event. This corresponds to 24 and 32 mm/hr for Site 1 and Site 2, respectively, occurring on March 30th 04:00 – 05:00 and March 30th 10:00 – 11:00 respectively. Such a rainfall event was described as a likely trigger for shallow landslides at the study sites (Spiekermann et al., 2021). To compare this event to a less extreme design event, we also model SlideforMAP with a 5-year return period, 12-hour duration for Site 2. This corresponds to a precipitation intensity of 4 mm/hr, based on the publicly available rainfall intensity return period grid HIRDs (Carey-Smith et al., 2018). An overview of miscellaneous SlideforMAP parameters is given in Table 6.3.

TABLE 6.3: An overview of all variable model parameters of SlideforMAP.

Parameter	Description	Value	Unit	Source
σ_d	Soil thickness, standard deviation	0.2	m	Estimate
σ_C	Soil cohesion, standard deviation	2.0	kPa	Estimate
σ_ϕ	Angle of internal friction, standard deviation	4.0	°	Estimate
ρ_{ls}	Density of the random generated landslides	0.3	HL/m^2	Computational limitation
ρ_{soil}	Dry soil density	1450	kg/m^3	Estimate
P_{min}	Precipitation intensity threshold for instability	1.2	mm/hr	Default value

Input for the shallow landslide surface area distribution are the areas of all inventoried 2010 slides in the extent the study area, bringing the total to 6947 shallow landslides. Further details on the landslide inventory are provided in section 6.2.4.1.

6.2.3.3 Allometric relationship between above and below-ground tree characteristics

Locations of single trees are determined based on the classification of individual tree crowns with UNet64. Tree height (H_{tree}) [m] is derived from the maximum value of a CHM, which is the difference between the digital terrain model and surface models within the crown's polygon, as used in Spiekermann et al. (2021). Tree height is related to tree DBH (DBH_{tree}) [m] via a general allometric relationship (given below), also used in van Zadelhoff et al. (2022). Tree DBH forms

the link between aboveground approximated tree size and the belowground assumptions on root density and root reinforcement:

$$DBH_{\text{tree}} = \frac{(H_{\text{tree}})^{1.25}}{100}, \tag{6.2}$$

Tree location, species, and DBH, from UNet64 (section 6.2.2.3), are applied in SlideforMAP directly. The first step in SlideforMAP is to compute the maximum lateral root reinforcement (RR_{max}) as a 2d raster, which is the lateral root reinforcement under infinite soil thickness. RR_{max} is a function of tree size and distance to said tree. Root reinforcement from multiple trees can overlap. RRmax is computed to the equation below (Gehring et al., 2019):

$$RR_{\text{max}} = (c \cdot DBH) \cdot \Gamma_{PDF}\left(\frac{D_{\text{trees}}}{DBH \cdot 18.5}\middle|\alpha_1, \beta_1\right), \tag{6.3}$$

where c is a fitting parameter in N/m^2; DBH is in m; and Γ_{PDF} is the gamma probability density function evaluated as function of the first term with shape parameter α_1 and scale parameter β_1. The shape and scale parameter are species specific to model the decrease in root reinforcement with increasing distance from the tree. Both α_1 and β_1 are dimensionless.

Due to lack of published calibration all species root reinforcement is related to Veronese Poplar (parametrized by Ngo et al. (2023)) via a multiplication factor and literature on root tensile strength measurements. The overview is given in Table 6.4. We recognise this approach has its shortcomings. It does not include species specific root architecture or compare in situ mechanical root reinforcement as would have been the case in root pull-out tests.

TABLE 6.4: Comparison of root tensile strength results from various sources for tree species in UNet64. Due to lack of data on root reinforcement, the sixth Unet64 class with indigenous species are classified as Kanuka. *only 2 – 3 mm roots measured.

UNet64 Species	**Assumed species**	**Tensile Strength (MPa), 1-4 mm roots**	**Multiplication factor of Veronese Poplar**	**Source**
PW	Veronese Poplar	40.10*	1.00	Watson et al. (2008)
Conifer	Pinus Radiata	17.52	0.44	Watson and Marden (2004)
Kanuka	Kanuka	34.11	0.85	Watson and Marden (2004)
Eucalyptus	Eucalyptus	55.39	1.38	Docker and Hubble (2008)
Acacia	Acacia	85.14	2.12	Docker and Hubble (2008)

A visualization of the development of RR_{max} with distance from a tree is given in Figure 6.3. Lateral root reinforcement and basal root reinforcement are derived from the maximum lateral root reinforcement (RR_{max}), as a function of soil thickness. This is outlined in van Zadelhoff et al. (2022).

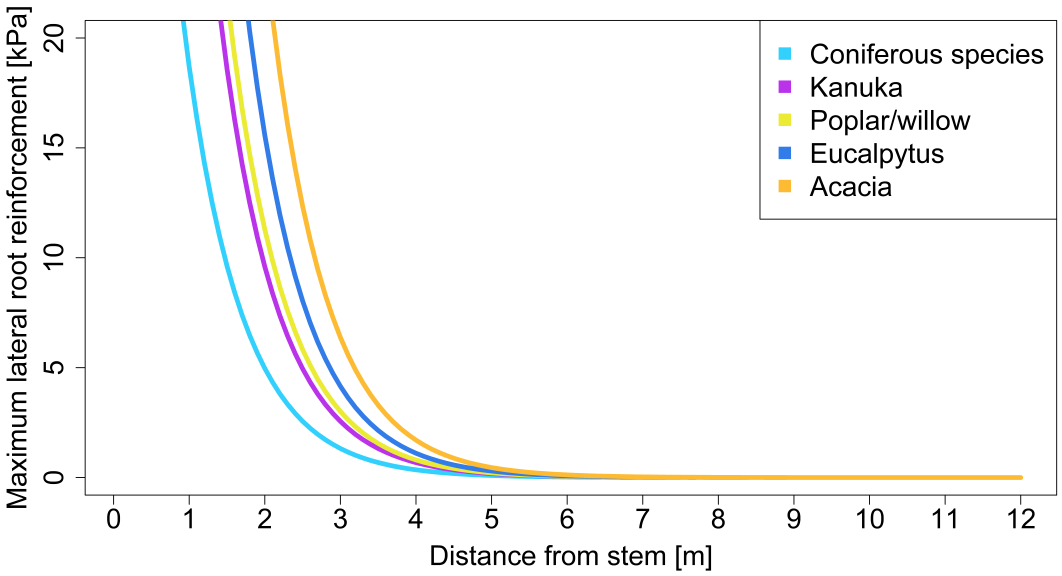

FIGURE 6.3: Maximum lateral root reinforcement as a function of distance to stem for a 0.4 m DBH for tree species as used in this study.

6.2.4 Statistical landslide susceptibility model

6.2.4.1 Model description

The landslide susceptibility model was developed according to the method described in (Spiekermann et al., 2021; Spiekermann et al., 2022b), using an inventory of 43,000 shallow landslides mapped in high resolution orthophotography from 2010 following landslide-triggering rainfall events between 2005 and 2010. Of these 43,000 shallow landslides, only those that intersect the study area (section 6.2.1) were selected to train a binary logistic regression (BLR) model. This reduced the number of landslides to 6,947 shallow landslides, with 4,751 from Site 1 and 2,196 from Site 2. For further information on the landslide inventory, we refer to Spiekermann et al. (2021) and Spiekermann et al. (2022b).

BLR is frequently used for statistical landslide susceptibility modelling since it models the probability of a binary response variable (Y=0 | 1), which corresponds to the absence (0) and presence (1) of landslides. We used a 1:1 balanced sample design, with an equal number of landslide presence and randomly generated landslide absence points. To increase the independence of landslide absence and presence points, a mask was created before the generation of absence points by buffering landslide polygons by 8.3 m (the 95th percentile of the radius r of the landslide scar inventory, assuming a circular shape).

BLR caters for both numerical and categorical independent variables, whereby the variability of Y is explained in terms of covariates $x_1, \ldots, x_i$. In BLR, the linear function takes on the form:

$$\text{logit} = \log \frac{p}{1-p} = (\beta_0) + \beta_1 x_1 + \ldots + \beta_i x_i) \tag{6.4}$$

where Y is the binary dependent variable of landslide occurrence; x_1 is the i-th explanatory variable; β_0 is a constant; β_i is the i-th regression coefficient; and logit is the link function used to convert log-odds ($\pm\infty$) to probability, which is sigmoidal in shape and always yields values between 0 and 1. The probability of landslide occurrence can thus be formulated as:

$$p(Y=1) = \frac{1}{(1+exp^{(-(\beta_0)+\beta_1 x_1+...+\beta_i x_i))}} \tag{6.5}$$

In the context of landslide susceptibility, the probabilities from logistic regression correspond to the predisposition of a given mapping unit to landsliding and are thus often referred to as spatial probabilities, as the probability makes no reference to time other than estimating the degree to which a given area is likely to be the site of a future landslide occurrence. BLR modelling was performed using the caret package (Kuhn, 2008) and the terra package (Hijmans, 2022) was used for model predictions, both within the open-source statistical software R (Team, 2021).

Logistic regression assumes independence of the independent variables. Therefore, the car package (Fox et al., 2012) was used to test for multicollinearity by quantifying the variance inflation factor (VIF) for all continuous variables. A predetermined VIF threshold of 2 was used to select variables for removal from the model ((Heckmann et al., 2014; O'brien, 2007; Smith et al., 2021; Van Den Eeckhaut et al., 2006). Moreover, all independent variables were removed with a test-statistic for the Wald test (z-statistic) of less than 2, which means the effect size is not significantly different from 0 (95% confidence level) and removal will not significantly affect model fit.

6.2.4.2 Independent predictor variables

The topographic predictor variables were derived from a 1-m LiDAR DEM and are the same as those used by Spiekermann et al. (2022b), including slope gradient (°), northernness (cosine transformation of slope aspect), and easternness (sine transformation of slope aspect). Refer to Spiekermann et al. (2022b) for further information on these variables and their physical process relevance for slope stability. One additional topographic variable was included here: the Topographic Wetness Index (TWI). The TWI is a measure of water accumulation or soil saturation (Moore et al., 1988) that may influence the propensity for landslide generation. For each tree class j (section 6.2.2.3), the TIMMS (M_j) were computed using the tree classification with the following logistical function (Spiekermann et al., 2022b):

$$M_j = 1 - \frac{1}{(1+e^{(\frac{(xmid-r)}{scal})})}, \tag{6.6}$$

where xmid is a parameter representing the r value at the inflection point of the curve; and scal a scale parameter on the input axis. Table 5 provides the values used for parameterising the TIMSS. As with the lateral root reinforcement model, the TIMSS assume the influence of trees contributing to slope stability at a given pixel to be additive. It does not account for variation in tree dimensions.

TABLE 6.5: Parameterisation of TIMSS for different tree classes

Tree class	xmid	scal	max r (m)
Conifer	6.98	3.12	17
Kanuka/Other native	7.51	2.71	17
Poplar/Willow/Acacia	8.58	3.44	20
Eucalyptus	6.86	1.93	13

Finally, lithological data (near-surface rock type) from the NZ Land Resource Inventory (Newsome et al., 2008) was included as a categorical variable, since the material type directly influences soil properties such as hydraulic conductivity and texture (Smith et al., 2021). Lithology was converted from vector format available at a scale of 1:50,000 to a grid at 1-m GSD. It is unavoidable that boundary and material type errors will result from using lithological data of

much lower resolution than for topographic variables. To ensure sufficient samples were gathered across all material types to safely infer the relationship, we remove lithology classes that are represented in less than 1% of combined presence and absence points (minimum 137 samples of balanced dataset). This led to the removal of two material types: "Gravels" (37 samples) and "Mudstone or fine siltstone — jointed" (82 samples), which reduced the landslide inventory to 6889 landslide scars and an equal number of landslide absence points.

6.2.5 Physical and statistical model performance measure

K-fold (k = 10) cross validation (CV) was used to test model predictive performance in the BLR model. The data were randomly partitioned into k folds, whereby k-1 folds are used to train the model, and the remaining fold used to test the predictive ability of the model. This is repeated until each of the ten folds has been used for model testing. To ensure the performance measures are not influenced by a particular data partitioning, this process is repeated 10 times, yielding a total of 100 performance metrics. The area under the receiver operator curve (AUROC) was used to estimate the model's predictive performance by plotting the true positive rate (sensitivity) against false positive rate (1 – specificity) across all potential cut-offs. The AUROC is well suited for balanced samples as it does not depend on the cut-off used to calculate classification accuracy (Hosmer, 2000). An AUROC score of 1 would mean the model can perfectly discriminate between the presence and absence of landslides in its predictions; a value of 0.5 corresponds to no discriminatory power. A good AUC score is between 0.8 and 0.9; an excellent score is > 0.9 (El Khouli et al., 2009).

Moreover, to enable a direct comparison of model performance using a standardised metric, AUROC with respect to the 2010 inventory is quantified using all data extracted from the raster predictions of the whole study area. Probability values coinciding with the rasterized landslide polygons (1-m resolution for BLR; 2-m resolution for SlideforMAP) were extracted and all other cells within the farm boundaries represented landslide absence cells. For SlideforMAP the AUROC is a near-independent measure of performance – the exception being that the shallow landslide surface area distribution used in SlideforMAP is based on the inventory surface area distribution.

6.2.6 Quantifying effectiveness of trees on slope stability at farm scale

Spatial predictions of landslide susceptibility were made for the two case study sites using both SlideforMAP and BLR models. We classified these spatial probabilities of landslide occurrence into three susceptibility classes of low, medium, and high (Lombardo & Mai, 2018; Petschko et al., 2014). This was done by extracting predicted probability values at each of the inventoried landslide points, ranking these in descending order and determining the probability thresholds of the 80th and 95th percentiles of landslide counts (Figure 6.4). This results in three landslide susceptibility classes of low, medium, and high. Thus, the high susceptibility class can be interpreted as the zones in which 80% of mapped landslides were triggered, the medium class where an additional 15% of landslides occurred, and the low class where the remaining 5% of past landslides were triggered.

The effect of the actual tree cover (S_1) was quantified by developing a treeless, pasture-only baseline scenario (S_0) and generating spatial predictions without any trees present. The same probability thresholds corresponding to the 80th and 95th percentiles of ranked landslides (based on predictions with the actual tree cover) were used to classify each of the predictions into the three classes of low to high. Reductions in landslide erosion at farm-scale are based on changes (CC, %) to the distribution of the three landslide susceptibility classes i for each farm:

$$CC_i = \frac{S1_i - S0_i}{S0_i} * 100, \tag{6.7}$$

where S1 and S0 are the proportions (0-1) of the three susceptibility classes of scenarios S_1 (actual trees) and S_0 (the baseline), respectively. We assume that future landsliding will follow the same pattern as in the past, such that the majority (80%) of landslides will occur in the high susceptibility zone, and so forth. Therefore, a reduction in the area occupied by the high susceptibility zone equates to a reduction in the number of future landslide erosion; the same is true for the medium susceptibility zone. This reduction in landsliding (LS_red) considers the rate (based on counts) of landsliding LR_i in each of the classes i = 0.8,0.15,0.05:

$$LS_{red} = \Sigma_{(i=3)}(CC_i \cdot LR_i), \tag{6.8}$$

To mitigate future landslide erosion, land managers require decision support on where to plant trees cost-effectively (Spiekermann et al., 2022b). To determine the potential implications of using a particular landslide susceptibility model, a spatial overlay between SlideforMAP and the BLR classifications was undertaken to quantify the level of agreement – both for the treeless baseline scenario (S0) and with the actual tree cover (S1) (Table 6.10). In this way, a spatially explicit comparison provides further insight beyond the difference in overall performance metrics and proportion of sites classified in the three landslide susceptibility classes (Table 6.9).

6.3 Results

6.3.1 Tree classification with CNN

The results of the tree classification are given in Table 6.6 and Table 6.7. Overall accuracy is 0.69, with average increasing to 0.79 when weighting by class size. Precision scores are overall significantly higher than recall scores, which means the model avoids large numbers of false positives. The poplar/willow class, with an f1 score of 0.93, has the highest overall classification accuracy. The lower recall scores indicate that false negatives are the most common source of error, as shown in the "Background" column of Table 6.7. This means the model struggled to detect and classify a reasonably large number of tree crowns. Yet, certain tree classes are more affected than others. The classes "Conifer", "Kānuka", and "Other Natives" were impacted most, as shown by their lower recall scores. For example, of the 13,661 samples, 5247 tree crowns of the Kānuka class (38.4%) were not detected and therefore classified as "Background". In terms of implications for the landslide susceptibility models, the low detection rate among these classes will result in an underestimation of mitigation effectiveness. Therefore, the results presented in the following sections can be interpreted as a conservative estimate of mitigation performance.

TABLE 6.6: Tree classification results, including precision, recall, f1-score statistics

Tree class	Precision	Recall	f1-score	Support
Background	0.01	1.00	0.02	69
Conifer	0.99	0.74	0.84	4339
Kānuka	0.95	0.61	0.74	13661
Poplar/Willow	0.98	0.88	0.93	5645
Eucalyptus	0.89	0.85	0.87	1414
Acacia	0.98	0.60	0.74	857
Other natives	0.96	0.51	0.67	2381
Accuracy			0.69	28366

TABLE 6.7: Confusion matrix

Tree class	Background	Conifer	Kānuka	Poplar/Willow	Eucalyptus	Acacia	Other natives	Total
Background	69	0	0	0	0	0	0	69
Conifer	1012	3194	13	23	67	8	22	4339
Kānuka	5247	7	8349	26	20	0	12	13661
Poplar/Willow	500	19	61	4983	63	4	15	5645
Eucalyptus	176	0	24	13	1200	0	1	1414
Acacia	266	10	15	44	4	512	6	857
Other natives	830	1	322	5	0	0	1223	2381
Accuracy	1.00	0.74	0.61	0.88	0.85	0.60	0.51	0.69

6.3.2 Landslide susceptibility modelling

Multicollinearity tests showed all continuous variables to have a VIF <2. Therefore, all continuous variables were retained in the model. Slope gradient was the most important variable in determining shallow landslide occurrence, followed by TWI (Table 6.8). Landslides occurred disproportionately on north- and east-facing slopes. As expected, the TIMSS had a significant stabilising effect. Except for "Limestone", all lithologies were removed from the BLR model as the coefficients were not significantly different from 0 and thus did not contribute to an improved model fit. Since most landslide presence and absence points are located in areas of either "Mudstone or fine siltstone – massive" (36.7%), "Loess" (30.1%), or "Sandstone or coarse siltstone — massive" (23.2%), these lithologies are effectively the reference category. The lack of significance of all lithologies besides Limestone (6.4% of data points) suggests that lithology plays a minor role in determining landslide occurrence in the study area, i.e., all other rock types are similarly susceptible to shallow landsliding.

TABLE 6.8: Standardized coefficients with associated standard errors and z-statistics for predictor variables of the BLR model (p-value of Wald's test and likelihood ratio test < 0.001 for all these variables)

Variable	Coefficient	SE	z statistic
(Intercept)	-0.41	0.03	-12.97
Slope	3.68	0.07	54.26
North	0.36	0.03	13.19
East	0.13	0.03	4.75
TWI	0.65	0.04	15.34
TIMSS	-0.43	0.03	-15.02
Li1	-1.34	0.13	-10.42

The AUROC of the final model was 0.94, which equates to an accuracy of 88.1% using an optimal cut-off of 0.50, and demonstrates an excellent model fit of the BLR. 10-fold cross-validation using 10 repeats was used to quantify the model's predictive performance (Figure 6.4). Median AUROC of the 100 train-test cycles was 0.94, with an IQR of 0.008, reflecting a stable performance in predicting the test data as either landslide presence or absence points.

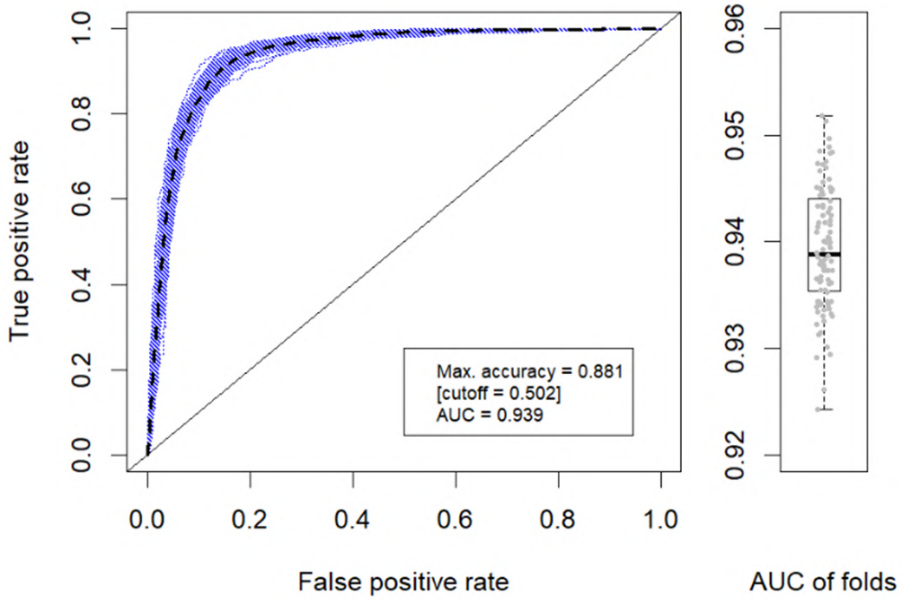

FIGURE 6.4: k-fold cross-validation results of BLR model.

The cumulative histograms show consistently higher class cut-offs for BLR, indicating the statistical model was slightly better at associating landslide scars with high probability values. The cut-offs from Figure 6.5 spatially divide the shallow landslide susceptibility predictions into three distinct classes, as displayed in Figure 6.7.

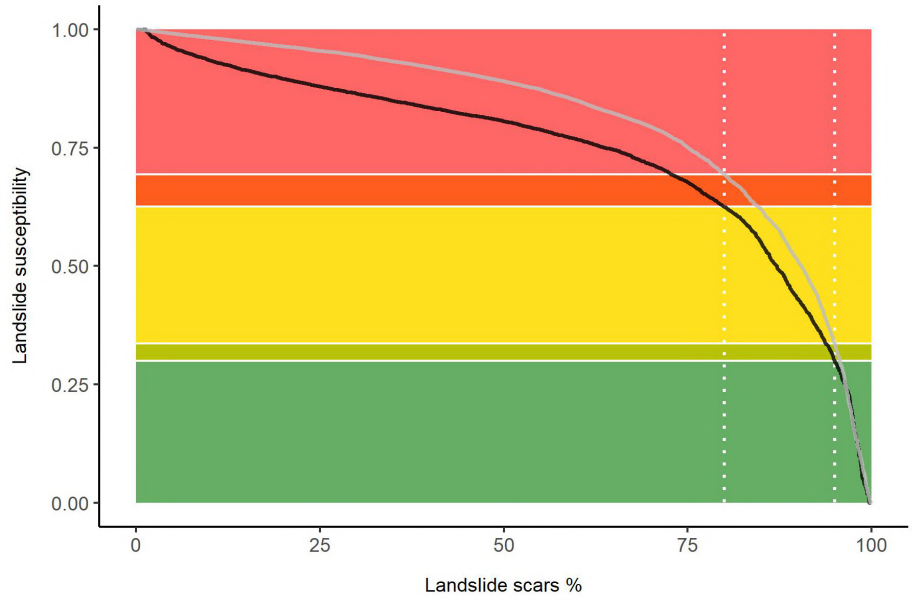

FIGURE 6.5: Decreasing rank order plot of SlideforMAP (black line) and binary logistic regression (grey line) susceptibility predictions for inventoried landslide scars for both farms combined. Predicted scar susceptibility is ranked in descending order with the percentage of scars with an equal or higher susceptibility given on the x-axis. The 80 % and 95 % percentage susceptibility cut-offs are at 0.65 and 0.31 for SlideforMAP respectively. For BLR the cut-offs are 0.69 and 0.34. These cut-offs determine the probability values used to classify predictions into three susceptibility classes of low, medium, and high.

The extent to which vegetation influences slope stability is dependent on the method used as shown in Figure 6.6. The maximum effective radius from the tree stem in SlideforMAP is 5 to 6 meters, corresponding to the most mature trees. The effective range for TIMMS is > 10 m, independent of tree dimension. This results in more overlap in the tree influence using TIMMS, and probably an overestimation of the effect of single trees of small dimensions (see single trees in the upper right corner of Figure 6.6).

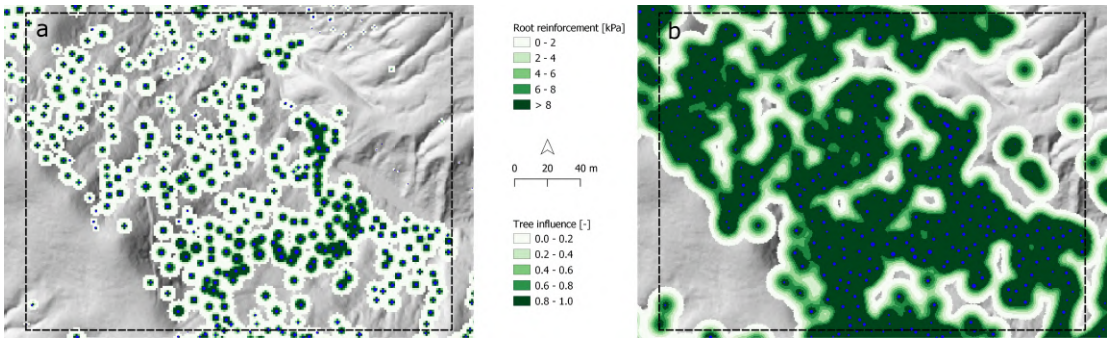

FIGURE 6.6: Spatial representation of individual tree (blue dots) effects for a selected area at Site 2. Insert a: maximum lateral root reinforcement in SlideforMAP. Insert b: Tree influence models on slope stability (TIMSS) as used in Binary logistic regression.

As can be seen from Figure 6.7, SlideforMAP appears to have a higher proportion of surface area classified as highly susceptible, both with and without vegetation. Instability is concentrated in the south-west of Site 2, coinciding with deeper soils. Binary logistic regression shows a more even distribution of susceptibility through the study area. Vegetation has a considerable influence on the shallow landslide susceptibility classification for both methods. In the little window we can see a reduction in landslide susceptibility in the vicinity of single trees, with larger trees giving a larger reduction in susceptibility for SlideforMAP. These patterns are, at least partly, responsible for the difference in susceptibility as shown in Figure 6.7.

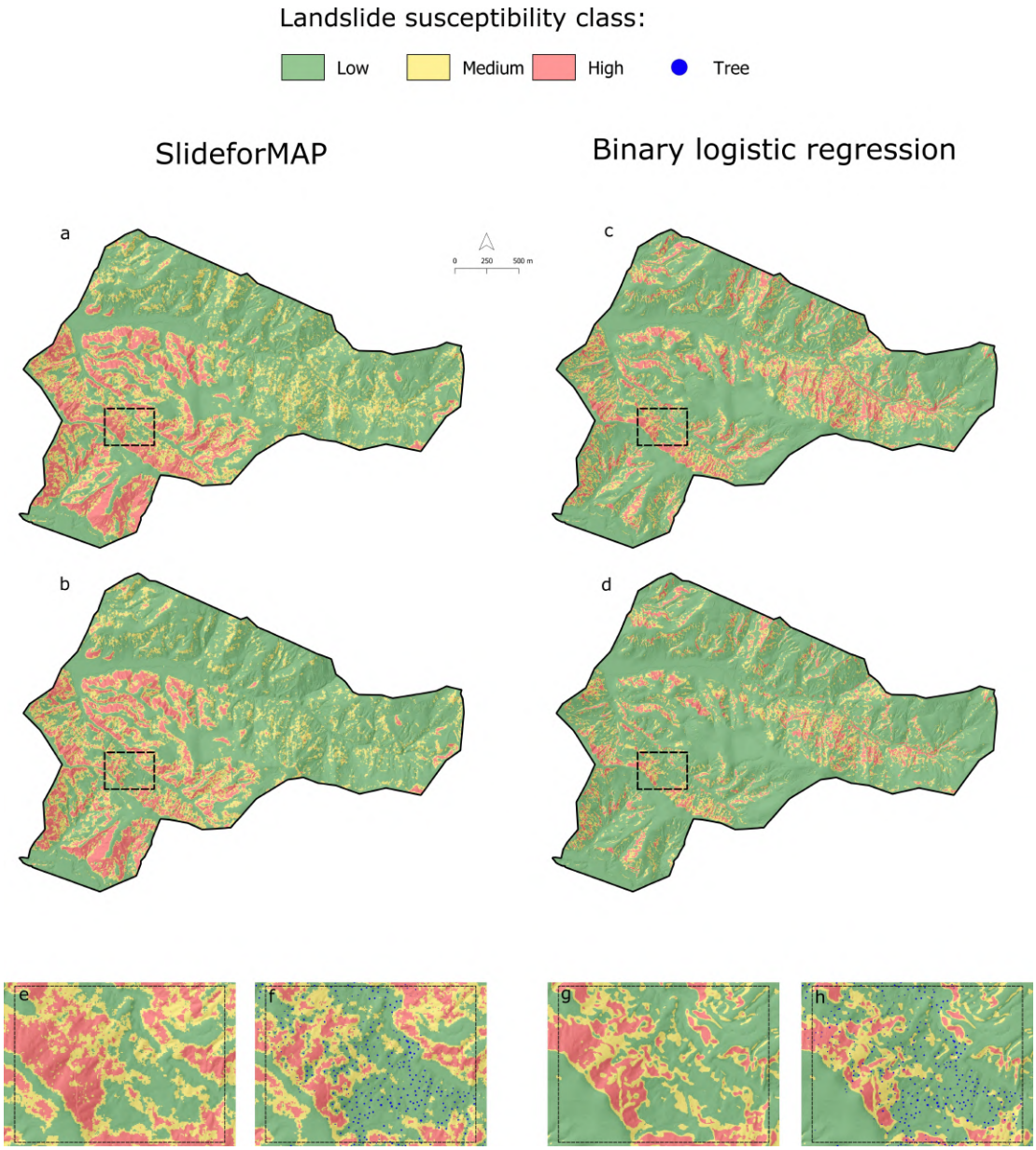

FIGURE 6.7: Comparison of landslide susceptibility at Site 2 between SlideforMAP (left column) and BLR (right column) based on three classes "low" to "high. Inserts a) and c) represent the treeless baseline scenario S0; Inserts b) and d) the actual tree cover S1. Inserts e) and f) show SlideforMAP landslide susceptibility classification without and with trees (blue dots); Inserts g) and h) do the same for the BLR classification, respectively.

The landslide susceptibility classifications of SlideforMAP and BLR are shown in Table 6.9 and includes both class distribution and the respective performance measure. As expected, the class distribution changes to a higher proportion in the low susceptibility class for both models under the actual tree cover. Despite adjusting the class cut-offs to landslide scar values (Figure 6.5), SlideforMAP has higher proportions of the study area in both the high and medium susceptibility classes – consistently for the baseline (S0) and when including the actual tree cover (S1). There is also less change in the distribution of susceptibility classes resulting from the tree cover compared with the BLR, which results in a lower estimate of mitigation performance. Based on equations 7 and 8, future landsliding (counts) is estimated to have been reduced by 3.2% at Site 1 and 16.4% at Site 2. This compares with estimates by the BLR model of 11.4% and 35.1%,

respectively.

Values of the AUROC performance measure based on the raster predictions for the study area extents (farm boundaries) are overall higher for BLR, with the best performance of 0.936 achieved at Site 2. SlideforMAP, in contrast, has its best performance at Site 1.

TABLE 6.9: Performance measurement and distribution of shallow landslide susceptibility classes (%) at Sites 1 and 2. Percentages are rounded and therefore do not always end up to 100% exactly

	SlideforMAP		**Binary logistic regression**	
	Site 1	Site 2	Site 1	Site 2
Treeless baseline S_0				
High	22.7	16.0	14.4	12.2
Medium	22.1	24.8	14.4	19.1
Low	55.2	59.2	71.2	68.7
Actual tree cover S_1				
High	21.8	13.0	12.4	7.3
Medium	22.0	21.6	13.6	15.1
Low	56.2	65.3	73.9	77.7
LS_{red} (%)	- 3.2	- 16.4	- 11.4	- 35.1
AUROC	0.871	0.826	0.911	0.936

Table 6.9 provides an overview of the level of agreement between SlideforMAP and the BLR landslide susceptibility classifications for the two study sites. In total, >70% of the spatial predictions are in agreement. In particular, the "Low" class of both models are almost in complete agreement. Interestingly, the greatest difference between the models is found in the medium class, with approximately 14% of the sites classified as "Medium" landslide susceptibility by SlideforMAP and "Low" landslide susceptibility by the BLR model. In general, SlideforMAP has a larger proportion of the sites classified as either "Medium" or "High" compared with the BLR model. Since the statistical approach fits a BLR model to the landslide inventory, the ability of the model to predict future sites of landslide occurrence is likely to be less than that quantified using cross-validation in this study. Therefore, the comparatively lower performance and less spatially refined predictions of SlideforMAP may not necessarily translate into a poorer predictive capability in terms of future landslide events. Considering the current tree cover, both models agreeing on "high" makes up approximately 8.2% of the study area. An additional 13.4% of the study area is classified as highly susceptible in either the SlideforMAP or BLR classification and should be considered for prioritising over the remaining 78.4% of the study area classified as either low or medium landslide susceptibility.

TABLE 6.10: Comparison of distribution of landslide susceptibility classes across the study area as predicted by SlideforMAP and the BLR model

BLR Class	**SlideforMAP Class**	**Treeless S0 (%)**	**Actual trees S1 (%)**
Low	**Low**	55.0	56.8
Medium	Low	2.1	2.0
High	Low	0.8	0.8
Low	Medium	13.9	14.5
Medium	**Medium**	5.8	5.2
High	Medium	1.8	1.5
Low	High	3.7	4.4
Medium	High	7.1	6.7
High	**High**	9.7	8.2
Total agreement		**70.5**	**70.1**

An added benefit of the physically based approach is the ability to compute the landslide susceptibility under different precipitation conditions. The comparison with BLR is performed under the extreme 2005 precipitation event that most likely left soils close to saturation. To contrast these results, the susceptibility classes in Table 6.11 are shown for the 5 yr. return period precipitation intensity (as defined in section 6.2.3.2). As can be seen using a lower precipitation intensity, there is only a slight decrease in the high-class proportions for both the vegetation and the non-vegetation scenario.

TABLE 6.11: Distribution of susceptibility proportion for SlideforMAP for a 5 yr. return period and 12-hour duration rainfall event. Thresholds from Figure 5 have been used to enable comparison to SlideforMAP class distribution under the extreme March 2005 event.

SlideforMAP 5 yr. return period design event	
	Site 2
Treeless baseline S_0	
Proportion High	15.6
Proportion Medium	24.8
Proportion Low	59.6
Actual tree cover S_1	
Proportion High	12.5
Proportion Medium	21.5
Proportion Low	65.9

6.4 Discussion

6.4.1 Evaluation of physical and statistical model predictions

The instability pattern in Site 2 appears to be driven by multiple factors in SlideforMAP, most notably slope angle and soil thickness. This can be well explained, as the soil thickness is noted as a highly sensitive parameter in the qualitative sensitivity analysis on SlideforMAP (van Zadelhoff et al., 2022). In Figure 6.7, the upper right of site 2 has shallow soils and the lower left deeper soils, directly mirroring the pattern in the instability with deep soils corresponding to higher landslide susceptibility.

In SlideforMAP only the mechanical effects of single trees are modelled, which have an effective distance of approximately 5-6 m, before the effect becomes negligible (Figures 6.3 and 6.6). This can also be seen in Figure 6.7f, with only large trees affecting the shallow landslide susceptibility class. This tree-size effect is an advantage as it enables modelling of the effects of tree development through time, either for existing trees or for proposed planting. Data related to tree growth rates (e.g. Matsushita et al., 2015) are required for estimating tree effects through time, as are allometric relationships between above and below ground tree biomass.

As mentioned in the introduction, the strength of the physically based approach is the evaluation of different rainfall scenarios, which can be actual events (SlideforMAP results in Table 6.9) or design events (results in Table 6.11). In this case, the March 2005 event corresponds to a return period greater than 100 years. Contrasting this to the design event, we see a larger proportion of high landslide susceptibility for both the vegetated and non-vegetated scenario. This scenario modelling can help to incorporate more frequent and more intense occurrence of landslide inducing rainfall events due to climate change. Scenario based calculations of benefits (in this case related to the mitigation of erosion) are fundamental for the application of cost-benefit analyses

for prioritizing nature-based mitigation measures.

The pattern of landslide susceptibility classes in BLR is more evenly distributed, with slope angle being the main driver for landslide susceptibility (Table 6.8). The sphere of influence of individual trees extends further that the lateral root reinforcement model (Table 6.5, Figures 6.3 and 6.6) and has a significant influence in determining landslide occurrence. The distribution of landslide susceptibility classes at Sites 1 and 2, and the estimation of mitigation performance (Table 6.9), are slightly different compared with that quantified by Spiekermann et al. (2022b) and overall are less susceptible. For example, at Site 1, the "High" class now occupies 14.3% instead of 15%, the "Medium" class 14.4% instead of 17.7% without trees. Besides being based on a subset of the landslide inventory used by Spiekermann et al. (2022b), these differences can also be attributed to the inclusion of the hydrological variable of TWI in the model, which has the effect of reducing landslide susceptibility in upper slopes where the upstream contributing area is reduced and thereby affecting soil moisture conditions.

The AUROC value for SlideforMAP indicates good performance (AUC > 0.8), indicating SlideforMAP can well identify regions susceptible to landsliding, without prior knowledge of the landslide events. The performance of BLR is excellent (AUC > 0.9). Although this is with tree influence calibrated to the landslide inventory, it shows that BLR is an effective method for discriminating landslide susceptible areas from stable areas.

6.4.2 Contrasting physical and statistical landslide susceptibility approaches

Assumptions and limitations of physically-based landslide susceptibility modelling

Since many abiotic (e.g., light, temperature, rainfall) and biotic (e.g., other trees, organisms in soil) factors influence the development of both tree crown and root system architecture (Iwasa et al., 1985; Lindh et al., 2018; Pierret et al., 2007), the hydrological and mechanical processes of a tree can vary considerably between and within tree species (Hales et al., 2009; Masi et al., 2021; Schmidt et al., 2001). This is particularly true when tree densities are such that competition for limited available resources (nutrients, water, light) is increased (Danjon et al., 2013). In their review of root systems of mixed-tree systems, Kumar and Jose (2018) found evidence that two or more tree species located in close proximity can cause reduced lateral spread of roots and/or increase root penetration at greater soil depths. Trees with similar root growth habit are more likely to have interlocking root systems that increase competitive interactions, whereas mixing tree species with different growth habits can result in temporal or spatial complementarity in use of above- and belowground resource (Kumar & Jose, 2018). This is due to phenotypic plasticity, which enables roots to respond to effects arising from i) variation in the abiotic environment (soil nutrients, water, light; Perona et al. (2022)), ii) the presence of neighbouring trees, and/or iii) herbivory (Callaway et al., 2003).

There is currently a paucity of species-specific data on root system architecture from widely spaced trees such as those found in agroforestry systems (Kumar & Jose, 2018; Schwarz et al., 2016). Most root extraction work aimed at characterising root system architecture of trees has been undertaken in forest stands (Hales, 2018), which means there is less data available to inform the development of root reinforcement models in silvopastoral systems or to calibrate root growth models (Schlüter et al., 2018). Knowledge of root systems in silvopastoral settings is limited to individual species of certain age classes (Marden et al., 2018; Phillips et al., 2014; Stone & Kalisz, 1991). This lack of data has direct implications for estimating the magnitude of lateral root reinforcement in fully mature adult trees, since the quantitative estimates rely on

knowledge of the spatial distribution of the roots (Cohen & Schwarz, 2017b). Moreover, the data requirements for developing estimates for species-specific, spatially distributed root reinforcement are not insignificant (Schwarz, Lehmann, et al., 2010). In fact, due to variability within root systems, it was found a minimum of four trees must be excavated to obtain sufficient root information to reduce the error associated with root reinforcement estimates to a level acceptable by geotechnical guidelines (Giadrossich et al., 2020). However, these requirements may change according to species and site specifics.

Therefore, the limiting factor to further develop root reinforcement models in silvopastoral systems is the lack of species-specific root data, which includes:

- Data pertaining to the strength and behaviour of different root diameter classes within the root-soil matrix (Schwarz, Lehmann, et al., 2010);
- Morphological data pertaining to the root system architecture, including the number of roots in different diameter classes with increasing distance from tree trunk and soil thickness;
- Root data of trees that grow in different environmental settings (e.g., substrate characteristics), spacings, and mixed-species vs. monoculture silvopastoral systems.

Given the current lack of observational data, the development of a root reinforcement model for a mixed-tree silvopastoral system requires assumptions during model parameterisation, particularly related to total and maximum root lengths and/or biomass (Stone & Kalisz, 1991). Moreover, the reductionist approach employed by root-reinforcement modelling is an inherent limitation (Masi et al., 2021). Reducing a tree to observations of the behaviour of its components (e.g., foliage, root system) cannot reveal the full extent of its properties – let alone a tree interacting within its environment composed of biotic and abiotic components. These properties that most natural systems have in addition to the sum of properties of the components are referred to as emergent properties of irreducible systems (Jorgensen, 2016). This concept of emergent properties promoted by Systems Ecology Science poses a challenge to physically-based models that follow an inherently reductionist approach to studying tree effects on slope stability.

Root reinforcement modelling versus TIMSS

While these limitations mean root reinforcement modelling in silvopastoral landscapes remains a challenge, there are advantages of a physical approach to quantifying individual tree effects on slope stability that include the ability to differentiate and weight the contribution of different mechanisms and processes allowing for their better understanding, quantification and for specific formulations of engineering solutions quantify both the mechanical reinforcement provided by root systems and the hydrological effects of trees on regulating soil moisture. The result is an estimate of the added contribution to soil strength as a measure of force (N/m) and can be used to consider how the margin of stability will change under any given hydrological scenario or change in land cover (Schwarz et al., 2016). This enables land managers and policy makers to design effective measures in relations to the occurrence probability (return periods as seen in Table 6.11) and the magnitude of triggering rainfall events and disposition factors with standardized return periods. A further key advantage of probabilistic-physically approaches is the use of allometric relationships between above and below-ground biomass. Thus, as advances in technology increase the ability to characterise above-ground properties of trees (Gunawardena et al., 2015), the main barrier to improved estimates of mechanical reinforcement stabilising effects of slopes by silvopastoral trees is the cost associated with empirical data collection. Nevertheless, a meaningful balance between the amount of data needed and the detail of model precision and

accuracy for solve a specific practical problem need to be discussed and found.

A limitation of the TIMSS method is the lack of a clear physical basis, as the TIMSS rely solely on patterns observed at landscape scale to infer what the physical parameters must be that render the relationships between the objects of interest, namely trees and landslide scars. This raises the question of plausibility, to which there are two helpful responses: The first is by way of a practical justification. Given the data scarcity with respect to root system architecture of adult trees, which have been established in an environment with negligible competition from neighbours, a validation of the TIMSS is only possible with reference to the limited root data available from widely spaced trees (see section 6.3). Both extracted root systems of younger trees (e.g. McIvor et al., 2009) and equivalent spatially distributed root reinforcement models (e.g. Schwarz et al., 2016) were similar to the TIMSS in terms of the sigmoidal shape of the curves despite the unit of measurement not being the same.

Secondly, the method of inquiry used follows a logical form guided by material induction theory (Norton, 2021). Based on a set of warranting facts, material inductive inference allows conclusions to be drawn that amplify pre-existing knowledge of the system (Norton, 2021). The warranting facts in this case can be summarised in the following statement: "Trees modify slope stability due to mechanical and hydrological mechanisms". Based on the assumption that these effects must manifest in such a way that can be observed at landscape scale, the TIMSS were developed using geospatial methods by testing whether landslide scars occur preferentially close to or remote from trees. The resulting TIMSS therefore infer the extent to which individual trees increase slope stability. The TIMSS raise some interesting questions, particularly related to the average maximum effective distance of an individual tree (e.g., 20 m for poplar/willow).

Lateral extent of effective root reinforcement is far less than the empirically-derived TIMSS (Figure 6.6). By definition, TIMMS reflect all single vegetation effects and possible synergies between these effects for the trees, landslides, and landslide absence areas to which it is calibrated. The compounding vegetation effects are attributed to the nearest trees from any given point in the landscape. SlideforMAP incorporates only the mechanical effects (lateral root reinforcement, basal root reinforcement and vegetation weight) and no synergies. Not having incorporated the hydrological effects of trees in SlideforMAP could be an important factor of difference. Local tree interception and reduction in antecedent moisture are unlikely to have a large influence under extreme precipitation conditions (Greenway, 1987) such as with the event we modelled here. However, a reduction in antecedent moisture, an increase in macropore lateral flow within a potential landslide and increase in storage capacity in a potential landslide contributing area is a more likely cumulative effect. An additional possibility is the limitation of landslides to occur between trees due to confinement between reinforced areas (Casadei et al., 2003; Cohen & Schwarz, 2017b). Where root reinforcement from neighbouring trees does not interconnect, tree roots likely decrease non-reinforced areas to such an extent that passive earth pressure prevents the potential landslides from initiating. If the tree confinement and contributing area are indeed a relevant effect, tree influence is not a primary tree-specific effect, rather it is a secondary site-specific effect as a function of tree dimensions, planting density and pattern. Further research is required to test the veracity of this hypothesis.

Assumptions and limitations of statistical landslide susceptibility modelling

The central assumption made in statistical landslide susceptibility models is that "the past is the key to the future" (van Westen et al., 2008). This assumption related to empirical inference is one made across the sciences, where past observations are used to establish causation and to

predict both what is likely to happen elsewhere under similar situations and the outcomes of future events. The limitation arising from this underlying assumption is that statistical landslide susceptibility models can only be used to predict future locations of landslide occurrences with similar causal mechanisms to the landslides used to train the model. However, slope stability is temporally dynamic due to changes in regolith depth, slope angle, land cover, etc. Indeed, the conceptual Terrain Event Resistance Model was proposed by Crozier and Preston (1999) and refers to the observations by Trustrum et al. (1984) that catchment landslide susceptibility changes are due to the progressive removal of susceptible regolith from parts of the catchment, reduction of lateral support, and related scar formation, etc. The combination of an evolving landscape with variable triggering mechanisms challenges the legitimacy of cross-validation using subsets of the same landslide inventory in testing the prediction skill of future events.

In the present study, a landslide inventory mapped on imagery from 2010 comprises a range of events from the period 2005–2009 – both summer and winter events of differing rainfall magnitudes (Spiekermann et al., 2021). While it remains unknown which event caused which landslide in the inventory, the model was trained using landslides that were triggered under a range of hydrological conditions, which – although not quantified – may increase the predictive skill for future events. If the study area is currently in an advanced stage of the Terrain Resistance Model due to multiple previous landslide events (De Rose, 2013; Spiekermann et al., 2022a) and requires increased triggering thresholds relative to historic events, then models trained with more recent landslide events are likely to outperform in future compared to models trained with historic events.

There are studies that have tested this assumption using multi-temporal landslide inventories. It is generally the case that multi-temporal landslide inventories are considered the preferred source of landslide information for susceptibility modelling (Reichenbach et al., 2018). Jones et al. (2021) used a 30-year inventory of monsoon-triggered landslides from Nepal to assess how well statistical models hindcast landslide occurrence in other years. They found models trained on extreme years unable to consistently hindcast landslide occurrence in other years. Landslide distributions were found to vary through time, which was due to different triggering mechanisms (storms, earthquakes, floods). However, developing models using increasingly long historical inventories showed that susceptibility models developed using >6–8 years of landslide data provide consistently reliable hindcasting accuracy. This affirms findings from similar studies (Guzzetti, Galli, et al., 2006; Smith et al., 2021; Spiekermann et al., 2022b), which demonstrate a dependency on sample size. A further example undertook a study to assess landslide susceptibility models based on event versus multi-temporal landslide inventories to better understand how inventory type affects model performance (Smith et al., 2021). The authors used three event-scale and three smaller multi-temporal study areas to fit models using the event-based data and test predictive performance with the multi-temporal data and vice versa. Multi-temporal records are generally restricted to smaller study areas, resulting in a less diverse range of lithologies and landforms. This was shown to reduce the transferability of the model to other areas. While the event-based models performed slightly better, the authors found no consistent improvement in model predictive performance when using the multi-temporal versus the event inventories. This lack of distinct improvement in model performance may reflect the event-scale landslide densities, which, if sufficiently high, could reduce the relative benefit of using a multi-temporal inventory for landslide susceptibility modelling. A similar assessment was undertaken by Spiekermann et al. (2022b) using a model developed by Spiekermann et al. (2022b) and tested with a landslide inventory from a 1977 storm event. Historic landslides were found more frequently on what is considered "moderately susceptible terrain" by a present-day susceptibility model, which was explained by differences in the triggering mechanism (long-duration rainfall with high antecedent moisture conditions in 1977 versus high intensity rainfall

events of 2005–2009). However, it was noted by the authors that the difference may also be an indication of terrain resistance.

While the Terrain Event Resistance Model (Crozier, 2005; Crozier & Preston, 1999) is conceptually plausible, the empirical evidence to support it remains inconclusive. It has been suggested that processes governing both failure location and associated off-slope sediment delivery are a more complex set of relationships relating to both slope properties and triggering conditions than the conceptual model supposes (Jones & Preston, 2012). A multi-temporal record of landslide events from 1943 to 2004 in the Waipaoa Catchment attempted to test the hypothesis that the relationship between landslide location and regolith exhaustion can be empirically observed as the soil mantle on lower slopes becomes increasingly below the critical depth for mass movement failure (Jones & Preston, 2012). However, the authors were unable to detect consistent upslope progression of the scars in relation to the channel in subsequent storm events in any of the five catchments and concluded that there was no predictable pattern in landslide locations over time. It is evident that further research is required to test the conceptual model of terrain resistance further to increase understanding of temporal dynamics in slope stability – both in terms of changes to terrain and triggering thresholds (D'Odorico & Fagherazzi, 2003). The development of future landslide susceptibility models should control not only for terrain and land cover effects but also for the triggering mechanism, e.g., through incorporation of rainfall data of adequate spatial and temporal resolution (e.g. Steger et al., 2022). Controlling for the triggering mechanism would allow model development for different rainfall events, which may render spatially variable predictions.

Implications for land management decisions

The shallow landslide susceptibility from either a statistical or physically based model can be interpreted as a measure of general landslide propensity or a specific propensity if estimated for a specific event. When done to a specific event with a corresponding inventory, the erosion volume and mass (depending on the assumption of soil density) can also be estimated. Physically-based scenario modelling is arguably better suited for estimating erosion for specific scenarios. We demonstrated this with SlideforMAP by estimating future landslide susceptibility for a specific design rainfall event with a given return period (Table 6.11). Statistical landslide susceptibility models, or hazard models, can also inform on the magnitude of the landslide response when data on the triggering mechanism (e.g., rainfall magnitude through use of interpolated precipitation or RADAR data) is available (e.g. Steger et al., 2022). While this research is limited to the current vegetation in our study area, the models can also be applied to analyse the effects of hypothetical tree planting Spiekermann et al. (2022b). This can help land managers and practitioners to effectively plan and better target the planting of new trees.

In terms of the utility of both approaches presented here, BLR can be used as a validation from the past to compensate for methodological uncertainty and/or inaccuracy in SlideforMAP. We therefore recommend decision makers prioritize areas for mitigation where SlideforMAP and BLR are in agreement within the high susceptibility class to achieve optimal outcomes. This will enable practitioners to reap the benefits from both the physical and statistical approaches, increasing the reliability of estimates for the future, while incorporating evidence from the past. However, it must also be recognised that in some areas of high slope instability, the effect of trees does not always increase stability sufficiently to avoid landsliding and establishment can be a significant challenge. Therefore, we recommend using the differences in unclassified probability maps as a supplemental source of information to guide decision-making with respect to planning tree planting. These maps of difference would show where the implementation of bioengineering measures would be most beneficial.

6.5 Conclusion

In the present study, we have shown how physical and statistical approaches to landslide susceptibility modelling are complementary in informing understanding of slope stability. It is uncommon to see process-based modelling alongside statistical modelling based on empirical data. A direct comparison of both models showed the strengths and limitations of the underlying assumptions. Both a statistically and physically based modelling approach to shallow landslide susceptibility for bio-engineering purposes has merit. Erosion can be mitigated by strategic planting of trees and both models can help in this regard. The main advantage in statistically based modelling is in the implicit inclusion of total tree effect, while the advantage of physically based models is the ability of precipitation event scenario modelling. Outputs from both models show an agreement of >70% for susceptibility class, with 8.2% of this agreement being in areas classified as highly susceptible. The <30% of the area where the models disagree in susceptibility classification can be attributed to differences in assumptions between the models and the better performance of the statistical approach since it fits the model using past observations of shallow landslides, resulting in improved spatial refinement of landslide susceptibility predictions. Land-managers aiming to optimize the targeted planting of trees are recommended to compare shallow landslide susceptibility under scenarios with potential trees and a treeless baseline (difference maps). This will help identify locations where new trees have the greatest protective effect excluding unstable areas that cannot be adequately stabilized by tree planting. Physically based models and non-linear statistical models (e.g., generalized additive mixed models) are best suited for such a comparison. Moreover, we recommend incorporating advantages of both approaches in this research and prioritizing areas for erosion mitigation where physical and statistical shallow landslide models agree within the highly susceptible class.

Declaration of competing interest

The authors declare no competing interests.

Acknowledgements

This research was supported by New Zealand Ministry of Business, Innovation and Employment research programs “Smarter Targeting of Erosion Control (STEC)” (Contract C09X1804) and “Bridging the gap between remote sensing and tree modelling with data science” (Contract C09X1923; Catalyst: Strategic Fund). We wish to acknowledge the contributions by Stella Belliss and Theresa Banning in form of on-screen digitization of tree crowns.

7 SlideforMAP application

Certain methodologies in the application of SlideforMAP or acquiring and assessing input parameters, are too detailed to have been included in any of the previous paper-based chapters. Nonetheless, these methodologies have been developed and/or analyzed during my PhD and therefore deserve mentioning. The sections below are dedicated to this purpose. Firstly, in section 7.1, fieldwork in New Zealand that was performed for calibrating root density and root reinforcement in poplar trees. Section 7.2 shows the application of SlideforMAP in assessing vegetation efficiency of current and hypothetical vegetation. Lastly, section 7.3 details a tiling approach to apply SlideforMAP to large study areas.

7.1 Fieldwork on poplar root architecture and root strength

As mentioned in chapter 5, poplar trees are often planted in New Zealand as a bio-engineering measure in slope stability. As part of my PhD, I conducted seven weeks of fieldwork in New Zealand, with the specific goal of obtaining field data to quantify lateral and basal root reinforcement of poplar trees. For this, a plantation at Ballantrae farm (near Woodville, Manawatu-Whanganui region) was chosen where four trees have had their root system excavated. The location of the study site and the four trees are displayed in Figure 7.1 below.

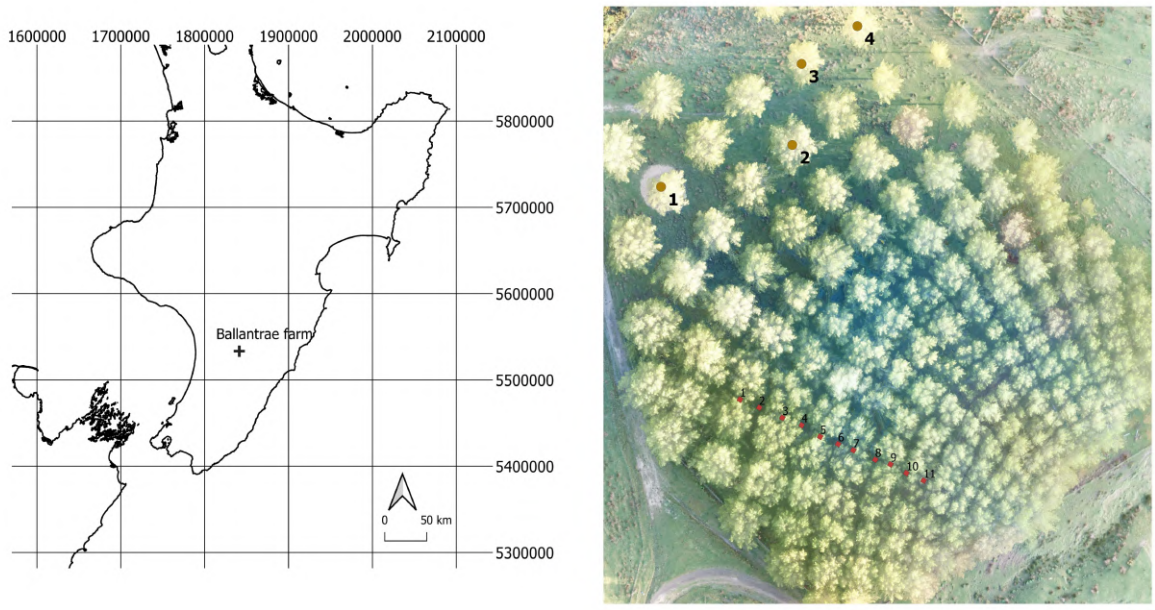

FIGURE 7.1: Left: location of the Ballantrae study site on the New Zealand north island. right: Aerial photo of the study site. Trees (1 to 4) are indicated of which the root system was excavated. The 11 transect holes are indicated as well

Trenches were dug around the four selected poplar trees, roots on the trench faces were counted and root diameter measured and arranged to distance and depth classes. The same method

was conducted to eleven 1 by 1 m transect holes on the plantation for validation purposes. A total of 64 in-situ pullout tests (section 2.4.2.1) on excavated roots on additional trees within the plantation were conducted. The calibration of the RBMw for poplar, as applied in this thesis for SlideforMAP, and further details of the fieldwork are presented in Ngo et al. (2023).

7.2 Vegetation mitigation scenarios

SlideforMAP can compute slope stability under hypothetical vegetation scenarios. For this, the input (either text or vector file) containing single tree detection results, is replaced with a data file of hypothetical trees. This data file is created from user input. Hypothetical forest can be generated under four dimensions of variation.

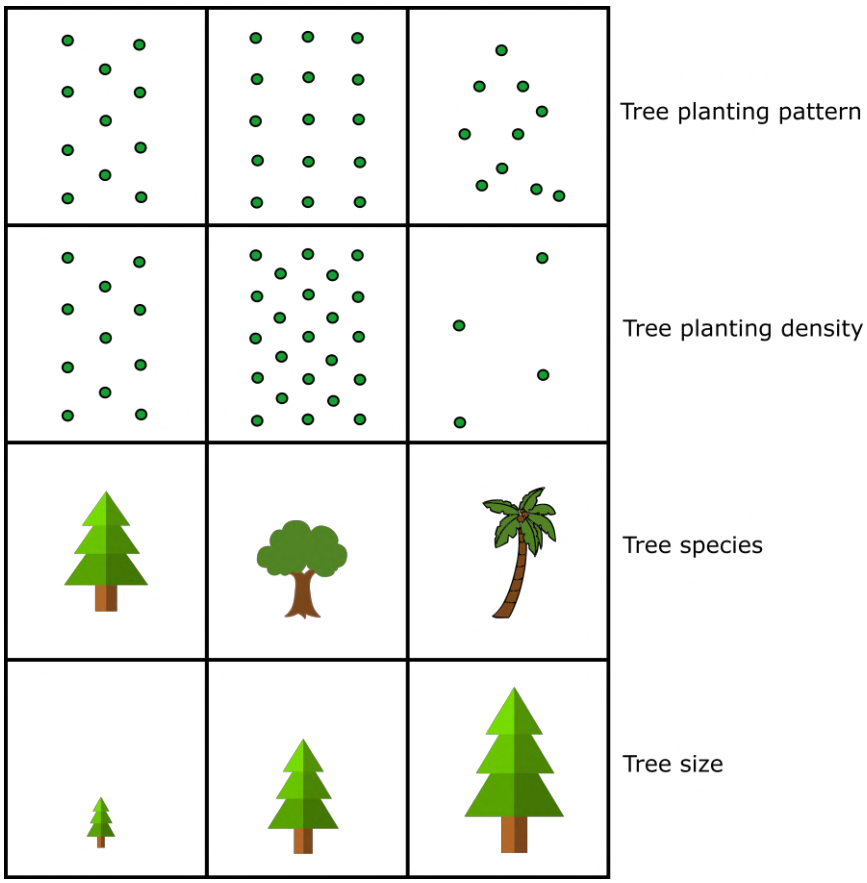

FIGURE 7.2: The four dimensions of variation in hypothetical forest generation. planting pattern (triangular, square or random), planting density (stems per hectare), planting tree species (provided RBMw calibration availability) and planting tree size (expressed in DBH).

For the locations of trees, tree density is given as well as desired pattern. Pattern can be cubic, triangular or random (with a user defined minimum distance between trees). Additional constraints, based on elevation, slope or topographic wetness index can be given as well to correct for tree suitability. Tree size [DBH] can be allocated uniformly or as samples from a normal distribution. Tree species can be defined uniformly, randomly from a distribution or conditionally to elevation, slope or TWI. Tree age and development through time, which is relevant in forest planning, is not explicitly accounted for in this method. This can be approximated by an increase in DBH. An example of two hypothetical vegetation scenarios in the St. Antönien study area (chapter 3) are given in Figure 7.3. These scenarios with lateral root reinforcement, shallow

landslide probability and relative reduction of probability are compared to the actual vegetation and a scenario without vegetation is used as reference.

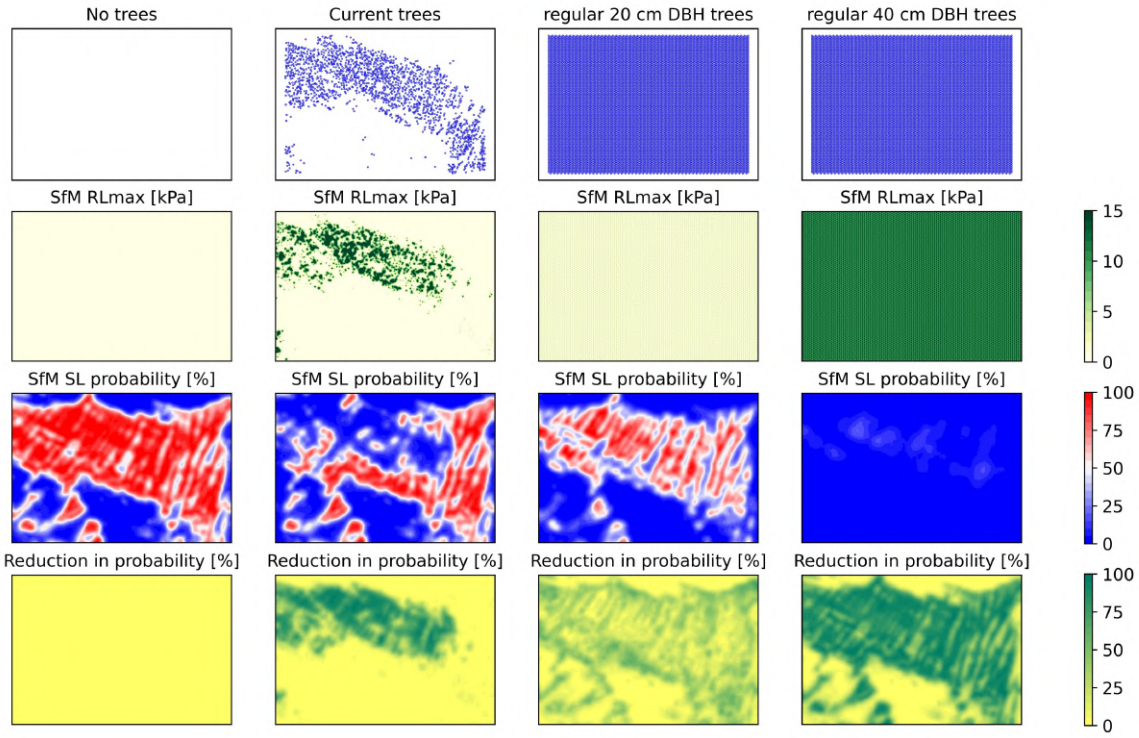

FIGURE 7.3: SlideforMAP modelled lateral root reinforcement and shallow landslide probability in the St. Antönien study area in Switzerland under four vegetation scenarios. first column: No vegetation used as a reference scenario. second column: Actual vegetation with single tree detection derived DBH. All trees assumed to be Beech. Third column: 150 stems per hectare, 20 cm DBH triangular pattern European beech plantation. Fourth column: 150 stems per hectare, 40 cm DBH triangular pattern European beech plantation. The first row displays location of the trees. The second row the spatial distribution of the maximum lateral root reinforcement. The third row displays the SlideforMAP computed shallow landslide susceptibility under default parametrization (chapter 4). The fourth row gives the reduction in shallow landslide reduction as compared to the no vegetation scenario.

It is important to note that the influence of vegetation on slope stability is controlled by geotechnical factors. For example, the basal root reinforcement contributing to shear resistance is a function of soil thickness, with the highest protective effect from basal root reinforcement in shallow soils (see chapter 4 for the physical relationship). The effectiveness of the vegetation scenarios, defined as the reduction in shallow landslide probability per 1000 trees is given in Table 7.1.

TABLE 7.1: Effectiveness in shallow landslide (SL) probability reduction of the vegetation scenarios from Figure 7.3.

	No vegetation	**Current vegetation**	**Plantation, 20 cm DBH**	**Plantation, 40 cm DBH**
Number of trees	0	1795	8701	8701
Mean SL probability [%]	54.4	34.6	32.9	1.9
Reduction per 1000 trees	-	11.03	2.47	6.04

Table 7.1 displays a high effectiveness of the current trees in reducing shallow landslide activity. This likely results from their function as protection forest, indicating they are target planted to prevent natural hazards. This is in contrast to the plantation, where no targeting is applied.

7.3 Tiling for regional application

At the time of writing, applying SlideforMAP over large scales (> 100 km^2) under low resolutions (< 5 m), the tiling of the study area is a computationally effective way to run SlideforMAP. A methodology using 25 km^2 tiles is developed. The flow accumulation and slope angle is computed from the DEM beforehand for the whole study area or per tile using an additional 2 km buffer. Figure 7.4 visualizes the process for a theoretical large catchment.

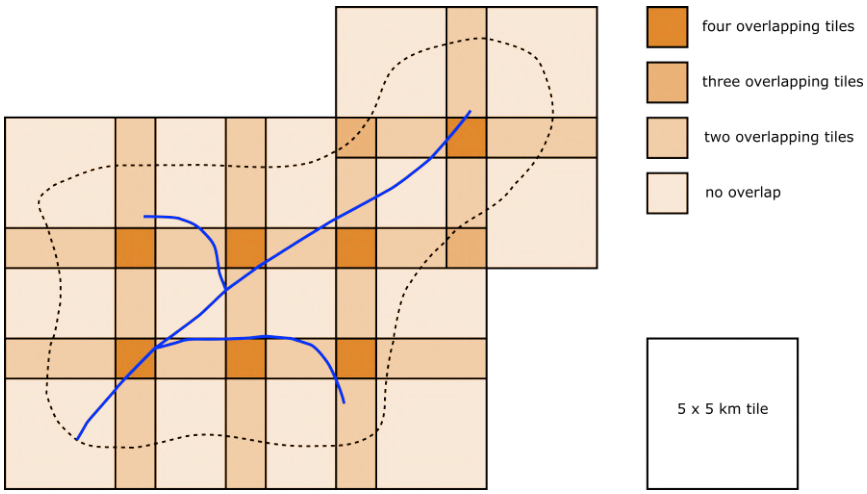

FIGURE 7.4: Visualized methodology of tiling for the application of SlideforMAP to a catchment study area (dotted line). In this example the total study area size is 140 km^2. The combined size of all tiles in the computation is 375 km^2. Despite the larger surface area, the computation is more effective within in the tiles and it prevents memory limit errors.

After running individual tiles with the SlideforMAP approach (chapter 4 or 5), the resulting shallow landslides probability rasters of the tiles are stitched together. Where the tiles do not overlap, the single probability value is taken. In areas where tiles overlap, the average value of shallow landslide probability is computed.

8 Synthesis

8.1 Introduction

This research aims to quantify the degree in which vegetation decreases shallow landslide initiation. Model development and the inclusion of novelties, as presented in this thesis, are a contribution to science. Simultaneously, the tool that has been developed, aims to be an aid for practitioners. It does this by limiting the number of input parameters and providing a robust framework, where using estimates of input parameters still provide good results. Simplifications in SlideforMAP are consciously chosen and attuned to the main goal of the model. Additionaly, the thesis includes: two calibrations of the model, a validation and an uncalibrated application of SlideforMAP.

8.2 Contribution to science

SlideforMAP is a physically based model, according to the definition as posed in section 2.2. The core safety factor computation and most parameters have a physical meaning. With its distinct modules (Figure 4.1), it follows a reductionist approach. Within the modules however, conceptual methods are included such as the TOPOG approach to hydrology and the runoff coefficient. The same holds for the RBMw approach to root reinforcement, which is essentially a calibration and conceptualization of physical measurements.

In the paper presented in chapter 4, the application of SlideforMAP with the RBMw model proved a significant gain in accuracy by including a single-tree based three-dimensional approach to root reinforcement, compared to a uniform value of root reinforcement. The calibration of the RBMw was adopted from Gehring et al. (2019) and is based on fieldwork. Our fieldwork (section 7.1) has laid the foundation for the poplar tree calibration of the RBMw.

The research presented in chapter 5 confirms results from other authors. Many approaches attempt to improve upon steady-state models (e.g Gascoin et al., 2009; Takeuchi et al., 2008), but found that the steady-state approach to predict water tables performs surprisingly well, despite its simplification (Moore & Thompson, 1996). Gains in accuracy by a dynamic approach are therefore often small. In addition to these main findings, specifically addressing model shortcomings, analyzing specific components and identifying model novelties, in the sections below aims to identify and place the contribution to science of SlideforMAP in context.

8.2.1 Model shortcomings

A direct and uncalibrated comparison to a statistical approach to shallow landslide susceptibility in New Zealand hill country (chapter 6) reveals several shortcomings in the SlideforMAP approach. This is in addition to the shortcomings as identified in the initial introduction to the model (chapter 4). A comprehensive overview is given below.

- No inclusion of evapotranspiration as well as other more minor hydrological effects (Greenway, 1987) simplifies the hydrological module. An indication of this simplification is in the

comparison of tree influence. A clear higher radius of influence of the statistical approach is given versus the extent of the lateral root reinforcement 6.6. It appears that hydrological influence of a tree extends further than the extent of its roots, although an explanation could also lie in the size confinement effect (see section 6.4.2).

- Antecedent moisture influences shallow landslide initiation (Baum & Godt, 2010; Guo et al., 2014; Jakob et al., 2012; Uchida et al., 2005). A fact that is even observed in our study areas (De Rose, 2013). Not having included this in SlideforMAP is a shortcoming. A counter argument could be that SlideforMAP focuses on extreme precipitation events, where antecedent moisture is of less influence (Feng et al., 2020). This does however, limit the applicability of SlideforMAP.

- The unexpectedly minor difference between the actual rainfall scenario and a design rainfall scenario (Table 6.9 and 6.11), illuminates the difficulty of using uncalibrated K_{sat} values. Calibrated values from chapter 5, a subsection of the same study area, show K_{sat} values in the order of 10^{-3} m/s, corresponding to macropore dominated lateral flux. Values in chapter 6 were orders of magnitude smaller, corresponding to matrix flow. Not calibrating leads to near total saturation as per the saturation degree equation, equation 4.12.

- The focus on water table development by sub-surface lateral flow rather than infiltration is a conscious choice. Whether this is a shortcoming is site-specific. Oftentimes lateral flux controls a local groundwater table, but in other cases it has been reported to be from vertical infiltration (e.g. Bordoni et al., 2015; Iverson, 2000).

8.2.2 Model components

Certain procedures of the model are not considered shortcomings, nor novelties, but their inclusion in the model is interesting and has potential for further development. Soil thickness proved to be a highly sensitive parameter in chapter 4. This is in line with findings in many other similar models (e.g. Liang & Chan, 2017). Deep soils have a significantly higher propensity for landslides than shallow ones, as seen in the calibration in chapter 4 and 5 and the spatial distribution of high risk in chapter 6, Figure 6.7. In the temporal sense it goes even further than sensitivity. Soil thickness and shallow landslide initiation constitute a mutual feedback mechanism (De Rose, 2013; Iida, 1999), being the basis of landscape evolution in certain environments, such as New Zealand hill country.

Shallow landslide surface area distribution is calibrated using the methodology by Malamud et al. (2004). In figure 5.13, we compare the distribution of the inventory to the unstable slides from SlideforMAP. The distributions are nearly identical, indicating good prediction of shallow landslide size. This could be related to the inclusion of passive earth pressure in the adapted version of SlideforMAP (chapter 5), which is the main controlling factor for shallow landslide size (Milledge et al., 2014).

8.2.3 Model novelties

Applying the single-tree based RBMw in a shallow landslide susceptibility is a novelty. It explicitly defines basal and lateral root reinforcement. Lateral root reinforcement is described by a propagation in root failure. It is quantified by adjusting for soil thickness and having it apply to half the circumference of an (assumed) oval shaped shallow landslide. Single-tree detection from new techniques such as the neural network, as presented in chapter 6, enables the wider application of the SlideforMAP procedure to mechanical vegetation effects. As far as we are aware, we are the first to compare a statistical model to a physically-based model, not only by

including the RBMw approach, but any single-tree based approach to shallow landslide susceptibility. An additional ability of our approach is to model tree development through time, by making assumptions on DBH increase.

The methodology from chapter 5 has multiple novelties in its hydrological module. These are i) Runoff coefficients, ii) Effective contributing area, iii) Representative rainfall intensity. These methods are generally applied to surface water and/or large scale hydrology, specifically predicting discharge at a defined outlet. The inclusion in, and adaption of, these concepts in small-scale sub-surface fluxes is novel. Representative rainfall intensity is particularly novel, as rainfall event characteristics and rainfall heterogeneity are important (e.g Cristiano et al., 2019), but only recent availability of RADAR data enables a reliable inclusion. Early warning systems based on intensity duration curves, consistently show this to be a shortcoming Tsai, 2008. For surface water relating rainfall to discharge is still extremely challenging. We adopted a surface hydrology inspired travel time/travel distance strategy and applied it to sub-surface water. This is still challenging, as many factors are of influence (see section 5.2.3.5). As far as we know, our strategy has not been applied with analytical equations on a regional scale. The effective contributing area defines the degree, to which the systems comes to steady-state and is quite the simplification of rainfall-runoff approaches, but still a novel inclusion. Land use dependent runoff coefficients are developed and applied as a means for runoff prediction on catchment scale (e.g. Markart et al., 2017; Scherrer & Naef, 2003). The use of these techniques explicitly for sub-surface lateral runoff on a smaller hillslope scale is, as far as we are aware, unique.

Passive earth pressure and root compression are often ignored in shallow landslide models (Murgia et al., 2022) . Including these in SlideforMAP makes for a model more close to reality and helps in correctly predicting shallow landslide size (Milledge et al., 2014). The SlideforMAP approach is not perfect though, as it is suggested passive earth pressure is at no stage fully mobilized in progressive failure (Cohen & Schwarz, 2017b).

8.3 Shallow landslide probability modelling

Having applied the model in both Switzerland and New Zealand, to a total of seven study areas, is a good indication of generalizability of the model. The study areas are both in energy-limited systems, indicating a permanent and relatively shallow groundwater system (Dingman, 2015). Land use is different though, with a silvopastoral system in the New Zealand study areas and sharply contrasting forests and meadows in the Switzerland study areas. Performance AUC values in chapter 4 (Eriz: 0.93, Trub: 0.93, StA: 0.64) and validation AUC values in chapter 5 (WA portion: 0.86, TW portion: 0.90) show that with adequate calibration, good AUC values can be achieved. The application in chapter 6 (WA farm: 0.83, TW farm 0.87), found good AUC values for an uncalibrated example as well.

The model is not designed to be an exact forecasting tool, despite the reasonable, good and very good AUC values (El Khouli et al., 2009). This is because the translation of shallow landslide probability as generated by SlideforMAP to actual hazard zones remains a challenge. Chung and Fabbri (2003) concisely describe that probabilities and subsequent classifications only have added value when a temporal component and magnitude is included. SlideforMAP does have a specific temporal component, as the modelled rainfall event has a associated statistical return period. It can therefore provide the highest shallow landslide probability in X years under the statistically likely highest precipitation intensity or lateral flux, when using the adapted, chapter 5, methodology. An estimate of magnitude can be made by relating SlideforMAP output to one or more past events and perform an interpolation or conversion. In this sense SlideforMAP

resembles other models, often statistical large scale models (Reichenbach et al., 2018), aiming to predict shallow landslide initiation by a relative susceptibility. In chapter 6, Figure 6.5, an empirical scheme is presented under this assumption. We define relative susceptibility classes, based on model output and shallow landslide locations in the past. As a relative measure, this is an acceptable procedure, assuming the past has predictive capacity for the future. Performing a deterministic run of SlideforMAP, replacing distributions with fixed values, could theoretically also provide a magnitude estimate. This is however untested and would remove benefits from the probabilistic approach, such as an estimation of shallow landslide size and other parameters.

The intended application of SlideforMAP, as defined before, is quantifying the influence of vegetation. This thesis poses that this can be achieved by comparing a relative rather than absolute reduction in shallow landslide probability, as seen in the example in section 7.3. Results from both chapter 4 and 6, compare current vegetation to a no vegetation reference scenario. In chapter 4 the average fraction of unstable hypothetical shallow landslides decreases from 0.475 to 0.336, corresponding to a 29% decrease due to vegetation. In chapter 6, SlideforMAP displays an average of 9.8% decrease in shallow landslide occurrence over both study areas. A potential explanation for the difference is methodological, as in chapter 4 it is measure of a model inner workings, i.e. the proportion of probabilistically generated landslides. In chapter 6 the reduction is correlated to a change in classification, which in turn is based on a shallow landslide inventory. Both have their inaccuracies, as both the inventory and the probabilistic modelling may not be representative of actual shallow landslide occurrence. The most likely reason for the difference though is study area heterogeneity. The study areas in Switzerland, as used in chapter 4, have a significantly larger averaged tree density (53 vs. 16 trees/ha) and averaged tree DBH (0.46 vs 0.27 m) than the New Zealand study areas. A visualization of the reduction in shallow landslide probability from chapter 4 and 6 per study area is given in Figure 8.1 below.

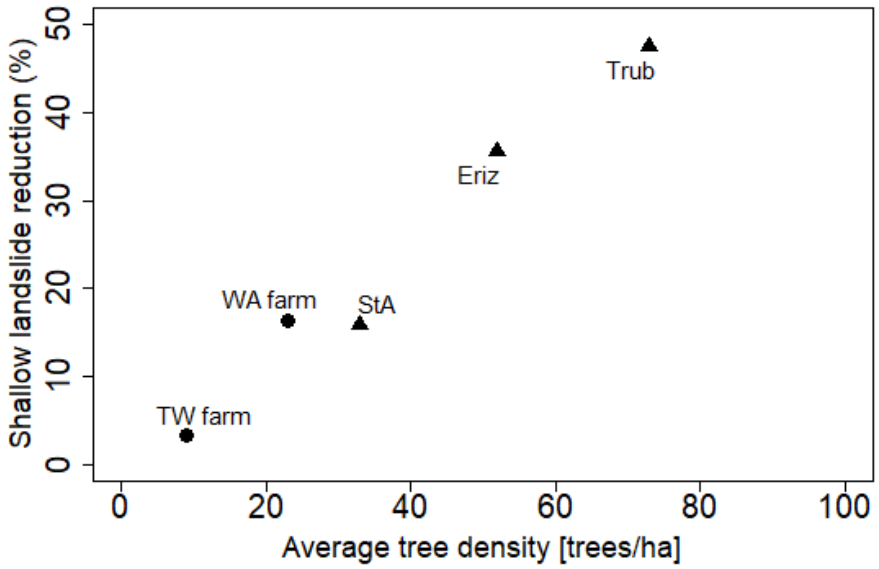

FIGURE 8.1: Reduction of shallow landslide probability by combining the results of chapter 4 and chapter 6. Study areas located in New Zealand given as circles, study areas in Switzerland as triangles. No trendline is inserted, as the data points are little and respective methodologies are incomparable.

The points in Figure 8.1 are generated from a different methodology, different rainfall assumptions and different tree size. They do however give an indication of the main point of this research, namely that trees have the potential to significantly decrease shallow landslide activity.

8.4 SlideforMAP application

Two distinct ways in the application for SlideforMAP can be identified. Firstly, method 1, for the identification of areas susceptible to shallow landslides and secondly, method 2, for the assessment of mitigation measures effectiveness. The outline of both methods is given in Figure 8.2 and 8.3 below.

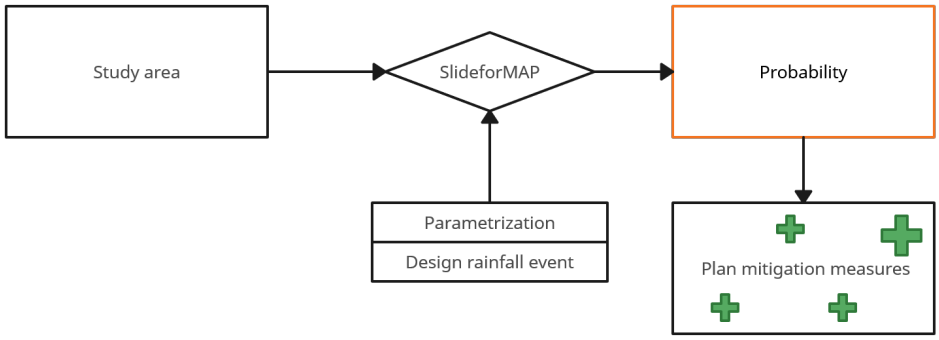

FIGURE 8.2: SlideforMAP application, method 1. Looking for areas where shallow landslide probability is high. These areas can likely, but not guaranteed, benefit from mitigation by tree planting.

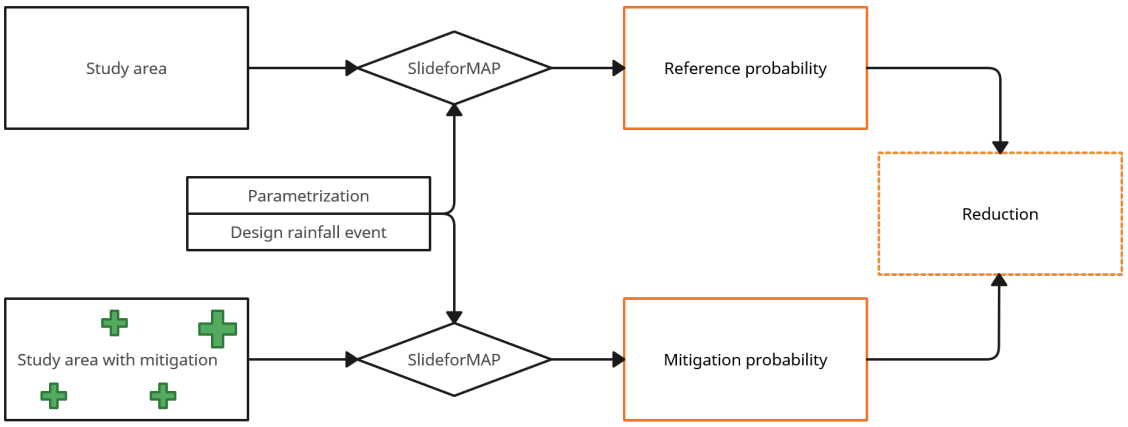

FIGURE 8.3: SlideforMAP application, method 2. Assessing the effectiveness of planned tree planting mitigation by comparing a scenario with and without said mitigation.

For efficient use of SlideforMAP, the application should be more of an iterative process. Consisting of method 1 for the calculation for possible sites under various (design) rainfall events and validating efficiency of potential scenarios with available resources with method 2. Tree development though time can be modelled by increasing tree size. Ideally, applying SlideforMAP is only a step in the mitigation process. The process is recommended to include a previous assessment of the problem and subsequent implementation and evaluation of mitigation measures (Spiekermann, 2022). In the assessment phase a holistic approach to tree placement and choice

should be undertaken (Mackay-Smith et al., 2021).

A special case for models such as SlideforMAP is the ability of back-calculation (e.g Papa et al., 2013; Salciarini et al., 2012). When provided with a representative and complete landslide inventory and knowledge on all but one (independent) parameter, this parameter can be back-calculated for each probabilistic landslide in the model. Spatially projecting all probabilistic landslides can subsequently compute the spatial field of the parameter of interest. Good applications for this approach is the analysis of rainfall and soil thickness heterogeneity.

8.5 Summary

In its methodology, SlideforMAP is among other state of the art models in predicting rainfall-event induced translational shallow landslide initiation, probabilistically. The core focus of SlideforMAP though is assessing the relative reduction in probability from specific targeted planting mitigation measures. For this root reinforcement is included in three dimension with the RBMw approach (section 4.2.5). The effectiveness of tree mitigation depends on tree planting density, pattern, species and size. A summary of results throughout this thesis with relative reduction versus tree density is presented in Figure 8.1. In order to correctly assess shallow landslide probability, the geotechnical and hydrological module of the model should realistically reflects processes happening in the soil. For this reason we introduced multiple novelties, specifically for the regional scale, which are: a representative rainfall intensity (section 5.2.3.5), an effective contributing area (section 5.2.3.6), runoff coefficient (section 5.2.3.3) and passive earth pressure (section 5.2.4). A methodology using SlideforMAP is presented in Figure 8.2, which is akin to most statistical susceptibility models, as it does not have a physical conversion to magnitude. This is used for identifying areas that could benefit from mitigation measures. A second methodology (Figure 8.3), specifically displays how to assess effectiveness of mitigation measures.

9 Conclusions and outlook

9.1 Conclusions

The main goal of this thesis, developing a state of the art model to quantify mitigation potential of trees on shallow landslide susceptibility, has been addressed throughout the previous five chapters. The model, named SlideforMAP, as presented in this thesis, has gone through the developmental and validation process in chapters 4, 5 and 7. It coupled the well known limit equilibrium and TOPOG approach to water table and slope stability computation, conditional on a precipitation intensity. The analytical functions provide the ability for a probabilistic approach, namely computing over a large number of hypothetical landslides, and the application on the regional scale. The local fraction of unstable hypothetical landslides, gives a relative shallow landslide probability that performs well (see summary in section 8.3). In chapter 6, we compare and benchmark SlideforMAP to a statistical approach. Finally, the synthesis (chapter 8) places the model in a broader context and seals its contribution to advance science. In the introduction, specific objectives were defined, subject to the main goal. These are addressed sequentially below:

- Root reinforcement of vegetation is included in three dimensions, using the state of the art RBMw approach and applied to single trees (as seen in Figures 4.9, 6.6 and 7.3). It distinguishes lateral and basal root reinforcement explicitly in the force balance. Total lateral root reinforcement is a calibrated function of tree species, tree DBH, lateral distance, and thickness to failure plane. Basal root reinforcement is a calibrated function of lateral root reinforcement, tree species, tree DBH and thickness to failure plane. Tree weight is included in the computation as well, leading to the representation of all potentially significant mechanical vegetation effects in SlideforMAP.

- Comparing the current single-tree approach to general approaches (uniform vegetation, forest stand uniform vegetation), shows a significant (> 99% confidence) increase in accuracy of the single-tree approach in two of three study areas in Switzerland. This observation and the physical basis of the model, indicate that SlideforMAP is a reliable tool to quantify the effect of potential trees on shallow landslide occurrence.

- In chapter 4, a calibration and subsequent performance measure is presented. Chapter 5, takes it a step further and gives a calibration and validation of SlideforMAP for two study areas in New Zealand (1.4 and 3.5 km^2). It includes RADAR-based hourly rainfall data, LiDAR-based single tree location and dimension and orthophoto-based tree species classification, providing excellent groundwork for shallow landslide modelling. A split-sample calibration and validation is performed on the model and an orthophoto-based shallow landslide inventory (total slides = 578). Validation AUC ranges between 0.814 and 0.896 (Table 5.8), depending on assumptions and version used (see chapter 5). As expected, the validation results are generally slightly lower than calibration results, but validation performance is still good.

- A non-steady state development is included in SlideforMAP (see chapter 5). It assumes a macropore-dominated lateral flux travel time. Travel times are computed for cells in the

contributing areas and a contributing fraction during a rainstorm event is included. The availability of RADAR-based rainfall data leads to a more informed assumption on representative rainfall intensity, which is the rainfall intensity representative for the modelled peak in lateral flux. Isolating the effect of the non-steady state from other model improvements is challenging. The non-steady state development has a significant influence on pore water pressure compared to a steady-state assumption with lower pressure in valleys, i.e. areas with a large contributing area (Figure 5.9).

- Vegetation-induced preferential flow is incorporated in SlideforMAP by the inclusion of a runoff coefficient, whose value is dependent on cumulative rainfall, soil thickness and lateral root reinforcement (as a proxy of root density). Comparing a hybrid version of SlideforMAP enables us to isolate the difference in performance for two study areas in New Zealand. This difference is negligible.

- Comparing the physically based SlideforMAP to a statistical logistical regression method, showed an approximately 70% agreement in classification between the models. Non-agreement is related to the difference in methodology and input data. Performance for the statistical method is excellent and very good for SlideforMAP. This is related to the calibration of the statistical method. An advantage of SlideforMAP is the ability to include susceptibility related to tree dimensions and specific rainfall events. In case of limited resources, practitioners are advised to focus on areas where both models are in agreement on high shallow landslide susceptibility.

All in all, the research presented in this thesis presents a model that can effectively quantify the effect of current and potential trees on the probability of shallow landslides.

The tool and concepts presented in this thesis can be of great value to practitioners, land managers and scientists. The well-considered application of SlideforMAP can optimize the planting and management of new trees and management of existing trees in areas where there is some minimal information on soil, topography and climate. The physical basis allows for the analysis of potential rainfall events that can be related to specific, preferably standardized, return periods. When recommendations, generated by SlideforMAP, are implemented on a large scale, shallow landslide probability can decrease substantially, with a minimized effect on land productivity. Properly considering vegetation co-benefits can further enhance the positive effects of trees.

9.2 Outlook

The increase in accuracy and availability of methods to detect single-trees locations and metrics, such as DBH and species, likely increases the applicability of single-tree based methods such as SlideforMAP. These methods can be of aid in the monitoring phase to check whether planted trees have developed as planned and, using SlideforMAP, whether the mitigation effect has developed as planned.

SlideforMAP presents a novel application of the RBMw model which distinguishes lateral and basal root reinforcement. Additionally it includes the novelty of relating groundwater flux to temporally heterogeneous rainfall and a runoff coefficient controlled by macropore presence, correlated to root reinforcement. Our hydrological improvements are still very much conceptual and have not definitively proven their merit. Simplifications in our application include a fixed macropore width, a macropore velocity dependent solely on precipitation intensity and a conceptual rainfall-runoff curve calibrated in Switzerland and previously applied on larger

scales. More research, improvements and test cases could advance the accuracy of shallow landslide models adopting a similar approach to lateral flux dominance.

In the RBMw approach, more tree species, such as native New Zealand trees like kanuka, can be parametrized. The RBMw assumes a constant species-specific root distribution as function of tree DBH. However numerous factors can potentially influence root distribution, such as slope angle, prevailing wind, water availability and competition from other roots (McIvor et al., 2009; Zhu et al., 2017). Root reinforcement is also assumed to be independent of environmental factors, but research suggests that soil moisture has a considerable influence (Masi et al., 2021). Further quantitative research on these factors and implementation in root distribution models can result in better predictions of root reinforcement.

The accuracy in quantifying tree effects by SlideforMAP is conditional to the accurate implementation of controlling factors for shallow landslide initiation. Methods that incorporate landscape evolution for estimating the spatial heterogeneity of soil depth are promising, such as those developed by D'Odorico and Fagherazzi (2003) and Marston (2010). These models are more reliable than extrapolations from limited measurements and the inclusion of the temporal domain opens the possibility of including soil development and shallow landslide activity as a feedback mechanism.

A holistic approach to tree placement is essential. The analysis for preventing shallow landslide occurrence, or any other type of natural hazard, by such trees is only part of the puzzle. A multitude of biological, economical and cultural considerations should be taken into account.

10 Supplementary material

Chapter 4: Introducing SlideforMAP; a probabilistic finite slope approach for modelling shallow landslide probability in forested situations

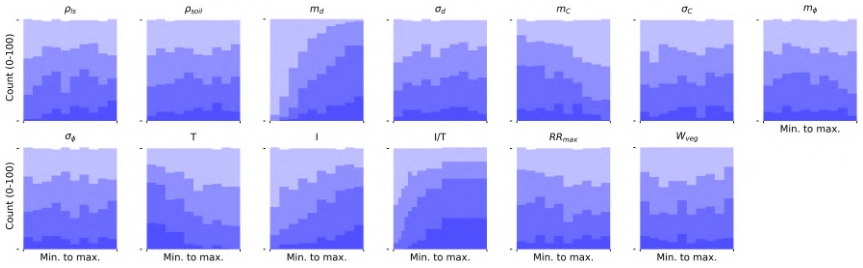

FIGURE 10.1: Histograms of different subsamples of the LHS parameter sets for the Eriz study area. The shading (from light to dark) corresponds to subsamples retaining only the x% best parameter sets in terms of AUC; the shown fractions are: 1, 0.7, 0.4, 0.1.

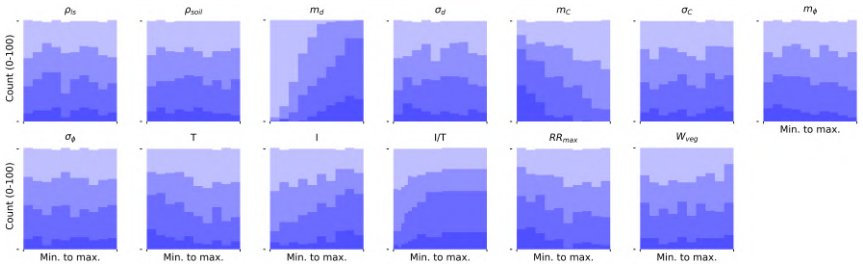

FIGURE 10.2: Histograms of different subsamples of the LHS parameter sets for the Eriz study area. The shading (from light to dark) corresponds to subsamples retaining only the x% best parameter sets in terms of Unstable ratio; the shown fractions are: 1, 0.7, 0.4, 0.1.

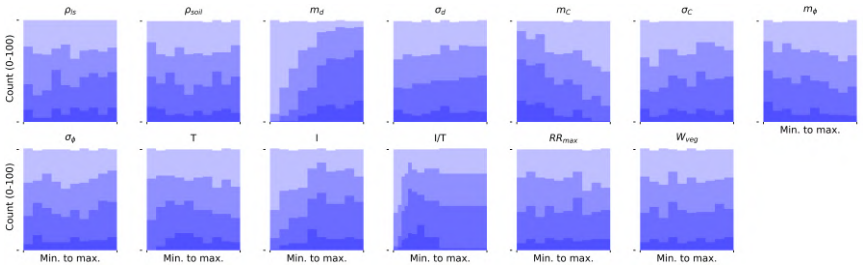

FIGURE 10.3: Histograms of different subsamples of the LHS parameter sets for the StA study area. The shading (from light to dark) corresponds to subsamples retaining only the x% best parameter sets in terms of AUC; the shown fractions are: 1, 0.7, 0.4, 0.1.

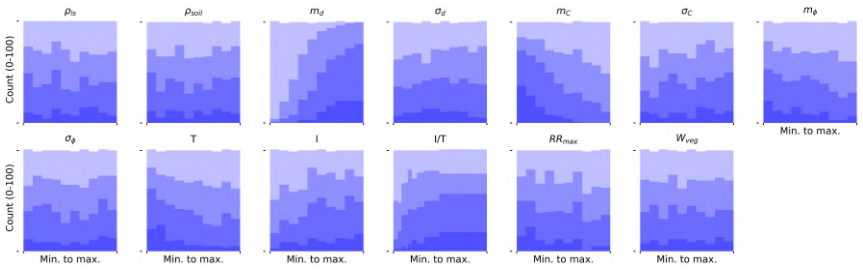

FIGURE 10.4: Histograms of different subsamples of the LHS parameter sets for the StA study area. The shading (from light to dark) corresponds to subsamples retaining only the x% best parameter sets in terms of Unstable ratio; the shown fractions are: 1, 0.7, 0.4, 0.1.

R-code constructing the precipitation intensity boundaries in the sensitivity analysis:

```
## Computation of the DDF curves ##
## Input intensities manually read from https://hydromaps.ch ->
Wasser in der Atmosphaere ->
B04 Extreme Punktniederschlaege
## method according to: https://hydrologischeratlas.ch/downloads/01/content/Text_Tafel24.de.pdf

#StAntonien rainfall intensity
#i_1h_100J<-42      #mm/h, 1 hour time period intensity, 100 year return period
#i_24h_100J<-115/24 #mm/h, 24 hour time period, 100 year return period
#i_1h_2p33J<- 21    #mm/h
#i_24h_2p33J<-57/24  #mm/h

#Bern_mittelland (Trub and Eriz study area) rainfall intensity
i_1h_100J<-47      #mm/h
i_24h_100J<-115/24 #mm/h
i_1h_2p33J<- 21    #mm/h
i_24h_2p33J<-62/24  #mm/h

T<-100 # Return period
d<- 1 # Duration
a<-0.315*log(i_24h_100J*24/i_1h_100J) # parameter 1
b<-0.315*log(i_24h_2p33J*24/i_1h_2p33J) # parameter 1

y<- -log(-log(1-1/T))
i_d_T_1<- i_1h_2p33J*(d^b) + 0.248*(i_1h_100J*(d^a) - i_1h_2p33J*(d^b))*(y-0.577)
print(i_d_T_1)
```

Python-code making and validating a log-normal distribution from a mean and a standard deviation:

```
import numpy as np
import scipy.special as sps
import matplotlib.pyplot as plt
from sklearn.metrics import mean_squared_error
from scipy.stats import norm
import pandas as pd

######### NORMAL TO LOGNORMAL DISTRIBUTION #########
LSFile = 'LS_data.csv'
LSinv_base = pd.read_csv(LSFile)
soil_depth_obs = LSinv_base['depth'].dropna().tolist() # get the list of the

#https://blogs.sas.com/content/iml/2014/06/04/simulate-lognormal-data-with-specified-mean-and-variance.html
m = np.mean(soil_depth_obs) # mean
v = np.std(soil_depth_obs)**2 # variance
phi = np.sqrt(v + m**2)
mu = np.log(m**2/phi) # lognormal par 1
sigma = np.sqrt(np.log(phi**2/m**2)) # lognormal par 2
n = 1000000

normalVals = np.random.normal(m,np.sqrt(v),n)       # draw soil depths from the distribution
LognormalVals = np.exp(np.random.normal(mu,sigma,n))       # draw soil depths from the distribution

plt.hist([normalVals, LognormalVals],bins = 500, histtype= 'step')
plt.xlabel('soil_depth')
plt.ylabel('n')

print(len(normalVals))
print(len(LognormalVals))
print(np.mean(normalVals))
print(np.mean(LognormalVals))
print(np.min(normalVals))
print(np.min(LognormalVals))
print(np.max(normalVals))
print(np.max(LognormalVals))
print(np.std(normalVals))
print(np.std(LognormalVals))
```

```
######## SOIL DEPTH OUR DISTRIBUTIONS VS. DATA #############
x = np.linspace(-1, 4, 5000)
pdf_log = (np.exp(-(np.log(x) - mu)**2 / (2 * sigma**2)) / (x * sigma * np.sqrt(2 * np.pi)))

points = plt.hist(soil_depth_obs, bins=int((max(soil_depth_obs)-min(soil_depth_obs))/0.2)\
, density = True, label = 'normalized data (n = 607)')
plt.plot(x, norm.pdf(x, m, np.sqrt(v)), label = 'fit normal distribution')
plt.plot(x, pdf_log, linewidth=2, color='r', label = 'fit lognormal distribution')
plt.axis('tight')
plt.xlabel('soil thickness (m)')
plt.ylabel('probability density')
plt.legend()
plt.savefig(r'C:\Users\vof1\Documents\Papers\paper_1\reviews\review_2\response\normallognormal.png',bbox_inches='tight'\
, dpi=200)
plt.show()

######## COMPUTE MEAN SQUARE ROOT ERRORS #############
LS_x = np.linspace(0.1, 2.9, 15)
LS_lognormals = np.nan_to_num((np.exp(-(np.log(LS_x) - mu)**2 / (2 * sigma**2)) / (LS_x * sigma * np.sqrt(2 * np.pi))))
LS_normals = norm.pdf(LS_x, m, np.sqrt(v))

# Mean Squared Error
MSE_normal = np.square(np.subtract(points[0],LS_normals)).mean()
MSE_lognormal = np.square(np.subtract(points[0],LS_lognormals)).mean()

print('The normal distribution MSE is ', np.round(MSE_normal,4))
print('The lognormal distribution MSE is ', np.round(MSE_lognormal,4))
```

R-code computing and plotting RRmax, Lateral root reinforcement and Basal root reinforcement:

```
#Data from Gehring et al. 2019. (https://doi.org/10.1038/s41598-019-45073-7) and applied SlideforMap
Distance <- seq(0.1,15,0.1)   # Range of horizontal distance [m]
depth<- seq(0,2,0.02)         # Range of soil depth [m]
DBH <-0.3                     # Diameter at Breast height of a tree [m]

# Horizontal root density Gamma function parameters
alpha_1 <- 0.862
beta_1 <- 3.225
c <- 25068.54

# Vertical root density Gamma function parameters
alpha_2 <- 1.284
beta_2 <- 3.688

# Check the maximum root reinforcement with alpha_1 and beta_1
root_max <- ifelse(Distance <18.5, ((c*DBH)*dgamma(Distance/(DBH*18.5), alpha_1, beta_1)),0)  #[N/m],
plot(Distance,root_max/1000, type = "b", pch = 16, col = '#FF8C00',\
main = 'RRmax, DBH = 0.3 m.', xlab = 'Distance from stem [m]', ylab = "Root reinforcement [kN/m]")
grid()

# lateral root reinforcement and basal root reinforcement with alpha_2 and beta_2
k <- 1 # [m^(-1)]
root_max_fix <- 1 # [kN/m]
degamma <- dgamma(depth,alpha_2,beta_2)
RRlat <- root_max_fix*pgamma(depth,alpha_2,beta_2) # [kN/m]
RRbas <- k * dgamma(depth,alpha_2,beta_2)*root_max_fix  # [kN/m^2]

plot(depth,degamma, type = "b", pch = 16, col = '#838B83', xlab = 'Soil thickness [m]', ylab = "Root reinforcement")
lines(depth, RRlat, type = "b", pch = 16, col = '#FF8C00')
lines(depth, RRbas, type = "b", pch = 16, col = '#1E90FF')
grid()
legend("topright",legend = c("Lateral [kN/m]", "Basal [kN/m2]"), col = c("#FF8C00", "#1E90FF"),pch = c(16, 16))

# Plot for an actual Random landslide
Surface_area = 50 # [m^2]
length_width_ratio <- 2 # [-]
ls_width = sqrt((Surface_area*4)/(pi*length_width_ratio)) # [m]
ls_length = ls_width*length_width_ratio  # [m]
Circumference = pi*(3*((ls_length/2)+(ls_width/2))-sqrt((3*(ls_length/2)+\
(ls_width/2))*((ls_length/2)+(3*(ls_width/2))))) # [m]

RRlat_l <- root_max_fix * pgamma(depth,alpha_2,beta_2) * Circumference * 0.5  # kN
RRbas_l <- root_max_fix * dgamma(depth,alpha_2,beta_2) * Surface_area         # kN

plot(depth,RRbas_l, type = "b", pch = 16, col = '#1E90FF',\
main = 'Random Landslide, area = 50 m2', xlab = 'Soil thickness [m]', ylab = "Root Force [kN]")
lines(depth, RRlat_l, type = "b", pch = 16, col = '#FF8C00')
grid()
legend("topright",legend = c("Lateral", "Basal"), col = c("#FF8C00", "#1E90FF"),pch = c(16, 16))
```

Chapter 5: Application and validation of SlideforMAP for assessing shallow landslide probability in New Zealand hill country

Precipitation event

RADAR-based precipitation data is used to compute the precipitation event with the highest return period for the time period of 2000-2010. The year 2000 is the first year of the data availability and 2010 is the year of the landslide inventory. A plot with the highest mean precipitation

intensity for events of a duration from 1 hour to 24 hours, with their start time and date are given in Figure 10.5.

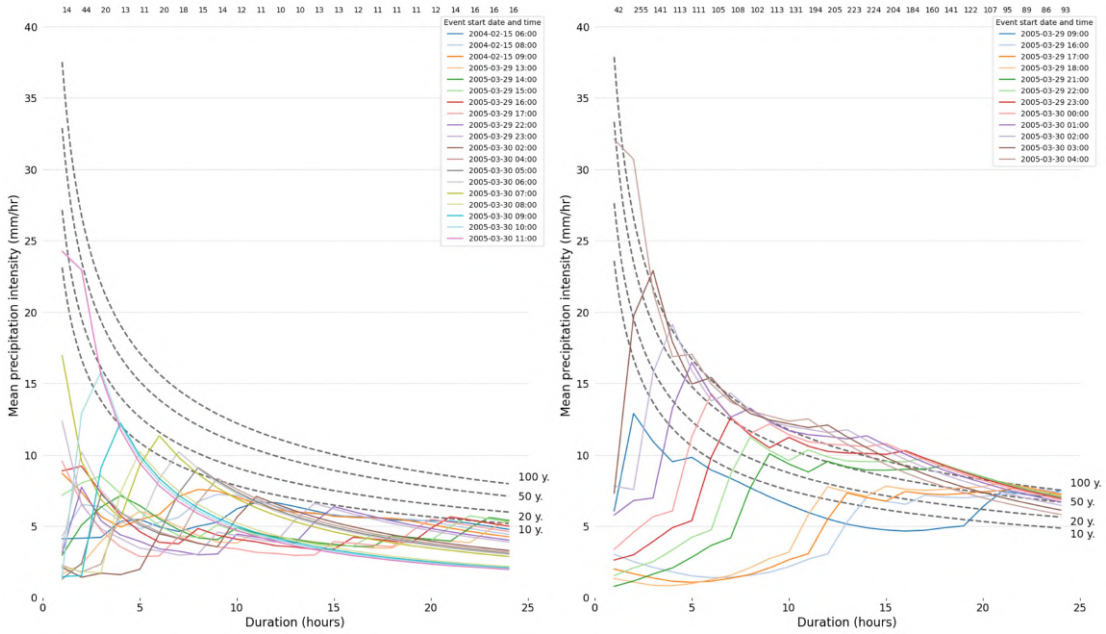

FIGURE 10.5: Intensity duration curves constructed from NIWA-HIRDS4 dataset (Carey-Smith et al., 2018) with return periods of 100, 50, 20 and 10 years. The return period is computed by minimal MSE fit of the NIWA-HIRDS4 dataset with a general function of $I = a * T^b$. Highest hourly interval intensity events over the years 2000-2010, preceding the landslide inventory, are plotted. The legend displays the date and time of their onset. Figure on the left for the Te Whanga area and Figure on the right for Waikoukou. Plotted lines are for the mean of the precipitation. Numbers above indicate the computed return periods of the event.

Relationship of precipitation intensity and maximum lateral flow

Our theoretical rainfall-runoff example for a contributing area in the Waikoukou study area. The example gives both an actual event and a constant mean precipitation of said event. This is shown in Figure 10.6.

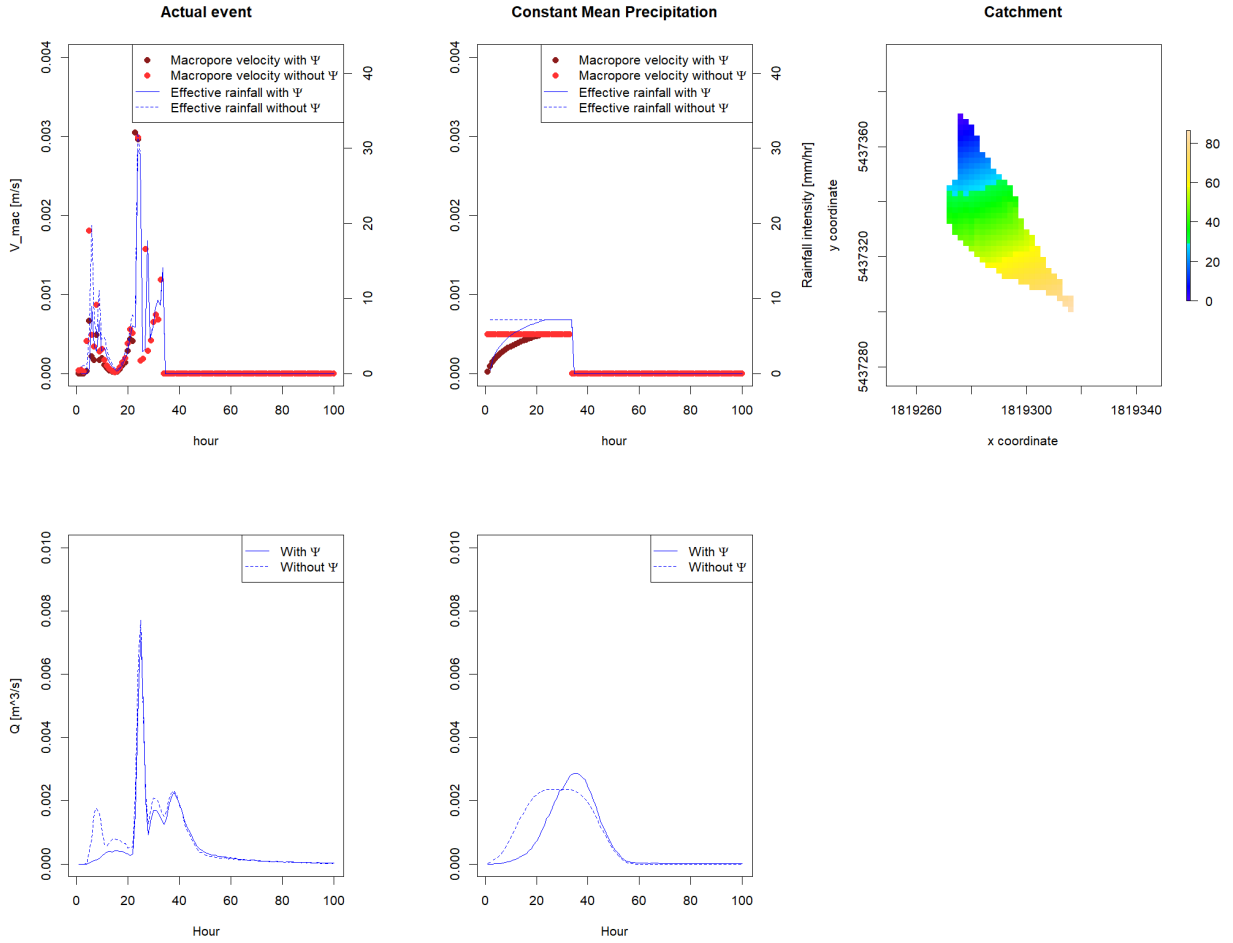

FIGURE 10.6: A rainfall-runoff example of lateral macropore flow as a response to the March 2005 rainfall event for an example contributing area in the Waikoukou study area. In the lower left and lower middle are the hydrograph and macropore velocity for the actual rainfall event and a constant mean precipitation event respectively. Both a scenario with and without a runoff coefficient is included. For the runoff coefficient we choose RT2, corresponding to slightly delayed runoff in shallow soils. Upper right is a visualization of the contributing area with distance to the outlet [m]. Lower left and middle left is the macropore flow rate at the outlet as a function of time for the actual event and the constant mean precipitation scenario.

In our example, the peak discharge under the constant mean precipitation (Figure 10.6 [lower middle]) with a runoff coefficient is higher than that under no runoff conditions. This seems contradictory, but is the resultant of our computation. We assume groundwater holds a constant velocity after infiltration, that is dependent on the infiltration intensity and a constant assumed macropore diameter. This approach enables the concentration of groundwater under different velocities at the outlet.

We applied the same methodology to a subset of the contributing areas in both the Waikoukou and Te Whanga study area and computed the ratio of macropore flow from a mean and an event precipitation. The results are plotted versus the contributing area size, which we expect to be the best and most practical predictor of this ratio in Figure 10.7, 10.8. These figures are for a scenario with no runoff coefficient and a fixed runoff coefficient. The version with a variable runoff coefficient is published in and applied in the main paper. The resolution of the digital

elevation model from which the D8 contributing areas are computed is 2 m.

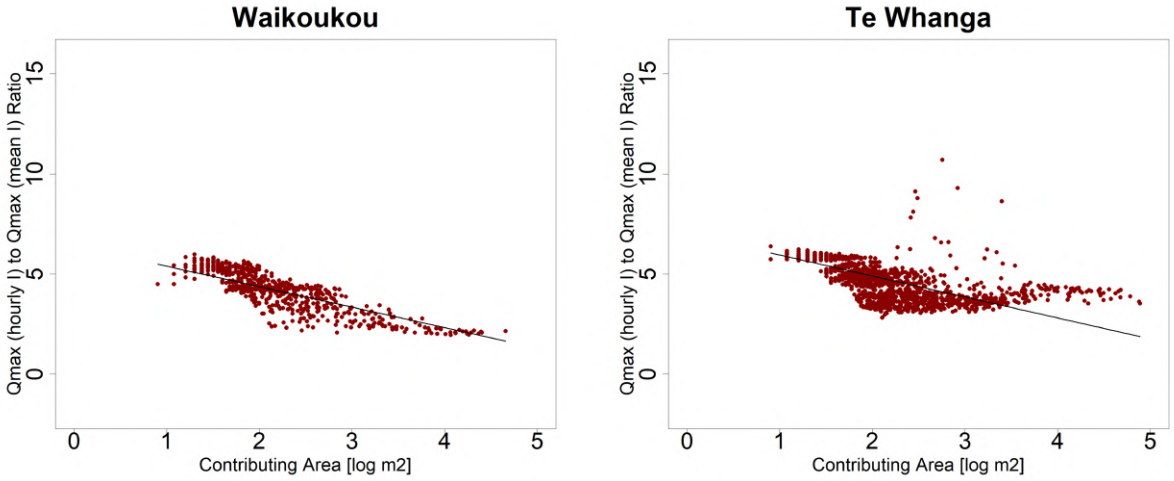

FIGURE 10.7: Ratio between the maximum lateral flow rate derived from an actual event and a constant mean precipitation with no runoff coefficient. The event is the March 2005 rainfall event and contributing areas are from both the Waikoukou and Te Whanga study area. A linear regression is performed to compute the relationship between this ratio and the contributing area size. The Waikoukou intercept and slope are 6.4 and -1.02 respectively. The Te Whanga intercept and slope are 7.0 and -1.05 respectively.

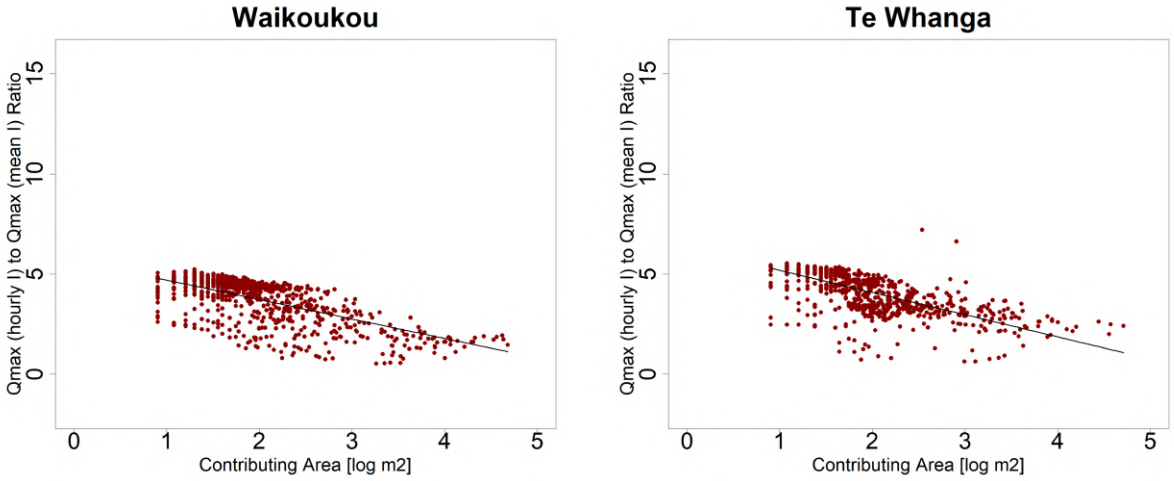

FIGURE 10.8: Ratio between the maximum lateral flow rate derived from an actual event and a constant mean precipitation with a runoff coefficient of Runoff Type 2. The event is the March 2005 rainfall event and contributing areas are from both the Waikoukou and Te Whanga study area. A linear regression is performed to compute the relationship between this ratio and the contributing area size. The Waikoukou intercept and slope are 5.7 and -0.83 respectively. The Te Whanga intercept and slope are 6.3 and -0.97 respectively.

Calibration and validation

The robustness of the calibration and validation method was tested by repeating the method 5 times for the Waikoukou study area with the original version of SlideforMAP as presented in this paper. This is limited for computational reasons. The resulting parameter values and

output metrics are given in Figure 10.9. Dotty plots displaying parameter narrowing for the best performing of the 5 calibration test runs are given in Figure 10.10 to 10.13.

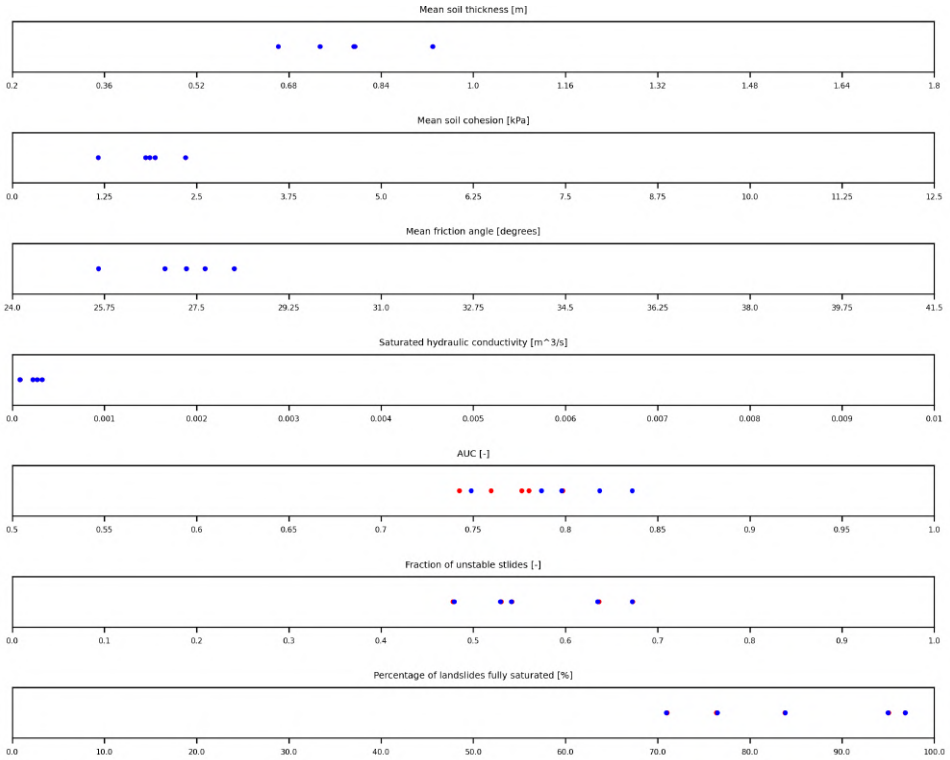

FIGURE 10.9: Development of the calibration and validation process. The upper four graphs show the resulting value of one of the calibration values. The lower three graphs give result variables with a blue dot for the calibration value and a red dot for validation values.

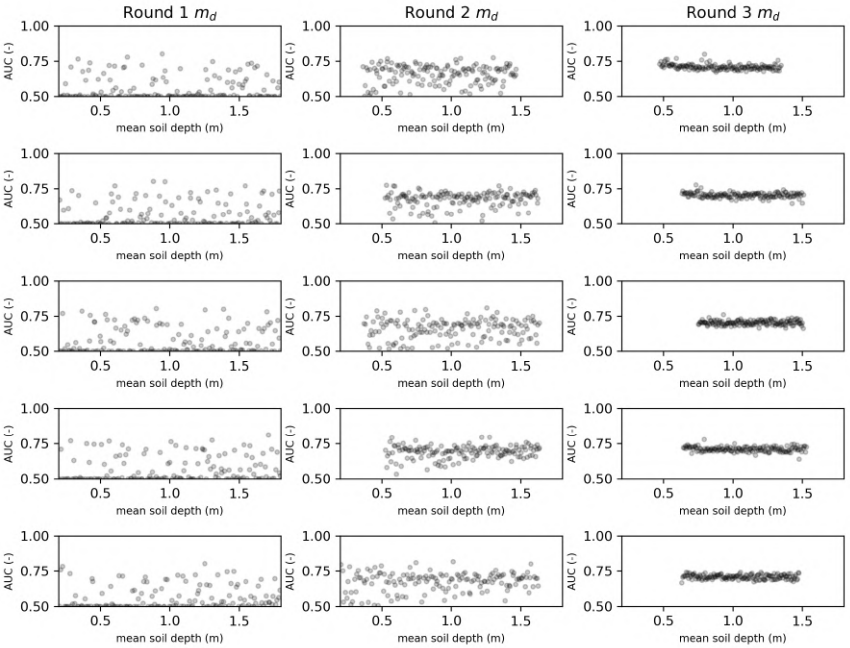

FIGURE 10.10: Dotty plots for the repeated calibration and validation process.The plot gives the parameter values of the mean soil thickness versus the resulting AUC for the three calibration rounds.

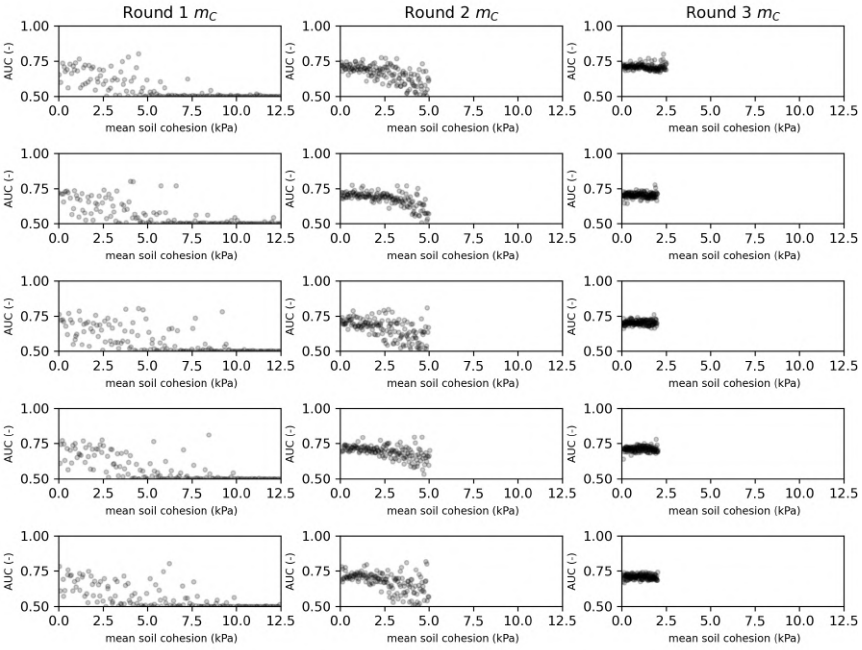

FIGURE 10.11: Dotty plots for the repeated calibration and validation process.The plot gives the parameter values of the mean saturated soil cohesion versus the resulting AUC for the three calibration rounds.

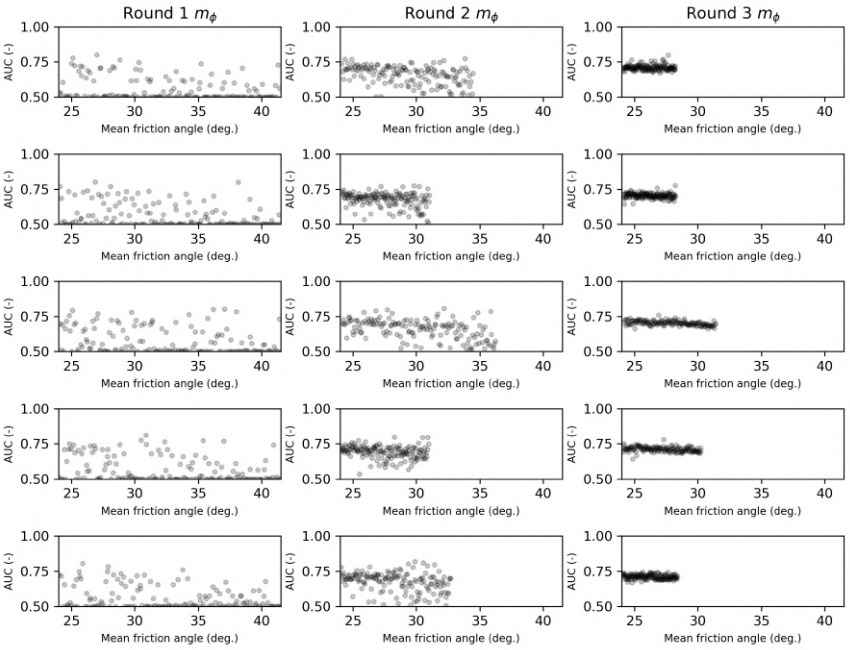

FIGURE 10.12: Dotty plots for the repeated calibration and validation process. The plot gives the parameter values of the mean friction angle versus the resulting AUC for the three calibration rounds.

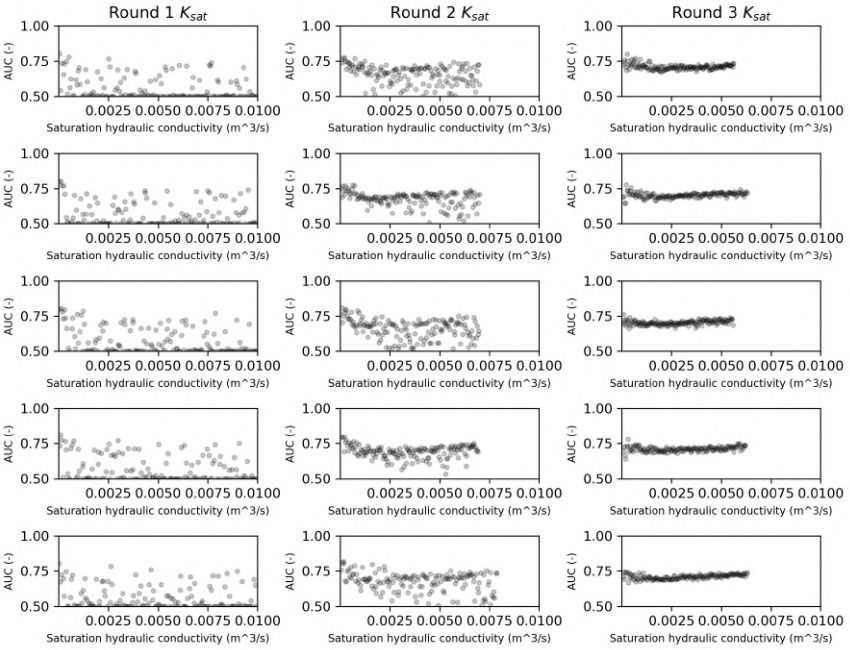

FIGURE 10.13: Dotty plots for the repeated calibration and validation process. The plot gives the parameter values of the saturated hydraulic conductivity versus the resulting AUC for the three calibration rounds.

Pore water pressure

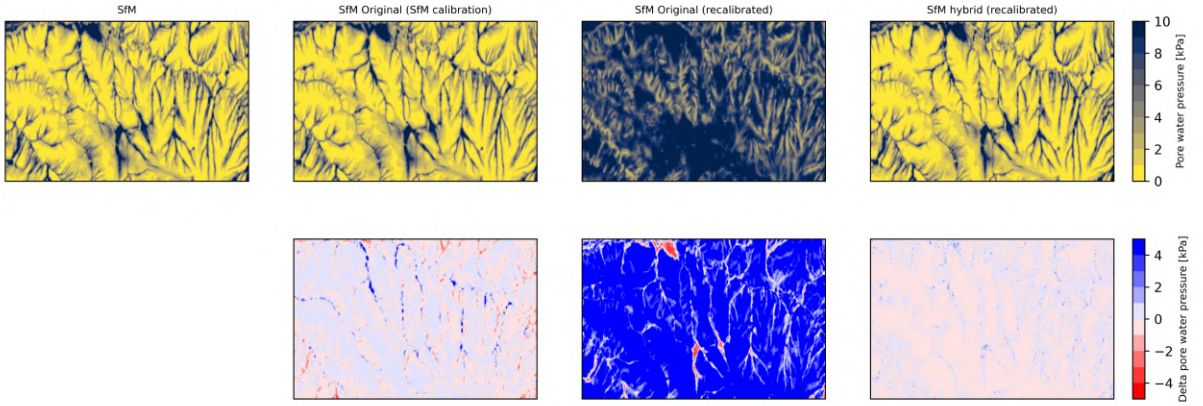

FIGURE 10.14: Calibrated pore water pressure in Waikoukou. Upper row, mean pore water pressure [kPa] from SfM, SfM org. with SfM parametrization, SfM org., with unique calibration and SfM no hybrid; Lower row list the absolute difference in pore water pressure of the versions as compared to SfM.

Bibliography

Ahuja, L., & El-Swaify, S. (1979). Determining soil hydrologic characteristics on a remote forest watershed by continuous monitoring of soil-water pressures, rainfall and runoff. *Journal of Hydrology*, *44*(1-2), 135–147. https://doi.org/10.1016/0022-1694(79)90151-3

Amatya, D. (Ed.). (2016). *Forest hydrology: Processes, management and assessment*. CAB International.

Ambroise, B., Beven, K., & Freer, J. (1996). Toward a Generalization of the TOPMODEL Concepts: Topographic Indices of Hydrological Similarity. *Water Resources Research*, *32*(7), 2135–2145. https://doi.org/10.1029/95WR03716

Amishev, D., Basher, L. R., Phillips, C. J., Hill, S., Marden, M., Bloomberg, M., & Moore, J. R. (2014). *New forest management approaches to steep hills* [OCLC: 900799046]. Ministry for Primary Industries.

Ang, A. H.-S., & Tang, W. H. (1975). *Probability Concepts in Engineering· Planning and Design*. John Wiley; Sons.

Antonetti, M. (2017). *Runoff generation during heavy rainfall events: Integrating expert knowledge about dominant runoff processes in conceptual hydrological models* (Doctoral dissertation). University of Zurich. https://doi.org/10.5167/UZH-148778

Antonetti, M., Scherrer, S., Kienzler, P. M., Margreth, M., & Zappa, M. (2017). Process-based hydrological modelling: The potential of a bottom-up approach for runoff predictions in ungauged catchments. *Hydrological Processes*, *31*(16), 2902–2920. https://doi.org/10.1002/hyp.11232

Arabameri, A., & Pourghasemi, H. R. (2019). Spatial Modeling of Gully Erosion Using Linear and Quadratic Discriminant Analyses in GIS and R. In *Spatial Modeling in GIS and R for Earth and Environmental Sciences* (pp. 299–321). Elsevier. https://doi.org/10.1016/B978-0-12-815226-3.00013-2

Arnone, E., Caracciolo, D., Noto, L. V., Preti, F., & Bras, R. L. (2016). Modeling the hydrological and mechanical effect of roots on shallow landslides. *Water Resources Research*, *52*(11), 8590–8612.

Arsenault, R., Brissette, F., & Martel, J.-L. (2018). The hazards of split-sample validation in hydrological model calibration. *Journal of Hydrology*, *566*, 346–362. https://doi.org/10.1016/j.jhydrol.2018.09.027

Askarinejad, A., Akca, D., & Springman, S. M. (2018). Precursors of instability in a natural slope due to rainfall: A full-scale experiment. *Landslides*, *15*(9), 1745–1759. https://doi.org/10.1007/s10346-018-0994-0

Askarinejad, A., Casini, F., Bischof, P., Beck, A., & Springman, S. M. (2012). Rainfall induced instabilities: A field experiment on a silty sand slope in northern Switzerland. *Rivista Italiana Di Geotecnica*, *3*(12), 50–71.

Aston, A. (1979). Rainfall interception by eight small trees. *Journal of Hydrology*, *42*(3-4), 383–396. https://doi.org/10.1016/0022-1694(79)90057-X

Badoux, A., Andres, N., Techel, F., & Hegg, C. (2016). Natural hazard fatalities in Switzerland from 1946 to 2015. *Natural Hazards and Earth System Sciences*, *16*(12), 2747–2768. https://doi.org/10.5194/nhess-16-2747-2016

Baeza, C., & Corominas, J. (2001). Assessment of shallow landslide susceptibility by means of multivariate statistical techniques. *Earth Surface Processes and Landforms*, *26*(12), 1251–1263. https://doi.org/10.1002/esp.263

Baiamonte, G. (2020). A rational runoff coefficient for a revisited rational formula. *Hydrological Sciences Journal*, *65*(1), 112–126. https://doi.org/10.1080/02626667.2019.1682150

Bárdossy, A. (2007). Calibration of hydrological model parameters for ungauged catchments. *Hydrology and Earth System Sciences*, *11*(2), 703–710. https://doi.org/10.5194/hess-11-703-2007

Barton, C. V. M., & Montagu, K. D. (2004). Detection of tree roots and determination of root diameters by ground penetrating radar under optimal conditions. *Tree Physiology*, *24*(12), 1323–1331. https://doi.org/10.1093/treephys/24.12.1323

Bartos, M. (2020). Pysheds: Simple and fast watershed delineation in python. https://doi.org/10.5281/zenodo.3822494

Basher, L., Betts, H., Lynn, I., Marden, M., McNeill, S., Page, M., & Rosser, B. (2018). A preliminary assessment of the impact of landslide, earthflow, and gully erosion on soil carbon stocks in New Zealand. *Geomorphology*, *307*, 93–106. https://doi.org/10.1016/j.geomorph.2017.10.006

Bast, A., Wilcke, W., Graf, F., Lüscher, P., & Gärtner, H. (2014). The use of mycorrhiza for eco-engineering measures in steep alpine environments: Effects on soil aggregate formation and fine-root development: *Earth Surface Processes and Landforms*, *39*(13), 1753–1763. https://doi.org/10.1002/esp.3557

Baum, R. L., & Godt, J. W. (2010). Early warning of rainfall-induced shallow landslides and debris flows in the USA. *Landslides*, *7*(3), 259–272. https://doi.org/10.1007/s10346-009-0177-0

Baum, R. L., Savage, W. Z., Godt, J. W., et al. (2002a). Trigrs—a fortran program for transient rainfall infiltration and grid-based regional slope-stability analysis. *US geological survey open-file report*, *424*, 38.

Baum, R. L., Savage, W. Z., & Godt, J. W. (2002b). TRIGRS—A Fortran Program for Transient Rainfall Infiltration and Grid-Based Regional Slope-Stability Analysis, Open file report 02-424, 25.

Beek, R. v. (2002). *Assessment of the influence of changes in land use and climate on landslide activity in a Mediterranean environment*. Koninklijk Nederlands Aardrijkskundig Genootschap.

Bellugi, D. G., Milledge, D. G., Cuffey, K. M., Dietrich, W. E., & Larsen, L. G. (2021). Controls on the size distributions of shallow landslides. *Proceedings of the National Academy of Sciences*, *118*(9), e2021855118. https://doi.org/10.1073/pnas.2021855118

Benoit, L., & Mariethoz, G. (2017). Generating synthetic rainfall with geostatistical simulations: Generating synthetic rainfall. *Wiley Interdisciplinary Reviews: Water*, *4*(2), e1199. https://doi.org/10.1002/wat2.1199

Bergström, S. (1976). *Development and application of a conceptual runoff model for scandinavian catchments*.

Betts, H., Basher, L., Dymond, J., Herzig, A., Marden, M., & Phillips, C. (2017). Development of a landslide component for a sediment budget model. *Environmental Modelling & Software*, *92*, 28–39. https://doi.org/10.1016/j.envsoft.2017.02.003

Beven, K. J. (2000). Uniqueness of place and process representations in hydrological modelling. *Hydrology and Earth System Sciences*, *4*(2), 203–213. https://doi.org/10.5194/hess-4-203-2000

Beven, K. J. (2012). *Rainfall-runoff modelling: The primer* (2nd ed). Wiley-Blackwell.

Beven, K. J., & Kirkby, M. J. (1979). A physically based, variable contributing area model of basin hydrology / Un modèle à base physique de zone d'appel variable de l'hydrologie du bassin versant. *Hydrological Sciences Bulletin*, *24*(1), 43–69. https://doi.org/10.1080/02626667909491834

Beven, K. (1997). TOPMODEL: A critique. *Hydrological Processes*, *11*(9), 1069–1085. https://doi.org/10.1002/(SICI)1099-1085(199707)11:9<1069::AID-HYP545>3.0.CO;2-O

Beven, K., & Binley, A. (1992). The future of distributed models: Model calibration and uncertainty prediction. *Hydrological Processes*, *6*(3), 279–298. https://doi.org/10.1002/hyp.3360060305

Beven, K., & Freer, J. (2001). A dynamic TOPMODEL. *Hydrological Processes*, *15*(10), 1993–2011. https://doi.org/10.1002/hyp.252

Beven, K., & Germann, P. (1982). Macropores and water flow in soils. *Water Resources Research*, *18*(5), 1311–1325. https://doi.org/10.1029/WR018i005p01311

Beven, K., & Germann, P. (2013). Macropores and water flow in soils revisited. *Water Resources Research*, *49*(6), 3071–3092. https://doi.org/10.1002/wrcr.20156

Beven, K. J., Lamb, R., Kirkby, M. J., & Freer, J. E. (2020). *A history of TOPMODEL* (preprint). Catchment hydrology/Modelling approaches. https://doi.org/10.5194/hess-2020-409

Bierkens, M. F. P. (Ed.). (2008). *Climate and the hydrological cycle*. International Association of Hydrological Sciences.

Binley, A. M., Beven, K. J., Calver, A., & Watts, L. G. (1991). Changing responses in hydrology: Assessing the uncertainty in physically based model predictions. *Water Resources Research*, *27*(6), 1253–1261. https://doi.org/10.1029/91WR00130

Bishop, A. W. (1955). The use of the Slip Circle in the Stability Analysis of Slopes. *Géotechnique*, *5*(1), 7–17. https://doi.org/10.1680/geot.1955.5.1.7

Blazkova, S., Beven, K., Tacheci, P., & Kulasova, A. (2002). Testing the distributed water table predictions of TOPMODEL (allowing for uncertainty in model calibration): The death of TOPMODEL?: The death of TOPMODEL? *Water Resources Research*, *38*(11), 39–1–39–11. https://doi.org/10.1029/2001WR000912

Bodner, G., Leitner, D., & Kaul, H.-P. (2014). Coarse and fine root plants affect pore size distributions differently. *Plant and Soil*, *380*(1-2), 133–151. https://doi.org/10.1007/s11104-014-2079-8

Bordoni, M., Meisina, C., Valentino, R., Lu, N., Bittelli, M., & Chersich, S. (2015). Hydrological factors affecting rainfall-induced shallow landslides: From the field monitoring to a simplified slope stability analysis. *Engineering Geology*, *193*, 19–37. https://doi.org/10.1016/j.enggeo.2015.04.006

Borga, M., Dalla Fontana, G., Gregoretti, C., & Marchi, L. (2002). Assessment of shallow landsliding by using a physically based model of hillslope stability. *Hydrological Processes*, *16*(14), 2833–2851. https://doi.org/10.1002/hyp.1074

Bouilloud, L., Chancibault, K., Vincendon, B., Ducrocq, V., Habets, F., Saulnier, G.-M., Anquetin, S., Martin, E., & Noilhan, J. (2010). Coupling the ISBA Land Surface Model and the TOPMODEL Hydrological Model for Mediterranean Flash-Flood Forecasting: Description, Calibration, and Validation. *Journal of Hydrometeorology*, *11*(2), 315–333. https://doi.org/10.1175/2009JHM1163.1

Brabb, E. E. (1984). *Innovative approaches to landslide hazard and risk mapping*. 4th International Symposium on Landslides. Toronto, Canada.

Buytaert, W., Reusser, D., Krause, S., & Renaud, J.-P. (2008). Why can't we do better than Topmodel? *Hydrological Processes*, *22*(20), 4175–4179. https://doi.org/10.1002/hyp.7125

Callaway, R. M., Pennings, S. C., & Richards, C. L. (2003). Phenotypic Plasticity and Interactions Among Plants. *Ecology*, *84*(5), 1115–1128. https://doi.org/10.1890/0012-9658(2003)084[1115:PPAIAP]2.0.CO;2

Carey-Smith, T., Henderson, R., & Singh, S. (2018). High intensity rainfall design system version 4. *NIWA Client Report 2018022CH, NIWA*.

Casadei, M., Dietrich, W. E., & Miller, N. (2003). Controls on shallow landslide size.

Cervi, F., Berti, M., Borgatti, L., Ronchetti, F., Manenti, F., & Corsini, A. (2010). Comparing predictive capability of statistical and deterministic methods for landslide susceptibility mapping: A case study in the northern Apennines (Reggio Emilia Province, Italy). *Landslides*, *7*(4), 433–444. https://doi.org/10.1007/s10346-010-0207-y

Chae, B.-G., Park, H.-J., Catani, F., Simoni, A., & Berti, M. (2017). Landslide prediction, monitoring and early warning: A concise review of state-of-the-art. *Geosciences Journal*, *21*(6), 1033–1070. https://doi.org/10.1007/s12303-017-0034-4

Chung, C.-J., & Fabbri, A. G. (2008). Predicting landslides for risk analysis — Spatial models tested by a cross-validation technique. *Geomorphology*, *94*(3-4), 438–452. https://doi.org/10.1016/j.geomorph.2006.12.036

Chung, C.-J. F., & Fabbri, A. G. (2003). Validation of Spatial Prediction Models for Landslide Hazard Mapping. *Natural Hazards*, *30*(3), 451–472. https://doi.org/10.1023/B:NHAZ.0000007172.62651.2b

Cislaghi, A., Chiaradia, E. A., & Bischetti, G. B. (2017). Including root reinforcement variability in a probabilistic 3D stability model: Root reinforcement variability in a probabilistic 3-D stability model. *Earth Surface Processes and Landforms*, *42*(12), 1789–1806. https://doi.org/10.1002/esp.4127

Cislaghi, A., Cohen, D., Gasser, E., Bischetti, G. B., & Schwarz, M. (2019). Field Measurements of Passive Earth Forces in Steep, Shallow, Landslide-Prone Areas. *Journal of Geophysical Research: Earth Surface*, *124*(3), 838–866. https://doi.org/10.1029/2017JF004557

Cislaghi, A., Rigon, E., Lenzi, M. A., & Bischetti, G. B. (2018). A probabilistic multidimensional approach to quantify large wood recruitment from hillslopes in mountainous-forested catchments. *Geomorphology*, *306*, 108–127. https://doi.org/10.1016/j.geomorph.2018.01.009

Cohen, D., Lehmann, P., & Or, D. (2009). Fiber bundle model for multiscale modeling of hydromechanical triggering of shallow landslides. *Water Resources Research*, *45*(10). https://doi.org/10.1029/2009WR007889

Cohen, D., & Schwarz, M. (2017a). SOSlope (v1.3) User manual of the „self organized slope“ model.

Cohen, D., Schwarz, M., & Or, D. (2011). An analytical fiber bundle model for pullout mechanics of root bundles. *Journal of Geophysical Research*, *116*(F3), F03010. https://doi.org/10.1029/2010JF001886

Cohen, D., & Schwarz, M. (2017b). Tree-root control of shallow landslides. *Earth Surface Dynamics*, *5*(3), 451–477. https://doi.org/10.5194/esurf-5-451-2017

Corominas, J., van Westen, C., Frattini, P., Cascini, L., Malet, J.-P., Fotopoulou, S., Catani, F., Van Den Eeckhaut, M., Mavrouli, O., Agliardi, F., Pitilakis, K., Winter, M. G., Pastor, M., Ferlisi, S., Tofani, V., Hervás, J., & Smith, J. T. (2014). Recommendations for the quantitative analysis of landslide risk. *Bulletin of Engineering Geology and the Environment*, *73*, 209–263. https://doi.org/10.1007/s10064-013-0538-8

Cristiano, E., Veldhuis, M.-c., Wright, D. B., Smith, J. A., & Giesen, N. (2019). The Influence of Rainfall and Catchment Critical Scales on Urban Hydrological Response Sensitivity. *Water Resources Research*, *55*(4), 3375–3390. https://doi.org/10.1029/2018WR024143

Croissant, T., Steer, P., Lague, D., Davy, P., Jeandet, L., & Hilton, R. G. (2019). Seismic cycles, earthquakes, landslides and sediment fluxes: Linking tectonics to surface processes using a reduced-complexity model. *Geomorphology*, *339*, 87–103. https://doi.org/10.1016/j.geomorph.2019.04.017

Crosta, G. B., & Frattini, P. (2003). Distributed modelling of shallow landslides triggered by intense rainfall. *Natural Hazards and Earth System Sciences*, *3*(1/2), 81–93. https://doi.org/10.5194/nhess-3-81-2003

Crozier, M. J. (2005). Multiple-occurrence regional landslide events in New Zealand: Hazard management issues. *Landslides*, *2*(4), 247–256. https://doi.org/10.1007/s10346-005-0019-7

Crozier, M. J., Eyles, R. J., Marx, S. L., McConchie, J. A., & Owen, R. C. (1980). Distribution of landslips in the Wairarapa hill country. *New Zealand Journal of Geology and Geophysics*, *23*(5-6), 575–586. https://doi.org/10.1080/00288306.1980.10424129

Crozier, M. J., & Preston, N. J. (1999). Modelling changes in terrain resistance as a component of landform evolution in unstable hill country [Series Title: Lecture Notes in Earth Sciences]. In *Process Modelling and Landform Evolution* (pp. 267–284). Springer-Verlag. https://doi.org/10.1007/BFb0009730

D'Amato Avanzi, G., Giannecchini, R., & Puccinelli, A. (2004). The influence of the geological and geomorphological settings on shallow landslides. An example in a temperate climate environment: The June 19, 1996 event in northwestern Tuscany (Italy). *Engineering Geology*, *73*(3-4), 215–228. https://doi.org/10.1016/j.enggeo.2004.01.005

Danjon, F., Stokes, A., & Bakker, M. R. (2013). Root systems of woody plants.

Darcy, H. (1856). *Les fontaines publiques de la ville de dijon: Exposition et application des principes à suivre et des formules à employer dans les questions de distribution d'eau... un appendice relatif aux fournitures d'eau de plusieurs villes au filtrage des eaux* (Vol. 1). Victor Dalmont, éditeur.

Day, R. W. (1997). State of the art: Limit equilibrium and finite-element analysis of slopes. *Journal of Geotechnical and Geoenvironmental Engineering*, *123*(9), 894. https://doi.org/10.1061/(ASCE)1090-0241(1997)123:9(894)

Dazio, E. (R., Conedera, M., & Schwarz, M. (2018a). Impact of different chestnut coppice managements on root reinforcement and shallow landslide susceptibility. *Forest Ecology and Management*, *417*, 63–76. https://doi.org/10.1016/j.foreco.2018.02.031

Dazio, E. (R., Conedera, M., & Schwarz, M. (2018b). Impact of different chestnut coppice managements on root reinforcement and shallow landslide susceptibility. *Forest Ecology and Management*, *417*(December 2017), 63–76. https://doi.org/10.1016/j.foreco.2018.02.031

De Rose, R. C. (2013). Slope control on the frequency distribution of shallow landslides and associated soil properties, North Island, New Zealand. *Earth Surface Processes and Landforms*, *38*(4), 356–371. https://doi.org/10.1002/esp.3283

De Vita, P., Reichenbach, P., Bathurst, J. C., Borga, M., Crosta, G., Crozier, M., Glade, T., Guzzetti, F., Hansen, A., & Wasowski, J. (1998). Rainfall-triggered landslides: A reference list. *Environmental Geology*, *35*(2-3), 219–233. https://doi.org/10.1007/s002540050308

Debele, S. E., Kumar, P., Sahani, J., Marti-Cardona, B., Mickovski, S. B., Leo, L. S., Porcù, F., Bertini, F., Montesi, D., Vojinovic, Z., & Di Sabatino, S. (2019). Nature-based solutions for hydro-meteorological hazards: Revised concepts, classification schemes and databases. *Environmental Research*, *179*, 108799. https://doi.org/10.1016/j.envres.2019.108799

de Jesús Arce-Mojica, T., Nehren, U., Sudmeier-Rieux, K., Miranda, P. J., & Anhuf, D. (2019). Nature-based solutions (NbS) for reducing the risk of shallow landslides: Where do we stand? *International Journal of Disaster Risk Reduction*, *41*, 101293. https://doi.org/10.1016/j.ijdrr.2019.101293

Dietrich, W. E., & Montgomery, D. R. (1998). Hillslopes, channels, and landscape scale. *Scale dependence and scale invariance in hydrology*, 30–60.

Dingman, S. L. (2015). *Physical hydrology* (Third edition). Waveland Press, Inc.

Division, C. E. (1986). Urban Hydrology for Small Watersheds.

Docker, B., & Hubble, T. (2008). Quantifying root-reinforcement of river bank soils by four Australian tree species. *Geomorphology*, *100*(3-4), 401–418. https://doi.org/10.1016/j.geomorph.2008.01.009

D'Odorico, P., & Fagherazzi, S. (2003). A probabilistic model of rainfall-triggered shallow landslides in hollows: A long-term analysis. *Water Resources Research*, *39*(9). https://doi.org/10.1029/2002WR001595

Dooge, J. C. I. (2005). Bringing it all together. *Hydrology and Earth System Sciences*, *9*(1/2), 3–14. https://doi.org/10.5194/hess-9-3-2005

Dorren, L. (2017). FINT – Find individual trees. User manual. *ecorisQ paper (www.ecorisq.org)*, 5 p.

Dorren, L., Sandri, A., Raetzo, H., & Arnold, P. (2009). Landslide risk mapping for the entire Swiss national road network. *Landslide Processes: from geomorphologic mapping to dynamic modeling, Strasbourg, France*, 6–7.

Douglas, G. B., Mcivor, I. R., Manderson, A. K., Koolaard, J. P., Todd, M., Braaksma, S., & Gray, R. A. J. (2013). Reducing shallow landslide occurrence in pastoral hill country using wide-spaced trees. *Land Degradation & Development*, *24*(2), 103–114. https://doi.org/10.1002/ldr.1106

Douglas, G. B., McIvor, I. R., & Lloyd-West, C. M. (2016). Early root development of field-grown poplar: Effects of planting material and genotype. *New Zealand Journal of Forestry Science*, *46*(1), 1. https://doi.org/10.1186/s40490-015-0057-4

Douglas, G. B., McIvor, I. R., Potter, J. F., & Foote, L. G. (2010). Root distribution of poplar at varying densities on pastoral hill country. *Plant and Soil*, *333*(1-2), 147–161. https://doi.org/10.1007/s11104-010-0331-4

Ducharne, A. (2009). Reducing scale dependence in TOPMODEL using a dimensionless topographic index. *Hydrology and Earth System Sciences*, *13*(12), 2399–2412. https://doi.org/10.5194/hess-13-2399-2009

Ducharne, A., Koster, R. D., Suarez, M. J., Stieglitz, M., & Kumar, P. (2000). A catchment-based approach to modeling land surface processes in a general circulation model: 2. Parameter estimation and model demonstration. *Journal of Geophysical Research: Atmospheres*, *105*(D20), 24823–24838. https://doi.org/10.1029/2000JD900328

Dymond, J. R., Herzig, A., Basher, L., Betts, H. D., Marden, M., Phillips, C. J., Ausseil, A.-G. E., Palmer, D. J., Clark, M., & Roygard, J. (2016). Development of a New Zealand SedNet model for assessment of catchment-wide soil-conservation works. *Geomorphology*, *257*, 85–93. https://doi.org/10.1016/j.geomorph.2015.12.022

Dysli, M., & Rybisar, J. (1992). *Statistique sur les caractéristiques des sols suisses- Statistische Behandlung der Kennwerte der Schweizer Boeden.* Bundesamt fuer Strassenbau.

Edwards, P. J., Williard, K. W., & Schoonover, J. E. (2015). Fundamentals of Watershed Hydrology. *Journal of Contemporary Water Research & Education*, *154*(1), 3–20. https://doi.org/10.1111/j.1936-704X.2015.03185.x

Ekanayake, J. C., Marden, M., Watson, A. J., & Rowan, D. (1997). Tree roots and slope stability: A comparison between Pinus Radiata and Kanuka. *New Zealand Journal of Forestry Science*, *27*(2), 216–233.

El Khouli, R. H., Macura, K. J., Barker, P. B., Habba, M. R., Jacobs, M. A., & Bluemke, D. A. (2009). Relationship of temporal resolution to diagnostic performance for dynamic contrast enhanced mri of the breast. *Journal of Magnetic Resonance Imaging: An Official Journal of the International Society for Magnetic Resonance in Medicine*, *30*(5), 999–1004.

Eysn, L., Hollaus, M., Lindberg, E., Berger, F., Monnet, J.-M., Dalponte, M., Kobal, M., Pellegrini, M., Lingua, E., Mongus, D., & Pfeifer, N. (2015). A Benchmark of Lidar-Based Single Tree Detection Methods Using Heterogeneous Forest Data from the Alpine Space. *Forests*, *6*(12), 1721–1747. https://doi.org/10.3390/f6051721

Fan, C.-C., Lu, J. Z., & Chen, H. H. (2021). The pullout resistance of plant roots in the field at different soil water conditions and root geometries. *CATENA*, *207*, 105593. https://doi.org/10.1016/j.catena.2021.105593

Fassnacht, F. E., Latifi, H., Stereńczak, K., Modzelewska, A., Lefsky, M., Waser, L. T., Straub, C., & Ghosh, A. (2016). Review of studies on tree species classification from remotely sensed data. *Remote Sensing of Environment*, *186*, 64–87. https://doi.org/10.1016/j.rse.2016.08.013

Fawcett, T. (2006). An introduction to ROC analysis. *Pattern Recognition Letters*, *27*(8), 861–874. https://doi.org/10.1016/j.patrec.2005.10.010

Feng, S., Liu, H., & Ng, C. (2020). Analytical analysis of the mechanical and hydrological effects of vegetation on shallow slope stability. *Computers and Geotechnics*, *118*, 103335. https://doi.org/10.1016/j.compgeo.2019.103335

Flury, M., Flühler, H., Jury, W. A., & Leuenberger, J. (1994). Susceptibility of soils to preferential flow of water: A field study. *Water Resources Research*, *30*(7), 1945–1954. https://doi.org/10.1029/94WR00871

Fox, J., Weisberg, S., Adler, D., Bates, D., Baud-Bovy, G., Ellison, S., Firth, D., Friendly, M., Gorjanc, G., Graves, S., et al. (2012). Package 'car'. *Vienna: R Foundation for Statistical Computing*, *16*.

Franks, S. W., Gineste, P., Beven, K. J., & Merot, P. (1998). On constraining the predictions of a distributed model: The incorporation of fuzzy estimates of saturated areas into the calibration process. *Water Resources Research*, *34*(4), 787–797. https://doi.org/10.1029/97WR03041

Frattini, P., Crosta, G., & Carrara, A. (2010). Techniques for evaluating the performance of landslide susceptibility models. *Engineering Geology*, *111*(1-4), 62–72. https://doi.org/10.1016/j.enggeo.2009.12.004

Freeze, R. A., & Cherry, J. A. (1979). *Groundwater*. Prentice-Hall.

Frehner, M., Wasser, B., & Schwitter, R. (2005). Nachhaltigkeit und Erfolgskontrolle im Schutzwald. Wagleitung fuer Pflegemassnahmen in Waeldern mit Schutzfuntion.

Frei, C., Isotta, F., & Schwanbeck, J. (2020). Mean Precipitation 1981-2010. In *Hydrological atlas of switzerland*. Geographisches Institut der Universität Bern.

Fuller, I. C., & Rutherfurd, I. D. (2022). Geomorphic Responses to Anthropogenic Land-Cover Change in Australia and New Zealand. In *Treatise on Geomorphology* (pp. 584–619). Elsevier. https://doi.org/10.1016/B978-0-12-818234-5.00104-8

Gao, M., Li, H.-Y., Liu, D., Tang, J., Chen, X., Chen, X., Blöschl, G., & Ruby Leung, L. (2018). Identifying the dominant controls on macropore flow velocity in soils: A meta-analysis. *Journal of Hydrology*, *567*, 590–604. https://doi.org/10.1016/j.jhydrol.2018.10.044

Gascoin, S., Ducharne, A., Ribstein, P., Carli, M., & Habets, F. (2009). Adaptation of a catchment-based land surface model to the hydrogeological setting of the Somme River basin (France). *Journal of Hydrology*, *368*(1-4), 105–116. https://doi.org/10.1016/j.jhydrol.2009.01.039

Gasser, E., Schwarz, M., Simon, A., Perona, P., Phillips, C., Hübl, J., & Dorren, L. (2019). A review of modeling the effects of vegetation on large wood recruitment processes in mountain catchments. *Earth-Science Reviews*, *194*, 350–373. https://doi.org/10.1016/j.earscirev.2019.04.013

Geertsema, M., Schwab, J. W., Blais-Stevens, A., & Sakals, M. E. (2009). Landslides impacting linear infrastructure in west central British Columbia. *Natural Hazards*, *48*(1), 59–72. https://doi.org/10.1007/s11069-008-9248-0

Gehring, E., Conedera, M., Maringer, J., Giadrossich, F., Guastini, E., & Schwarz, M. (2019). Shallow landslide disposition in burnt European beech (Fagus sylvatica L.) forests. *Scientific Reports*, *9*(1), 8638. https://doi.org/10.1038/s41598-019-45073-7

Gerke, H. H., & van Genuchten, M. T. (1993). A dual-porosity model for simulating the preferential movement of water and solutes in structured porous media. *Water Resources Research*, *29*(2), 305–319. https://doi.org/10.1029/92WR02339

Germann, P., & Beven, K. (1981). Water flow in soil macropores I. An experimental approach. *Journal of Soil Science*, *32*(1), 1–13. https://doi.org/10.1111/j.1365-2389.1981.tb01681.x

Germann, P. F., & Beven, K. (1985). Kinematic Wave Approximation to Infiltration Into Soils With Sorbing Macropores. *Water Resources Research*, *21*(7), 990–996. https://doi.org/10.1029/WR021i007p00990

Gessesse, A. A., & Melesse, A. M. (2019). Temporal relationships between time series CHIRPS-rainfall estimation and eMODIS-NDVI satellite images in Amhara Region, Ethiopia. In *Extreme Hydrology and Climate Variability* (pp. 81–92). Elsevier. https://doi.org/10.1016/B978-0-12-815998-9.00008-7

Giadrossich, F., Schwarz, M., Cohen, D., Cislaghi, A., Vergani, C., Hubble, T., Phillips, C., & Stokes, A. (2017). Methods to measure the mechanical behaviour of tree roots: A review. *Ecological Engineering*, *109*, 256–271. https://doi.org/10.1016/j.ecoleng.2017.08.032

Giadrossich, F., Schwarz, M., Cohen, D., Preti, F., & Or, D. (2013). Mechanical interactions between neighbouring roots during pullout tests. *Plant and Soil*, *367*(1-2), 391–406. https://doi.org/10.1007/s11104-012-1475-1

Giadrossich, F., Schwarz, M., Marden, M., Marrosu, R., & Phillips, C. (2020). Minimum representative root distribution sampling for calculating slope stability in Pinus radiata D.Don plantations in New Zealand. *New Zealand Journal of Forestry Science*, *50*. https://doi.org/10.33494/nzjfs502020x68x

Glade, T. (2003). Landslide occurrence as a response to land use change: A review of evidence from New Zealand. *CATENA*, *51*(3-4), 297–314. https://doi.org/10.1016/S0341-8162(02)00170-4

Glade, T., Anderson, M., & Crozier, M. J. (Eds.). (2005). *Landslide hazard and risk*. J. Wiley.

González-Ollauri, A., & Mickovski, S. B. (2014). Integrated Model for the Hydro-Mechanical Effects of Vegetation Against Shallow Landslides [Artwork Size: 37-61 Pages Publisher: Alma Mater Studiorum - University of Bologna]. *EQA - International Journal of Environmental Quality*, 37–61 Pages. https://doi.org/10.6092/ISSN.2281-4485/4535

Gorsevski, P. V., Gessler, P. E., Boll, J., Elliot, W. J., & Foltz, R. B. (2006). Spatially and temporally distributed modeling of landslide susceptibility. *Geomorphology*, *80*(3-4), 178–198. https://doi.org/10.1016/j.geomorph.2006.02.011

Grabs, T., Seibert, J., Bishop, K., & Laudon, H. (2009). Modeling spatial patterns of saturated areas: A comparison of the topographic wetness index and a dynamic distributed model. *Journal of Hydrology*, *373*(1-2), 15–23. https://doi.org/10.1016/j.jhydrol.2009.03.031

Graf, F., Frei, M., & Böll, A. (2009). Effects of vegetation on the angle of internal friction of a moraine. *For. Snow Landsc. Res.*, *82*(1), 61–77.

Green, W., & Ampt, G. (1911). The flow of air and water through soils. *J. Agric. Sci*, *4*, 1–24.

Greenway, D. (1987). Greenway, beter leesbaar.pdf. In *Slope stability: Geotechnical engineering and geomorphology/edited by MG Anderson and KS Richards*.

Griffiths, D. V., Huang, J., & Fenton, G. A. (2009). Influence of Spatial Variability on Slope Reliability Using 2-D Random Fields. *Journal of Geotechnical and Geoenvironmental Engineering*, *135*(10), 1367–1378. https://doi.org/10.1061/(ASCE)GT.1943-5606.0000099

Gunawardena, A., Nissanka, S., Dayawansa, N., & Fernando, T. (2015). Estimation of above ground biomass in horton plains national park, sri lanka using optical, thermal and radar remote sensing data.

Guo, L., Chen, J., & Lin, H. (2014). Subsurface lateral preferential flow network revealed by time-lapse ground-penetrating radar in a hillslope. *Water Resources Research*, *50*(12), 9127–9147. https://doi.org/10.1002/2013WR014603

Guzzetti, F., Galli, M., Reichenbach, P., Ardizzone, F., & Cardinali, M. (2006). Landslide hazard assessment in the Collazzone area, Umbria, Central Italy. *Natural Hazards and Earth System Sciences*, *6*(1), 115–131. https://doi.org/10.5194/nhess-6-115-2006

Guzzetti, F., Reichenbach, P., Ardizzone, F., Cardinali, M., & Galli, M. (2006). Estimating the quality of landslide susceptibility models. *Geomorphology*, *81*(1-2), 166–184. https://doi.org/10.1016/j.geomorph.2006.04.007

HADES. (2020). https://hydrologischeratlas.ch/downloads/01/content/Text_Tafel24.de.pdf.

Hales, T. C., Ford, C. R., Hwang, T., Vose, J. M., & Band, L. E. (2009). Topographic and ecologic controls on root reinforcement. *Journal of Geophysical Research*, *114*(F3), F03013. https://doi.org/10.1029/2008JF001168

Hales, T. C. (2018). Modelling biome-scale root reinforcement and slope stability: Biome driven root reinforcement change. *Earth Surface Processes and Landforms*, *43*(10), 2157–2166. https://doi.org/10.1002/esp.4381

Hawley, G., & Dymond, R. (1988). How much do trees reduce landsliding? *Soil and Water Conservation Society*, *43*(6), 495–498.

He, K., Gkioxari, G., Dollár, P., & Girshick, R. (2017). Mask r-cnn. *Proceedings of the IEEE international conference on computer vision*, 2961–2969.

Heckmann, T., Gegg, K., Gegg, A., & Becht, M. (2014). Sample size matters: Investigating the effect of sample size on a logistic regression susceptibility model for debris flows. *Natural Hazards and Earth System Sciences*, *14*(2), 259–278. https://doi.org/10.5194/nhess-14-259-2014

Hendriks, M. R. (2010). *Introduction to physical hydrology* [ISBN: 978-0-19-929684-2]. Oxford University Press.

Herwitz, S. R. (1985). Interception storage capacities of tropical rainforest canopy trees. *Journal of Hydrology*, *77*(1-4), 237–252. https://doi.org/10.1016/0022-1694(85)90209-4

Hess, D. M., Leshchinsky, B. A., Bunn, M., Benjamin Mason, H., & Olsen, M. J. (2017). A simplified three-dimensional shallow landslide susceptibility framework considering topography and seismicity. *Landslides*, *14*(5), 1677–1697. https://doi.org/10.1007/s10346-017-0810-2

Hijmans, R. J. (2022). Terra: Spatial data analysis.(1.5-17).

Holcombe, E., Smith, S., Wright, E., & Anderson, M. G. (2012). An integrated approach for evaluating the effectiveness of landslide risk reduction in unplanned communities in the Caribbean. *Natural Hazards*, *61*(2), 351–385. https://doi.org/10.1007/s11069-011-9920-7

Hosmer, D. (2000). Lemeshow s. applied logistic regression.

Hu, X., Li, X.-Y., Li, Z.-C., Gao, Z., Wu, X.-c., Wang, P., Lyu, Y.-L., & Liu, L.-y. (2020). Linking 3-D soil macropores and root architecture to near saturated hydraulic conductivity of typical meadow soil types in the Qinghai Lake Watershed, northeastern Qinghai–Tibet Plateau. *CATENA*, *185*, 104287. https://doi.org/10.1016/j.catena.2019.104287

Huang, G., Zheng, M., & Peng, J. (2021). Effect of Vegetation Roots on the Threshold of Slope Instability Induced by Rainfall and Runoff (J. Mádl-Szonyi, Ed.). *Geofluids*, *2021*, 1–19. https://doi.org/10.1155/2021/6682113

Hubble, T., Docker, B., & Rutherfurd, I. (2010). The role of riparian trees in maintaining riverbank stability: A review of Australian experience and practice. *Ecological Engineering*, *36*(3), 292–304. https://doi.org/10.1016/j.ecoleng.2009.04.006

Iida, T. (1999). A stochastic hydro-geomorphological model for shallow landsliding due to rainstorm. *CATENA*, *34*(3-4), 293–313. https://doi.org/10.1016/S0341-8162(98)00093-9

Ivanov, V. Y., Bras, R. L., & Vivoni, E. R. (2008). Vegetation-hydrology dynamics in complex terrain of semiarid areas: 2. Energy-water controls of vegetation spatiotemporal dynamics and topographic niches of favorability: ENERGY-WATER CONTROLS IN SEMIARID TERRAIN. *Water Resources Research*, *44*(3). https://doi.org/10.1029/2006WR005595

Iverson, R. M. (2000). Landslide triggering by rain infiltration. *Water Resources Research*, *36*(7), 1897–1910. https://doi.org/10.1029/2000WR900090

Iwasa, Y., Cohen, D., & Leon, J. A. (1985). Tree height and crown shape, as results of competitive games. *Journal of Theoretical Biology*, *112*(2), 279–297. https://doi.org/10.1016/S0022-5193(85)80288-5

Jakob, M., Owen, T., & Simpson, T. (2012). A regional real-time debris-flow warning system for the District of North Vancouver, Canada. *Landslides*, *9*(2), 165–178. https://doi.org/10.1007/s10346-011-0282-8

Jensen, H., Lang, H., & Rinderknecht, J. (1997). Extreme Punktregen unterschiedlicher Dauer und Wiederkehrperioden 1901-1970, Tafel 2.4. In *Hydrologischer atlas der schweiz*. Geographisches Institut der Universität Bern.

Johnson, N. L., & Kotz, S. (1970). *Continuous univariate distributions*. Houghton Mifflin, Boston.

Jones, J. N., Boulton, S. J., Bennett, G. L., Stokes, M., & Whitworth, M. R. Z. (2021). Temporal Variations in Landslide Distributions Following Extreme Events: Implications for Landslide Susceptibility Modeling. *Journal of Geophysical Research: Earth Surface*, *126*(7). https://doi.org/10.1029/2021JF006067

Jones, K. E., & Preston, N. J. (2012). Spatial and temporal patterns of off-slope sediment delivery for small catchments subject to shallow landslides within the Waipaoa catchment, New Zealand. *Geomorphology*, *141-142*, 150–159. https://doi.org/10.1016/j.geomorph.2011.12.037

Jorgensen, S. (2016). *Introduction to systems ecology* (Vol. 4). CRC Press.

Keijsers, J., Schoorl, J., Chang, K.-T., Chiang, S.-H., Claessens, L., & Veldkamp, A. (2011). Calibration and resolution effects on model performance for predicting shallow landslide locations in Taiwan. *Geomorphology*, *133*(3-4), 168–177. https://doi.org/10.1016/j.geomorph.2011.03.020

Kirkby, M. (1975). Hydrograph modelling strategies, 69–90. *Peel R, Chisholm M, Haggert P, Processes in Physical and Human Geography, Heineman, London*.

Kjekstad, O., & Highland, L. (2009a). Economic and Social Impacts of Landslides. In *Landslides – Disaster Risk Reduction* (pp. 573–587). Springer Berlin Heidelberg. https://doi.org/10.1007/978-3-540-69970-5_30

Kjekstad, O., & Highland, L. (2009b). Economic and social impacts of landslides. In K. Sassa & P. Canuti (Eds.), *Landslides – disaster risk reduction* (pp. 573–587). Springer Berlin Heidelberg. https://doi.org/10.1007/978-3-540-69970-5_30

Klemeš, V. (1986). Operational testing of hydrological simulation models. *Hydrological Sciences Journal*, *31*(1), 13–24. https://doi.org/10.1080/02626668609491024

Knevels, R., Brenning, A., Gingrich, S., Heiss, G., Lechner, T., Leopold, P., Plutzar, C., Proske, H., & Petschko, H. (2021). Towards the Use of Land Use Legacies in Landslide Modeling: Current Challenges and Future Perspectives in an Austrian Case Study. *Land*, *10*(9), 954. https://doi.org/10.3390/land10090954

Knevels, R., Petschko, H., Proske, H., Leopold, P., Maraun, D., & Brenning, A. (2020). Event-Based Landslide Modeling in the Styrian Basin, Austria: Accounting for Time-Varying Rainfall and Land Cover. *Geosciences*, *10*(6), 217. https://doi.org/10.3390/geosciences10060217

Koestel, J., & Jorda, H. (2014). What determines the strength of preferential transport in undisturbed soil under steady-state flow? *Geoderma*, *217-218*, 144–160. https://doi.org/10.1016/j.geoderma.2013.11.009

Korpela, I., Dahlin, B., Schäfer, H., Bruun, E., Haapaniemi, F., Honkasalo, J., Ilvesniemi, S., Kuutti, V., Linkosalmi, M., Mustonen, J., Salo, M., Suomi, O., & Virtanen, H. (2007). Single-tree forest inventory using lidar and aerial images for 3D treetop positioning, species recognition, height and crown width estimation. *In Proceedings of ISPRS workshop on laser scanning*, 12–14.

Korpela, I. (2004). Individual tree measurements by means of digital aerial photogrammetry. *Silva Fennica Monographs*, *2004*(3). https://doi.org/10.14214/sf.sfm3

Koster, R. D., Suarez, M. J., Ducharne, A., Stieglitz, M., & Kumar, P. (2000). A catchment-based approach to modeling land surface processes in a general circulation model: 1. Model structure. *Journal of Geophysical Research: Atmospheres*, *105*(D20), 24809–24822. https://doi.org/10.1029/2000JD900327

Kuhn, M. (2008). Building Predictive Models in *R* Using the **caret** Package. *Journal of Statistical Software*, *28*(5). https://doi.org/10.18637/jss.v028.i05

Kumar, B. M., & Jose, S. (2018). Phenotypic plasticity of roots in mixed tree species agroforestry systems: Review with examples from peninsular India. *Agroforestry Systems*, *92*(1), 59–69. https://doi.org/10.1007/s10457-016-0012-2

Kuriakose, S. L., van Beek, L. P. H., & van Westen, C. J. (2009). Parameterizing a physically based shallow landslide model in a data poor region. *Earth Surface Processes and Landforms*, *34*(6), 867–881. https://doi.org/10.1002/esp.1794

Kutílek, M., & Nielsen, D. R. (1994). *Soil hydrology: Textbook for students of soil science, agriculture, forestry, geoecology, hydrology, geomorphology or other related disciplines*. Catena-Verl.

Lamb, R., Beven, K., & Myrabø, S. (1997). Discharge and water table predictions using a generalised TOPMODEL formulation. *Hydrological Processes*, *11*(9), 1145–1167. https://doi.org/10.1002/(SICI)1099-1085(199707)11:9<1145::AID-HYP550>3.0.CO;2-C

Lambert, M. G., Trustrum, N. A., & Costall, D. A. (1984). Effect of soil slip erosion on seasonally dry Wairarapa hill pastures. *New Zealand Journal of Agricultural Research*, *27*(1), 57–64. https://doi.org/10.1080/00288233.1984.10425732

Lateltin, O. (1997). Berticksichtigung der massenbewegungsgefahren bei raumwirksamen tatigkeiten. naturgefahren, empfehlungen. *Bern, Bundesamt für Raumplanung (BRP), Bundesamt für Wasserwirtschaft (BWW), Bundesamt für Umwelt, Wald und Landschaft (BUWAL)*.

Lateltin, O., Haemmig, C., Raetzo, H., & Bonnard, C. (2005). Landslide risk management in Switzerland. *Landslides*, *2*(4), 313–320. https://doi.org/10.1007/s10346-005-0018-8

Lau, A., Calders, K., Bartholomeus, H., Martius, C., Raumonen, P., Herold, M., Vicari, M., Sukhdeo, H., Singh, J., & Goodman, R. (2019). Tree Biomass Equations from Terrestrial LiDAR: A Case Study in Guyana. *Forests*, *10*(6), 527. https://doi.org/10.3390/f10060527

Lee, J., & Begg, J. (2002). *Geology of the wairarapa area* (Vol. 11).

Lehmann, P., Gambazzi, F., Suski, B., Baron, L., Askarinejad, A., Springman, S. M., Holliger, K., & Or, D. (2013). Evolution of soil wetting patterns preceding a hydrologically induced landslide inferred from electrical resistivity survey and point measurements of volumetric water content and pore water pressure: EVOLUTION OF WETTING PATTERNS PRECEDING A RAPID LANDSLIDE. *Water Resources Research*, *49*(12), 7992–8004. https://doi.org/10.1002/2013WR014560

Leonarduzzi, E., Molnar, P., & McArdell, B. W. (2017). Predictive performance of rainfall thresholds for shallow landslides in Switzerland from gridded daily data. *Water Resources Research*, *53*(8), 6612–6625. https://doi.org/10.1002/2017WR021044

Lepore, C., Arnone, E., Noto, L. V., Sivandran, G., & Bras, R. L. (2013). Physically based modeling of rainfall-triggered landslides: A case study in the Luquillo forest, Puerto Rico. *Hydrology and Earth System Sciences*, *17*(9), 3371–3387. https://doi.org/10.5194/hess-17-3371-2013

Li, W. C., Lee, L. M., Cai, H., Li, H. J., Dai, F., & Wang, M. L. (2013). Combined roles of saturated permeability and rainfall characteristics on surficial failure of homogeneous soil slope. *Engineering Geology*, *153*, 105–113. https://doi.org/10.1016/j.enggeo.2012.11.017

Liang, W.-L., & Chan, M.-C. (2017). Spatial and temporal variations in the effects of soil depth and topographic wetness index of bedrock topography on subsurface saturation generation in a steep natural forested headwater catchment. *Journal of Hydrology*, *546*, 405–418. https://doi.org/10.1016/j.jhydrol.2017.01.033

Lin, H., Bouma, J., Wilding, L., Richardson, J., Kutílek, M., & Nielsen, D. (2005). Advances in Hydropedology. In *Advances in Agronomy* (pp. 1–89). Elsevier. https://doi.org/10.1016/S0065-2113(04)85001-6

Lindh, M., Falster, D. S., Zhang, L., Dieckmann, U., & Brännström, Å. (2018). Latitudinal effects on crown shape evolution. *Ecology and Evolution*, *8*(16), 8149–8158. https://doi.org/10.1002/ece3.4275

Liu, D., Guo, S., Wang, Z., Liu, P., Yu, X., Zhao, Q., & Zou, H. (2018). Statistics for sample splitting for the calibration and validation of hydrological models. *Stochastic Environmental*

Research and Risk Assessment, *32*(11), 3099–3116. https://doi.org/10.1007/s00477-018-1539-8

Loat, R. (2003). *Risk management of natural hazards in Switzerland* (tech. rep.).

Loat, R., & Petrascheck, A. (1997). Consideration of flood hazards for activities with spatial impact. *Federal Office for the Environment (FOEN): Bern, Switzerland*.

Lombardo, L., & Mai, P. M. (2018). Supplementary Materials: Presenting Logistic Regression-based landslide susceptibility results.

Lu, N., Godt, J. W., & Wu, D. T. (2010). A closed-form equation for effective stress in unsaturated soil. *Water Resources Research*, *46*(5). https://doi.org/10.1029/2009WR008646

Luo, Y., He, S.-m., Chen, F.-z., Li, X.-p., & He, J.-c. (2015). A physical model considered the effect of overland water flow on rainfall-induced shallow landslides. *Geoenvironmental Disasters*, *2*(1), 8. https://doi.org/10.1186/s40677-015-0017-6

Mackay-Smith, T. H., Burkitt, L., Reid, J., López, I. F., & Phillips, C. (2021). A Framework for Reviewing Silvopastoralism: A New Zealand Hill Country Case Study. *Land*, *10*(12), 1386. https://doi.org/10.3390/land10121386

Malamud, B. D., Turcotte, D. L., Guzzetti, F., & Reichenbach, P. (2004). Landslide inventories and their statistical properties. *Earth Surface Processes and Landforms*, *29*(6), 687–711. https://doi.org/10.1002/esp.1064

Manaaki Whenua - Landcare Research. (2019). S-map - New Zealand's national digital soil map. 10.7931/L1WC7.

Marden, M., Lambie, S., & Rowan, D. (2018). Root system attributes of 12 juvenile indigenous early colonising shrub and tree species with potential for mitigating erosion in New Zealand. *New Zealand Journal of Forestry Science*, *48*(1), 11. https://doi.org/10.1186/s40490-018-0115-9

Markart, G., Kohl, B., Sotier, B., Klebinder, K., Schauer, T., Bunza, G., Pirkl, H., & Stern, R. (2011). A Simple Code of Practice for the Assessment of Surface Runoff Coefficients for Alpine Soil-/Vegetation Units in Torrential Rain (Version 2.0) [Publisher: Unpublished]. https://doi.org/10.13140/RG.2.1.3406.5441

Markart, G., Kohl, B., Sotier, B., Schauer, T., Bunza, G., & Stern, R. (2006). Geländeanleitung zur Abschätzung des Oberflächenabflussbeiwertes bei Starkregen–Grundzüge und erste Erfahrungen.

Markart, G., Römer, A., Bieber, G., Pirkl, H., Klebinder, K., Hörfarter, C., Ita, A., Jochum, B., Kohl, B., & Motschka, K. (2015). Assessment of Shallow Interflow Velocities in Alpine Catchments for the Improvement of Hydrological Modelling. In *Engineering Geology for Society and Territory - Volume 3* (pp. 611–615). Springer International Publishing. https://doi.org/10.1007/978-3-319-09054-2_122

Markart, G., Sotier, B., Stepanek, L., Lechner, V., & Kohl, B. (2017). Waldwirkung auf die Abflussbildung bei unterschiedlichen Betrachtungsmaßstäben. *Wildbach Lawinenverbau*, (180), 100–115.

Marston, R. A. (2010). Geomorphology and vegetation on hillslopes: Interactions, dependencies, and feedback loops. *Geomorphology*, *116*(3-4), 206–217. https://doi.org/10.1016/j.geomorph.2009.09.028

Masi, E. B., Segoni, S., & Tofani, V. (2021). Root Reinforcement in Slope Stability Models: A Review. *Geosciences*, *11*(5), 212. https://doi.org/10.3390/geosciences11050212

Matsushita, M., Takata, K., Hitsuma, G., Yagihashi, T., Noguchi, M., Shibata, M., & Masaki, T. (2015). A novel growth model evaluating age–size effect on long-term trends in tree growth (E. Sayer, Ed.). *Functional Ecology*, *29*(10), 1250–1259. https://doi.org/10.1111/1365-2435.12416

McDonnell, J. J., Sivapalan, M., Vaché, K., Dunn, S., Grant, G., Haggerty, R., Hinz, C., Hooper, R., Kirchner, J., Roderick, M. L., Selker, J., & Weiler, M. (2007). Moving beyond heterogeneity

and process complexity: A new vision for watershed hydrology. *Water Resources Research*, *43*(7). https://doi.org/10.1029/2006WR005467

McDonnell, J. J. (2014). The two water worlds hypothesis: Ecohydrological separation of water between streams and trees? *WIREs Water*, *1*(4), 323–329. https://doi.org/10.1002/wat2.1027

McGuire, L. A., Rengers, F. K., Kean, J. W., Coe, J. A., Mirus, B. B., Baum, R. L., & Godt, J. W. (2016). Elucidating the role of vegetation in the initiation of rainfall-induced shallow landslides: Insights from an extreme rainfall event in the Colorado Front Range. *Geophysical Research Letters*, *43*(17), 9084–9092. https://doi.org/10.1002/2016GL070741

McIvor, I. R., Douglas, G. B., & Benavides, R. (2009). Coarse root growth of Veronese poplar trees varies with position on an erodible slope in New Zealand. *Agroforestry Systems*, *76*(1), 251–264. https://doi.org/10.1007/s10457-009-9209-y

McIvor, I. R., Douglas, G. B., Hurst, S. E., Hussain, Z., & Foote, A. G. (2007). Structural root growth of young Veronese poplars on erodible slopes in the southern North Island, New Zealand. *Agroforestry Systems*, *72*(1), 75–86. https://doi.org/10.1007/s10457-007-9090-5

McIvor, I., Douglas, G., Dymond, J., Eyles, G., & Marde, M. (2011). Pastoral Hill Slope Erosion in New Zealand and the Role of Poplar and Willow Trees in Its Reduction. In *Soil Erosion Issues in Agriculture*. InTech. https://doi.org/10.5772/24365

McKay, M. D., Beckman, R. J., & Conover, W. J. (1979). Comparison of three methods for selecting values of input variables in the analysis of output from a computer code. *Technometrics*, *21*(2), 239–245. https://doi.org/10.1080/00401706.1979.10489755

McMillan, H., Jackson, B., Clark, M., Kavetski, D., & Woods, R. (2011). Rainfall uncertainty in hydrological modelling: An evaluation of multiplicative error models. *Journal of Hydrology*, *400*(1-2), 83–94. https://doi.org/10.1016/j.jhydrol.2011.01.026

Menk, J., Dorren, L., Heinzel, J., Marty, M., & Huber, M. (2017). Evaluation automatischer Einzelbaumerkennung aus luftgestützten Laserscanning-Daten. *Schweizerische Zeitschrift fur Forstwesen*, *168*(3), 151–159. https://doi.org/10.3188/szf.2017.0151

Metz, C. E. (1978). Basic principles of ROC analysis. *Seminars in Nuclear Medicine*, *8*(4), 283–298. https://doi.org/10.1016/S0001-2998(78)80014-2

Milledge, D. G., Bellugi, D., McKean, J. A., Densmore, A. L., & Dietrich, W. E. (2014). A multidimensional stability model for predicting shallow landslide size and shape across landscapes. *Journal of Geophysical Research: Earth Surface*, *119*(11), 2481–2504. https://doi.org/10.1002/2014JF003135

Moana Project Team. (2021). Moana Project releases Hau-Moana: NZ atmospheric Hindcast downscaling data.

Montgomery, D. R., & Dietrich, W. E. (1994). A physically based model for the topographic control on shallow landsliding. *Water Resources Research*, *30*(4), 1153–1171. https://doi.org/10.1029/93WR02979

Montgomery, D. R., & Dietrich, W. E. (2004). Reply to comment by Richard M. Iverson on "Piezometric response in shallow bedrock at CB1: Implications for runoff generation and landsliding": COMMENTARY. *Water Resources Research*, *40*(3). https://doi.org/10.1029/2003WR002815

Montgomery, D. R., Dietrich, W. E., & Heffner, J. T. (2002). Piezometric response in shallow bedrock at CB1: Implications for runoff generation and landsliding. *Water Resources Research*, *38*(12), 10–1–10–18. https://doi.org/10.1029/2002WR001429

Montgomery, D. R., Schmidt, K. M., Greenberg, H. M., & Dietrich, W. E. (2000). Forest clearing and regional landsliding. *Geology*, *28*(4), 311. https://doi.org/10.1130/0091-7613(2000)28<311:FCARL>2.0.CO;2

Montrasio, L., & Valentino, R. (2008). A model for triggering mechanisms of shallow landslides. *Natural Hazards and Earth System Sciences*, *8*(5), 1149–1159. https://doi.org/10.5194/nhess-8-1149-2008

Montrasio, L., Valentino, R., & Losi, G. L. (2011). Towards a real-time susceptibility assessment of rainfall-induced shallow landslides on a regional scale. *Natural Hazards and Earth System Sciences*, *11*(7), 1927–1947. https://doi.org/10.5194/nhess-11-1927-2011

Mooney, S. J., & Morris, C. (2008). A morphological approach to understanding preferential flow using image analysis with dye tracers and X-ray Computed Tomography. *CATENA*, *73*(2), 204–211. https://doi.org/10.1016/j.catena.2007.09.003

Moore, I. D., O'Loughlin, E. M., & Burch, G. J. (1988). A contour-based topographic model for hydrological and ecological applications. *Earth Surface Processes and Landforms*, *13*(4), 305–320. https://doi.org/10.1002/esp.3290130404

Moore, R. D., & Thompson, J. C. (1996). Are Water Table Variations in a Shallow Forest Soil Consistent with the TOPMODEL Concept? *Water Resources Research*, *32*(3), 663–669. https://doi.org/10.1029/95WR03487

Moos, C. (2018). *Valuing the protective effect of forests against rockfall: A risk-based approach* (Doctoral dissertation). Philosophisch-naturwissenschaftliche Fakultät Universität Bern.

Moos, C., Bebi, P., Graf, F., Mattli, J., Rickli, C., & Schwarz, M. (2016). How does forest structure affect root reinforcement and susceptibility to shallow landslides?: A Case Study in St Antönien, Switzerland. *Earth Surface Processes and Landforms*, *41*(7), 951–960. https://doi.org/10.1002/esp.3887

Mosley, M. (1982). Subsurface flow velocities through selected forest soils, South Island, New Zealand. *Journal of Hydrology*, *55*(1-4), 65–92. https://doi.org/10.1016/0022-1694(82)90121-4

Mulvaney, T. J. (1851). On the use of self-registering rain and flood gauges in making observations of the relations of rainfall and flood discharges in a given catchment. *Proceedings of the institution of Civil Engineers of Ireland*, *4*, 19–31.

Munich RE. (2018). Relevant hydrological events worldwide 1980 - 2018. *NatCatService*.

Murgia, I., Giadrossich, F., Mao, Z., Cohen, D., Capra, G. F., & Schwarz, M. (2022). Modeling shallow landslides and root reinforcement: A review. *Ecological Engineering*, *181*, 106671. https://doi.org/10.1016/j.ecoleng.2022.106671

Naef, F., Scherrer, S., & Faeh, A. (1994). *How does a catchment behave under extreme precipitation? Old and new ideas and experiments* (tech. rep.). Versuchsanstalt für Wasserbau Hydrologie und Glaziologie ETH Zentrum.

Newsome, P., Wilde, R., & Willoughby, E. (2008). *Land resource information system spatial: Data layers*. Landcare Research New Zealand.

Ngo, H. M., Zadelhoff, F. B. V., Gasparini, I., Plaschy, J., Flepp, G., Dorren, L., Phillips, C., Giadrossich, F., & Schwarz, M. (2023). Analysis of poplar ' s (Populus nigra ita .) root system for the assessment of ecosystem services in NZ pastoral hillcountry; in preparation, 1–35.

Norton, J. D. (2021). *The Material Theory of Induction*. University of Calgary Press. https://doi.org/10.2307/j.ctv25wxcb5

O'brien, R. M. (2007). A Caution Regarding Rules of Thumb for Variance Inflation Factors. *Quality & Quantity*, *41*(5), 673–690. https://doi.org/10.1007/s11135-006-9018-6

O'Callaghan, J. F., & Mark, D. M. (1984). The Extraction of Drainage Networks from Digital Elevation Data. *Computer vision, graphics, and image processing*, *28*(3), 323–344.

O'Loughlin, E. M. (1986). Prediction of Surface Saturation Zones in Natural Catchments by Topographic Analysis. *Water Resources Research*, *22*(5), 794–804. https://doi.org/10.1029/WR022i005p00794

Pack, R. T., Tarboton, D. G., & Goodwin, C. N. (1998). The SINMAP Approach to Terrain Stability Mapping. *8th Congress of the International Association of Engineering Geology, Vancouver, British Columbia*, *2*, 1157–1166.

Papa, M. N., Medina, V., Ciervo, F., & Bateman, A. (2013). Derivation of critical rainfall thresholds for shallow landslides as a tool for debris flow early warning systems. *Hydrology and Earth System Sciences*, *17*(10), 4095–4107. https://doi.org/10.5194/hess-17-4095-2013

Park, H. J., Lee, J. H., & Woo, I. (2013). Assessment of rainfall-induced shallow landslide susceptibility using a GIS-based probabilistic approach. *Engineering Geology*, *161*, 1–15. https://doi.org/10.1016/j.enggeo.2013.04.011

Pechlivanidis, I., Jackson, B., McIntyre, N., & Wheater, H. (2011). Catchment scale hydrological modelling: A review of model types, calibration approaches and uncertainty analysis methods in the context of recent developments in technology and applications. *Global NEST Journal*, *13*(3), 193–214.

Perona, P., Flury, R., Barry, D. A., & Schwarz, M. (2022). Tree root distribution modelling in different environmental conditions. *Ecological Engineering*, *185*, 106811. https://doi.org/10.1016/j.ecoleng.2022.106811

Petschko, H., Brenning, A., Bell, R., Goetz, J., & Glade, T. (2014). Assessing the quality of landslide susceptibility maps – case study Lower Austria. *Natural Hazards and Earth System Sciences*, *14*(1), 95–118. https://doi.org/10.5194/nhess-14-95-2014

Phillips, C., Hales, T., Smith, H., & Basher, L. (2021). Shallow landslides and vegetation at the catchment scale: A perspective. *Ecological Engineering*, *173*, 106436. https://doi.org/10.1016/j.ecoleng.2021.106436

Phillips, C., & Marden, M. (2005). Reforestation Schemes to Manage Regional Landslide Risk. In *Landslide Hazard and Risk* (1st ed., pp. 517–547). Wiley. https://doi.org/10.1002/9780470012659.ch18

Phillips, C. J., Marden, M., & Suzanne, L. M. (2014). Observations of root growth of young poplar and willow planting types. *New Zealand Journal of Forestry Science*, *44*(1), 15. https://doi.org/10.1186/s40490-014-0015-6

Pierret, A., Doussan, C., Capowiez, Y., Bastardie, F., & Pagès, L. (2007). Root Functional Architecture: A Framework for Modeling the Interplay between Roots and Soil. *Vadose Zone Journal*, *6*(2), 269–281. https://doi.org/10.2136/vzj2006.0067

Plakman, V., Janssen, T., Brouwer, N., & Veraverbeke, S. (2020). Mapping Species at an Individual-Tree Scale in a Temperate Forest, Using Sentinel-2 Images, Airborne Laser Scanning Data, and Random Forest Classification. *Remote Sensing*, *12*(22), 3710. https://doi.org/10.3390/rs12223710

Pollen, N., & Simon, A. (2005). Estimating the mechanical effects of riparian vegetation on stream bank stability using a fiber bundle model. *Water Resources Research*, *41*(7). https://doi.org/10.1029/2004WR003801

Ponce, V. M., & Hawkins, R. H. (1996). Runoff Curve Number: Has It Reached Maturity? *Journal of Hydrologic Engineering*, *1*(1), 11–19. https://doi.org/10.1061/(ASCE)1084-0699(1996)1:1(11)

Post, D. A., & Jakeman, A. J. (1996). Relationship between catchment attributes and hydrological response characteristics in small australian mountain ash catchments. *Hydrological Processes*, *10*(6), 877–892. https://doi.org/10.1002/(SICI)1099-1085(199606)10:6<877::AID-HYP377>3.0.CO;2-T

Power, I., Thorrold, B., & Balks, M. (2003). Soil properties and nitrogen availability in silvopastoral plantings of Acacia melanoxylon in North Island, New Zealand. *Agroforestry Systems*, *57*(3), 225–237. https://doi.org/10.1023/A:1024838311287

Prancevic, J. P., Lamb, M. P., McArdell, B. W., Rickli, C., & Kirchner, J. W. (2020). Decreasing Landslide Erosion on Steeper Slopes in Soil-Mantled Landscapes. *Geophysical Research Letters*, *47*(10). https://doi.org/10.1029/2020GL087505

Price, B., Gomez, A., Mathys, L., Gardi, O., Schellenberger, A., Ginzler, C., & Thürig, E. (2017). Tree biomass in the Swiss landscape: Nationwide modelling for improved accounting for

forest and non-forest trees. *Environmental Monitoring and Assessment*, *189*(3), 106. https://doi.org/10.1007/s10661-017-5816-7

Rallison, R. E. (1980). Origin and evolution of the scs runoff equation.

Ratto, M., Tarantola, S., & Saltelli, A. (2001). Sensitivity analysis in model calibration: GSA-GLUE approach. *Computer Physics Communications*, *136*(3), 212–224. https://doi.org/10.1016/S0010-4655(01)00159-X

Refsgaard, J. C. (1997). Parameterisation, calibration and validation of distributed hydrological models. *Journal of Hydrology*, *198*(1-4), 69–97. https://doi.org/10.1016/S0022-1694(96)03329-X

Reichenbach, P., Busca, C., Mondini, A. C., & Rossi, M. (2014). The Influence of Land Use Change on Landslide Susceptibility Zonation: The Briga Catchment Test Site (Messina, Italy). *Environmental Management*, *54*(6), 1372–1384. https://doi.org/10.1007/s00267-014-0357-0

Reichenbach, P., Rossi, M., Malamud, B. D., Mihir, M., & Guzzetti, F. (2018). A review of statistically-based landslide susceptibility models. *Earth-Science Reviews*, *180*, 60–91. https://doi.org/10.1016/j.earscirev.2018.03.001

Reid, L., & Page, M. (2003). Magnitude and frequency of landsliding in a large New Zealand catchment. *Geomorphology*, *49*(1-2), 71–88. https://doi.org/10.1016/S0169-555X(02)00164-2

Reubens, B., Poesen, J., Danjon, F., Geudens, G., & Muys, B. (2007). The role of fine and coarse roots in shallow slope stability and soil erosion control with a focus on root system architecture: A review. *Trees*, *21*(4), 385–402. https://doi.org/10.1007/s00468-007-0132-4

Richards, L. A. (1931). Capillary conduction of liquids through porous mediums. *Physics*, *1*(5), 318–333. https://doi.org/10.1063/1.1745010

Rickli, C., & Graf, F. (2009). Effects of forests on shallow landslides – case studies in Switzerland. *Forest Snow and Landscape Research*, *82*(1), 33–44.

Rickli, C., Graf, F., Bebi, P., Bast, A., Loup, B., & McArdell, B. (2019). Schützt der Wald vor Rutschungen? Hinweise aus der WSL-Rutschungsdatenbank. *Schweizerische Zeitschrift fur Forstwesen*, *170*(6), 310–317. https://doi.org/10.3188/szf.2019.0310

Rinaldo, A., Botter, G., Bertuzzo, E., Uccelli, A., Settin, T., & Marani, M. (2006). Transport at basin scales: 1. Theoretical framework. *Hydrology and Earth System Sciences*, *10*(1), 19–29. https://doi.org/10.5194/hess-10-19-2006

Rinderer, M., & Seibert, J. (2012). Soil Information in Hydrologic Models: Hard Data, Soft Data, and the Dialog between Experimentalists and Modelers. In *Hydropedology* (First edition, pp. 515–536). Elsevier.

Robinson, J. S., Sivapalan, M., & Snell, J. D. (1995). On the relative roles of hillslope processes, channel routing, and network geomorphology in the hydrologic response of natural catchments. *Water Resources Research*, *31*(12), 3089–3101. https://doi.org/10.1029/95WR01948

Roering, J. J., Schmidt, K. M., Stock, J. D., Dietrich, W. E., & Montgomery, D. R. (2003). Shallow landsliding, root reinforcement, and the spatial distribution of trees in the Oregon Coast Range. *Canadian Geotechnical Journal*, *40*(2), 237–253. https://doi.org/10.1139/t02-113

Ronneberger, O., Fischer, P., & Brox, T. (2015). U-net: Convolutional networks for biomedical image segmentation. *International Conference on Medical image computing and computer-assisted intervention*, 234–241.

Rossi, G., Catani, F., Leoni, L., Segoni, S., & Tofani, V. (2013). HIRESSS: A physically based slope stability simulator for HPC applications. *Natural Hazards and Earth System Sciences*, *13*(1), 151–166. https://doi.org/10.5194/nhess-13-151-2013

SafeLand. (2011). *Living with landslide risk in Europe: Assessment, effects of global change, and risk management strategies; Deliverable D2.8* (Recommended Procedures for Validating Landslide Hazard and Risk Models and Maps No. D2.8). Safeland.

Sakals, M. E., & Sidle, R. C. (2004). A spatial and temporal model of root cohesion in forest soils. *Canadian Journal of Forest Research*, *34*(4), 950–958. https://doi.org/10.1139/x03-268

Salciarini, D., Fanelli, G., & Tamagnini, C. (2017). A probabilistic model for rainfall—induced shallow landslide prediction at the regional scale. *Landslides*, *14*(5), 1731–1746. https://doi.org/10.1007/s10346-017-0812-0

Salciarini, D., Tamagnini, C., Conversini, P., & Rapinesi, S. (2012). Spatially distributed rainfall thresholds for the initiation of shallow landslides. *Natural Hazards*, *61*(1), 229–245. https://doi.org/10.1007/s11069-011-9739-2

Salvatici, T., Tofani, V., Rossi, G., D'Ambrosio, M., Tacconi Stefanelli, C., Masi, E. B., Rosi, A., Pazzi, V., Vannocci, P., Petrolo, M., Catani, F., Ratto, S., Stevenin, H., & Casagli, N. (2018). Application of a physically based model to forecast shallow landslides at a regional scale. *Natural Hazards and Earth System Sciences*, *18*(7), 1919–1935. https://doi.org/10.5194/nhess-18-1919-2018

Savenije, H. H. G. (2009). HESS Opinions;The art of hydrology. *Hydrology and Earth System Sciences*, *13*(2), 157–161. https://doi.org/10.5194/hess-13-157-2009

Savenije, H. H. G. (2010). HESS Opinions "Topography driven conceptual modelling (FLEX-Topo)" *Hydrology and Earth System Sciences*, *14*(12), 2681–2692. https://doi.org/10.5194/hess-14-2681-2010

Schaefli, B., & Gupta, H. V. (2007). Do Nash values have value? *Hydrological Processes*, *21*(15), 2075–2080. https://doi.org/10.1002/hyp.6825

Scheidl, C., Heiser, M., Kamper, S., Thaler, T., Rammer, W., Seidl, R., Klebinder, K., Lechner, V., Nagl, F., Kohl, B., & Markart, G. (2022). Influence of Canopy Disturbances on Runoff and Landslide Disposition after Heavy Rainfall Events. In M. Teich, C. Accastello, F. Perzl, & K. Kleemayr (Eds.), *Protective Forests as Ecosystem-based Solution for Disaster Risk Reduction (Eco-DRR)*. IntechOpen. https://doi.org/10.5772/intechopen.99511

Scherrer, S. C., Fischer, E. M., Posselt, R., Liniger, M. A., Croci-Maspoli, M., & Knutti, R. (2016). Emerging trends in heavy precipitation and hot temperature extremes in Switzerland: Trends in Swiss Climate Extremes. *Journal of Geophysical Research: Atmospheres*, *121*(6), 2626–2637. https://doi.org/10.1002/2015JD024634

Scherrer, S. (1996). *Abflussbildung bei Starkniederschlägen: Identifikation von Abflussprozessen mittels künstlicher Niederschläge* (Doctoral dissertation) [Artwork Size: 180 Bl. Medium: application/pdf Pages: 180 Bl.]. ETH Zurich. https://doi.org/10.3929/ETHZ-A-001735502

Scherrer, S., & Naef, F. (2003). A decision scheme to indicate dominant hydrological flow processes on temperate grassland. *Hydrological Processes*, *17*(2), 391–401. https://doi.org/10.1002/hyp.1131

Schlüter, S., Blaser, S. R. G. A., Weber, M., Schmidt, V., & Vetterlein, D. (2018). Quantification of Root Growth Patterns From the Soil Perspective via Root Distance Models. *Frontiers in Plant Science*, *9*, 1084. https://doi.org/10.3389/fpls.2018.01084

Schmaltz, E. M., & Mergili, M. (2018). Integration of root systems into a GIS-based slip surface model: Computational experiments in a generic hillslope environment. *Landslides*, *15*(8), 1561–1575. https://doi.org/10.1007/s10346-018-0970-8

Schmaltz, E. M., Steger, S., & Glade, T. (2017). The influence of forest cover on landslide occurrence explored with spatio-temporal information. *Geomorphology*, *290*, 250–264. https://doi.org/10.1016/j.geomorph.2017.04.024

Schmaltz, E. M., Van Beek, L., Bogaard, T. A., Kraushaar, S., Steger, S., & Glade, T. (2019). Strategies to improve the explanatory power of a dynamic slope stability model by enhancing land cover parameterisation and model complexity. *Earth Surface Processes and Landforms*, *44*(6), 1259–1273. https://doi.org/10.1002/esp.4570

Schmidt, K. M., Roering, J. J., Stock, J. D., Dietrich, W. E., Montgomery, D. R., & Schaub, T. (2001). The variability of root cohesion as an influence on shallow landslide susceptibility in the Oregon Coast Range. *Canadian Geotechnical Journal*, *38*, 995–1024.

Schwarz, M., Cohen, D., & Or, D. (2011). Pullout tests of root analogs and natural root bundles in soil: Experiments and modeling. *Journal of Geophysical Research: Earth Surface*, *116*(F2). https://doi.org/10.1029/2010JF001753

Schwarz, M., Cohen, D., & Or, D. (2012). Spatial characterization of root reinforcement at stand scale: Theory and case study. *Geomorphology*, *171-172*, 190–200. https://doi.org/10.1016/j.geomorph.2012.05.020

Schwarz, M., Giadrossich, F., & Cohen, D. (2013). Modeling root reinforcement using a root-failure Weibull survival function. *Hydrology and Earth System Sciences*, *17*(11), 4367–4377. https://doi.org/10.5194/hess-17-4367-2013

Schwarz, M., Lehmann, P., & Or, D. (2010). Quantifying lateral root reinforcement in steep slopes - from a bundle of roots to tree stands. *Earth Surface Processes and Landforms*, *35*(3), 354–367. https://doi.org/10.1002/esp.1927

Schwarz, M., Phillips, C., Marden, M., McIvor, I. R., Douglas, G. B., & Watson, A. (2016). Modelling of root reinforcement and erosion control by 'Veronese' poplar on pastoral hill country in New Zealand. *New Zealand Journal of Forestry Science*, *46*(1), 4. https://doi.org/10.1186/s40490-016-0060-4

Schwarz, M., Preti, F., Giadrossich, F., Lehmann, P., & Or, D. (2010). Quantifying the role of vegetation in slope stability: A case study in Tuscany (Italy). *Ecological Engineering*, *36*(3), 285–291. https://doi.org/10.1016/j.ecoleng.2009.06.014

Schwarz, M., Rist, A., Cohen, D., Giadrossich, F., Egorov, P., Büttner, D., Stolz, M., & Thormann, J.-J. (2015). Root reinforcement of soils under compression. *Journal of Geophysical Research: Earth Surface*, *120*(10), 2103–2120. https://doi.org/10.1002/2015JF003632

Seibert, J. (1996). HBV light. User's manual.

Shao, W., Bogaard, T. A., Bakker, M., & Greco, R. (2015). Quantification of the influence of preferential flow on slope stability using a numerical modelling approach. *Hydrology and Earth System Sciences*, *19*(5), 2197–2212. https://doi.org/10.5194/hess-19-2197-2015

Shou, K.-J., & Chen, J. (2021). On the rainfall induced deep-seated and shallow landslide hazard in Taiwan. *Engineering Geology*, *288*, 106156. https://doi.org/10.1016/j.enggeo.2021.106156

Sidle, R. C. (1992). A theoretical model of the effects of timber harvesting on slope stability. *Water Resources Research*, *28*(7), 1897–1910. https://doi.org/10.1029/92WR00804

Sidle, R. C., & Bogaard, T. A. (2016). Dynamic earth system and ecological controls of rainfall-initiated landslides. *Earth-Science Reviews*, *159*, 275–291. https://doi.org/10.1016/j.earscirev.2016.05.013

Sidle, R. C., Noguchi, S., Tsuboyama, Y., & Laursen, K. (2001). A conceptual model of preferential flow systems in forested hillslopes: Evidence of self-organization. *Hydrological Processes*, *15*(10), 1675–1692. https://doi.org/10.1002/hyp.233

Sidle, R. C., & Ochiai, H. (2006). Natural factors influencing landslides. *Landslides: Processes, Prediction, and Land Use*, *18*, 41–119.

Sitterson, J., Knightes, C., Parmar, R., Wolfe, K., Avant, B., & Muche, M. (2018). An Overview of Rainfall-Runoff Model Types.

Sivapalan, M., Blöschl, G., Zhang, L., & Vertessy, R. (2003). Downward approach to hydrological prediction. *Hydrological Processes*, *17*(11), 2101–2111. https://doi.org/10.1002/hyp.1425

Sivapalan, M., Woods, R. A., & Kalma, J. D. (1997). Variable bucket representation of TOPMODEL and investigation of the effects of rainfall heterogeneity. *Hydrological Processes*, *11*(9), 1307–1330. https://doi.org/10.1002/(SICI)1099-1085(199707)11:9<1307::AID-HYP562>3.0.CO;2-Y

Smith, H. G., Spiekermann, R., Betts, H., & Neverman, A. J. (2021). Comparing methods of landslide data acquisition and susceptibility modelling: Examples from New Zealand. *Geomorphology*, *381*, 107660. https://doi.org/10.1016/j.geomorph.2021.107660

Spiekermann, R., Kienberger, S., Norton, J., Briones, F., & Weichselgartner, J. (2015). The Disaster-Knowledge Matrix – Reframing and evaluating the knowledge challenges in disaster risk reduction. *International Journal of Disaster Risk Reduction*, *13*, 96–108. https://doi.org/10.1016/j.ijdrr.2015.05.002

Spiekermann, R. I., McColl, S., Fuller, I., Dymond, J., Burkitt, L., & Smith, H. G. (2021). Quantifying the influence of individual trees on slope stability at landscape scale. *Journal of Environmental Management*, *286*, 112194. https://doi.org/10.1016/j.jenvman.2021.112194

Spiekermann, R. I., Smith, H. G., McColl, S., Burkitt, L., & Fuller, I. C. (2022a). Development of a morphometric connectivity model to mitigate sediment derived from storm-driven shallow landslides. *Ecological Engineering*, *180*, 106676. https://doi.org/10.1016/j.ecoleng.2022.106676

Spiekermann, R. I., Smith, H. G., McColl, S., Burkitt, L., & Fuller, I. C. (2022b). Quantifying effectiveness of trees for landslide erosion control. *Geomorphology*, *396*, 107993. https://doi.org/10.1016/j.geomorph.2021.107993

Spiekermann, R. I. (2022). *Quantifying the performance of silvopastoralism for landslide erosion and sediment control in New Zealand's hill country* (Doctoral dissertation). Massey University. Palmerston North, New Zealand.

Steger, S., Brenning, A., Bell, R., Petschko, H., & Glade, T. (2016). Exploring discrepancies between quantitative validation results and the geomorphic plausibility of statistical landslide susceptibility maps. *Geomorphology*, *262*, 8–23. https://doi.org/10.1016/j.geomorph.2016.03.015

Steger, S., Moreno, M., Crespi, A., Zellner, P. J., Gariano, S. L., Brunetti, M. T., Melillo, M., Peruccacci, S., Marra, F., Kohrs, R., Goetz, J., Mair, V., & Pittore, M. (2022). *Deciphering seasonal effects of triggering and preparatory precipitation for improved shallow landslide prediction using generalized additive mixed models* (preprint). Landslides and Debris Flows Hazards. https://doi.org/10.5194/nhess-2022-271

Steinacher, R., Medicus, G., Fellin, W., & Zangerl, C. (2009). The Influence of Deforestation on Slope (In-) Stability. *Austrian Journal of Earth Sciences*, *102*(2), 90–99.

Sternagel, A., Loritz, R., Wilcke, W., & Zehe, E. (2019). Simulating preferential soil water flow and tracer transport using the Lagrangian Soil Water and Solute Transport Model. *Hydrology and Earth System Sciences*, *23*(10), 4249–4267. https://doi.org/10.5194/hess-23-4249-2019

Stokes, A., Douglas, G. B., Fourcaud, T., Giadrossich, F., Gillies, C., Hubble, T., Kim, J. H., Loades, K. W., Mao, Z., McIvor, I. R., Mickovski, S. B., Mitchell, S., Osman, N., Phillips, C., Poesen, J., Polster, D., Preti, F., Raymond, P., Rey, F., … Walker, L. R. (2014). Ecological mitigation of hillslope instability: Ten key issues facing researchers and practitioners. *Plant and Soil*, *377*(1-2), 1–23. https://doi.org/10.1007/s11104-014-2044-6

Stone, E., & Kalisz, P. (1991). On the maximum extent of tree roots. *Forest Ecology and Management*, *46*(1-2), 59–102. https://doi.org/10.1016/0378-1127(91)90245-Q

Styczen, M., & Morgan, R. (2003). Engineering properties of vegetation. In *Slope stabilization and erosion control: A bioengineering approach* (pp. 16–72). Taylor & Francis.

Swiss Re Institute. (2019). Natural catastrophes and man-made disasters in 2018: "secondary" perils on the frontline. *Sigma*, *2*(2), 1–36.

Swisstopo. (2017). SWISSIMAGE. Luftbilder Level 2 (25 cm) Wabern: Bern.

Swisstopo. (2018). SwissALTI3D Das hoch auf-gelöste Terrainmodell der Schweiz.

Swisstopo. (2020). Switzerland forest cover map.

Takeuchi, K., Hapuarachchi, P., Zhou, M., Ishidaira, H., & Magome, J. (2008). A BTOP model to extend TOPMODEL for distributed hydrological simulation of large basins. *Hydrological Processes*, *22*(17), 3236–3251. https://doi.org/10.1002/hyp.6910

Team, R. C. (2021). R: A language and environment for statistical computing. r foundation for statistical computing, vienna, austria. 2012.

Torres, R., Dietrich, W. E., Montgomery, D. R., Anderson, S. P., & Loague, K. (1998). Unsaturated zone processes and the hydrologic response of a steep, unchanneled catchment. *Water Resources Research*, *34*(8), 1865–1879. https://doi.org/10.1029/98WR01140

Trustrum, N., Thomas, V., & Lambert, M. (1984). Soil slip erosion as a constraint to hill country pasture porduction. *Proceedings of the New Zealand Grassland Association*, 66–76. https://doi.org/10.33584/jnzg.1984.45.1676

Tsai, T.-L. (2008). The influence of rainstorm pattern on shallow landslide. *Environmental Geology*, *53*(7), 1563–1569. https://doi.org/10.1007/s00254-007-0767-x

Uchida, T., Tromp-van Meerveld, I., & McDonnell, J. J. (2005). The role of lateral pipe flow in hillslope runoff response: An intercomparison of non-linear hillslope response. *Journal of Hydrology*, *311*(1-4), 117–133. https://doi.org/10.1016/j.jhydrol.2005.01.012

Uhlenbrook, S., & Leibundgut, C. (2002). Process-oriented catchment modelling and multiple-response validation. *Hydrological Processes*, *16*(2), 423–440. https://doi.org/10.1002/hyp.330

Van Beek, L., Wint, J., Cammeraat, L., & Edwards, J. (2007). Observation and simulation of root reinforcement on abandoned mediterranean slopes. In *Eco-and ground bio-engineering: The use of vegetation to improve slope stability* (pp. 91–109). Springer.

Van Den Eeckhaut, M., Vanwalleghem, T., Poesen, J., Govers, G., Verstraeten, G., & Vandekerckhove, L. (2006). Prediction of landslide susceptibility using rare events logistic regression: A case-study in the Flemish Ardennes (Belgium). *Geomorphology*, *76*(3-4), 392–410. https://doi.org/10.1016/j.geomorph.2005.12.003

van Genuchten, M. T. (1980). A Closed-form Equation for Predicting the Hydraulic Conductivity of Unsaturated Soils. *Soil Science Society of America Journal*, *44*(5), 892–898. https://doi.org/10.2136/sssaj1980.03615995004400050002x

van Kraayenoord, C. (1968). Poplars and willows in New Zealand with particular reference to their use in erosion control.

van Schaik, N. (2009). Spatial variability of infiltration patterns related to site characteristics in a semi-arid watershed. *CATENA*, *78*(1), 36–47. https://doi.org/10.1016/j.catena.2009.02.017

van Westen, C. J., Castellanos, E., & Kuriakose, S. L. (2008). Spatial data for landslide susceptibility, hazard, and vulnerability assessment: An overview. *Engineering Geology*, *102*(3-4), 112–131. https://doi.org/10.1016/j.enggeo.2008.03.010

van Zadelhoff, F. B., Albaba, A., Cohen, D., Phillips, C., Schaefli, B., Dorren, L., & Schwarz, M. (2022). Introducing SlideforMAP: A probabilistic finite slope approach for modelling shallow-landslide probability in forested situations. *Natural Hazards and Earth System Sciences*, *22*(8), 2611–2635. https://doi.org/10.5194/nhess-22-2611-2022

Varnes, D. (1978). *Slope movement types and processes* (tech. rep. No. 176).

VAW. (1993). Die Grösse extremer Hochwasser der Saltina; Bericht Nr. 4080.

Vergani, C., Giadrossich, F., Buckley, P., Conedera, M., Pividori, M., Salbitano, F., Rauch, H., Lovreglio, R., & Schwarz, M. (2017). Root reinforcement dynamics of European coppice woodlands and their effect on shallow landslides: A review. *Earth-Science Reviews*, *167*, 88–102. https://doi.org/10.1016/j.earscirev.2017.02.002

Vergani, C., Schwarz, M., Cohen, D., Thormann, J., & Bischetti, G. (2014). Effects of root tensile force and diameter distribution variability on root reinforcement in the Swiss and Italian Alps. *Canadian Journal of Forest Research*, *44*(11), 1426–1440. https://doi.org/10.1139/cjfr-2014-0095

Vergani, C., Schwarz, M., Soldati, M., Corda, A., Giadrossich, F., Chiaradia, E. A., Morando, P., & Bassanelli, C. (2016). Root reinforcement dynamics in subalpine spruce forests following timber harvest: A case study in Canton Schwyz, Switzerland. *CATENA*, *143*, 275–288. https://doi.org/10.1016/j.catena.2016.03.038

Vine, M. (1980). *Root systems of some poplar trees* (Internal report No. 14). Aokautere Science centre.

von Ruette, J., Lehmann, P., & Or, D. (2013). Rainfall-triggered shallow landslides at catchment scale: Threshold mechanics-based modeling for abruptness and localization. *Water Resources Research*, *49*(10), 6266–6285. https://doi.org/10.1002/wrcr.20418

VSS-Kommission. (1998). *Geotechnische Erkundung und Untersuchung; Geotechnische Kenngrössen, Characteristic Coefficients of soils, Association of Swiss Road and Traffic Engineers, 670 010, 2011. https://www.mobilityplatform.ch/de/vss-shop/product/SN-670010* (tech. rep.). Schweizer Norm.

VSS-Kommission, A. o. S. R., & Engineers, T. (2011). *Schweizer Norm, 670 010 Geotechnische Erkundung und Untersuchung; Geotechnische Kenngrössen, Characteristic Coefficients of soils, https://www.mobilityplat shop/product/SN-670010* (tech. rep.). Schweizer Norm.

Waldron, L. J. (1977). The Shear Resistance of Root-Permeated Homogeneous and Stratified Soil. *Soil Science Society of America Journal*, *41*(5), 843–849. https://doi.org/10.2136/sssaj1977.03615995004100050005x

Wang, X., Huang, F., Fan, X., Shahabi, H., Shirzadi, A., Bian, H., Ma, X., Lei, X., & Chen, W. (2022). Landslide susceptibility modeling based on remote sensing data and data mining techniques. *Environmental Earth Sciences*, *81*(2), 50. https://doi.org/10.1007/s12665-022-10195-1

Watson, A., McIvor, I., & Douglas, G. (2008). Live root-wood tensile strength of Populus x euramericana, 'Veronese poplar'. *The New Zealand Poplar*, 1–8.

Watson, A., Phillips, C., & Marden, M. (1999). Root strength, growth, and rates of decay: Root reinforcement changes of two tree species and their contribution to slope stability. *Plant and Soil*, *217*, 39–47. https://doi.org/10.1007/978-94-017-3469-1_4

Watson, A. J., & Marden, M. (2004). Live root-wood tensile strengths of some common New Zealand indigenous and plantation tree species. *New Zealand Journal of Forestry Science*, *34*(3).

Weiler, M., & McDonnell, J. J. (2007). Conceptualizing lateral preferential flow and flow networks and simulating the effects on gauged and ungauged hillslopes. *Water Resources Research*, *43*(3). https://doi.org/10.1029/2006WR004867

Weiler, M., & Naef, F. (2003). An experimental tracer study of the role of macropores in infiltration in grassland soils. *Hydrological Processes*, *17*(2), 477–493. https://doi.org/10.1002/hyp.1136

Welch, B. L. (1947). The Generalization of 'Student's' Problem when Several Different Population Variances are Involved. *Biometrika*, *34*(1/2), 28. https://doi.org/10.2307/2332510

Wiekenkamp, I., Huisman, J., Bogena, H., Lin, H., & Vereecken, H. (2016). Spatial and temporal occurrence of preferential flow in a forested headwater catchment. *Journal of Hydrology*, *534*, 139–149. https://doi.org/10.1016/j.jhydrol.2015.12.050

Wilkinson, A. (1999). Poplars and willows for soil erosion control in New Zealand. *Biomass and Bioenergy*, *16*(4), 263–274. https://doi.org/10.1016/S0961-9534(99)00007-0

Williams, D. G., & Scott, R. L. (2009). Vegetation-Hydrology Interactions. *Ecology and Conservation of the San Pedro River*, 37–56.

Wolock, D. M., & McCabe, G. J. (1995). Comparison of Single and Multiple Flow Direction Algorithms for Computing Topographic Parameters in TOPMODEL. *Water Resources Research*, *31*(5), 1315–1324. https://doi.org/10.1029/95WR00471

Wu, T. H. (1984). *Effect of Vegetation on Slope Stability* (Transportation Research Report 965).

Wu, T. H., McKinnell III, W. P., & Swanston, D. N. (1979). Strength of tree roots and landslides on Prince of Wales Island, Alaska. *Canadian Geotechnical Journal*, *16*(1), 19–33. https://doi.org/10.1139/t79-003

Wu, W., & Sidle, R. C. (1995). A Distributed Slope Stability Model for Steep Forested Basins. *Water Resources Research*, *31*(8), 2097–2110. https://doi.org/10.1029/95WR01136

Wu, Y., Kirillov, A., Massa, F., Lo, W., & Girshick, R. (2019). Detectron2 [www document]. *URL https://github. com/facebookresearch/detectron2 (accessed 3.3. 21)*.

Xu, C., Xu, X., Dai, F., & Saraf, A. K. (2012). Comparison of different models for susceptibility mapping of earthquake triggered landslides related with the 2008 Wenchuan earthquake in China. *Computers & Geosciences*, *46*, 317–329. https://doi.org/10.1016/j.cageo.2012.01.002

Xue, L., Yang, F., Yang, C., Wei, G., Li, W., & He, X. (2018). Hydrological simulation and uncertainty analysis using the improved TOPMODEL in the arid Manas River basin, China. *Scientific Reports*, *8*(1), 452. https://doi.org/10.1038/s41598-017-18982-8

Yang, D., Herath, S., & Musiake, K. (2000). Comparison of different distributed hydrological models for characterization of catchment spatial variability. *Hydrological Processes*, *14*(3), 403–416. https://doi.org/10.1002/(SICI)1099-1085(20000228)14:3<403::AID-HYP945>3.0.CO;2-3

Zevenbergen, L. W., & Thorne, C. R. (1987). Quantitative analysis of land surface topography. *Earth Surface Processes and Landforms*, *12*(1), 47–56. https://doi.org/10.1002/esp.3290120107

Zhang, C., Chu, J., & Fu, G. (2013). Sobols sensitivity analysis for a distributed hydrological model of Yichun River Basin, China. *Journal of Hydrology*, *480*, 58–68. https://doi.org/10.1016/j.jhydrol.2012.12.005

Zhang, L., Wu, F., Zheng, Y., Chen, L., Zhang, J., & Li, X. (2018). Probabilistic calibration of a coupled hydro-mechanical slope stability model with integration of multiple observations. *Georisk: Assessment and Management of Risk for Engineered Systems and Geohazards*, *12*(3), 169–182. https://doi.org/10.1080/17499518.2018.1440317

Zhang, S., Zhao, L., Delgado-Tellez, R., & Bao, H. (2018). A physics-based probabilistic forecasting model for rainfall-induced shallow landslides at regional scale. *Natural Hazards and Earth System Sciences*, *18*(3), 969–982. https://doi.org/10.5194/nhess-18-969-2018

Zhu, H., Zhang, L., Xiao, T., & Li, X. (2017). Enhancement of slope stability by vegetation considering uncertainties in root distribution. *Computers and Geotechnics*, *85*, 84–89. https://doi.org/10.1016/j.compgeo.2016.12.027

Zieher, T., Rutzinger, M., Schneider-Muntau, B., Perzl, F., Leidinger, D., Formayer, H., & Geitner, C. (2017). Sensitivity analysis and calibration of a dynamic physically based slope stability model. *Natural Hazards and Earth System Sciences*, *17*(6), 971–992. https://doi.org/10.5194/nhess-17-971-2017

Zörner, J., Dymond, J., Shepherd, J., Wiser, S., & Jolly, B. (2018). LiDAR-Based Regional Inventory of Tall Trees—Wellington, New Zealand. *Forests*, *9*(11), 702. https://doi.org/10.3390/f9110702

Declaration of Authorship

gemäss Art. 18 PromR Phil.nat 2019

Name/vorname: van Zadelhoff, Feiko Bernard

Matrikelnummer: 20-125-159

Studiengang: Dissertation in Geography

Titel der Arbeit: Quantification of vegetation effects on shallow landslide probability at regional scales

Leiter der Arbeit: Prof. Dr. Bettina Schaefli

"I declare herewith that this thesis is my own work and that I have not used any sources other than those stated. I have indicated the adoption of quotations as well as thoughts taken from other authors as such in the thesis. I am aware that the Senate pursuant to Article 36 paragraph 1 literature of the University Act of September 5th, 1996 and Article 69 of the University Statute of June 7th, 2011 is authorized to revoke the doctoral degree awarded on the basis of this thesis. For the purposes of evaluation and verification of compliance with the declaration of originality and the regulations governing plagiarism, I hereby grant the University of Bern the right to process my personal data and to perform the acts of use this requires, in particular, to reproduce the written thesis and to store it permanently in a database, and to use said database, or to make said database available, to enable comparison with theses submitted by others."

Place and date: Bern 29-03-2023

Signature: